SPIN STATE ISOMERISM AND MOLECULAR MAGNETISM FROM SITE-SPECIFICALLY SUBSTITUTED BIS(INDENYL) TRANSITION METAL COMPLEXES

By

Jeffrey Allen Crisp

Dissertation
Submitted to the Faculty of the
Graduate School of Vanderbilt University
in partial fulfillment of the requirements
for the degree of

DOCTOR OF PHILOSOPHY
in
Chemistry

August, 2009

Nashville, Tennessee

Approved:
Professor Timothy P. Hanusa
Professor Charles M. Lukehart
Professor David Wright
Professor Eva Harth
Professor Bridget R. Rodgers

FOR MOM AND DAD

Acknowledgements

First and foremost, I would like to thank my parents, Allen and Susan Crisp, for the opportunities in this life that they have been able to give to me through their hard work and sacrifice. Without their love, patience, and understanding this would not have been possible.

I would also like to thank my advisor, Professor Timothy P. Hanusa, for enriching my education during my time here at Vanderbilt University. His willingness to teach everyone around him is nothing short of inspirational, and he has instilled in me a passion for learning that has changed my life. It has been an absolute privilege to work for him. The rest of my committee members are thanked as well for the challenges they brought to my experience as a chemist.

My treasured friend Gabrielle Lehr has been my biggest supporter over the final half of this process. She has permitted me the time and space I needed to accomplish the work while offering only sincere encouragement. Her positive outlook has helped keep me a balanced individual, and I have been truly blessed for having her on this part of the journey.

I would also like to thank past Hanusa-lab members, specifically Brett Meredith and Keith Quisenberry, who took their time to train me in air-sensitive handling techniques. It was also a joy to have the opportunity to work with Rosemary White and Cameron Gren. Cameron has been a dear friend, and I wish him all the best in his career.

This work was made possible by ACS-PRF, and so I thank them for their financial support.

TABLE OF CONTENTS

LIST OF TABLES

Table Page

LIST OF FIGURES

Figure Page

Cp	cyclopentadienyl
Cp*	pentamethylcyclopentadienyl
Ind	indenyl
Ind^{Me-1}	1-methylindenyl
Ind^{Me-2}	2-methylindenyl
Ind^{Me-4}	4-methylindenyl
Ind^{Me-5}	5-methylindenyl
$Ind^{2Me-4,7}$	4,7-dimethylindenyl
$Ind^{3Me-1,2,3}$	1,2,3-trimethylindenyl
$Ind^{3Me-2,4,7}$	2,4,7-trimethylindenyl
$Ind^{4Me-4,5,6,7}$	4,5,6,7-tetramethylindenyl
$Ind^{5Me-2,4,5,6,7}$	2,4,5,6,7-pentamethylindenyl
Ind^{7Me} or Ind*	1,2,3,4,5,6,7-heptamethylindenyl
$Ind^{Bzo-5,6}$	benz[*f*]indenyl
Ind^{Si-2}	2-trimethylsilylindenyl
$Ind^{2Si-1,3}$	1,3-bis(trimethylsilyl)indenyl
Ind^{Me-1}	1-methylindenyl
TCNE	tetracyanoethylene
TCNQ	7,7,8,8-tetracyano-*p*-quinodimethane
DCID	2-(dicyanomethylene)indane-1,3-dione
DCNQ	2,3-dicyanonaphtho-1,4-quinone

INTRODUCTION

The indenyl ligand has been used for over 50 years in organometallic transition metal chemistry.[1] In many cases, it may be regarded as a benzannulated derivative of the cyclopentadienyl ring (Cp), and is known to form sandwich complexes of iron(II) and cobalt(III) as analogues of ferrocene and the cobaltocenium cation.[2]

Early first row transition metal complexes with the indenyl ring have been used as propylene polymerization catalysts to produce specific tacticities of the polymer.[3] These complexes are often in high oxidation states (such as Ti^{IV}) with a highly bent metallocene structure that accommodates the propylene monomers. The classic Cp sandwich framework of 3*d* metals is not obtained in groups 3 or 4 (with the exceptions of $[C_5Me_4(SiMe_2{}^tBu)]_2Ti$ and $[(P_5)_2Ti]^{2-}$),[4,5] and yet vanadocene was crystallographically characterized 30 years ago.[6] The difficulty in attaining Cp sandwich structures of scandium and titanium extends to the indenyl ligand, but bis(indenyl)vanadium(II) has been known for over 20 years.[7] Surprisingly, there have been no papers published on the effects of substitution on the indenyl rings of homoleptic vanadium and manganese complexes, although such complexes of chromium have been more recently examined.[8-10]

The use of electron-donating substituents has proven to be an effective tool in manipulating the spin-state of manganocene.[11-13] Large numbers of sufficiently bulky donor groups on Cp rings (specifically, the tetraisopropylcyclopentadienyl ring) have also been

shown to produce the high-spin state in chromocene and manganocene due to steric repulsions of the substituents.[14,15] The manipulation of the ligand field strength by variations in the electron donation and steric demand of the ligand can influence the electronic properties of transition metals in bis(indenyl) complexes that have readily accessible high- and low-spin states. This control of the spin-state of an organometallic complex then affects the accessibility of the metal centers due to the adjustments in the average M–C bond lengths.

When compared with transition metal complexes of the cyclopentadienyl ligand, the corresponding complexes formed with the indenyl ring offer reactivities that are often several-fold higher.[16] This difference has been linked to the ability of the indenyl ring to undergo an aromatization of the C_6 ring,[16] while the 5-membered ring is only delocalized over C(1), C(2), and C(3), with a formal double bond between C(8) and C(9),[17] yielding allylic bonding to a metal center. This η^5 to η^3 haptotropic slip, termed the "indenyl ligand effect" by Basolo and Rerek,[18] opens a coordination site on the metal center, which is particularly useful for binding a two-electron donor.[19] This same haptotropic slip is energetically disfavored by the Cp ligand due to the accompanying bend at the allylic positions (Figure 1) and decrease in aromaticity, leading to a much lower reactivity of metal complexes along with diminished lability of ancillary ligands.[20]

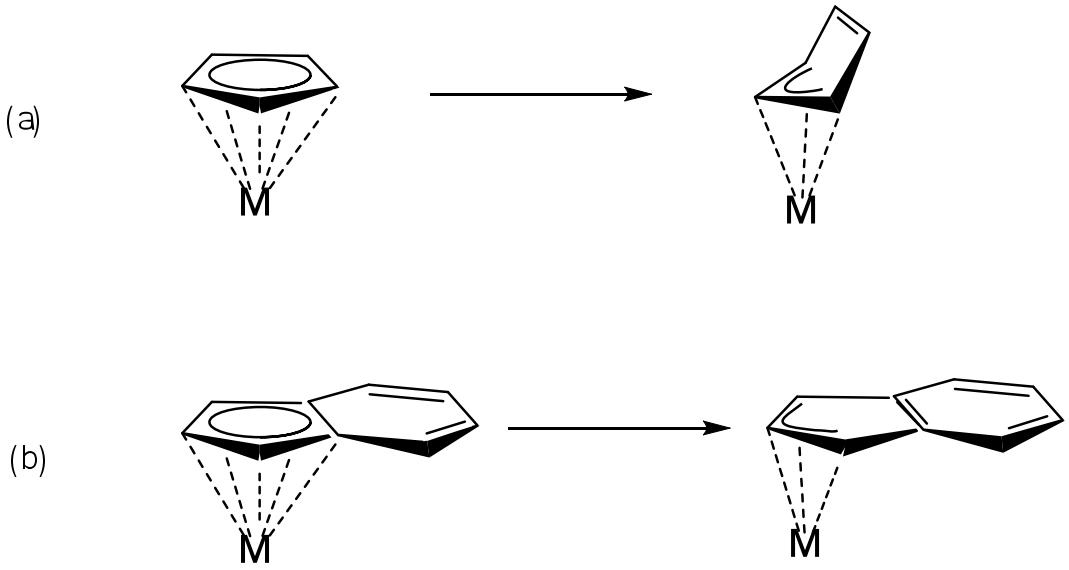

Figure 1. Comparison of the η^5 to η^3 haptotropic slip of the Cp ring (a) and the indenyl ring (b).

The enhanced reactivity of transition metal complexes employing the indenyl ligand, along with their potentially tunable spin states, generates considerable interest in these molecules. In fact, the chromium derivatives have already been shown to exhibit high-spin, low-spin, and spin-crossover behavior in both the solid state and in solution.[8,21] But there are still unanswered questions as to the spin-state determining factors in these complexes. Could similar principles be applied to other early 3*d* metals? If so, the induced variations in the spin state of the complexes may cause their reactivities to be markedly influenced.

Throughout this text, references to calculations of various bond distances and bending angles will be used for comparison among relevant compounds. The average metal to car-

bon distance (av M–C) is calculated from the average of the distances of the 5-membered ring carbons considered to be within bonding distance to the metal center (Figure 2). The slip parameter (Δ_{M-C}) is defined as the difference in the average bond lengths of the metal to carbon atoms C(1), C(2), and C(3) and the metal to the adjacent carbon atoms C(8) and C(9). The hinge angle is the angle formed at the intersection of planes defined by carbon atoms C(1), C(2), C(3) and C(1), C(3), C(8), C(9). The fold angle is the angle formed at the intersection of planes defined by carbon atoms C(1), C(3), C(8), C(9) and C(4), C(7), C(8), C(9). The twist angle is the angle observed by the amount of rotation between two indenyl rings on a metal center.[22] Finally, the angle between C_5 rings is the angle measured from parallel 5-membered rings in sandwich complexes.

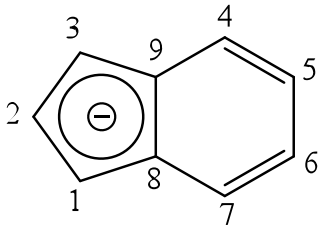

Figure 2. Numbering scheme of the indenyl ring

CHAPTER I

THE EFFECT OF BENZO-RING SUBSTITUTION ON THE STERIC AND ELECTRONIC PROPERTIES OF BIS(INDENYL)CHROMIUM(II) COMPLEXES

Introduction

Although chromocene was reported in 1953,[23,24] bis(indenyl)chromium(II) remained undiscovered until 1977 when it was patented as a polymerization catalyst.[25] It wasn't fully structurally characterized until 1996, at which time it was reported as a dimer,[26] in contrast to the earlier report of bis(1,2,3,4,5,6,7-heptamethylinenyl)chromium(II) which was found to be a monomeric, low-spin species like chromocene.[27] This ligand behavior with chromium(II) is also found in homoleptic allyl complexes, where the unsubstituted molecule is dimeric in nature,[28] but trimethylsilyl substituents prevent dimerization.[29,30]

The ability of the indenyl ligand to adopt an η^3 or η^5 coordination in chromium complexes led to the investigation of steric and electronic effects of indenyl ligand substitution. In 2002, the discovery of the influence of molecular symmetry on the spin-state of substituted bis(indenyl)chromium(II) species was reported.[8] This achievement, in conjunction with the documentation of the influence on the spin-state by variations in number and location of methyl substituents, has effectively mapped the strength of electron donation from each position on the indenyl ring. However, the contribution of backside (C_6) ring substituents alone has not been examined for their ability to disrupt dimerization or

donate to the metal center. Comparing the staggered high-spin $(Ind^{Me\text{-}2})_2Cr$ and predominantly low-spin $(Ind^{5Me\text{-}2,4,5,6,7})_2Cr$,[9,10] it can be seen that the addition of backside methyl groups lowered the spin-state of the molecule, while not affecting its conformation. Although it crystallizes with both staggered and eclipsed molecules in the unit cell, the staggered $(Ind^{3Me\text{-}2,4,7})_2Cr$ molecule exhibits spin-crossover behavior in the solid state. The predominant conformation in solution is not known, but spin-crossover behavior is observed there as well.[10] Thus the addition of methyl groups to the 5- and 6-positions in $(Ind^{5Me\text{-}2,4,5,6,7})_2Cr$ is enough to increase the HOMO/LUMO gap to a level that increases spin-pairing.

That these four additional methyl groups (5,6 on both rings) tip the scale toward the low-spin state in an already hexamethylated complex is not surprising; however, the fact that they have an observable influence on the metal center given their distance from the metal makes the system ideal for characterizing the relative donor strengths of backside substitution. Along with the determination of a more comprehensive picture of the positional effects of methyl substitution on the entire indenyl ring, backside substituted indenyl ligands are the systems that will be investigated here.

Experimental

General Considerations. Unless otherwise noted, all manipulations were performed with the rigorous exclusion of air and moisture using Schlenk or glovebox tech-

niques. Proton (^{1}H) NMR experiments were obtained on a Bruker DPX-300 spectrometer at 300 MHz, or a Bruker DPX-400 at 400 MHz, and were referenced to the residual proton resonances of THF-d_8 (δ 3.58) and $CDCl_3$ (δ 7.26). Elemental analyses were performed by Desert Analytics (Tucson, AZ). Melting points were determined on a Laboratory Devices Mel-Temp apparatus in sealed capillaries. Mass spectra were obtained using a Hewlett-Packard 5890 Series II gas chromatograph/mass spectrometer.

Materials. Anhydrous chromium(II) chloride was purchased from Strem Chemicals and used as received. Aluminum(III) chloride, 4-methylindanone, *p*-xylene, 3-chloropropanoyl chloride, acryloyl chloride, 3-*p*-tolyl propionic acid, carbon disulfide (CS_2) and anhydrous tetrahydrofuran (THF), sodium iodide, 2-cyclopentenone, and α,α,α′α′-tetrabromo-*o*-xylene were purchased from Aldrich and used as received. 1,2,3,4-Tetramethylbenzene (90%) was purchased from TCI and used as received. Hexanes, toluene, and diethyl ether were distilled under nitrogen from potassium benzophenone ketyl. Anhydrous pentane was purchased from Acros and used as received. Dimethylformamide was purchased from Aldrich, dried over an alumina column, and kept over 4A molecular sieves prior to use. $CDCl_3$ (Cambridge Isotope) was dried with 4A molecular sieves prior to use. Toluene-d_8 (Aldrich) and THF-d_8 (Cambridge Isotope) were distilled under vacuum from Na/K (22/78) alloy and stored over 4A molecular sieves prior to use.

Magnetic Measurements. Solution magnetic susceptibility measurements were performed on a Bruker DRX-400 spectrometer using the Evans' NMR method.[31-35] 5–10

mg of the paramagnetic material was dissolved in toluene-d_8 in a 1.0 mL volumetric flask. The solution was thoroughly mixed, and approximately 0.5 mL was placed in a NMR tube containing a toluene-d_8 capillary. The calculations required to determine the number of unpaired electrons based on the data collected have been described elsewhere.[36]

Solid state magnetic susceptibility data were obtained by Prof. Gordon T. Yee (Virginia Tech) on a Quantum Designs MPMS SQUID magnetometer in a field of 70,000 G. Control of the sample temperature ranges from 1.8 to 300 K. To handle the extremely air- and moisture-sensitive compounds, the previously described sample holder was used;[14] the diamagnetic susceptibility of the sample holder was accepted as the average value of the measurements on several identical sample holders. The diamagnetic correction for each complex was estimated from Pascal's constants.

Synthesis of 4,5,6,7-Tetramethylindene, HInd$^{4Me\text{-}4,5,6,7}$. In a N_2 flushed 500 mL Schlenk flask, 28.86 g (0.2164 mol) of $AlCl_3$ was added to a solution of 1,2,3,4-tetramethylbenzene (18.08 g, 0.2164 mol) in 200 mL of CS_2. The flask was chilled in an ice bath before acryloyl chloride (12.19 g, 0.2164 mol) was added and the reaction was allowed to warm to room temperature. With a drying tube attached, the reaction was brought to reflux for 2 h, during which time the color changed from orange to black, and the evolution of HCl was observed. The mixture was then stirred overnight at room temperature. The reaction was brought to reflux for 2 h before it was cooled to room temperature, poured over 50 mL of HCl in 500 g of ice, and slurried for 3 h. The organic layer was

separated and neutralized with dilute $NaHCO_3$, then dried over $MgSO_4$. After filtration of the $MgSO_4$, excess CS_2 was removed by rotary evaporation resulting in a dark orange oil.

The oil was kept at 4 °C overnight, and it formed a dark orange resin in the flask. A mixture of 10% hexanes in methanol (250 mL) was heated and added to dissolve the resin. The solution was filtered to remove undissolved material and the remaining solution was kept at -20 °C. Overnight, a light orange powder became suspended in the solution above a black tar. The solution and powder were kept while the black tar was discarded. This process was repeated twice to further purify the 4,5,6,7-tetramethylindan-1-one product (6.620 g, 16%) confirmed by GC/MS ($m^+ = 188$).

The indanone (6.620 g, 0.03516 mol) was dissolved in 125 mL of anhydrous diethyl ether and chilled to 0 °C in a 250 mL Schlenk flask under N_2. $Li[AlH_4]$ (36 mL of 1.0 M in diethyl ether) was slowly syringed into the flask over 20 min with stirring. After the mixture had been stirred overnight, a condenser was attached, and the reaction was refluxed for 2 h. The mixture was cooled to 0 °C, and the reaction was quenched by the dropwise addition of 10 mL of cold water and a subsequent 150 mL of dilute NH_4Cl solution. Upon stirring, the mixture rapidly evolved a gas. Diethyl ether was added and a separation performed. The ether layer was dried with $MgSO_4$, filtered, and the ether was removed by rotary evaporation to leave a waxy orange solid. This solid was dissolved in 250 mL of toluene and added to a 500 mL round-bottom flask fitted with a Dean-Stark trap and condenser. A few crystals of *p*-toluenesulfonic acid were added to the solution. The solu-

tion was refluxed until approximately 0.5 mL of water was collected in the trap. After cooling to room temperature, the solution was dried over $MgSO_4$, and the toluene was removed by rotary evaporation to yield dark brown crystals of 4,5,6,7-tetramethylindene (1.294 g, 0.007511 mol). Overall synthesis resulted in 3.5% yield. ^{1}H NMR (400 MHz) in $CDCl_3$: δ 2.30 (multiplet, 12H, 4 *CH*$_3$); 3.35 (doublet, 2H, *CH*$_2$); 6.50 (doublet, 1H, *CH* in 1-position); 6.75 (multiplet, 1H, *CH* in 2-position). GC/MS characterization was consistent with the expected molecular ion peak of this compound (m^+ = 172).

Synthesis of 4,7-Dimethylindene, HInd$^{2Me-4,7}$. In a N_2-flushed 500 mL Schlenk flask, 31.40 g (0.2355 mol) of $AlCl_3$ was added to a solution of *p*-xylene (25.00 g, 0.2355 mol) in 200 mL of CS_2. The flask was chilled in an ice bath before 3-chloropropanoyl chloride (29.90 g, 0.2355 mol) was added and the reaction was allowed to warm to room temperature. With a drying tube attached, the reaction was brought to reflux for 2 h, during which time the color changed from yellow to red, and the evolution of HCl was observed. The mixture was then stirred overnight at room temperature. The reaction was poured over 500 g of ice and slurried until it became yellow. The organic layer was neutralized with dilute $NaHCO_3$ and dried over $MgSO_4$. After removal of the $MgSO_4$ by filtration, excess CS_2 was removed by rotary evaporation to afford a yellow oil of 3-chloro-1-(2,5-dimethylphenyl)-1-propanone (40.0 g, 86%) confirmed by GC/MS (m^+ = 196).

The yellow oil was added dropwise to excess concentrated H_2SO_4 over 15 min with stirring to give an orange, then red, mixture that was subsequently heated to 80 °C for 2 h, accompanied by the evolution of HCl. The mixture was poured on ice and slurried for 20 min, yielding a light red aqueous layer. The product was separated with diethyl ether, neutralized with $NaHCO_3$, and dried with $MgSO_4$. Rotary evaporation of the solvent left a white waxy solid. For purification, the solid was redissolved in methanol and placed in a freezer overnight at –20 °C. White crystals precipitated and were filtered to yield 24.6 g (76%) of 4,7-dimethyl-1-indanone, as confirmed by GC/MS ($m^+ = 160$).

The indanone (24.6 g, 0.154 mol) was dissolved in anhydrous diethyl ether and chilled to 0 °C in a 500 mL Schlenk flask under N_2. 100 mL of 1.0 M $Li[AlH_4]$ in diethyl ether was syringed into the flask over 20 min with stirring. After the mixture had stirred overnight, a condenser was attached, and the reaction was refluxed for 5 h. The mixture was cooled to 0 °C, and the reaction was quenched by the dropwise addition of 2 mL of cold water, 4 mL of dilute NaOH solution, and 100 mL of cold water. A white solid precipitated from solution. The mixture was filtered, separated from the water layer, and dried over $MgSO_4$. After rotary evaporation, large opaque crystals of the 4,7-dimethyl-1-indanol (19.34 g, 77%) formed and were confirmed by GC/MS ($m^+ = 162$).

The alcohol was redissolved in 200 mL of toluene and added to a 500 mL round-bottom flask fitted with a Dean-Stark trap and condenser. A few crystals of *p*-toluenesulfonic acid were added to the solution. The solution was refluxed until approxi-

mately 2 mL of water was collected in the trap. After cooling to room temperature, the solution was washed with dilute $NaHCO_3$ solution and dried over $MgSO_4$. The toluene was removed by rotary evaporation to yield 4,7-dimethylindene (15.4 g, 90%) as a tan liquid. ^1H NMR and GC/MS characterization of 4,7-dimethylindene were consistent with the expected spectra of the compound. Overall synthesis resulted in 45% yield.

Synthesis of 5-Methylindene, $HInd^{Me-5}$. In a 250 mL round bottom flask, 10.0 g (0.0609 mol) of 3-*p*-tolylpropionic acid was dissolved in excess thionyl chloride and heated to reflux for 4 h. The evolution of SO_2 and HCl was observed. After cooling to room temperature, the reaction was stirred for an additional 14 h. The thionyl chloride solvent was removed under vacuum, and the resulting 3-p-tolylpropanoyl chloride was dissolved in 100 mL of CS_2 and placed in a dropping funnel. In a 500 mL Schlenk flask purged with N_2, approximately 10 g of $AlCl_3$ was slurried in 200 mL of CS_2. The flask was chilled to 0 °C before the dropwise addition of the 3-*p*-tolylpropanoyl chloride solution. The reaction immediately turned from a light green to a dark green and finally to a muddy brown. After stirring for 14 h at room temperature, the reaction was heated to reflux for 3 h. The flask was chilled to 0 °C, and the reaction was quenched by the addition of cold water. A separation was performed following the addition of 2 × 50 mL of dilute $NaHCO_3$ solution and 100 mL of cold water. The CS_2 layer was then separated from the water layer, and dried over $MgSO_4$. After rotary evaporation, an orange oil of the 5-

methyl-1-indanone was isolated and confirmed by GC/MS (m^+ = 146) in 81% yield. Upon standing, large orange crystals of the indanone formed in the flask.

5-Methyl-1-indanone (7.48 g, 0.0512 mol) was dissolved in anhydrous diethyl ether and chilled to 0 °C in a 500 mL Schlenk flask under N_2. $Li[AlH_4]$ (34 mL of a 1.0 M solution in diethyl ether) was syringed into the flask over 20 min while stirring. Immediately a brown precipitate formed but was redissolved upon complete addition of the $Li[AlH_4]$. After the mixture had stirred overnight, a condenser was attached, and the reaction was refluxed for 4 h. The yellow-orange mixture was cooled to 0 °C, and the reaction was quenched by the successive addition of 2 mL of cold water, 4 mL of dilute NaOH solution, and 100 mL of cold water. The ether layer was then separated from the water layer, and dried over $MgSO_4$. After rotary evaporation, an orange oil of the 5-methyl-1-indanol was isolated and confirmed by GC/MS (m^+ = 148).

The full amount of 5-methyl-1-indanol was redissolved in 100 mL of toluene and added to a 500 mL round-bottom flask fitted with a Dean-Stark trap and condenser. A few crystals of *p*-toluenesulfonic acid were added to the solution. The solution was refluxed for 3 h until slightly more than 0.5 mL of water was collected in the trap. After cooling to room temperature, the solution was washed with dilute $NaHCO_3$ solution and dried under $MgSO_4$. The toluene was removed by rotary evaporation to yield 5-methylindene (6.51 g, 0.0500 mol, 98%) as a yellow oil. GC/MS characterization of 5-

methylindene was consistent with the expected spectrum of the compound (m^+ = 130). The overall yield was 82%.

Synthesis of 4-Methylindene, $HInd^{Me-4}$. 4-Methyl-1-indanone (5.00 g, 0.0342 mol) was dissolved in anhydrous diethyl ether and chilled to 0 °C in a 500 mL Schlenk flask under N_2. $Li[AlH_4]$ (30 mL of a 1.0 M solution in diethyl ether) was syringed into the flask over 20 min while stirring. After the mixture had stirred overnight, a condenser was attached, and the reaction was refluxed for 5 h. The mixture was cooled to 0 °C, and the reaction was quenched by the successive addition of 2 mL of cold water, 4 mL of dilute NaOH solution, and 100 mL of cold water. The ether layer was then separated from the water layer, and dried over $MgSO_4$. After rotary evaporation, a light yellow powder of the 4-methyl-1-indanol (5.02 g, 0.339 mol, 99%) was isolated and confirmed by GC/MS (m^+ = 148).

The full amount of 4-methyl-1-indanol was redissolved in 100 mL of toluene and added to a 500 mL round-bottom flask fitted with a Dean-Stark trap and condenser. A few crystals of *p*-toluenesulfonic acid were added to the solution. The solution was refluxed until approximately 0.5 mL of water was collected in the trap. After cooling to room temperature, the solution was washed with dilute $NaHCO_3$ solution, separated, and dried over $MgSO_4$. The toluene was removed by rotary evaporation to yield 4-methylindene (3.93 g, 0.0302 mol, 89%) as a yellow oil. ^1H NMR and GC/MS characteri-

zation of 4-methylindene were consistent with the expected spectra of the compound. The overall yield was 88%.

Synthesis of Benz[*f*]indene, $HInd^{Bzo\text{-}5,6}$. This synthesis has been modified from a literature preparation.[37] Sodium iodide (45.0 g, 0.300 mol) was slurried and partially dissolved in 250 mL of warm (80 °C), dry DMF in a 500 mL Schlenk flask. The solution was cooled back to room temperature before 25.0 g (0.0593 mol) of α,α,α′,α′-tetrabromo-*o*-xylene was added to the DMF, and the resulting mixture turned light golden. Upon the dropwise addition of 5.00 g (0.0610 mol) of 2-cyclopentenone, the solution immediately turned dark orange and eventually black. The reaction was returned to 80 °C and stirred for 15 h. Water was added to quench the reaction and dissolve any remaining sodium iodide. Diethyl ether (6×50 mL) was added, and several extractions were performed. The diethyl ether layer was dried over $MgSO_4$ before filtering and removing the solvent by rotary evaporation. The product that remained was a viscous dark brown substance that was redissolved in a minimum amount of hot ethanol. This solution was slowly cooled to near 0 °C and left for 12 h. A light brown powder precipitated from solution and was isolated by vacuum filtration to leave 15.4 g (0.0845 mol, 25% yield) of the benz[*f*]indanone. The indanone was placed in a 250 mL Schlenk flask under N_2 and was partially dissolved in 100 mL of dry diethyl ether. The flask was chilled to 0 °C before 20 mL of 1.0 M lithium aluminum hydride was syringed into the flask. The reaction quickly

turned light orange and fully dissolved the remaining precipitate. It was allowed to warm to room temperature and stir for 6 h; no visible change occurred.

The reaction was quenched with cold water, forming copious amounts of white precipitate. Extraction with diethyl ether, followed by drying over $MgSO_4$ and removal of the solvent, yielded pure, white, crystalline benz[*f*]indanol in 94% yield (14.6 g, 0.0793 mol). Under N_2, 5.0 g of this benz[*f*]indanol was dissolved in 200 mL of toluene in a 500 mL round bottom flask fitted with a stir bar and a Dean-Stark apparatus. A catalytic amount of *p*-toluenesulfonic acid was added and the mixture brought to reflux for 6 h. The temperature of the reaction was further increased until slightly more than 1 mL of H_2O was collected in the trap. The reaction was cooled before water was added and a separation was performed. The organic layer was dried over $MgSO_4$, filtered, and the toluene was removed by rotary evaporation. The remaining product (1.30 g, 13% yield) was a light brown power and confirmed to be benz[*f*]indene by GC/MS ($m^+ = 166$).

Synthesis of Potassium 4,5,6,7-tetramethylindenide, K[4,5,6,7-$(CH_3)_4C_9H_3$] ($KInd^{4Me\text{-}4,5,6,7}$). 4,5,6,7-Tetramethylindene (1.294 g, 7.511 mmol) was dissolved in 30 mL of toluene in a 250 mL Erlenmeyer flask. Potassium bis(trimethylsilyl)amide $K[N(SiMe_3)_2]$ (1.199 g, 6.010 mmol) was dissolved in toluene and added dropwise to the indene while stirring. The reaction was stirred 12 h before adding 150 mL of hexanes. A light red-purple precipitate formed and was filtered over a medium-porosity glass frit. The precipitate was washed with hexanes (2 × 30 mL) and dried under

vacuum to yield 0.408 g (1.89 mmol, 31%) of potassium 4,5,6,7-tetramethylindenide. The product was confirmed to contain K[$Ind^{4Me-4,5,6,7}$] (^{1}H NMR in THF-d_8); the crude product was used without further purification.

Synthesis of Potassium 4,7-dimethylindenide, K[4,7-$(CH_3)_2C_9H_5$] ($KInd^{2Me-4,7}$). 4,7-Dimethylindene (5.00 g, 0.0347 mol) was redissolved in 80 mL of toluene in a 250 mL Erlenmeyer flask. Potassium bis(trimethylsilyl)amide K[$N(SiMe_3)_2$] (6.23 g, 0.0312 mol) was dissolved in toluene and added dropwise to the indene while stirring. The reaction was stirred 24 h before adding 150 mL of hexanes. A bright yellow precipitate formed and was filtered over a medium-porosity glass frit. The precipitate was washed with hexanes (2 × 30 mL) and dried under vacuum to yield 4.89 g (86%) of the indenide salt. The product was confirmed to be K[$Ind^{2Me-4,7}$] by ^{1}H NMR (400 MHz) in toluene-d_8: δ 2.34 (singlet, 6H, CH_3 in 4,7-positions); 6.56 (multiplet, 3H, *CH* in 1,2,3-position); 7.20 (doublet, 2H, *CH* in 5,6-positions).

Synthesis of Potassium 5-Methylindenide, K[Ind^{Me-5}]. 5-Methylindene (2.50 g, 0.0192 mol) was degassed and dissolved in 20 mL of toluene in a 250 mL Erlenmeyer flask. Potassium bis(trimethylsilyl)amide K[$N(SiMe_3)_2$] (3.64 g, 0.0182 mol) was dissolved in toluene and added dropwise to the indene while stirring. The reaction was stirred 14 h before adding 150 mL of hexanes. A bright yellow precipitate formed and was filtered over a medium-porosity glass frit. The precipitate was washed with hexanes (2 × 30 mL) and dried under vacuum to yield 2.05 g (67%) of the indenide salt as a yellow pow-

der. The product was confirmed to contain K[Ind^{Me-5}] (^{1}H NMR in THF-d_8); the crude product was used without further purification.

Synthesis of Potassium 4-Methylindenide, K[Ind^{Me-4}]. 4-Methylindene (3.93 g, 0.0302 mol) was degassed and dissolved in 20 mL of toluene in a 250 mL Erlenmeyer flask. Potassium bis(trimethylsilyl)amide K[$N(SiMe_3)_2$] (5.72 g, 0.0287 mol) was dissolved in toluene and added dropwise to the indene while stirring. The reaction was stirred 24 h before adding 150 mL of hexanes. A bright yellow precipitate formed and was filtered over a medium-porosity glass frit. The precipitate was washed with hexanes (2 × 30 mL) and dried under vacuum to yield 3.83 g (67%) of the indenide salt. The product was confirmed to be K[Ind^{Me-4}] by ^{1}H NMR (400 MHz) in toluene-d_8: δ 2.24 (singlet, 3H, CH_3); 6.54 (multiplet, 3H, *CH* in 1,2,3-position); 7.38 (multiplet, 3H, *CH* in 5,6,7-position).

Synthesis of Potassium Benz[*f*]indenide, K[$Ind^{Bzo-5,6}$]. Dry, solid benz[*f*]indene (1.30 g, 7.82 mmol) was dissolved in 20 mL of toluene in a 250 Erlenmeyer flask. Potassium bis(trimethylsilyl)amide K[$N(SiMe_3)_2$] (1.48 g, 7.42 mmol) was dissolved in toluene and added dropwise to the indene while stirring. A bright red solid immediately precipitated from solution and the reaction mixture was allowed to stir for 2 h. For complete separation of the product, 150 mL of hexanes was added, and the mixture was filtered over a medium-porosity glass frit. The red precipitate was washed with hexanes

(2 × 30 mL) and dried under vacuum to yield 1.16 g (73%) of the potassium benz[*f*]indenide.

Attempted Synthesis of Bis(4,5,6,7-tetramethylindenyl)chromium(II), $(Ind^{4Me-4,5,6,7})_2Cr$. Anhydrous $CrCl_2$ (0.1192 g, 0.9703 mmol) was added to a 125 mL Erlenmeyer flask along with a magnetic stirring bar and 30 mL of THF. Potassium 4,5,6,7-tetramethylindenide (0.408 g, 1.89 mmol) was dissolved in 10 mL of THF and added dropwise to the flask while stirring. The mixture turned black, and it was allowed to stir for 3 h. The solvent was removed under vacuum, and 30 mL of hexanes was added to dissolve the residue. The mixture was filtered through a medium-porosity glass frit, and the filtrate was collected in a 250 mL Schlenk flask, which was placed in a -30 °C freezer. After 48 h, no crystals were observed so the solution was placed on the Schlenk line and pumped to dryness. A viscous black oil remained that was uncharacterizable by NMR methods, possibly the result of impurities in the potassium indenide.

Synthesis of Bis(4,7-dimethylindenyl)chromium(II), $(Ind^{2Me-4,7})_2Cr$. Anhydrous $CrCl_2$ (0.500 g, 4.07 mmol) was added to a 125 mL Erlenmeyer flask along with a magnetic stirring bar and 30 mL of THF. Potassium 4,7-dimethylindenide (1.483 g, 8.15 mmol) was dissolved in 10 mL of THF and added dropwise to the flask while stirring. The mixture initially turned dark green, then black, and it was allowed to stir overnight. The solvent was removed under vacuum, and 50 mL of hexanes was added to dissolve the residue. The mixture was filtered through a medium-porosity glass frit, and the

filtrate was collected in a 250 mL modified (via sidearm fused gas inlet and 14/20 ground glass joint) round bottom flask, which was placed in a –30 °C freezer. After 48 h, dark green crystals of $(Ind^{2Me\text{-}4,7})_2Cr$ were observed and isolated by cannulation of the mother liquor on a Schlenk line. The crystals were dried under vacuum and brought into the glovebox (0.283 g, 21%) mp 155–160 °C. Anal. Calcd. for $C_{22}H_{22}Cr$: C, 78.08; H, 6.55. Found: C, 77.84; H, 6.55. Solution magnetic susceptibility (μ_{eff}^{298K}): 3.4.

Attempted Synthesis of Bis(4-methylindenyl)chromium(II), $(Ind^{Me\text{-}4})_2Cr$. Anhydrous $CrCl_2$ (0.864 g, 7.03 mmol) was added to a 125 mL Erlenmeyer flask along with a magnetic stirring bar and 20 mL of THF. Potassium 4-methylindenide (2.36 g, 14.0 mmol) was dissolved in 15 mL of THF and added dropwise to the flask while stirring. The mixture turned brown-black, and it was allowed to stir for 14 h. The solvent was removed under vacuum, and the remaining solid was divided into two portions. The first fraction was washed with hexanes (2 × 10 mL), filtered, and placed in the freezer at –40 °C. No crystals were observed from this solution. The second fraction was washed with toluene (2 × 7 mL), filtered, and collected in two vials. The first vial was placed in the freezer –40 °C, and crystals too small for x-ray analysis formed. In the second vial, hexanes was allowed to diffuse slowly in over a period of 2 days at room temperature. Brown-black needles formed that were suitable for x-ray crystallography, but they were unstable at room temperature over two days, depositing white and green powders. The crystals were found to be $(Ind^{Me\text{-}4})_3Cr_2Cl$ (0.274 g, 72.2%).

Synthesis of Bis(benz[*f*]indenyl)chromium(II), $(Ind^{Bzo\text{-}5,6})_2Cr$. Anhydrous $CrCl_2$ (0.0602 g, 0.490 mmol) was added to a 125 mL Erlenmeyer flask along with a stir bar and 10 mL of THF. Potassium benz[*f*]indenide (0.200 g, 0.979 mmol) was dissolved in 10 mL of THF and added dropwise to the flask while stirring. The mixture immediately turned red-black, and it was allowed to stir overnight. The solvent was removed under vacuum, and 10 mL of toluene was added to dissolve the chromium complex. The mixture was filtered through a medium-porosity glass frit, and the filtrate was collected in a 125 mL Erlenmeyer flask. Upon evaporation of solvent, x-ray quality, long black needles formed in 66% yield (0.124 g). Once formed, the crystals were insoluble in organic solvents, preventing characterization by NMR methods. Anal. Calcd. for $C_{26}H_{18}Cr$: C, 81.66; H, 4.74. Found: C, 80.84; H, 4.45.

Computational Details. Geometry optimizations and frequency calculations were performed using the GAUSSIAN 03 suite of programs.[38] Density functional theory was employed with the use of the TPSSh functional, which is based on the meta-generalized gradient approximation (MGGA) of Tao, Perdew, and Staroverov, with the admixture of 10% exact (Hartree–Fock) exchange;[39] it has been demonstrated to give good results with transition-metal systems.[40] Calculations used the standard 6-31+G(d) Pople basis sets (for Cr, this is (23s, 18p, 5d, 1f)/[6s, 6p, 3d, 1f][41]). In the case of the indenyl anions, some comparative calculations were conducted with the B3LYP functional[42-44] and the aug-cc-pVTZ basis set.

General Procedures for X-ray Crystallography. A suitable crystal of each sample was located, attached to a glass fiber, and mounted on a Bruker SMART Platform CCD diffractometer for data collection at 173(2) K or 100(2) K. Data collection and structure solutions for all molecules were conducted at the X-ray Crystallography Laboratory at the University of Minnesota by Dr. William W. Brennessel and Benjamin E. Kucera, or at the University of California, San Diego by Dr. Arnold L. Rheingold. Data resolution of 0.84 Å was considered in the data reduction (SAINT 6.01 and SAINT 6.35, Bruker Analytical Systems, Madison, WI). The intensity data were corrected for absorption and decay (SADABS). All calculations were performed using the current SHELXTL suite of programs.[45] Final cell constants were calculated from a set of strong reflections measured during the actual data collection. Relevant crystal and data collection parameters for each of the compounds are given in Appendix B.

The space groups were determined based on systematic absences and intensity statistics. A direct-methods solution was calculated that provided most of the non-hydrogen atoms from the *E*-map. Several full-matrix least-squares/difference Fourier cycles were performed that located the remainder of the non-hydrogen atoms. All non-hydrogen atoms were refined with anisotropic displacement parameters. All hydrogen atoms were placed in ideal positions and refined as riding atoms with relative isotropic displacement parameters.

X-ray Crystallography of $(Ind^{2Me-4,7})_2Cr$. Dark green crystals of $(Ind^{2Me-4,7})_2Cr$ were harvested by preparing a concentrated hexanes solution, which was cooled to –30 °C. The crystals were separated from the mother liquor via cannulation and dried under vacuum prior to data collection. An initial set of cell constants was calculated from reflections produced from three sets of 20 frames. These sets of frames were oriented such that orthogonal wedges of reciprocal space were surveyed. This produced orientation matrices determined from 40 reflections. The final cell constants were calculated from the *xyz* centroids of 2603 strong reflections as described in the general procedures.

Data was collected using MoKα radiation (graphite monochromator) with a frame time of 60 s and a detector distance of 4.83 cm. A randomly oriented region of reciprocal space was surveyed to the extent of 1 sphere, and to a resolution of 0.84 Å. Three major sections of frames were collected with 0.30° steps in ω at four different ϕ settings and a detector position of –28° in 2θ.

The space group *Cc* was determined as described in the general procedures. The space group was later confirmed with PLATON[46] to be certain that space group *C*2/*c* was not a possibility. The refinement required modeling for inversion twinning (74:26). The final full matrix least-squares refinement converged to $R1 = 0.0364$ and $wR2 = 0.0893$ (F^2, all data).

X-ray Crystallography of $(Ind^{Me-4})_3Cr_2Cl$. Dark brown crystals of $(Ind^{Me-4})_3Cr_2Cl$ were harvested by preparing a concentrated toluene solution, into which hexanes

was allowed to diffuse at room temperature. The crystals were separated from the mother liquor and dried under vacuum prior to data collection. An initial set of cell constants was calculated from reflections produced from three sets of 20 frames. These sets of frames were oriented such that orthogonal wedges of reciprocal space were surveyed. This produced orientation matrices determined from 22 reflections. The final cell constants were calculated from the *xyz* centroids of 3284 strong reflections as described in the general procedures.

Data was collected using MoKα radiation (graphite monochromator) with a frame time of 90 s and a detector distance of 4.920 cm. A randomly oriented region of reciprocal space was surveyed to the extent of 1 sphere, and to a resolution of 0.84 Å. Three major sections of frames were collected with 0.30° steps in ω at four different ϕ settings and a detector position of –28° in 2θ.

The space group $P2_1/c$ was determined as described in the general procedures. The structure was modeled as disordered over two of the three indenyl positions (78:22) and the methyl indenyl ligand on Cr2 was modeled as disordered over two positions (87:13). There appears to be a THF molecule disordered over an inversion center; however, attempts to refine it were unsuccessful, and the program SQUEEZE[46] was used to model the electron density. The total solvent accessible void space was 334.1 $Å^3$ per unit cell, containing roughly 113 electrons. The THF molecule was included in the molecular formula in order to achieve a correct molecular volume. The final full matrix least-squares refinement converged to $R1 = 0.0849$ and $wR2 = 0.2190$ (F^2, all data).

X-ray Crystallography of $[(Ind^{Bzo\text{-}5,6})_2Cr]_2$. Dark purple crystals of $[(Ind^{Bzo\text{-}5,6})_2Cr]_2$ were grown by preparing a concentrated toluene solution and allowing the solvent to slowly evaporate at room temperature. The crystals were separated from the mother liquor and dried under vacuum prior to data collection. An initial set of cell constants was calculated from reflections produced from three sets of 20 frames. These sets of frames were oriented such that orthogonal wedges of reciprocal space were surveyed. This produced orientation matrices determined from 40 reflections. The final cell constants were calculated from the *xyz* centroids of 2916 strong reflections as described in the general procedures.

Data was collected using MoKα radiation (graphite monochromator) with a frame time of 90 s and a detector distance of 4.83 cm. A randomly oriented region of reciprocal space was surveyed to the extent of 1 sphere, and to a resolution of 0.84 Å. Three major sections of frames were collected with 0.30° steps in ω at four different ϕ settings and a detector position of –28° in 2θ.

The space group *C*2/*c* was determined as described in the general procedures. The final full matrix least-squares refinement converged to $R1 = 0.0789$ and $wR2 = 0.2043$ (F^2, all data).

Results

Ligand synthesis. Various alkylated and benzannulated indenes were prepared by modifications of standard procedures.[27,37,47-49] These included $HInd^{Me\text{-}4}$, $HInd^{Me\text{-}5}$, $HInd^{2Me\text{-}4,7}$,

$HInd^{4Me-4,5,6,7}$, and $HInd^{Bzo-5,6}$. As opposed to methylation on the frontside (C_5 ring) of the parent indene, substitution on the 4-,5-,6-, or 7-positions of the indene ring is only possible through the use of methylated starting materials. Friedel-Crafts acylation of a methylated benzene ring is the C_5 ring-closing step (Figure 3) or the frontside addition to the benzene ring prior to ring closure (Figure 4). Benzannulation of the 5- and 6-positions of the indene ring is achieved by the synthesis shown in Figure 5.

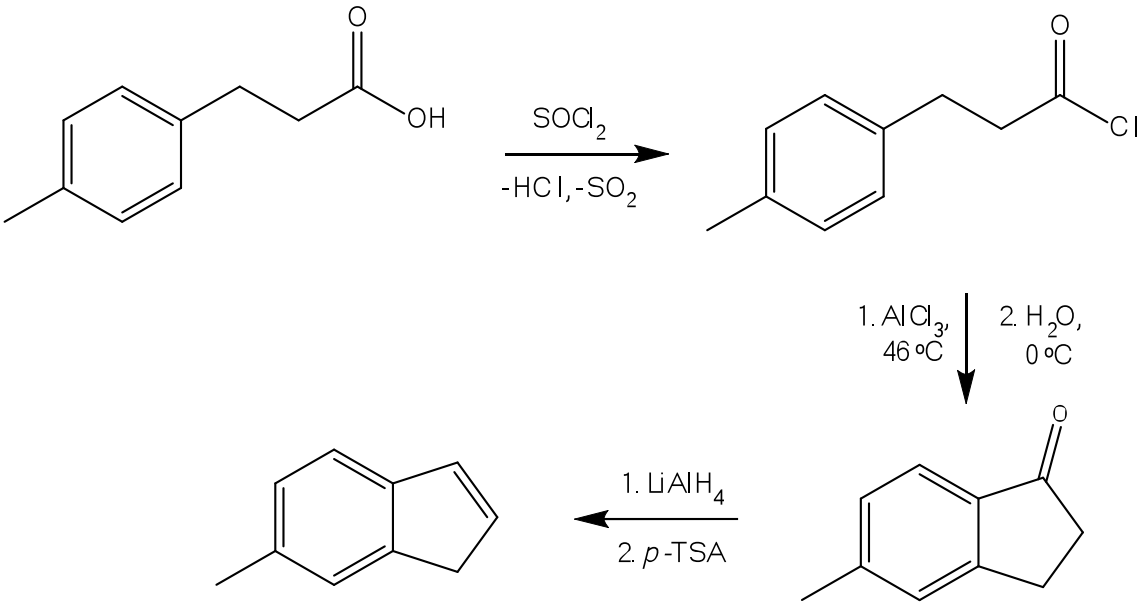

Figure 3. Synthesis of 5-methylindene based on Friedel-Crafts acylation, followed by reduction and dehydration.

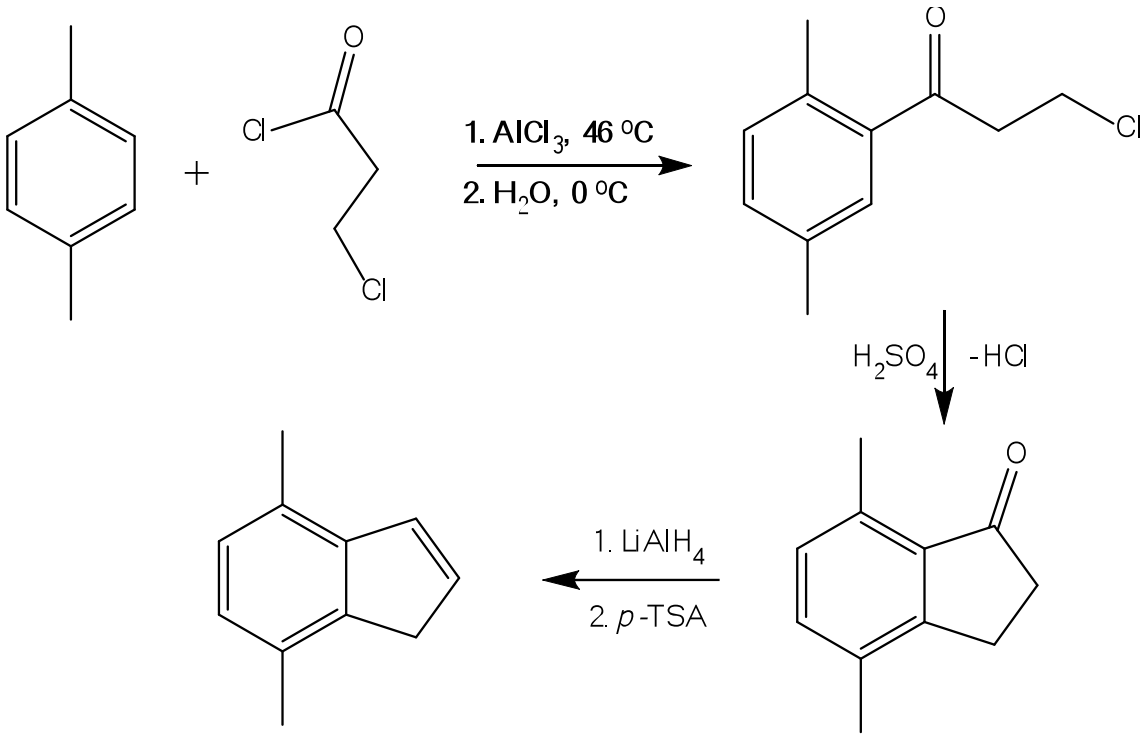

Figure 4. Synthesis of 4,7-dimethylindene based on Friedel-Crafts acylation, followed by reduction and dehydration.

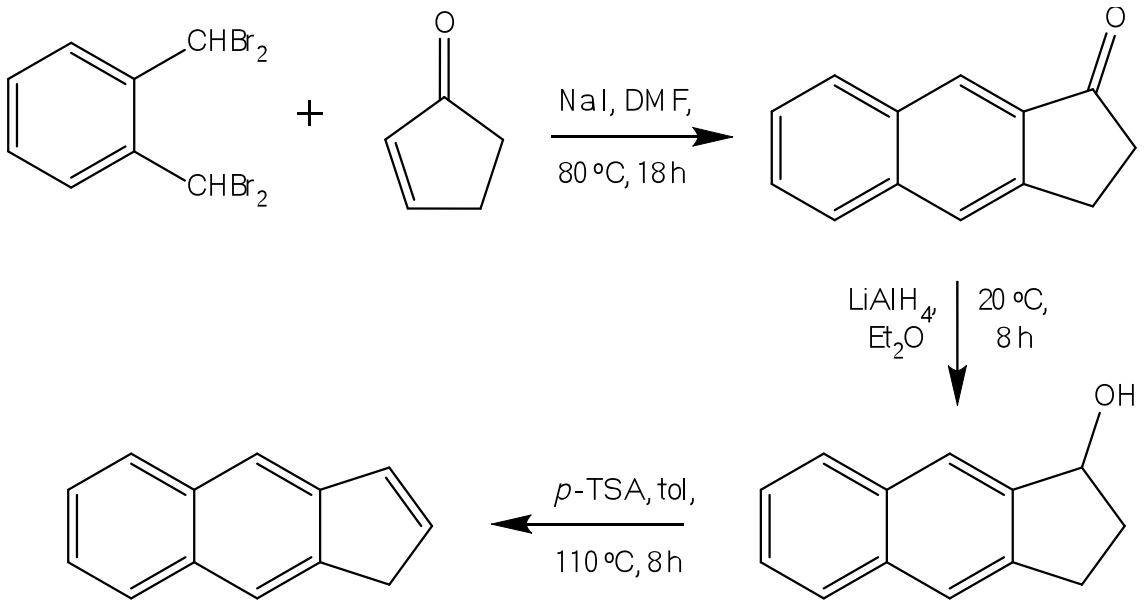

Figure 5. Synthesis of benz[*f*]indene.

Once the desired indene was synthesized and purified by vacuum distillation, the alkali metal indenide salt was prepared via deprotonation reaction with a strong base. Reactions with potassium bis(trimethylsilyl)amide were performed in toluene, followed by precipitation of the potassium indenide salt by the addition of hexanes (eq 1). The indenides were isolated from the resulting bis(trimethylsilyl)amine by filtration and rigorous washing with additional hexanes. The potassium indenides were dried under vacuum prior to reactions with chromium chloride.

$$HInd' + K[N(SiMe_3)_2] \xrightarrow{Tol} \xrightarrow{Hex\ or\ Pent} K[Ind'] + HN(SiMe_3)_2 \qquad (1)$$

Synthesis of Substituted Bis(indenyl)metal Complexes of Cr(II). Once the appropriate indenide salts were prepared, the corresponding bis(indenyl)chromium(II) complexes could be readily synthesized by salt metathesis elimination reactions. In each case, two equivalents of the appropriate alkali metal indenide salt were allowed to react with anhydrous chromium(II) chloride in THF (eq 2); the resulting mixtures were generally stirred overnight to ensure complete reaction. Following the removal of THF under vacuum, a less polar solvent (pentane, hexanes, or toluene) was added to extract the transition metal species, precipitating the alkali metal chloride in the process. The solubility of these bis(indenyl)chromium complexes in even the most non-polar solvents provides an

efficient means by which to separate the desired materials from the rest of the reaction mixture.

$$2\,A[Ind'] + CrCl_2 \xrightarrow{THF} \xrightarrow{Hex\ or\ Pent} (Ind')_2Cr + 2\,ACl \qquad (2)$$

$$A = Li\ or\ K$$

Solid State (SQUID) Magnetic Susceptibility Measurement of Bis(4,7-dimethyl-indenyl)chromium(II). A crystalline sample of $(Ind^{2Me\text{-}4,7})_2Cr$ was examined with a SQUID magnetometer, and complete data from that measurement can be found in Appendix C. Figure 6 shows the recorded magnetic moment (μ_{eff}) of $(Ind^{2Me\text{-}4,7})_2Cr$ as a function of temperature.

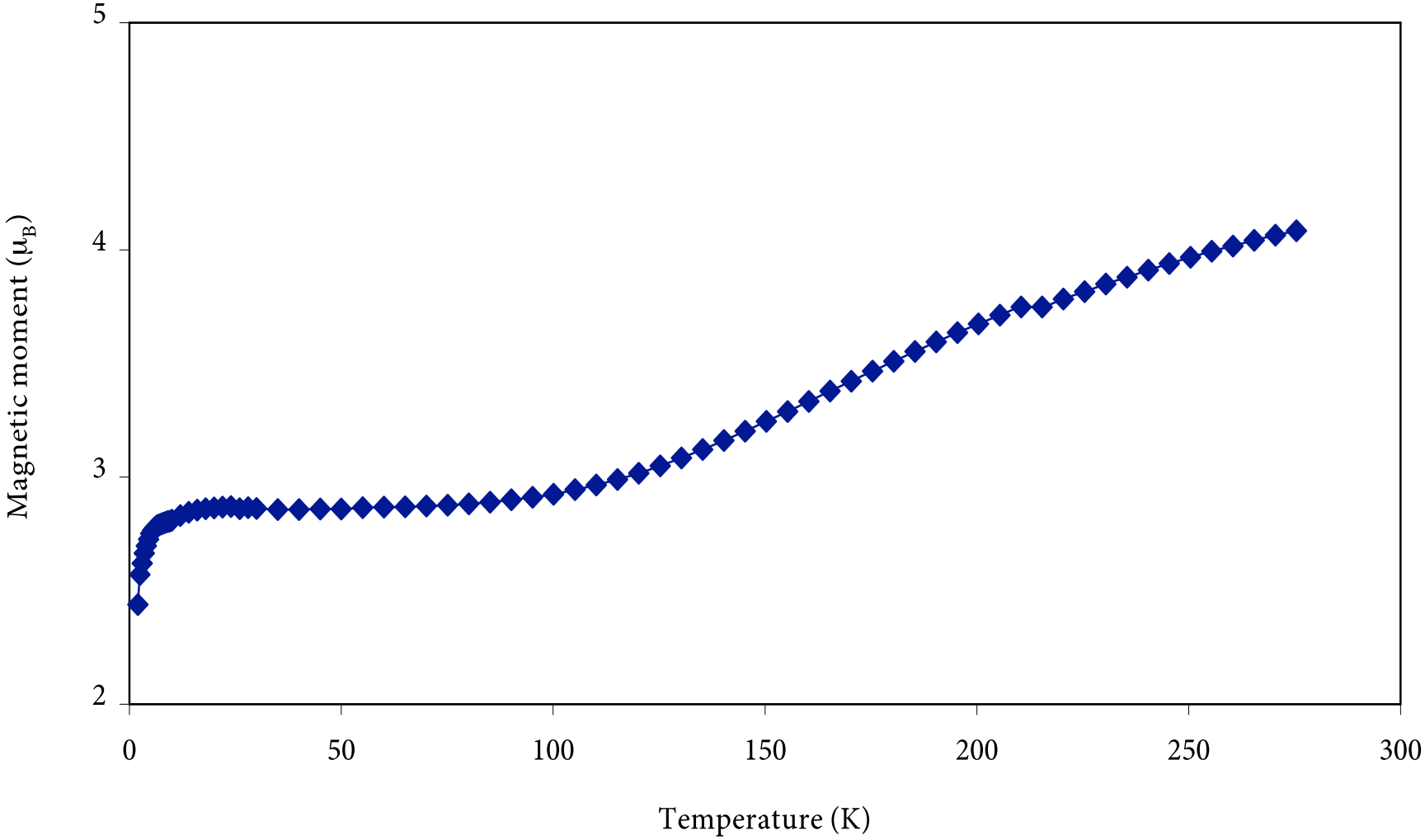

Figure 6. SQUID data for $(Ind^{2Me\text{-}4,7})_2Cr$ showing the compound's spin-crossover behavior in the solid state.

Solid State Structures

$(Ind^{Me-4})_3Cr_2Cl$. Crystals of $(Ind^{Me-4})_3Cr_2Cl$ were harvested from a toluene and hexanes solution as dark brown needles. An ORTEP of the molecule is given in Figure 7, which indicates the numbering scheme referred to in the text; selected bond lengths and angles are shown in Table 1.

Disorder in the indenyl ligands lowers the accuracy of the structure, but it is clear that the compound is isostructural with Ind_3Cr_2Cl.[26] The Cr–Cr bond distance of 2.325(2) Å is slightly longer than that found for the nonmethylated compound (2.317(1) Å). There are two terminal η^5-indenyl ligands, each one bound to a separate metal center. The molecule is completed by a μ,η^3-indenyl ligand and a bridging chloride. The three indenyl ligands form a tripod-like arrangement around the two chromium centers, but are splayed out to accommodate the μ-Cl ligand. This arrangement leads to two of the methyl groups pointing toward each other, although the closest intramolecular Me···Me′ contacts are at 4.5 Å, outside the sum of van der Waals radii. These methyl groups are bent out of the C_6 ring plane (4.44° and 2.76° for the methyl groups on C(19) and C(9), respectively) more so than the methyl without close contacts (0.51° for the methyl group on C(29)). Of the three indenyl rings, the bridging ligand unsurprisingly displays the largest hinge (6.46°) and fold angles (4.11°) due to its slipped η^3 coordination.

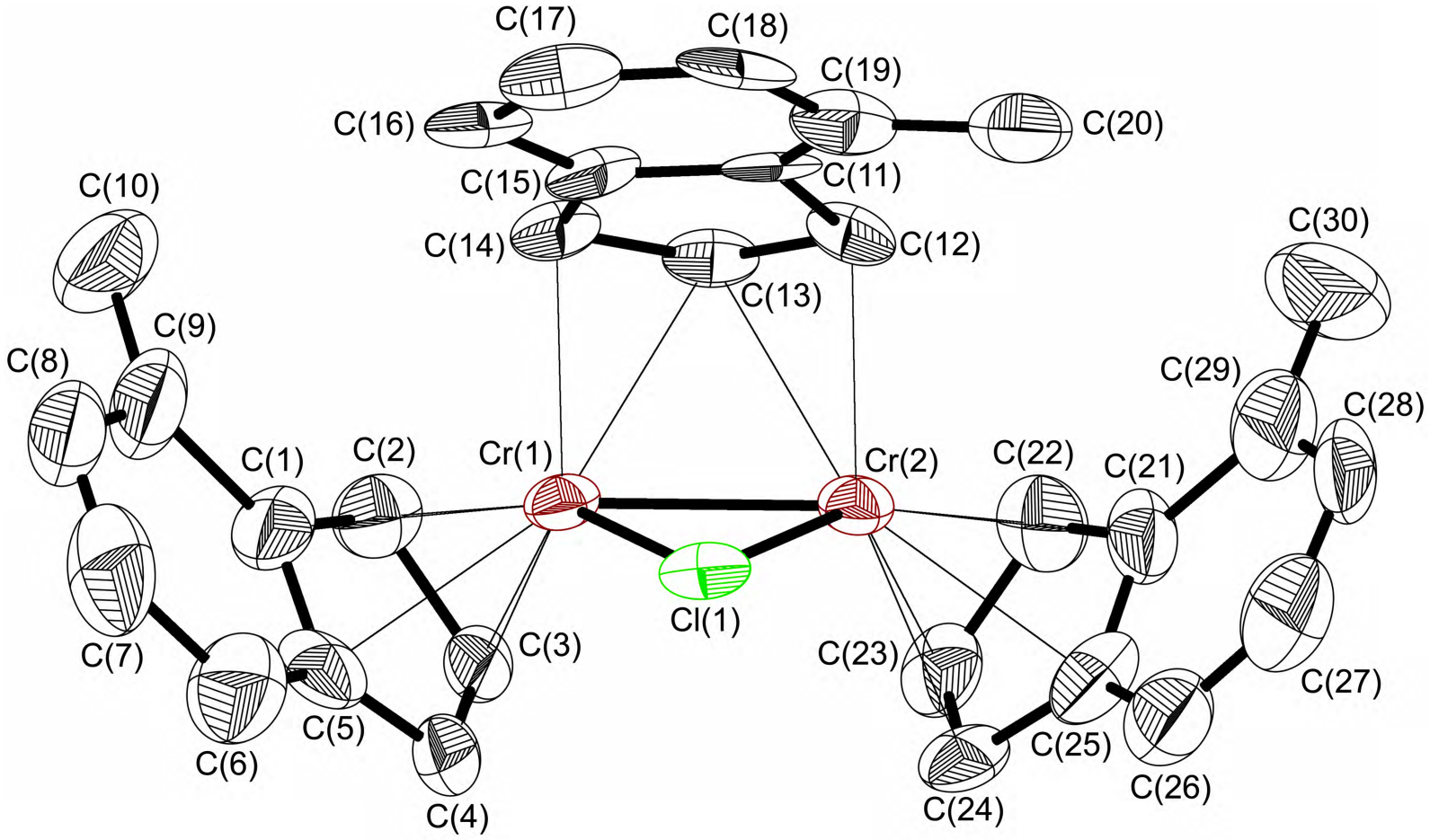

Figure 7. ORTEP of the non-hydrogen atoms of $(Ind^{Me-4})_3Cr_2Cl$ illustrating the numbering scheme used in the text. Thermal ellipsoids are shown at the 50% level.

Table 1. Selected Bond Distances and Angles for $(Ind^{Me-4})_3Cr_2Cl$.

Bridging		Terminal	
Atoms	Distance (Å)	Atoms	Distance (Å)
Cr(1)–C(12)	2.153(8)	Cr(1)–C(1)	2.331(8)
Cr(1)–C(13)	2.377(9)	Cr(1)–C(2)	2.239(8)
Cr(2)–C(13)	2.360(8)	Cr(1)–C(3)	2.246(8)
Cr(2)–C(14)	2.149(8)	Cr(1)–C(4)	2.237(7)
		Cr(1)–C(5)	2.343(8)
hinge = 6.46°			
fold = 4.11°		hinge = 6.15°	
		fold = 2.04°	
		Δ_{M-C} = 0.096 Å	
Cr(1)–Cl(1)	2.330(2)		
Cr(2)–Cl(1)	2.336(2)	Cr(2)–C(21)	2.357(8)
Cr(1)–Cr(2)	2.3246(17)	Cr(2)–C(22)	2.256(9)
		Cr(2)–C(23)	2.223(8)
		Cr(2)–C(24)	2.260(8)
		Cr(2)–C(25)	2.325(9)
		hinge = 2.65°	
		fold = 2.80°	
		Δ_{M-C} = 0.095 Å	

$(Ind^{2Me-4,7})_2Cr$. Crystals of $(Ind^{2Me-4,7})_2Cr$ were harvested from a hexanes solution as dark green plates. An ORTEP of the molecule is given in Figure 8, which indicates the numbering scheme referred to in the text; selected bond lengths and angles are shown in Table 2.

There are two independent molecules in the asymmetric unit, both with very similar bond distances and angles. No intermolecular π-stacking is observed; however, the six-membered rings are nearly eclipsed (twist angles of 8.6 and 9.0° for molecules Cr(1) and Cr(2), respectively) on each molecule. The Cr–C ring distances (average 2.18(1) Å for

Cr(1) and 2.17(1) Å for Cr(2)) are consistent with low-spin chromium(II) centers. The two indenyl ligands are bound to the chromium center in an η^5 fashion; the slip parameter (Δ_{M-C} = 0.078 Å for both independent molecules) is typical for low-spin Ind′$_2$Cr complexes (cf. the value for the low-spin (Ind^{7Me})$_2$Cr, Δ_{M-C} = 0.098 Å).[21] Contact distances for the methyl groups (average 3.81(1) Å for Cr(1) and 3.73(1) Å for Cr(2)) are close enough to imply van der Waals attraction as an added source for stabilization of the eclipsed conformation. The indenyl planes of each molecule are nearly parallel, forming angles of 3.2(1)° and 1.9(1)° for Cr(1) and Cr(2), respectively.

Table 2. Selected Bond Distances and Angles for (Ind$^{2Me-4,7}$)$_2$Cr.

Atoms	Distance (Å)	Atoms	Distance (Å)
Cr(1)–C(1)	2.219(3)	Cr(1)–C(12)	2.244(4)
Cr(1)–C(2)	2.150(4)	Cr(1)–C(13)	2.178(4)
Cr(1)–C(3)	2.128(4)	Cr(1)–C(14)	2.121(4)
Cr(1)–C(4)	2.164(4)	Cr(1)–C(15)	2.145(4)
Cr(1)–C(5)	2.251(4)	Cr(1)–C(16)	2.236(4)
Δ_{M-C}		0.098 Å	
hinge angles		1.007°, 2.023°	
fold angles		2.458°, 3.766°	
angle between C_5 ring planes		6.021°	
twist		8.561°	

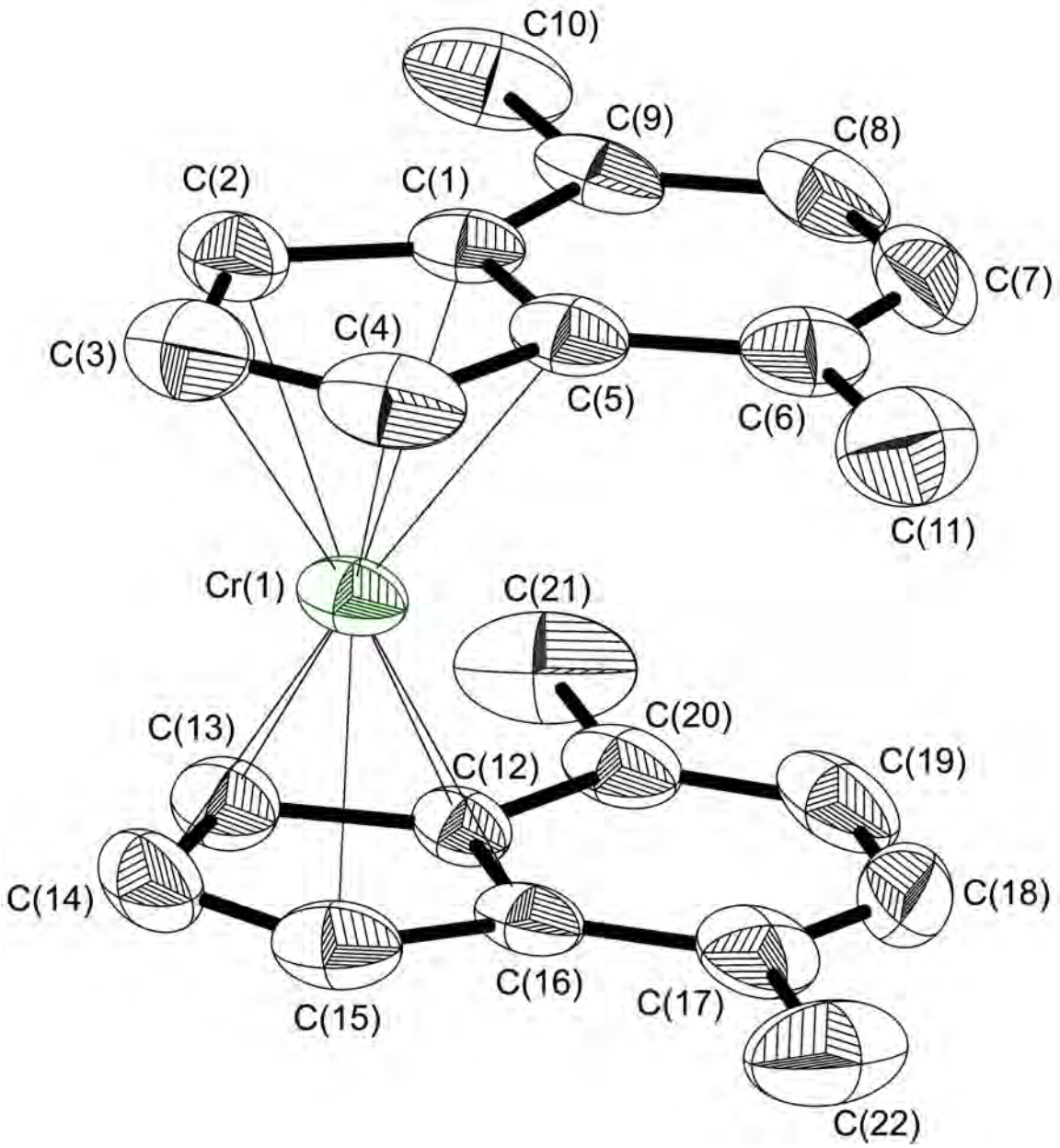

Figure 8. ORTEP of the non-hydrogen atoms of $(Ind^{2Me-4,7})_2Cr$ illustrating the numbering scheme used in the text. Thermal ellipsoids are shown at the 50% level.

$(Ind^{Bzo-5,6})_4Cr_2$. Crystals of $(Ind^{Bzo-5,6})_4Cr_2$ were harvested from a toluene solution as black needles. An ORTEP of the molecule is given in Figure 9, which indicates the numbering scheme referred to in the text; selected bond lengths and angles are shown in Table 3.

It is clear that the compound is isostructural with Ind_4Cr_2.[26] There is one toluene molecule in the lattice for every chromium dimer. The Cr–Cr bond distance of 2.113(2) Å is appreciably shorter than that found for the parent indenyl compound (2.175(1) Å). Just as in Ind_4Cr_2, there are two terminal η^5-indenyl ligands, each one bound to a separate metal center, along with two μ,η^3-indenyl ligands. The average Cr–C distance is 2.33(3) Å for the terminal ligands and 2.24(3) Å for the bridging ligands.

Table 3. Selected Bond Distances and Angles for $(Ind^{Bzo-5,6})_4Cr_2$.

Bridging		Terminal	
Atoms	Distance (Å)	Atoms	Distance (Å)
Cr(1)–C(21)	2.338(8)	Cr(1)–C(1)	2.218(9)
Cr(1)–C(33)	2.168(9)	Cr(1)–C(2)	2.249(8)
Cr(2)–C(21)	2.379(9)	Cr(1)–C(3)	2.437(10)
Cr(2)–C(22)	2.190(8)	Cr(1)–C(12)	2.440(11)
		Cr(1)–C(13)	2.270(10)
Cr(1)–C(41)	2.265(10)		
Cr(1)–C(53)	2.174(9)	Cr(2)–C(61)	2.222(9)
Cr(2)–C(41)	2.286(10)	Cr(2)–C(62)	2.251(8)
Cr(2)–C(42)	2.159(9)	Cr(2)–C(63)	2.449(10)
		Cr(2)–C(72)	2.495(10)
hinge	13.09°, 8.39°	Cr(2)–C(73)	2.281(9)
fold	2.63°, 6.21°		
		hinge	8.44°, 7.21°
Cr(1)–Cr(2)	2.113(2)	fold	2.27°, 1.51°

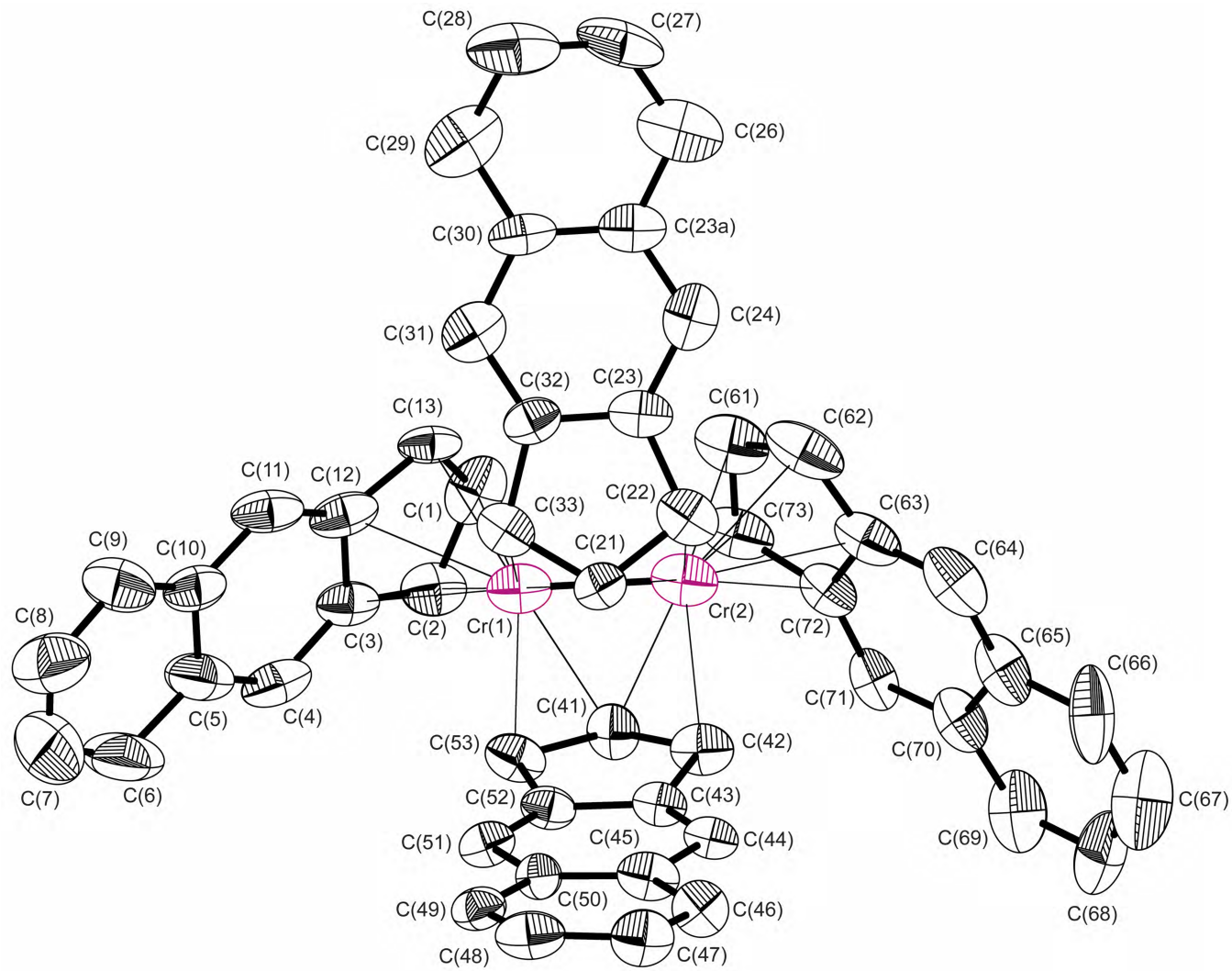

Figure 9. ORTEP of the non-hydrogen atoms of $(Ind^{Bzo\text{-}5,6})_4Cr_2$ illustrating the numbering scheme used in the text. Thermal ellipsoids are shown at the 50% level.

Computational Results

Consideration of the HOMO-*n* orbitals of the indenyl anion (Figure 10) makes it apparent that substitution on the 4,7-positions should most strongly affect the energy of the LUMO (π_6), HOMO (π_5), and HOMO-2 (π_3) orbitals. Although the last orbital is sometimes considered not to be substantially involved in bonding in transition-metal bis(indenyl) complexes,[27] calculations on the $[Ind^{2Me\text{-}4,7}]^-$ anion (TPSSh/6-31+G(d)) indicate that the energy of the π_3 orbital is raised by 0.30 eV relative to the unsubstituted anion; in contrast, the energy of π_4 is lowered, but by only 0.02 eV. This conclusion is relatively insensitive to the level of theory employed. With the B3LYP functional and the larger aug-cc-pVTZ basis set, for example, the energy of the π_3 orbital of the $[Ind^{2Me\text{-}4,7}]^-$ anion is raised by 0.33 eV relative to the unsubstituted anion; the energy of π_4 is again lowered by 0.02 eV.

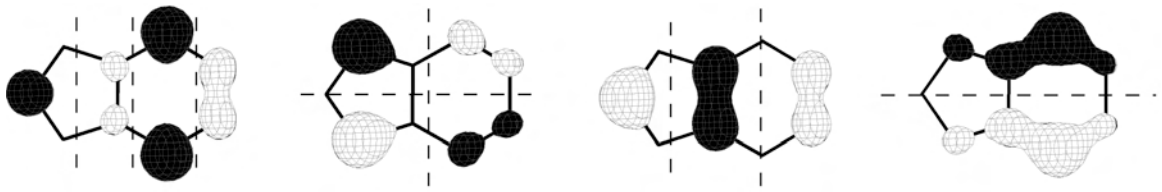

LUMO (π_6) HOMO (π_5) HOMO-1 (π_4) HOMO-2 (π_3)

Figure 10. Frontier π-orbitals of the indenyl anion. The π_n notation is the same as that used by previous authors.[50]

To determine how these changes affect the molecular orbitals of a complex, calculations were performed at the TPSSh/6-31+G(d) level on high- and low-spin Ind_2Cr and $(Ind^{2Me\text{-}4,7})_2Cr$. The Ind_2Cr diagrams are similar to that calculated at the B3PW91/LANL2DZ level for the unsubstituted complex.[8] There are many closely spaced energy levels in the diagrams for $(Ind^{2Me\text{-}4,7})_2Cr$ (Figure 11), but no truly degenerate molecular orbitals ($\Delta E \geq 0.04$ eV). For the staggered $(Ind^{2Me\text{-}4,7})_2Cr$ complex that is calculated in the high-spin state, the π_3-associated orbitals are raised to within 0.05 eV of those associated with π_4. This in turn affects the π_4/d_{xz} orbitals, raising the energy of the bonding combination and conversely lowering the energy of the antibonding combination, which is the HOMO. If the molecule is placed in the low-spin state, the π_3 orbitals drop in energy, with a gap of 0.34 eV below the π_4/d_{xz} combination. The reduced electron repulsion has the effect of lowering the energy of the entire molecule by 2.4 kJ mol^{-1}, a small amount consistent with spin-crossover effects.[51-53]

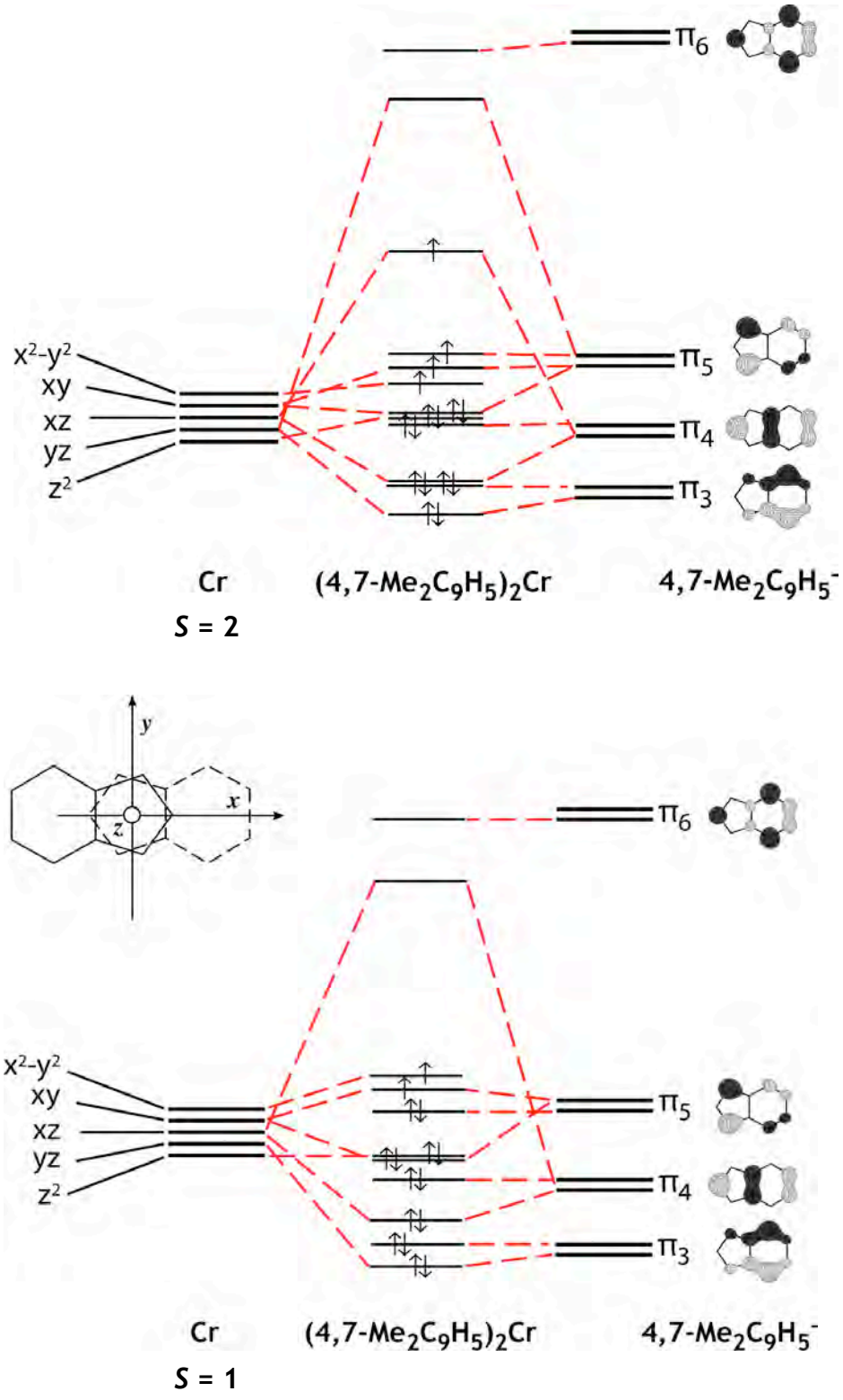

Figure 11. MO diagrams for the hypothetical high-spin (top) and low-spin (bottom) staggered $(Ind^{2Me\text{-}4,7})_2Cr$ complex.

Discussion

Previous investigation into the substitutions necessary to break apart the dimeric nature of bis(indenyl)chromium(II) revealed that a single methyl on the allylic portion of the ring was sufficient to prevent dimerization.[9] Presumably, backside (C_6 ring) methylation should be more likely to maintain the dimeric structure, rather than form monomeric species. Substitution on the 5- and 6-positions has been shown to be sterically undemanding in the complex $(Ind^{Bzo\text{-}5,6})_4Cr_2$, with ligands that are more electron withdrawing than their parent indenyl counterparts, resulting in a shorter Cr–Cr bond distance. A single methyl in the 4-position of the indenyl ring would not be expected to donate enough electron density to break the Cr–Cr bond and form a monomer, and yet a dimeric species ($[Cr(Ind^{Me\text{-}4})_2]_2$) similar to the known bis(indenyl)chromium dimer[26] is presumably prevented by the steric hindrance of the 4 methyl groups. Rather, the dinuclear species formed does not undergo complete metathesis even upon the addition of excess potassium 4-methylindenide.

Addition of a second methyl group to the backside ring, forming the 4,7-dimethylindenyl ligand, also yields a monomeric chromium compound. Increased steric effects from another methyl substituent, in conjunction with the discovery that the π_3 indenyl orbital (see Figure 11) facilitates strong electronic donation from the 4- and 7-positions of this ligand, add to the molecule's preference for a monomeric state.

Molecular symmetry and electron donation from the ligands interact in complex ways in the monomeric compounds of bis(indenyl)chromium(II). Largely unpredictable crystal packing forces have a prominent effect on the former, and some instances of spin-crossover behavior are observed only in the solid state, where intermolecular cooperative effects are operative. In this regard, it is notable that staggered and eclipsed conformations are the only arrangements found in the solid state with the methylated compounds; the gauche arrangements observed in $[1,3\text{-}(t\text{-Bu or } SiMe_3)_2C_9H_5]_2Cr$ appear to require the presence of groups more sterically demanding than methyl or even isopropyl.[8]

The eight known bis(indenyl)chromium(II) compounds with methylated ligands comprise a set in which several trends involving ligand conformation, substitution and magnetic properties are evident. Owing to the compact size of methyl groups, intramolecular steric interactions are not significant here. Instead, the two most clearly defined patterns are the following:

1) *Symmetry is an important, but not completely determinant, influence on the spin state.* There is now strong empirical and computational evidence that a staggered ligand conformation (specifically, one with C_i symmetry) supports a high-spin state in bis(indenyl)chromium(II) complexes (Figure 12), that an eclipsed conformation is less supportive (and associated with spin-crossover molecules), and that a twisted (gauche) conformation is associated with low spin molecules (Figure 13).[8,9] That the symmetry restrictions are not absolute is indicated by $(Ind^{7Me})_2Cr$, which is staggered in the solid state,

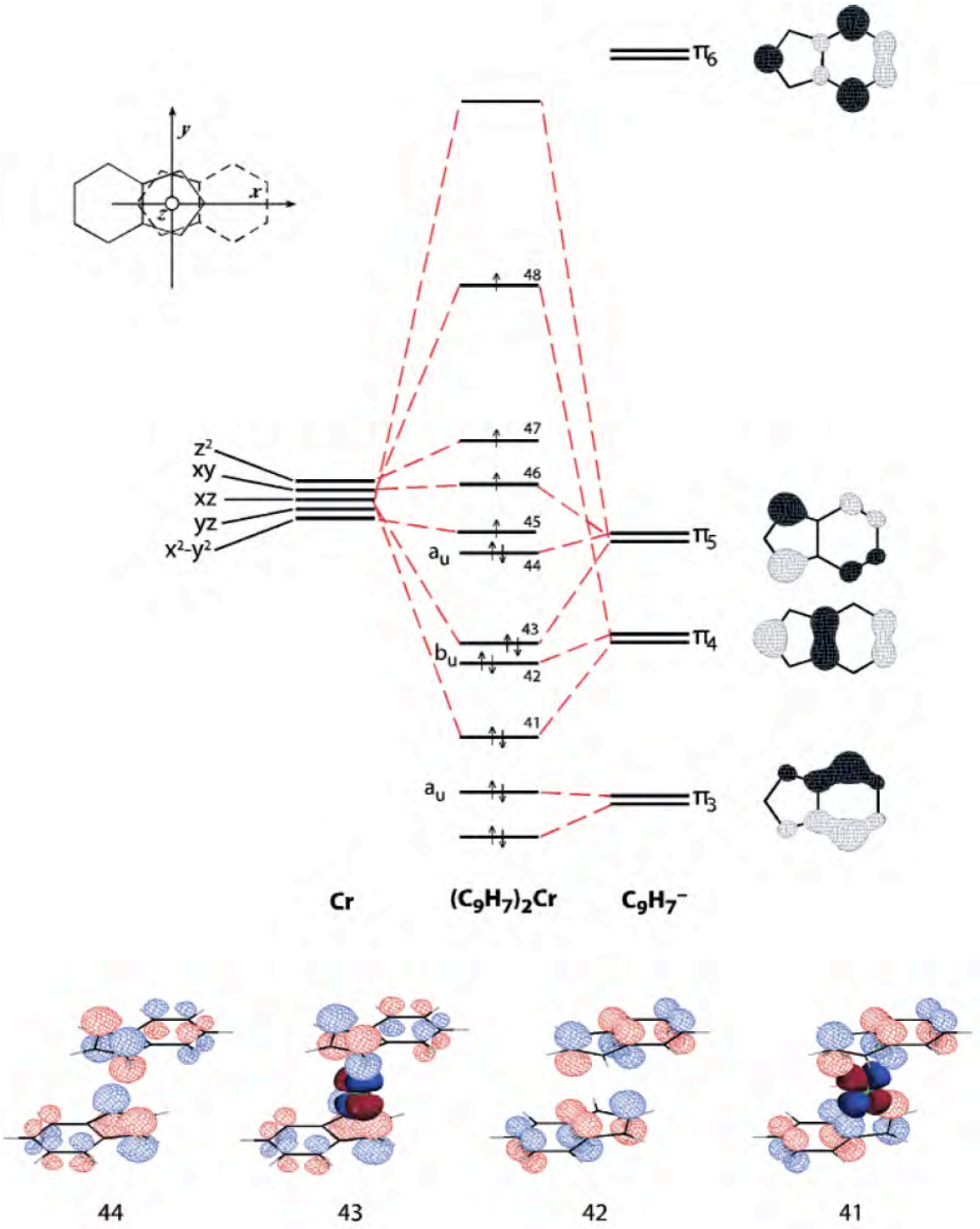

Figure 12. Qualitative MO diagram for high-spin, staggered Ind_2Cr. Energy levels were derived from extended Hückel calculations. Nonbonding orbitals 44 and 42 are forbidden by symmetry from interacting with the metal *d* orbitals.[8]

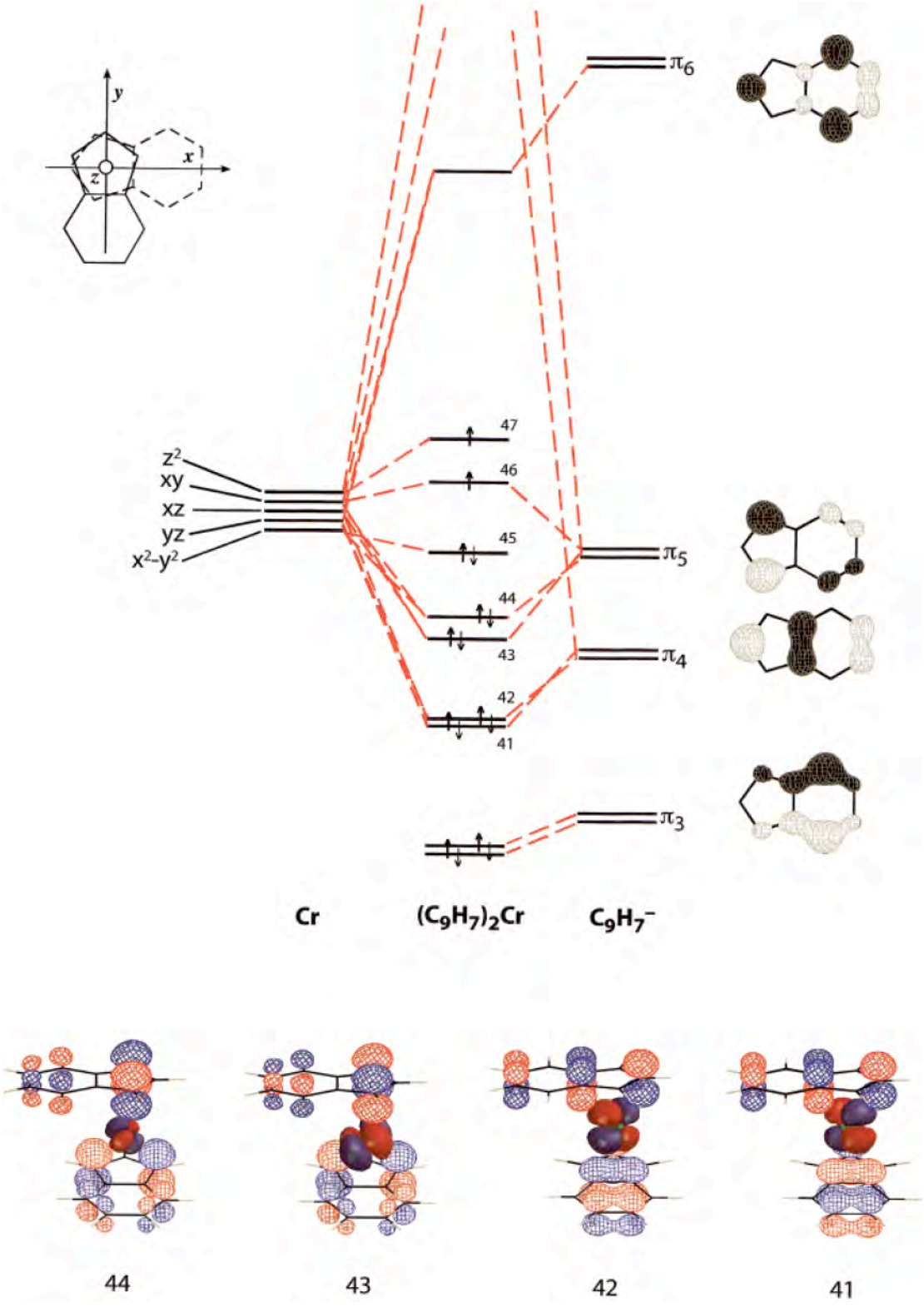

Figure 13. Qualitative MO diagram for low-spin, gauche Ind_2Cr. Energy levels were derived from extended Hückel calculations.[8]

but at all measured temperatures is low spin.

2) *Increasing methylation supports a lower spin state*. Apart from symmetry effects, it is apparent that more complete methylation is associated with lower spin state molecules. Between the extremes of $(Ind^{7Me})_2Cr$ and $(Ind^{Me\text{-}2})_2Cr$ are molecules that undergo thermally induced spin crossovers. This phenomenon is reminiscent of that of manganocene, Cp_2Mn, and its ring-substituted derivatives. Although the parent compound is high-spin ($S = {}^5/_2$) at all measured temperatures, 1,1-dimethylmanganocene is high-spin ($S = {}^5/_2$; $\mu_B = 5.50$) at 373 K, but converts to a low-spin species ($S = {}^1/_2$; $\mu_B = 1.99$) at lower temperatures (193 K).[54] Alkylation of the cyclopentadienyl ring increases the *d*-orbital splitting and preference for spin pairing, so that $(C_5Me_5)_2Mn$, for example, is low-spin ($\mu_B = 2.18$) over a large temperature range.[55]

In the case of the molecules discussed here, the exact type of behavior observed (i.e., whether the spin transitions are complete or not) is a function not only of the number of substituents but also of their *location* on the indenyl ligand. The way in which symmetry and the degree/location of methylation affects the magnetic properties can be summarized as follows:

$(Ind^{Me\text{-}2})_2Cr$: This is the most straightforward case, as the molecule is minimally substituted, adopts a staggered conformation in the solid state, and is high spin both in solution and the solid state at all temperatures.[9]

$(Ind^{Me-1})_2Cr$: Although the molecule exhibits spin-crossover behavior in the solid state, this is certainly the result of its eclipsed configuration, which is dictated by crystal packing forces. In solution, it is high spin, and likely adopts a staggered conformation.[9]

$(Ind^{3Me-1,2,3})_2Cr$: This molecule demonstrates the increasing effect of ligand methylation, as it displays spin-crossover behavior in the solid state, despite its staggered configuration. Nevertheless, it is high spin in solution, indicating that even with the front ring completely methylated, cooperative effects in the solid state are necessary to overcome the symmetry-imposed preference for a high-spin state.

$(Ind^{3Me-2,4,7})_2Cr$, $(Ind^{2Me-4,7})_2Cr$: Conceptually, $(Ind^{3Me-2,4,7})_2Cr$ can be derived from $(Ind^{3Me-1,2,3})_2Cr$ by moving two methyl groups to the benzo ring. The fact that both eclipsed and staggered conformations are found in the solid state is a consequence of crystal packing, but also indicates that they are essentially equienergetic. In solution, a magnetic moment not characteristic of either high spin or low spin is observed, suggesting that comparable populations of eclipsed and staggered conformations are present in spin equilibrium. $(Ind^{2Me-4,7})_2Cr$ has a similar magnetic moment in solution, indicating that the single methyl group on the five-membered ring plays a minor role in determining the magnetic behavior. The fact that the latter is eclipsed in the solid state produces its spin-crossover behavior, which is similar to that of the eclipsed $(Ind^{Me-1})_2Cr$.[9]

As the number of methyl groups is the same in $(Ind^{3Me-2,4,7})_2Cr$ and $(Ind^{3Me-1,2,3})_2Cr$, the former's lower magnetic moment in solution is clearly related to the loca-

tion of the methyl groups on the ligands. The data suggest that substitution on the benzo ring has at least as strong an influence on spin state as when substitution occurs on the five-membered ring. Solid-state data are also consistent with this; to the extent that increasing methylation supports a low-spin state, it can be noted that the average Cr–C distance in the staggered conformation of $(Ind^{3Me\text{-}2,4,7})_2Cr$ at 173 K (2.172(4) Å) is 3% shorter than that in the staggered $(Ind^{3Me\text{-}1,2,3})_2Cr$ (2.239(11) Å) at the same temperature. It should be pointed out that similar positional effects have not been observed in the UV/vis or cyclic voltammetry (CV) data of methyl-substituted bis(indenyl)iron(II) complexes;[56] the UV/vis data are relatively insensitive to the substitution pattern (a consequence of an essentially constant HOMO/LUMO gap), and the CV data reflect the energy of the HOMO only, for which substitution on the benzo ring has less of an effect than methylation on the five-membered ring.

Conclusion

The bis(indenyl)chromium(II) system has proved to be an excellent framework for mapping the electronic effects of site-specific methylation along with how backside ring substituents affect the Cr–Cr bond in dinuclear complexes. The surprising amount of electronic donation derived from the 4- and 7-positions has been shown to be essentially equal to that from allylic positions of the C_5 ring. The absence of available complexes with methylation solely on the 5- and 6-positions of the indenyl ligand leaves open the ques-

tion of the ability of methyl groups in those locations to donate to the metal. However, a comparison of the known spin states of the known, staggered complexes ($(Ind^{3Me\text{-}2,4,7})_2Cr$ and $(Ind^{5Me\text{-}2,4,5,6,7})_2Cr$) suggests that the methyl groups in the 5- and 6-positions have a noticeable, yet smaller effect than those in the 4- and 7-positions. This is confirmed by the addition of an electron withdrawing benzo group in the 5- and 6-positions (as exists in the $[(Ind^{Bzo\text{-}5,6})_2Cr]_2$ complex); the resulting complex contains a shorter Cr–Cr bond than that in the parent indenyl complex.

These results are applicable to transition metal indenyl systems where the electronic properties of the metal require adjustability without influencing its accessibility, such as in polymerization catalysis[57,58] or the binding of small molecules.[59,60] In cases where the one dimensional stacking of transition metal complexes is imperative, methyl substituents add a minimal increase in steric bulk while substantially manipulating the electron donor properties of the metal. This principle should be applicable to the design of magnetic materials with charge-transfer salt donors based on the bis(indenyl) transition metal framework.[61]

CHAPTER II

THE DESIGN OF METALLOCENE-LIKE ELECTRON DONORS FOR THE APPLICATION OF TUNABLE MOLECULAR MAGNETISM

Introduction

In the 1960s, H. M. McConnell developed the idea of an electron-transfer salt-based ferromagnetic material. He developed this concept from the discovery of ferromagnetic coupling reported in picrylaminocarbazyl (PAC) and Wurster's blue perchlorate at very cold temperatures (1.5–4 K).[62] These compounds, being free radicals, would be expected to have spins coupled antiparallel with respect to one another in the solid state. However, according to McConnell's mechanism, if alternating regions of strongly positive spin density and weakly negative spin density[63,64] are coupled, ferromagnetic exchange would result. The structure of PAC was shown to have atoms which would exhibit negative spin density and atoms with positive spin density, and together with proper overlap in the solid state, PAC does indeed produce ferromagnetic coupling.[65] From here, McConnell evolved the idea of obtaining radicals that stack in one dimension with alternating regions of positive and negative spin density. The use of charge-transfer (CT) salts to produce this magnetic behavior was also proposed by McConnell and has had a lasting impact on the field of molecular magnetism.[66]

Decamethylferrocene 7,7,8,8-tetracyanoquinonide, $[FeCp^*_2]^+[TCNQ]^-$, was the first CT salt compound discovered to exhibit ferromagnetic coupling.[67-70] It and related compounds are synthesized from electron-rich organometallic donors (e.g., $FeCp^*_2$) and electron-poor acceptors (usually an olefin or quinone substituted with electron withdrawing groups).[71] These metallocene donors provide a suitable shape to be paired with the typically flat electron acceptors. The π-π interactions between donor and acceptor allow for stacking in one dimension, which happens to be an excellent framework for promoting ferromagnetic spin coupling.[65] The bulk of the charge from the radical electron on the donor remains localized in a metal orbital. This electron induces an antiparallel spin density on the Cp rings. The radical electron on the acceptor also couples to this Cp spin density, ensuring the ferromagnetic coupling between the radicals on both the donor and acceptor. Long-range ordering between stacks, allowing for a bulk ferromagnetic material, results from the orthogonality of the radical orbitals in adjacent stacks.[72]

Attempts to vary the donors in magnetic CT salts have been limited almost exclusively to close analogues of the decamethylmetallocenes, such as decaethylferrocene[73] and octamethylferrocene.[74] It has only been more recently that the use of donors other than Cp^*_2M has been effective in retaining the desired magnetism.[61]

The choice of an electron donor and acceptor pair is based principally on their reversible electrochemical characteristics. Although such considerations are important, we describe here the applications of an additional design principle derived from crystal engi-

neering,[75] i.e., the matching of the donor with an acceptor of roughly the same size, shape, and symmetry. Using this concept as a guide, we have produced the first non-metallocene CT salt in its class that exhibits long-range magnetic order.

The first CT salts to be prepared from a bis(indenyl)metal complex were derived from bis(1,2,3,4,5,6,7-heptamethylindenyl)iron(II) and the acceptors tetracyanoethylene (TCNE), 7,7,8,8-tetracyano-*p*-quinodimethane (TCNQ) and 2,3-dichloro-5,6-dicyanobenzoquinone (DDQ).[76] The TCNQ salt was crystallographically characterized, but no magnetic measurements were made for any of the three compounds that would establish if they were magnetically ordered materials (e.g., ferromagnets or antiferromagnets). Compared to the donor-acceptor centering often observed in Cp*-based molecular magnets, the crystal structure of the bis(indenyl)iron/TCNQ compound displayed a mis-

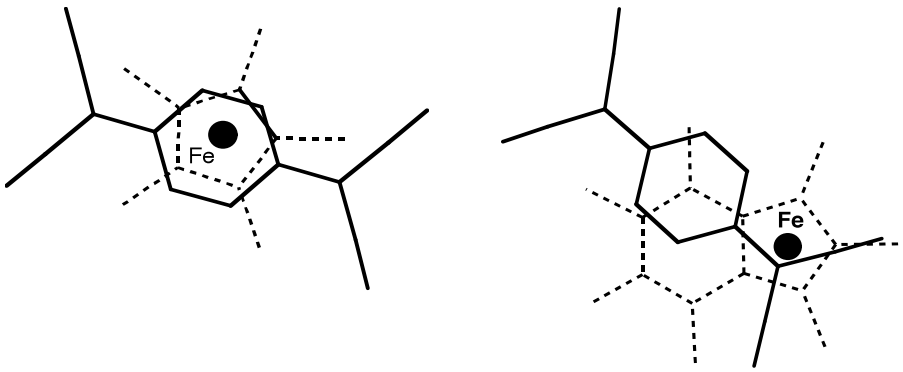

Figure 14. Projections perpendicular to the donor-acceptor planes in $[FeCp^*_2]^+[TCNQ]^-$ (left) and in $[Fe(Me_7C_9)_2]^+[TCNQ]^-$ (right). The TCNQ (solid line) is on top, with the adjacent ligand of the iron complex (dashed line) next. The iron centers (black dots) are in back.

alignment of the donor and acceptor units (Figure 14). The poor overlap of the donating 5-member rings on the indenyl ligand with the organic polycyano molecule's electron accepting region may be partially responsible for the lack of ordered magnetic behavior.

The indenyl ligand has been used for over 40 years in organometallic transition metal chemistry. In many cases, it may be regarded as a benzannulated derivative of the cyclopentadienyl ring (Cp). Our group has previously investigated alkyl- and silyl-substituted bis(indenyl)metal complexes that exhibit various magnetic properties including spin crossover behavior.[8-10] Unlike Cp'_2M, the bis(indenyl) architecture should provide a tunable platform for new CT salt synthesis, directed at improving our understanding of the magnetic coupling in this class of compounds.

Experimental

General Considerations. All manipulations were performed with the rigorous exclusion of air and moisture using Schlenk or glovebox techniques. Proton (^{1}H) NMR experiments were obtained on a Bruker DPX-300 spectrometer at 300 MHz, or a Bruker DPX-400 at 400 MHz, and were referenced to residual proton resonances of THF-d_8 (δ 3.58) and $CDCl_3$ (δ 7.26). Elemental analyses were performed by Desert Analytics (Tucson, AZ); however, the CT salt complexes analyzed consistently low in their C and H percentages, so these results are not discussed. Melting points were determined on a Laboratory Devices Mel-Temp apparatus in sealed capillaries. Melting points of CT salt

complexes were noted to be > 300 °C. Mass spectra were obtained using a Hewlett-Packard 5890 Series II gas chromatograph/mass spectrometer.

Materials. Anhydrous iron(II) chloride and chromium(II) chloride were purchased from Strem Chemicals and used as received. Anhydrous manganese(II) chloride was purchased from Alfa Aesar and used as received. 2,3-Dichloro-1,4-naphthoquinone, 7,7,8,8-tetracyano-*p*-quinodimethane, tetracyanoethylene, 2-bromoindan-1-ol, tiglic acid, thionyl chloride, *n*-butyl lithium, potassium bis(trimethylsilyl)amide, and *p*-toluenesulfonic acid were purchased from Aldrich and used as received. 2-(Dicyanomethylene)indane-1,3-dione was donated by William Tyree (Virginia Tech). Hexanes, toluene, and diethyl ether were distilled under nitrogen from potassium benzophenone ketyl. Benzene and anhydrous tetrahydrofuran (THF) was purchased from Aldrich and used as received. Chlorotrimethylsilane and anhydrous pentane were purchased from Acros and used as received. $CDCl_3$ (Cambridge Isotope) was dried with 4A molecular sieves prior to use. Toluene-d_8 (Aldrich) and THF-d_8 (Cambridge Isotope) were vacuum distilled from Na/K (22/78) alloy and stored over 4A molecular sieves prior to use.

Magnetic Measurements. Solid state magnetic susceptibility data were obtained by Prof. Gordon T. Yee (Virginia Tech) on a Quantum Designs MPMS SQUID magnetometer in a field of 70,000 G. Control of the sample temperature ranges from 1.8 to 300 K. To handle the extremely air- and moisture-sensitive compounds, the previously described sample holder was used;[14] the diamagnetic susceptibility of the sample holder was

accepted as the average value of the measurements on several identical sample holders. The diamagnetic correction for each complex was estimated from Pascal's constants.

Synthesis of 2-Trimethylsilylindene, $HInd^{Si-2}$. In a 500 mL round bottom flask, 2-bromoindan-1-ol (10.0 g, 0.0469 mol) was dissolved in 250 mL of toluene, and the flask was fitted with a Dean-Stark trap and condenser. The solution was warmed to 50 °C for full dissolution of the indanol. A few crystals of *p*-toluenesulfonic acid were added to the solution, and the solution was refluxed until slightly more than 0.5 mL of water was collected in the trap. After cooling to room temperature, the solution was washed with dilute $NaHCO_3$ solution and separated into aqueous and organic layers. The aqueous layer was washed twice with 20 mL of toluene, and the organic layers were combined and dried over $MgSO_4$. After filtration, the toluene was removed by rotary evaporation to yield 2-bromoindene (7.96 g, 0.0408 mol, 87%) as orange crystals. ^1H NMR and GC/MS characterization of 2-bromoindene were consistent with the expected spectra of this compound.

2-Bromoindene was brought into the glovebox and added to 35 mL of anhydrous THF in a 125 mL addition funnel. Magnesium turnings (4.0 g, 0.163 mol) and 50 mL of anhydrous THF were added to a 500 mL 3-neck round bottom flask fitted with the addition funnel, gas inlet atop a reflux condenser, magnetic stir bar, and a rubber septum. The flask was placed on a Schlenk line, and 2 mL of bromoethane was syringed into the flask to activate the magnesium turnings. After about 5 min, the THF began to boil, so this solution was syringed out of the flask and discarded. To avoid contamination with trace

amounts of ethyl magnesium bromide, the turnings were washed 3 times with 40 mL of anhydrous THF. Eighty mL of THF was added to the Mg^0 turnings before 5 mL of the solution of 2-bromoindene was quickly added to the flask to initiate the reaction. The remaining solution was added dropwise over 90 minutes while the reaction was cooled to -15 °C. Upon complete addition of the 2-bromoindene solution, the reaction was warmed to room temperature, and 4.5 g (5.2 mL, 0.0414 mol) of trimethylsilyl chloride was added over 5 min. The reaction was refluxed for 1 h with constant stirring. After being allowed to cool to room temperature, the reaction was stirred for 14 h. Cold water was added to quench the reaction, and magnesium bromide chloride precipitated from solution. The mixture was decanted to remove any unreacted magnesium, and the mixture was washed with water until no more MgBrCl was noticeable. Diethyl ether (200 mL) was also added to the mixture to separate the organic and aqueous layers. The ether layer was dried over $MgSO_4$ before filtration. The removal of solvent via rotary evaporation resulted in a yellow-orange oil. This product was purified to a clear, colorless liquid by vacuum distillation over 45–48 °C and 110 mTorr pressure. The overall product yield was 19% (1.71 g). It was confirmed to be 2-trimethylsilylindene by GC/MS ($m^+ = 188$).

Synthesis of 1,3-Dimethyl-2-trimethylsilylindene, $HInd^{2Me\text{-}1,3/Si\text{-}2}$. 2-Trimethylsilyl-indene (3.14 g, 16.7 mmol) was dissolved in 50 mL of pentane and added to a 125 mL Erlenmeyer flask fitted with a stir bar. *n*-Butyl lithium (6.7 mL, 2.5 M) was slowly added to the flask. The reaction was allowed to stir overnight producing an ex-

tremely viscous oil. Approximately 5 mL of diethyl ether was introduced to the flask. After 10 minutes of stirring with a metal spatula, an off-white solid precipitated. This solid was collected by filtration over a medium-porosity glass frit, washed with pentane (2×20 mL), and dried under vacuum to yield 2.65 g (82%) of lithium 2-trimethylsilylindenide, Li[Ind^{Si-2}].

Li[Ind^{Si-2}] (2.65 g, 13.6 mmol) was dissolved in 100 mL of anhydrous diethyl ether in a 250 mL Schlenk flask fitted with a stir bar and addition funnel. Methyl iodide (1.95 g, 13.7 mmol) was dissolved in 10 mL of diethyl ether and added via syringe to the addition funnel. The MeI solution was added dropwise overnight. To quench the reaction, 20 mL of 0.1 M HCl was added to the flask. The organic layer was subsequently separated and washed with dilute $NaHCO_3$ solution and deionized water. The organic layer was dried over $MgSO_4$ and filtered before rotary evaporation left a clear, colorless oil in 77% yield (2.12 g).

A second methyl group was added to the 3-position by this same process which produced 1.77 g of 1,3-dimethyl-2-trimethylsilylindene in 49% overall yield. The product was confirmed by GC/MS (m^+ = 216).

Synthesis of 4,7-Dimethylindene, $HInd^{2Me-4,7}$. Synthesis of this compound was described in Chapter 1.

Synthesis of 1,2,3-Trimethylindene, $HInd^{3Me-1,2,3}$. Thionyl chloride (200 mL) and tiglic acid (24.8 g, 0.248 mol) were introduced into a 500 mL round bottom

flask fitted with a stir bar and a reflux condenser. The solution was refluxed for 3.5 h. The pale yellow solution was transferred to a 500 mL round bottom flask fitted with a distillation head. Excess thionyl chloride was distilled, leaving tigloyl chloride (23.5 g, 80% yield) in the flask.

Anhydrous $AlCl_3$ (26.5 g, 0.199 mol) and benzene (200 mL) were introduced to a 500 mL three-neck flask fitted with a reflux condenser, an addition funnel, and a stir bar. The mixture was cooled to 0 °C and tigloyl chloride (23.5 g, 0.199 mol) was slowly added via the addition funnel. The mixture was warmed to room temperature and stirred for 30 min before the reaction was brought to reflux for 48 h. The mixture was cooled to room temperature and poured into a beaker of ice (400 g) and conc. HCl (90 mL). The organic layer was extracted 4 times with 100 mL portions of a sodium bicarbonate solution and dried over $MgSO_4$. The excess benzene was removed by distillation to afford an orange oil. This oil was purified over a silica gel column using increasing concentrations of methylene chloride in hexanes. After removal of the solvents using rotary evaporation, 28.6 g (0.179 mol, 90% yield) of 2,3-dimethyl-1-indanone was recovered.

The indanone was dissolved in 100 mL of anhydrous ether and added to a 500 mL Schlenk flask fitted with a stir bar. After the flask was chilled to 0 °C, methyl lithium (100 mL, 1.5 M in ether) was slowly syringed into the solution with stirring. The mixture was allowed to stir for 14 h at room temperature before being cooled to 0 °C and being quenched with a few mL of cold water. The organic layer was separated, dried over

$MgSO_4$, and the solvent was removed by rotary evaporation. The resulting alcohol was redissolved in 250 mL of toluene and transferred to a 500 mL round bottom flask fitted with a Dean-Stark trap and a condenser. A catalytic amount of *p*-toluenesulfonic acid (50 mg) was added, and the solution was refluxed until approximately 3 mL of water was collected in the trap. The reaction was cooled to room temperature, and the toluene was removed by rotary evaporation to afford a black oil. The oil was distilled under vacuum (65 °C, 17 mTorr) to give a yellow fraction (2.48 g). The product was formed in 6.3% overall yield and confirmed to be 1,2,3-trimethylindene by comparison of its spectra (^{1}H NMR and GC/MS) with literature values.[48]

Synthesis of Lithium 1,3-Dimethyl-2-trimethylsilylindenide, Li[Ind$^{2Me-1,3/Si-2}$]. 1,3-Dimethyl-2-trimethylsilylindene (1.77 g, 8.18 mmol) was dissolved in 50 mL of pentane and added to a 125 mL Erlenmeyer flask fitted with a stir bar. *n*-Butyl lithium (3.3 mL, 2.5 M) was slowly added to the flask. The reaction was allowed to stir overnight. Approximately 5 mL of diethyl ether was introduced to the flask. An off-white solid precipitated from the mixture. This solid was collected by filtration over a medium-porosity glass frit, washed with pentane (2×20 mL), and dried under vacuum to yield 1.52 g (84% yield) of lithium 1,3-dimethyl-2-trimethylsilylindenide, Li[Ind$^{2Me-1,3/Si-2}$].

Synthesis of Potassium 1,2,3-Trimethylindenide, K[Ind$^{3Me-1,2,3}$]. 1,2,3-Trimethylindene (2.48 g, 0.0157 mol) was dissolved in 30 mL of toluene in a 250 mL Erlenmeyer flask fitted with a stir bar. Potassium bis(trimethylsilyl)amide (2.66 g, 0.0133

mol) was dissolved in toluene and added dropwise to the indene while stirring. The reaction was stirred 14 h before adding 100 mL of hexanes. A bright yellow precipitate formed and was filtered over a medium-porosity glass frit. The precipitate was washed with hexanes (2 × 30 mL) and dried under vacuum to yield 2.34 g (90% yield) of K[$Ind^{3Me-1,2,3}$].

Synthesis of Potassium 4,7-Dimethylindenide, K[$Ind^{2Me-4,7}$]. Synthesis of this compound was described in Chapter 1.

Synthesis of Potassium 2-Trimethylsilylindenide, K[Ind^{Si-2}]. 2-Trimethylsilylindene (1.71 g, 9.10 mmol) was degassed and dissolved in 20 mL of toluene in a 250 mL Erlenmeyer flask. Potassium bis(trimethylsilyl)amide (1.72 g, 8.64 mmol), was dissolved in toluene and added dropwise to the indene while stirring. The reaction was stirred 14 h before adding 100 mL of hexanes. A white precipitate formed and the mixture was filtered over a medium-porosity glass frit. The precipitate was washed with hexanes (2 × 30 mL) and dried under vacuum. The product was confirmed to be K[Ind^{Si-2}] by ^{1}H NMR (400 MHz) in THF-d_8: δ 0.34 (singlet, 9H, $Si(CH_3)_3$); 5.67 (singlet, 2H, *CH* in 1,3-position); 6.31 (doublet of doublets, 2H, *CH* in 4,7-position); 7.09 (multiplet, 2H, *CH* in 5,6-position). The product was formed in 88% yield (2.06 g).

Synthesis of Bis(2-trimethylsilylindenyl)iron(II), $(Ind^{Si-2})_2Fe$. $FeCl_2$ (0.256 g, 2.02 mmol) was added to a 125 mL Erlenmeyer flask along with 30 mL of THF and a stir bar. Potassium 2-trimethylsilylindenide (1.205 g, 4.04 mmol) was dissolved in 10 mL of anhydrous THF. Upon the dropwise addition of K[Ind^{Si-2}] into the flask, the re-

action mixture turned a dark green-blue and was allowed to stir overnight. The following day, the nearly black solution was placed under vacuum to remove the solvent. Extraction into hexanes (40 mL), followed by filtration of the solution over a medium-porosity glass frit, allowed for the isolation of the iron product from KCl. The deep blue-purple hexanes solution was red by transmitted light. After the hexanes solvent had been allowed to evaporate slowly, dark blue crystalline material formed (0.532 g, 46% yield); the crystals were acicular and unsuitable for x-ray crystallography. Anal. Calcd for $C_{24}H_{30}Si_2Fe$: C, 66.96; H, 7.02; Fe, 12.97. Found: C, 67.36; H, 7.68; Fe, 13.4. ^{1}H NMR was consistent with the dark blue oil reported by Fern, et al.[77]

Synthesis of Bis(4,7-dimethylindenyl)iron(II), $(Ind^{2Me\text{-}4,7})_2Fe$. $FeCl_2$ (0.2242 g, 1.77 mmol) was added to a 125 mL Erlenmeyer flask along with 30 mL of THF and a stir bar. Potassium 4,7-dimethylindenide (0.645 g, 3.54 mmol) was dissolved in 10 mL of anhydrous THF. Upon the dropwise addition of the $K[Ind^{2Me\text{-}4,7}]$ to the flask, the reaction mixture turned a dark purple and was allowed to stir overnight. The following day, the nearly black solution was placed under vacuum to remove the solvent. Extraction into pentane (40 mL), followed by filtration of the solution over a medium-porosity glass frit, allowed for the isolation of the iron product from KCl. After the hexanes solvent had been allowed to evaporate slowly, a dark purple crystalline material was isolated (0.512 g, 85% yield). Anal. Calcd for $C_{22}H_{22}Fe$: C, 77.21; H, 6.48. Found: C, 77.01; H, 6.17.

Synthesis of Bis(1,3-dimethyl-2-trimethylsilylindenyl)iron(II), ($Ind^{2Me-1,3/Si-2}$)$_2$Fe. $FeCl_2$ (0.1076 g, 0.849 mmol) was added to a 125 mL Erlenmeyer flask along with 30 mL of THF and a stir bar. Lithium 1,3-dimethyl-2-trimethylsilylindenide (0.3769 g, 1.70 mmol) was dissolved in 10 mL of anhydrous THF. Upon the dropwise addition of Li[$Ind^{2Me-1,3/Si-2}$] into the flask, the reaction mixture turned dark purple and was allowed to stir overnight. The following day, the nearly black solution was placed under vacuum to remove the solvent. Extraction into hexanes (40 mL), followed by filtration of the solution over a medium-porosity glass frit, allowed for the isolation of the iron product from LiCl. The deep purple crystals were obtained in 86% yield (0.357 g). Anal. Calcd for $C_{28}H_{38}Si_2Fe$: C, 69.11; H, 7.87; Fe, 11.48. Found: C, 69.74; H, 8.56; Fe, 11.7.

Synthesis of Bis(1,2,3-trimethylindenyl)iron(II), ($Ind^{3Me-1,2,3}$)$_2$Fe. $FeCl_2$ (0.161 g, 1.27 mmol) was added to a 125 mL Erlenmeyer flask along with 30 mL of THF and a stir bar. Potassium 1,2,3-trimethylindenide (0.500 g, 2.55 mmol) was dissolved in 10 mL of anhydrous THF. Upon the dropwise addition of the K[$Ind^{3Me-1,2,3}$] to the flask, the reaction mixture turned a dark purple and was allowed to stir overnight. The following day, the nearly black solution was placed under vacuum to remove the solvent. Extraction into hexanes (40 mL), followed by filtration of the solution over a medium-porosity glass frit, allowed for the isolation of the iron product from KCl. The deep purple hexanes solution was added to a modified round bottom flask and placed in the freezer at -30 °C. Large purple crystals were grown from the solution and isolated by cannulation of the mother

liquor on a Schlenk line. The crystals were dried under vacuum and brought into the glovebox (0.348 g, 74% yield). The ^{1}H NMR spectrum was consistent with the known compound.[78]

Synthesis of Bis(1,2,3-trimethylindenyl)chromium(II), $(Ind^{3Me\text{-}1,2,3})_2Cr$. Following the previously described synthesis,[10] $CrCl_2$ (0.200 g, 1.63 mmol) was added to a 125 mL Erlenmeyer flask along with 30 mL of THF and a stir bar. Potassium 1,2,3-trimethylindenide (0.5 g, 2.55 mmol) was dissolved in 10 mL of anhydrous THF. Upon the dropwise addition of the $K[Ind^{3Me\text{-}1,2,3}]$ to the flask, the reaction mixture turned a dark purple and was allowed to stir overnight. The following day, the nearly black solution was placed under vacuum to remove the solvent. Extraction into hexanes (40 mL), followed by filtration of the solution over a medium-porosity glass frit, allowed for the isolation of the iron product from KCl. The purple hexanes solution was added to a modified round bottom flask and placed in the freezer at -30 °C. Two large purple crystalline blocks were grown from the solution and isolated by cannulation of the mother liquor on a Schlenk line. The crystals were dried under vacuum and brought into the glovebox (0.125 g, 21% yield). The mp (233–236 °C) was consistent with the known compound.[10]

Synthesis of 2,3-Dicyano-1,4-naphthoquinone, DCNQ. 2,3-Dichloro-1,4-naphthoquinone (5.00 g, 22.0 mmol) was dissolved in 75 mL of ethanol in a 250 mL Erlenmeyer flask fitted with a stir bar and an addition funnel and surrounded by a water bath. Sodium cyanide (6.0 g, 122 mmol) was dissolved in 50 mL of ethanol and slowly

dropped into the flask via the addition funnel. The reaction mixture turned a deep red, and after 1 hour of stirring, 10 mL of cold conc. HCl was added to quench the reaction. The white product was isolated by filtration and thoroughly rinsed with H_2O. After being dried, 5.3 g of the material was dispersed in acetic acid, heated to 100 °C, and 15 mL of 30% nitric acid was added over 1 h. This solution was diluted with H_2O and placed in the freezer for 1.5 h. A yellow solid was isolated by filtration and purified by recrystallization from dichloromethane to produce 1.5 g (33% yield) of yellow needles. Characterization of the product was consistent with the known literature.[79]

Synthesis of Bis(1,2,3-trimethylindenyl)iron(III) 2-(Dicyanomethylene)indane-1,3-dione, $[Fe(Ind^{3Me\text{-}1,2,3})_2]^+[DCID]^-$. Bis(1,2,3-trimethylindenyl)iron(II) (115 mg, 0.31 mmol) was dissolved in 2 mL of THF in a Schlenk tube fitted with a stir bar. DCID (75 mg, 0.36 mmol) dissolved in 5 mL of THF was added to the solution, and the reaction was stirred for 1 h. Diethyl ether (15 mL) was slowly added to precipitate the charge transfer salt. The mixture was filtered over a medium-porosity glass frit and washed twice with hexanes (10 mL). Dark red-purple microcrystals were obtained (102 mg, 57% yield).

Synthesis of Bis(1,2,3-trimethylindenyl)iron(III) Tetracyanoethylene, $[Fe(Ind^{3Me\text{-}1,2,3})_2]^+[TCNE]^-$. Bis(1,2,3-trimethylindenyl)iron(II) (123 mg, 0.33 mmol) was dissolved in 2 mL of THF in a Schlenk tube fitted with a stir bar. TCNE (48 mg, 0.38 mmol) dissolved in 5 mL of THF was added to the solution, and the reaction was stirred

for 1 h. Diethyl ether (15 mL) was slowly added to precipitate the charge transfer salt. The mixture was filtered over a medium-porosity glass frit and washed twice with hexanes (10 mL). Deep purple microcrystals were obtained (138 mg, 83% yield).

Synthesis of Bis(1,2,3-trimethylindenyl)iron(III) 7,7,8,8-Tetracyano-*p*-quino-dimethane, $[Fe(Ind^{3Me\text{-}1,2,3})_2]^+[TCNQ]^-$. Bis(1,2,3-trimethylindenyl)iron(II) (125 mg, 0.34 mmol) was dissolved in 2 mL of THF in a Schlenk tube fitted with a stir bar. TCNQ (67 mg, 0.33 mmol) dissolved in 5 mL of THF was added to the solution, and the reaction was stirred for 1 h. Diethyl ether (15 mL) was slowly added to precipitate the charge transfer salt. The mixture was filtered over a medium-porosity glass frit and washed twice with hexanes (10 mL). Black microcrystals were obtained (145 mg, 77% yield).

Synthesis of Bis(1,2,3-trimethylindenyl)iron(III) 2,3-Dicyano-1,4-naphthoquinonide, $[Fe(Ind^{3Me\text{-}1,2,3})_2]^+[DCNQ]^-$. Bis(1,2,3-trimethylindenyl)iron(II) (118 mg, 0.32 mmol) was dissolved in 2 mL of THF in a Schlenk tube fitted with a stir bar. DCNQ (68 mg, 0.33 mmol) dissolved in 5 mL of THF was added to the solution, and the reaction was stirred for 1 h. Diethyl ether (15 mL) was slowly added to precipitate the charge transfer salt. The mixture was filtered over a medium-porosity glass frit and washed twice with hexanes (10 mL). Maroon microcrystals were obtained (160 mg, 86% yield). Decomp. > 300 °C. Anal. Calcd for $C_{36}H_{30}FeN_2O_2$: C, 74.75; H, 5.23; N, 4.84. Found: C (average of two determinations), 70.03; H (average of two determinations), 4.96; N, 4.81. Although the carbon analysis is low, the molar ratio

of C:H is 1.19:1 or 35.6:30, which is close to the expected value. X-ray quality crystals were obtained by slow diffusion of the reagents at –78 °C. Specifically, DCNQ (68 mg, 0.33 mmol) was dissolved in a minimal amount of THF in a Schlenk tube. THF (2 mL) was slowly added on top of the DCNQ solution to separate the two reactants. A concentrated solution of bis(1,2,3-trimethylindenyl)iron(II) (121 mg, 0.33 mmol) in THF was gently layered above the mixture, which was subsequently kept at –78 °C for 24 h. Filtration yielded air stable, maroon needles.

Synthesis of Bis(2-trimethylsilylindenyl)iron(III) 2-(Dicyanomethylene)indane-1,3-dione, $[Fe(Ind^{Si\text{-}2})_2]^+[DCID]^-$. Bis(2-trimethylsilylindenyl)iron(II) (124 mg, 0.288 mmol) was dissolved in 2 mL of THF in a Schlenk tube fitted with a stir bar, and the solution was cooled to –30 °C. DCID (60 mg, 0.288 mmol) dissolved in 5 mL of cold THF was added to the solution, and the reaction was stirred for 1 h. Hexanes (10 mL) was slowly added to precipitate the charge transfer salt. Immediately, an orange precipitate formed in a blue-green solution. The mixture was filtered over a medium-porosity glass frit and washed twice with hexanes (10 mL). An orange powder (0.143 g) was collected in 78% yield.

Synthesis of Bis(1,3-dimethyl-2-trimethylsilylindenyl)iron(III) 2-(Dicyanomethylene) indane-1,3-dione, $[Fe(Ind^{2Me\text{-}1,3/Si\text{-}2})_2]^+[DCID]^-$. Bis(1,3-dimethyl-2-trimethylsilylindenyl) iron(II) (290 mg, 0.60 mmol) was dissolved in 2 mL of THF in a Schlenk tube fitted with a stir bar, and the solution was cooled to –25 °C. DCID

(132 mg, 0.63 mmol) dissolved in 5 mL of cold THF was added to the solution, and the reaction was stirred for 1 h. Pentane (15 mL) was slowly added to precipitate the charge transfer salt. The mixture was filtered over a medium-porosity glass frit and washed twice with pentane (10 mL). Black microcrystals (0.228 g) were collected in 54% yield.

Synthesis of Bis(4,7-dimethylindenyl)iron(III) 2,3-Dicyano-1,4-naphthoquinonide, $[Fe(Ind^{2Me\text{-}4,7})_2]^+[DCNQ]^-$. Bis(4,7-dimethylindenyl)iron(II) (194 mg, 0.567 mmol) was dissolved in 4 mL of THF in a Schlenk tube fitted with a stir bar, and the solution was cooled to –25 °C. DCNQ (118 mg, 0.567 mmol) dissolved in 5 mL of cold THF was added to the solution, and the reaction was stirred for 1 h. Pentane (15 mL) was slowly added to precipitate the charge transfer salt. The mixture was filtered over a medium-porosity glass frit and washed twice with pentane (10 mL). Black microcrystals (200 mg) were collected in 64% yield.

Synthesis of Bis(4,7-dimethylindenyl)iron(III) 2,3-Dicyano-1,4-naphthoquinonide, $[Fe(Ind^{2Me\text{-}4,7})_2]^+[DCID]^-$. Bis(4,7-dimethylindenyl)iron(II) (194 mg, 0.567 mmol) was dissolved in 4 mL of THF in a Schlenk tube fitted with a stir bar, and the solution was cooled to –25 °C. DCNQ (118 mg, 0.567 mmol) dissolved in 7 mL of cold THF was layered above the solution, and the reaction was kept in the freezer overnight. Pentane (15 mL) was slowly added to precipitate the charge transfer salt. The mixture was filtered over a medium-porosity glass frit and washed twice with pentane (10 mL). Black microcrystals (200 mg) were collected in 64% yield.

Synthesis of Bis(1,2,3-trimethylindenyl)chromium(III) 2,3-Dicyano-1,4-naphtho-quinonide, $[Cr(Ind^{3Me-1,2,3})_2]^+[DCNQ]^-$. Bis(1,2,3-trimethylindenyl)chromium(II) (60 mg, 0.16 mmol) was dissolved in 2 mL of THF in a Schlenk tube fitted with a stir bar at –30 °C. DCNQ (34 mg, 0.16 mmol) was dissolved in 5 mL of THF at –30 °C, slowly added to the solution, and the reaction was stirred for 30 min. Diethyl ether (5 mL) was added to precipitate the charge transfer salt. The mixture was filtered over a medium-porosity glass frit and washed twice with diethyl ether (5 mL). A yellow-brown powder was obtained (75 mg, 80% yield).

Synthesis of Bis(1,2,3-trimethylindenyl)chromium(III) 2-(Dicyanomethylene)in-dane-1,3-dione, $[Cr(Ind^{3Me-1,2,3})_2]^+[DCID]^-$. Bis(1,2,3-trimethylindenyl)chromium(II) (60 mg, 0.16 mmol) was dissolved in 2 mL of cold THF in a Schlenk tube fitted with a stir bar. DCID (34 mg, 0.16 mmol) dissolved in 5 mL of cold THF was added to the solution, and the reaction was stirred for 30 min. Diethyl ether (5 mL) was slowly added to precipitate the charge transfer salt. The mixture was filtered over a medium-porosity glass frit and washed twice with diethyl ether (5 mL). A deep purple powder was obtained (68 mg, 72% yield).

Synthesis of Bis(4,7-dimethylindenyl)manganese(III) 2,3-Dicyano-1,4-naphtho-quinonide, $[Mn(Ind^{2Me-4,7})_2]^+[DCNQ]^-$. Bis(4,7-dimethylindenyl)manganese(II) (104 mg, 0.305 mmol) was dissolved in 2 mL of THF in a Schlenk tube fitted with a stir bar, and the solution was cooled to –25 °C. DCNQ (63

mg, 0.567 mmol) dissolved in 5 mL of cold THF was added to the solution, and the reaction was stirred for 1 h. Pentane (15 mL) was slowly added to precipitate the charge transfer salt. The mixture was filtered over a medium-porosity glass frit and washed twice with pentane (10 mL). An olive green powder (55 mg) was collected in 33% yield.

Synthesis of Bis(2-trimethylsilyl)indenyl)manganese(III) 2,3-Dicyano-1,4-naph-thoquinonide, $[Mn(Ind^{Si\text{-}2})_2]^+[DCNQ]^-$. Bis(2-trimethylsilyl)indenyl)manganese(II) (76.2 mg, 0.133 mmol) was dissolved in 2 mL of THF in a Schlenk tube fitted with a stir bar, and the solution was cooled to –25 °C. DCNQ (27.6 mg, 0.133 mmol) dissolved in 5 mL of cold THF was added to the solution, and the reaction was stirred for 1 h. Pentane (15 mL) was slowly added to precipitate the charge transfer salt. The mixture was filtered over a medium-porosity glass frit and washed twice with pentane (10 mL). A dark brown powder (27 mg) was collected in 26% yield.

General Procedures for X-ray Crystallography. A suitable crystal of each sample was located, attached to a glass fiber, and mounted on a Bruker SMART Platform CCD diffractometer for data collection at 173(2) K or 100(2) K. Data collection and structure solutions for all molecules were conducted at the X-ray Crystallography Laboratory at the University of Minnesota by Dr. William W. Brennessel, or at the University of California, San Diego by Dr. Arnold L. Rheingold. Data resolution of 0.84 Å was considered in the data reduction (SAINT 6.01 and SAINT 6.35, Bruker Analytical Systems, Madison, WI). The intensity data were corrected for absorption and decay (SADABS). All

calculations were performed using the current SHELXTL suite of programs.[45] Final cell constants were calculated from a set of strong reflections measured during the actual data collection. Relevant crystal and data collection parameters for each of the compounds are given in Appendix B.

The space groups were determined based on systematic absences and intensity statistics. A direct-methods solution was calculated that provided most of the non-hydrogen atoms from the E-map. Several full-matrix least-squares/difference Fourier cycles were performed that located the remainder of the non-hydrogen atoms. All non-hydrogen atoms were refined with anisotropic displacement parameters. All hydrogen atoms were placed in ideal positions and refined as riding atoms with relative isotropic displacement parameters.

X-ray Crystallography of $[Fe(Ind^{3Me\text{-}1,2,3})_2]^+[DCNQ]^-$. A dark maroon crystal of $[Fe(Ind^{3Me\text{-}1,2,3})_2]^+[DCNQ]^-$ was grown from the slow diffusion of the electron donor and acceptor solutions kept at –78 °C for one day. The crystal was separated from the mother liquor via filtration and dried under vacuum prior to data collection. An initial set of cell constants was calculated from reflections produced from three sets of 20 frames. These sets of frames were oriented such that orthogonal wedges of reciprocal space were surveyed. This produced orientation matrices determined from 28 reflections. The final cell constants were calculated from the *xyz* centroids of 2566 strong reflections as described in the general procedures.

Data was collected using MoKα radiation (graphite monochromator) with a frame time of 90 s and a detector distance of 4.83 cm. A randomly oriented region of reciprocal space was surveyed to the extent of 1 sphere, and to a resolution of 0.84 Å. Three major sections of frames were collected with 0.30° steps in ω at four different ϕ settings and a detector position of –28° in 2θ.

The space group *Pbca* was determined as described in the general procedures. The final full matrix least-squares refinement converged to $R1 = 0.0580$ and $wR2 = 0.1664$ (F^2, all data).

X-ray Crystallography of $(Ind^{2Me\text{-}1,3/Si\text{-}2})_2Fe$. Dark green crystals of $(Ind^{2Me\text{-}1,3/Si\text{-}2})_2Fe$ were harvested by preparing a concentrated pentane solution which was allowed to slowly evaporate at room temperature. The crystals were separated from the mother liquor and dried under vacuum prior to data collection. An initial set of cell constants was calculated from reflections produced from three sets of 20 frames. These sets of frames were oriented such that orthogonal wedges of reciprocal space were surveyed. This produced orientation matrices determined from 40 reflections. The final cell constants were calculated from the *xyz* centroids of 7494 strong reflections as described in the general procedures.

Data was collected using MoKα radiation (graphite monochromator) with a frame time of 60 s and a detector distance of 4.83 cm. A randomly oriented region of reciprocal space was surveyed to the extent of 1 sphere, and to a resolution of 0.84 Å. Three major

sections of frames were collected with 0.30° steps in ω at four different ϕ settings and a detector position of –28° in 2θ.

The space group *Cc* was determined as described in the general procedures. The final full matrix least-squares refinement converged to $R1 = 0.0372$ and $wR2 = 0.0936$ (F^2, all data).

Results

Ligand Synthesis. Various alkylated and trimethylsilylated indenes were prepared by modifications of standard procedures.[27,37,47-49] These included $HInd^{3Me-1,2,3}$, $HInd^{2Me-4,7}$, $HInd^{2Me-1,3/Si-2}$, $HInd^{Bzo-5,6}$, $HInd^{Si-2}$. The addition of a trimethylsilyl group to the 2-position of the indene ring was performed through a Grignard intermediate (Figure 15). Substitution on the C_5 ring can also be achieved by Friedel-Crafts acylation of a benzene ring using a methylated chloropropenone as in Figure 16.

Once the desired hydrocarbon ring was synthesized and purified by vacuum distillation, the alkali metal indenide salt was prepared via deprotonation reaction with a strong base. Reactions with potassium bis(trimethylsilyl)amide were performed in toluene, followed by precipitation of the potassium indenide salt by the addition of hexanes. The indenides were isolated from bis(trimethylsilyl)amine by filtration and rigorous washing with additional hexanes. Reactions with *n*-butyl lithium were performed in a combination of pentane and hexanes, followed by precipitation of the lithium indenide salt by the ad-

dition of a small volume of diethyl ether. The indenides were similarly isolated and washed prior to reactions with transition metal salts.

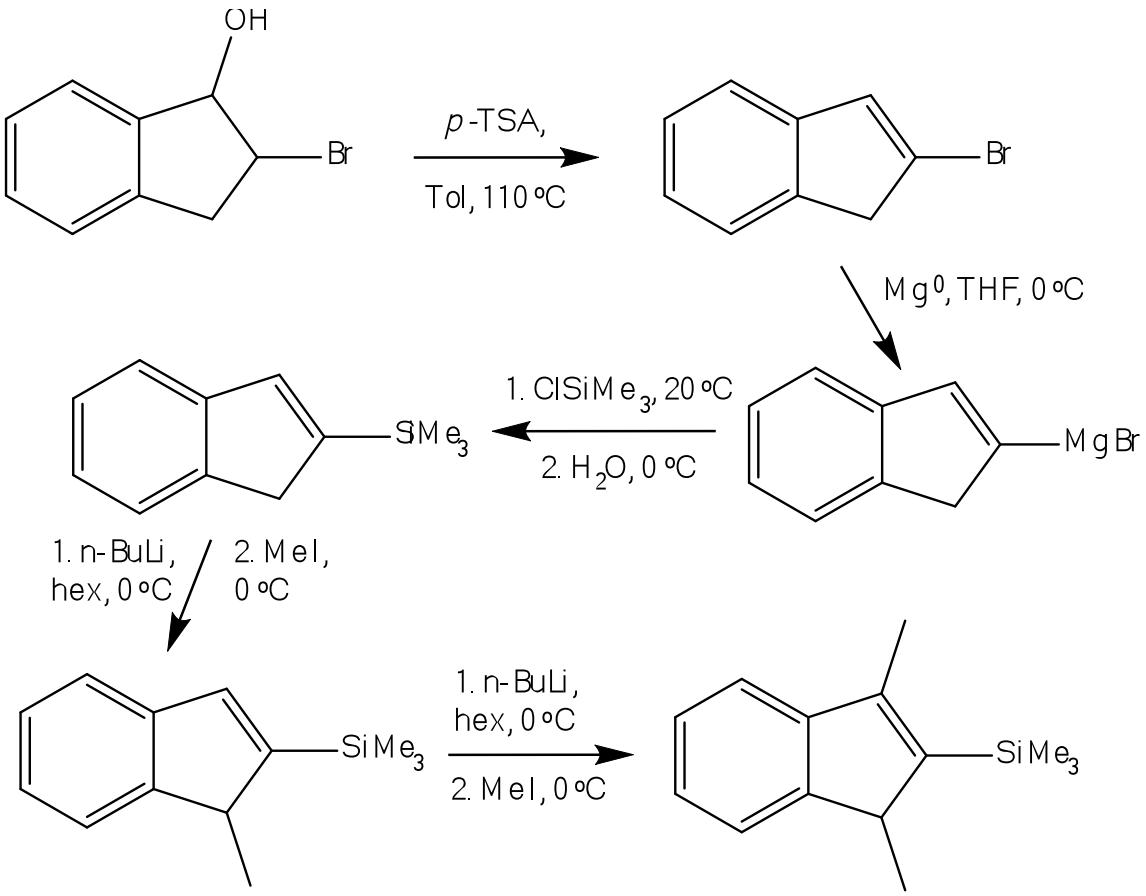

Figure 15. Synthesis of 2-trimethylsilylindene, followed by deprotonation and methylation of the 1- and 3-positions of the ring.

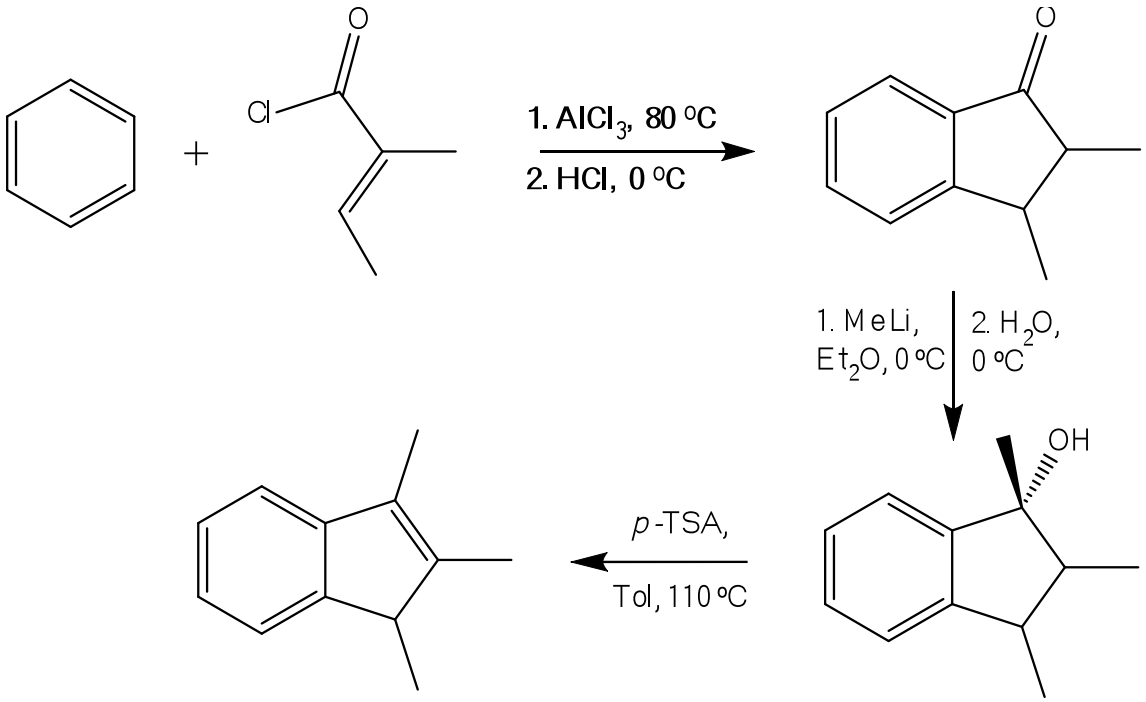

Figure 16. Synthesis of 1,2,3-trimethylindene.

Synthesis of Substituted Bis(indenyl)metal Complexes of Fe(II), Mn(II), and Cr(II). Once the appropriate indenide salts were prepared, the corresponding bis(indenyl)iron, manganese, and chromium complexes could be readily synthesized by salt metathesis elimination reactions. In each case, two equivalents of the appropriate alkali metal indenide salt were allowed to react with anhydrous iron(II), manganese(II), or chromium(II) chloride in THF (eq 3); the resulting mixtures were generally stirred overnight to ensure complete reaction. Following the removal of THF under vacuum, a less polar solvent (pentane, hexanes, or toluene) was added to extract the transition metal species, precipitating the alkali metal chloride in the process. The solubility of these bis(indenyl) transition metal complexes in even the most non-polar solvents pro-

vides an efficient means by which to separate the desired materials from the rest of the reaction mixture.

$$2\,A[Ind'] + MCl_2 \xrightarrow{THF} \xrightarrow{Hex\ or\ Pent} (Ind')_2M + 2\,ACl \qquad (3)$$

$$A = Li\ or\ K$$
$$M = Cr, Mn, or\ Fe$$

The CT salt synthesis is performed in THF at room temperature in the case of iron, and at –30 °C for manganese or chromium. A solution of the acceptor is added to a solution of the Ind′$_2$M complex, typically producing a crystalline precipitate of the CT salt upon the addition of diethyl ether or in some cases a less polar solvent. The products were isolated by filtration and their magnetic properties analyzed with a SQUID magnetometer.

Solid State Structures

$(Ind^{2Me\text{-}1,3/Si\text{-}2})_2Fe$. Crystals of $(Ind^{2Me\text{-}1,3/Si\text{-}2})_2Fe$ were harvested from a pentane solution as purple needles. An ORTEP of the molecule is given in Figure 17, which indicates the numbering scheme referred to in the text; selected bond lengths and angles are shown in Table 4.

The average Fe-C ring distance observed for this species (2.073(6) Å) is only slightly lengthened from that observed in unsubstituted Ind_2Fe (2.065(4) Å).[22] Furthermore, the

M–C distances compare favorably to those observed in other substituted bis(indenyl)iron(II) complexes such as $(Ind^{2i\text{-}1,3})_2Fe$ (2.068(6) Å)[80] and bis(heptamethylindenyl)iron(II) (2.074(4) Å).[22] The range of Fe–C distances in the 5-membered rings (2.048–2.100(2) Å) is consistent with η^5 binding to the iron; the small amount of slippage (Δ_{M-C} = 0.034 Å) observed in the complex is also comparable to that observed in other substituted bis(indenyl)iron(II) complexes. One notable feature is the trimethylsilyl groups are substantially bent out of the 5-membered ring plane (0.43 Å). This is probably due to the steric bulk of the ligand, since the closest contact to the other ring (C(12) to C(31)) is 3.67 Å—smaller than the sum of the van der Waals radii for two methyl groups. The methyl group nearest each opposing trimethylsilyl group is bent out of the C_5 plane by 0.10 Å, while the other methyl groups lie in the plane. The degree of rotation of the ligands from eclipsed (112.3°) is unlike other bis(indenyl)iron(II) complexes. Typically, the ligands are completely eclipsed,[22,78] gauche (near 90°),[77,80] or, in the singular case of the bis(heptamethylindenyl)iron(II), 151.3°.[22] The hinge and fold angles observed are consistent with the known $(Ind)_2Fe$ and $(Ind^*)_2Fe$ structures,[22] so any steric crowding must be relieved by the amount of ligand rotation and the out-of-plane bending of the substituents.

Table 4. Selected Bond Distances and Angles for $(Ind^{2Me-1,3/Si-2})_2Fe$.

Atoms	Distance (Å)	Atoms	Distance (Å)
Fe(1)–C(26)	2.048(2)	Fe(1)–C(6)	2.055(2)
Fe(1)–C(27)	2.074(2)	Fe(1)–C(7)	2.074(2)
Fe(1)–C(28)	2.054(2)	Fe(1)–C(8)	2.056(2)
Fe(1)–C(29)	2.095(2)	Fe(1)–C(9)	2.097(2)
Fe(1)–C(25)	2.100(2)	Fe(1)–C(5)	2.083(2)

Δ_{M-C}	0.034 Å
hinge angle	3.73°
fold angle	0.020°
angle between C_5 ring planes	0.898°
twist	112.3°

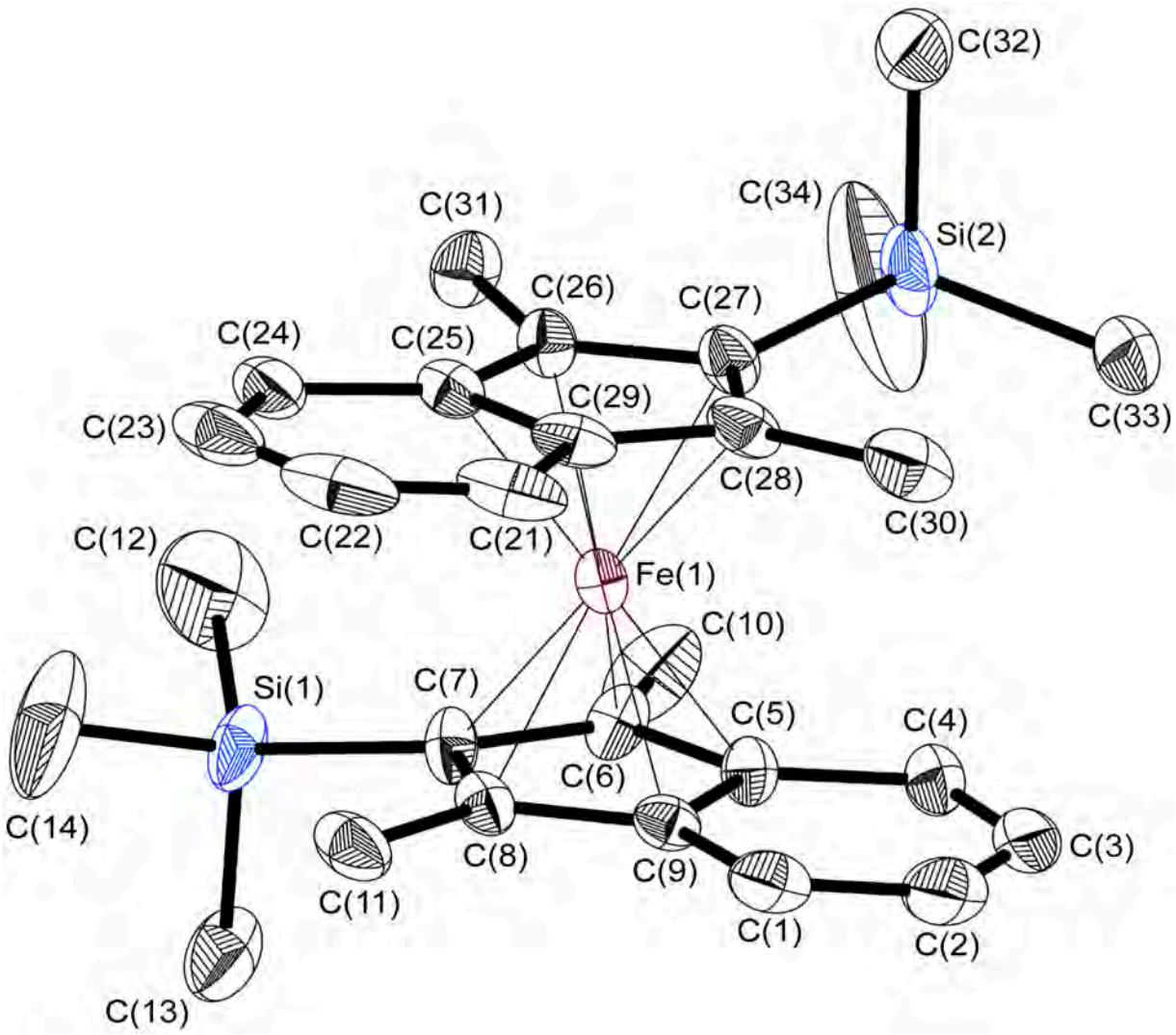

Figure 17. ORTEP of the non-hydrogen atoms of $(Ind^{2Me\text{-}1,3/Si\text{-}2})_2Fe$ illustrating the numbering scheme used in the text. Thermal ellipsoids are shown at the 50% level.

$[(Ind^{3Me\text{-}1,2,3})_2Fe]^+[DCNQ]^-$. Crystals of $[(Ind^{3Me\text{-}1,2,3})_2Fe]^+[DCNQ]^-$ were harvested from cold THF as maroon needles. An ORTEP of the molecule is given in Figure 18, which indicates the numbering scheme referred to in the text; selected bond lengths and angles are shown in Table 5.

The average Fe–C distance (2.113(18) Å) is similar to the average Fe–C distance reported in the complex bis(1,2,3,4,5,6,7-heptamethylindenyl)iron(III) 7,7,8,8-tetracyano-*p*-quinodimethanide (2.108(8) Å);[76] however it is slightly longer than the distance reported for the known ferromagnet decamethylferrocenium tetracyanoethanide (2.086 Å).[69] As in the other two molecules selected for comparison, the indenyl rings are bound in a η^5 fashion to the iron centers. The methyl groups are not substantially bent out of the C_5 plane (0.05 Å), owing to the lack of steric congestion. The hinge and fold angles of 4.56° and 4.61°, respectively, are similar to those found in the neutral bis(heptamethylindenyl)iron(II), indicating the oxidation of the metal complex has had little effect on the planarity of the ring. However, the rotation of the ligands at 102.5° is substantially closer to a gauche conformation than the $(Ind^*)_2Fe$ complex (151.3°).[22] This amount of rotation between ligands is tracked very well with the acceptor $DCNQ^-$ anions. As the indenyl rings are stacked along the *z* axis of the unit cell, the torsion angle between the two centroids of an indenyl ring and the two centroids of a $DCNQ^-$ anion is only 0.35°. This alignment is corroborated by the apparent π–π interaction between the donor and acceptor; the centroids of the two rings in the $DCNQ^-$ anion are 3.43 Å (front)

and 3.67 Å (back) from the plane of the indenyl ring. The distance between the least-squares plane of the anion and the iron center is 5.09 Å, which is comparable to magnetically ordered molecules.[69,76,81]

Each one-dimensional CT salt stack is surrounded by six other salt stacks, allowing a single ion to have a total of eight nearest neighboring ions. Of these eight neighbors, two of them are of the same charge (see Figure 19), meaning that for every bis(1,2,3-trimethylindenyl)iron(III) cation, there are six surrounding 2,3-dicyano-1,4-naphthoquinonide anions and two cations.

Table 5. Selected Bond Distances and Angles for $[(Ind^{3Me\text{-}1,2,3})_2Fe]^+$ $[DCNQ]^-$.

Atoms	Distance (Å)	Atoms	Distance (Å)
Fe(1)–C(14)	2.067(6)	Fe(1)–C(16)	2.109(6)
Fe(1)–C(4)	2.076(6)	Fe(1)–C(13)	2.134(6)
Fe(1)–C(2)	2.093(6)	Fe(1)–C(5)	2.143(6)
Fe(1)–C(15)	2.099(6)	Fe(1)–C(17)	2.153(5)
Fe(1)–C(3)	2.099(6)	Fe(1)–C(1)	2.155(5)

Δ_{M-C}	0.056 Å
hinge angle	4.56°
fold angle	4.61°
angle between C_5 ring planes	1.115°
twist between Ind′ rings	102.5°
twist between D^+ and A^-	0.35°

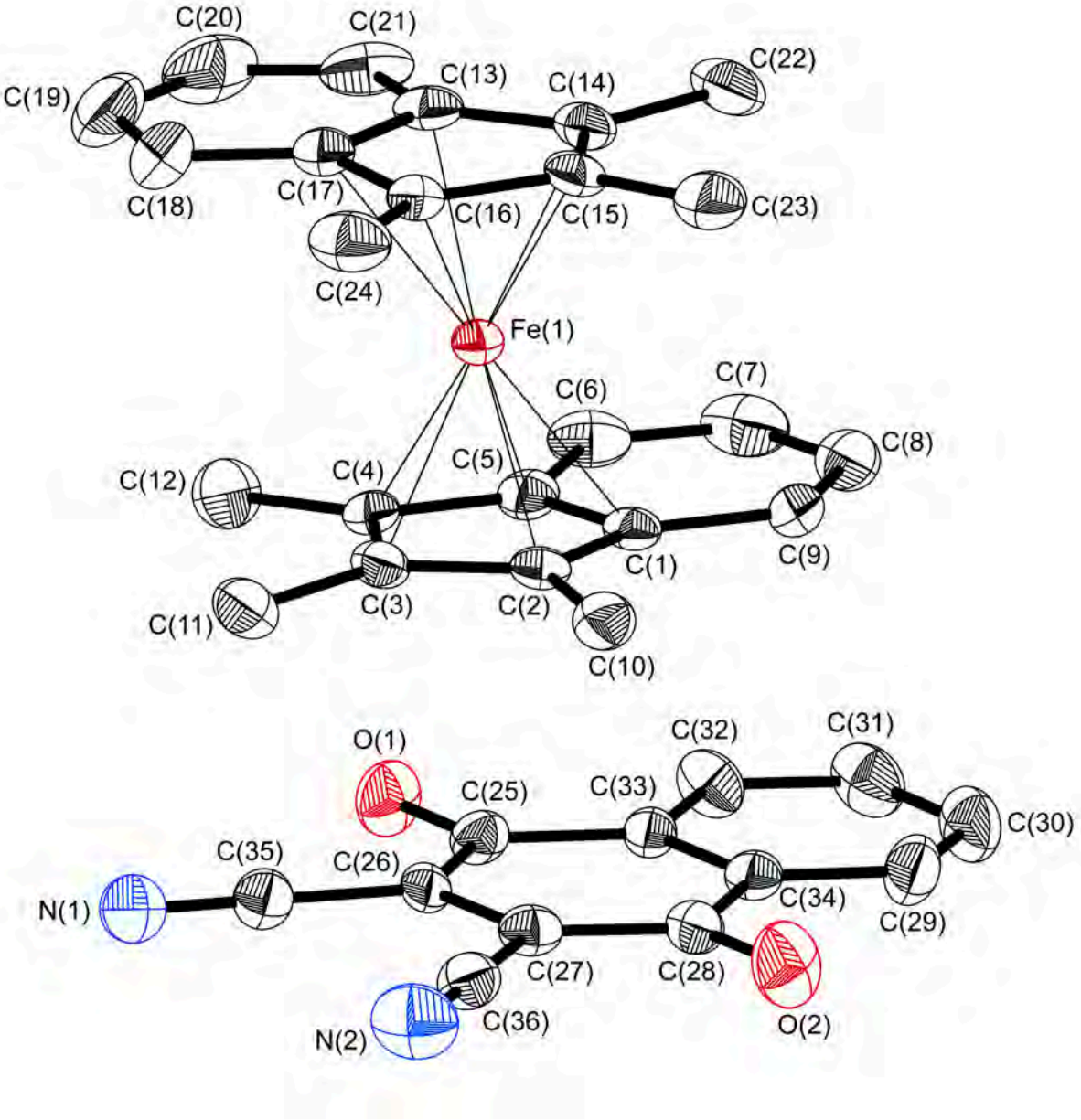

Figure 18. ORTEP of the non-hydrogen atoms of a single ion pair of $[(Ind^{3Me\text{-}1,2,3})_2Fe]^+[DCNQ]^-$, illustrating the numbering scheme used in the text. Thermal ellipsoids are shown at the 50% level.

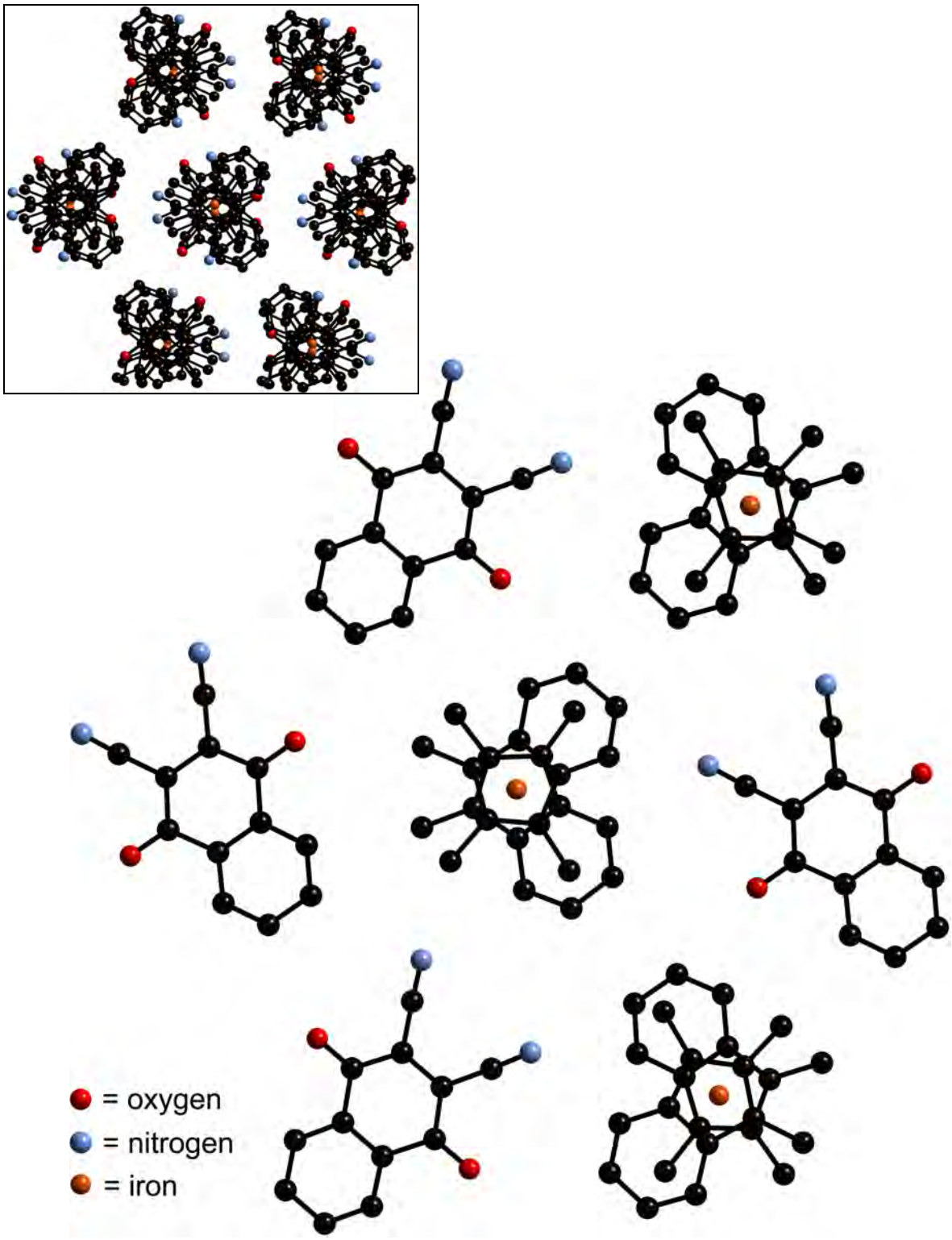

Figure 19. Cross-sectional view from above the *c*-axis of 7 CT salt ions showing 6 of the 8 closest ions to the central cation (the other 2 anions are above and below the plane). The inset shows the hexagonal arrangement of stacks. Hydrogen atoms are omitted for clarity.

Magnetic Measurements

$[(Ind^{3Me-1,2,3})_2Fe]^+[DCNQ]^-$. A microcrystalline sample (50 mg) was analyzed by SQUID magnetometry to determine the type of magnetism (para-, ferro-, antiferro-, etc.) present in the CT salt. AC susceptibility data were acquired to determine if the sample was a spin-glass. The results of the experiments are plotted in Figures 20–22. All other compounds proved to be simple paramagnetic species only (i.e., no ordering was observed down to 1.8 K). A plot of χT and 1/χ (Figure 23) for the complex $[(Ind^{2Me-1,3/Si-2})_2Fe]^+[DCID]^-$ is shown as an example of simple paramagnetism.

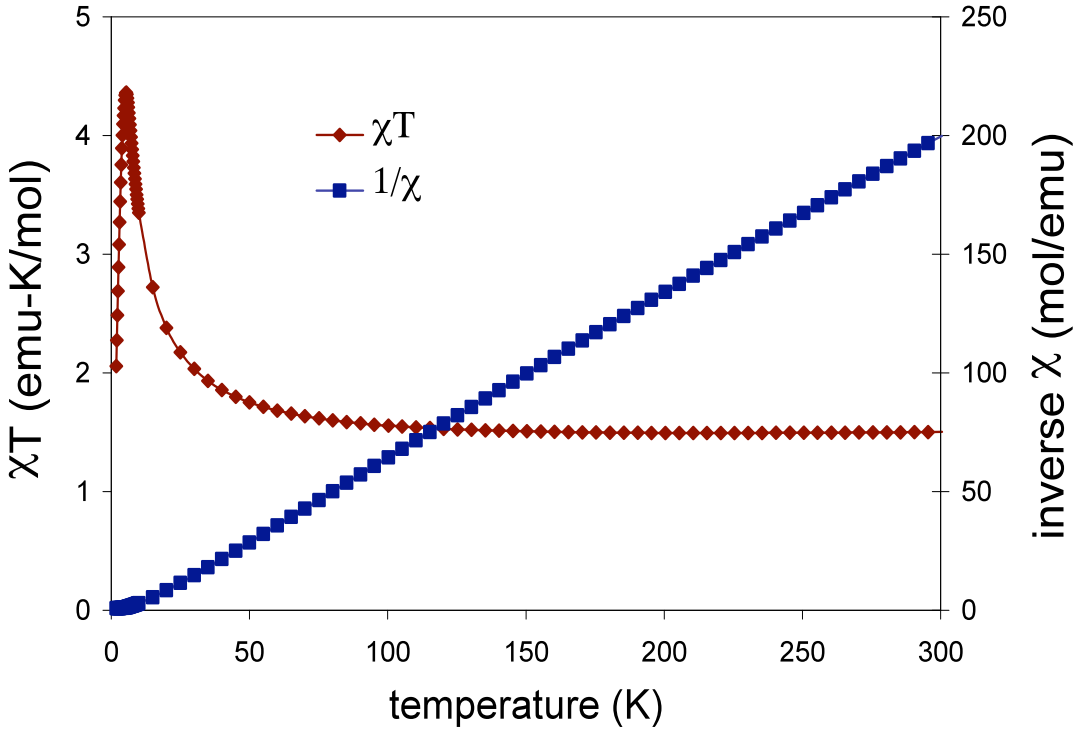

Figure 20. χT vs. T and inverse χ vs. T for $[(Ind^{3Me-1,2,3})_2Fe]^+[DCNQ]^-$ measured in 5000 G applied field.

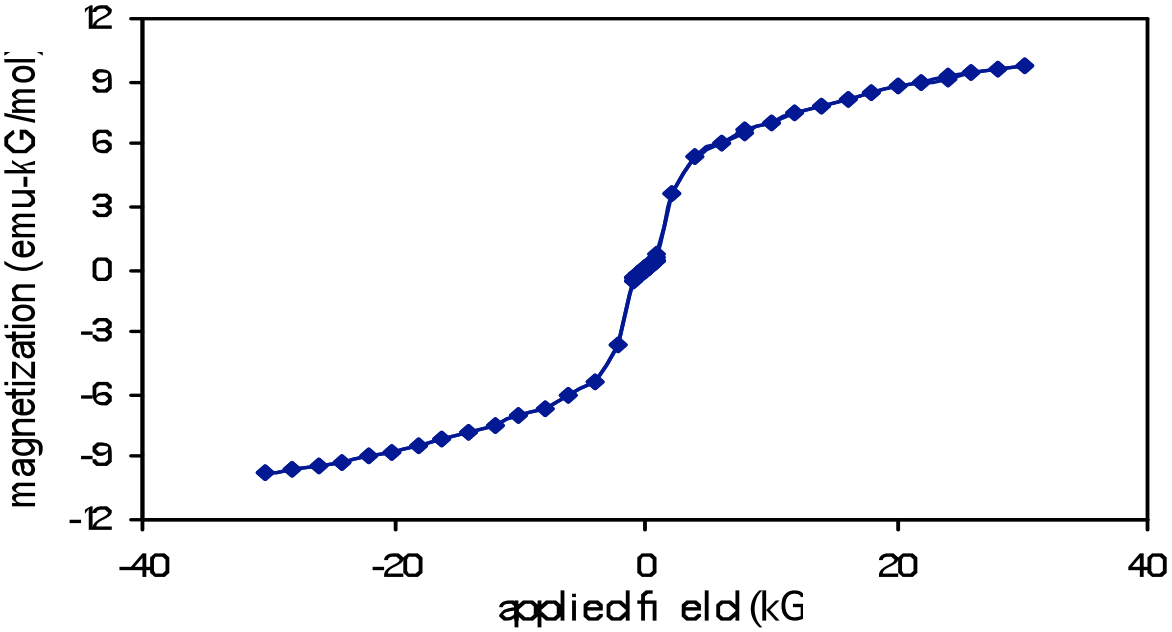

Figure 21. Magnetization vs. applied field for $[(Ind^{3Me\text{-}1,2,3})_2Fe]^+[DCNQ]^-$ at 1.8 K.

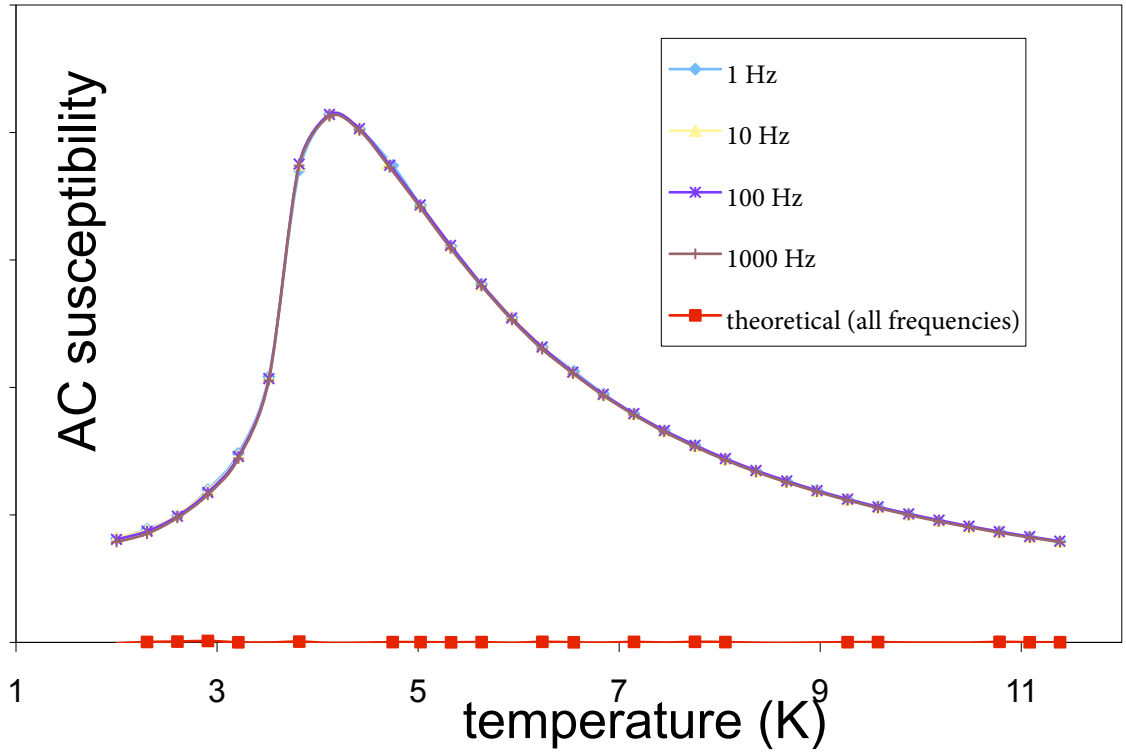

Figure 22. AC susceptibility data for $[(Ind^{3Me\text{-}1,2,3})_2Fe]^+[DCNQ]^-$.

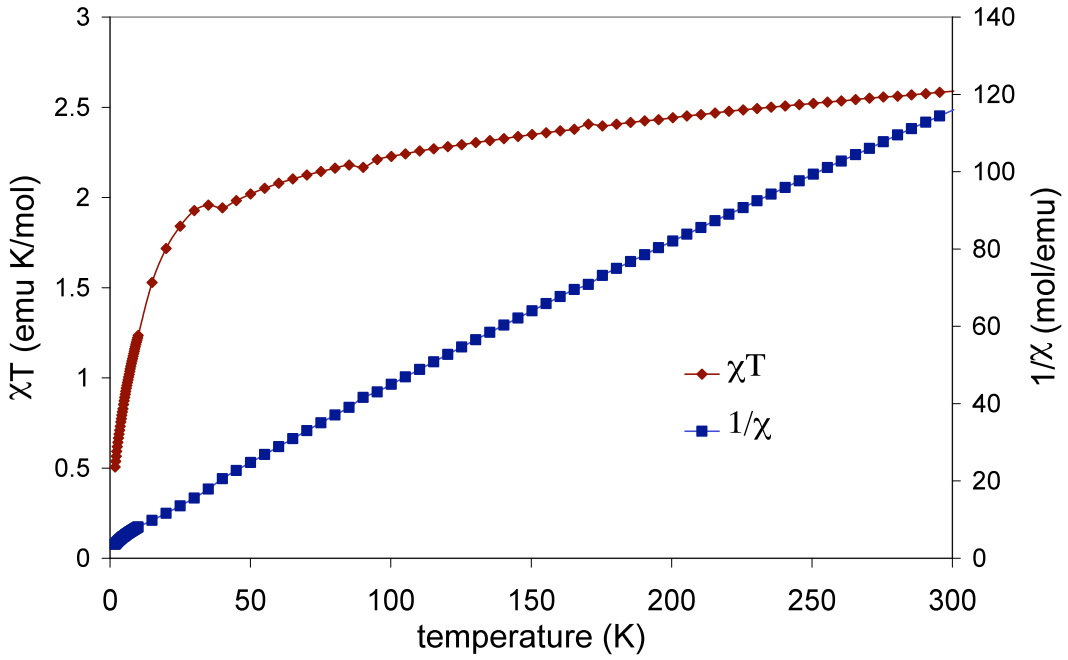

Figure 23. χT vs. T and 1/χ vs. T for $[(Ind^{2Me-1,3/Si-2})_2Fe]^+[DCID]^-$ measured in a 5000 G applied field.

Discussion

Since the time when McConnell laid the groundwork for the theory of molecular magnetism, a great number of molecules exhibiting various forms of magnetism have been synthesized. Among the first were $[Cp^*_2Fe]^+[TCNE]^-$ and $[Cp^*_2Fe]^+[TCNQ]^-$; however, broadening the range of materials that demonstrate this ordering has proven a difficult task, in part because the mechanism for long-range ordering remains controversial.[72,76,82]

Almost all the compounds of this type that exhibit long-range order (i.e. ferromagnetism or antiferromagnetism) employ a decamethylmetallocene, MCp^*_2 (M = Cr, Mn, Fe or Ni), in the role of the donor, but there has been an effort to discover other effective examples. Although various other CT salts based on alkyl-substituted ferrocenes such as decaethylferrocene[73] and octaethylferrocene[74] have been examined, the most relevant to the present discussion is a report of the reaction of bis(permethylindenyl)iron(II) and tetracyanoethylene (TCNE), 7,7,8,8-tetracyano-*p*-quinodimethane (TCNQ), and 2,3-dichloro-5,6-dicyanobenzoquinone (DDQ).[76] Although none of these three compounds unequivocally orders magnetically (i.e., no AC susceptibility or low field DC data were reported), the TCNQ analogue is reported to exhibit ferromagnetic coupling with $\theta = 6(1)$ K.

Here we describe the structure and/or magnetic properties of certain $(Ind')_2M$ (M = Cr, Mn, Fe) compounds as electron donors in CT salt complexes. We have prepared electron acceptors that more closely match the geometry of the indenyl ligand than the traditional acceptors, TCNE and TCNQ. These multi-ring donors and acceptors should be more likely to exhibit π-π interactions, leading to long range, one-dimensional stacking. According to Olivier Kahn,[72] this stacking in the solid state should lead to ferromagnetic ordering within a single $D^+A^-D^+A^-\ldots$ chain. The idea of alternating strongly positive and weakly negative spin densities (the McConnell I mechanism) along each stack in $[Cp^*_2Fe]^+[TCNE]^-$ has recently been upheld by DFT calculations.[83] However, coupling of

the spins *between* stacks is less easily controlled due to the unpredictability of nearest-neighbor packing. One might expect the arrangement of ions around each positively charged donor to be only negatively charged acceptors, although in the plane orthogonal to each 1-D chain, this is not always the case (see Figure 19).

Compared with $[Cp^*_2Fe]^+[TCNQ]^-$, the weaker magnetic ordering of $[(Ind^*)_2Fe]^+[TCNQ]^-$ may be partially explained by the fact that there are widely varying distances between iron centers (8.74 Å to 12.98 Å) resulting from the canting of the 1-D chains. This canting is likely due to crystal packing forces, but it could be influenced by the mismatched sizes and shapes of the donor and acceptor molecules. Consequential to the wide range of ion–ion distances in nearby stacks, there is likely a mix of ferromagnetic and antiferromagnetic coupling, decreasing the overall ordering of the bulk material.[76]

To attempt to address these interchain interaction problems observed in 1994 by Murphy and O'Hare, the choice of electron acceptor was varied. Bis(1,2,3-trimethylindenyl)iron(III) 2,3-dicyanonaphtho-1,4-quinonide, $[(Ind^{3Me\text{-}1,2,3})_2Fe]^+[DCNQ]^-$ orders as a metamagnet below 4.1 K (Figure 15). (A metamagnet orders antiferromagnetically in the absence of a field, and becomes a ferromagnet in the presence of a field.) We had targeted this particular compound because of the similarity between the footprint of an indenyl ring and the DCNQ acceptor. We do in fact observe π-π stacking, indicated by the donor–acceptor ring distance (3.43 to 3.67 Å) and the eclipsing of the rings, sup-

porting favorable magnetic interactions. Other CT salts described in this work employing the $(Ind^{3Me\text{-}1,2,3})_2Fe$ cation with alternate acceptors, including TCNE, TCNQ, and DCID do not magnetically order. Although the critical temperature (T_C = 6.8 K) for $[(Ind^{3Me\text{-}1,2,3})_2Fe]^+[DCNQ]^-$ is not particularly notable, the compound represents a proof of concept that efficacious non-metallocene donors exist as potential building blocks for CT salt magnets and that our ideas of crystal engineering and magnet design by pairing suitably geometrically matched donors and acceptors hold merit.

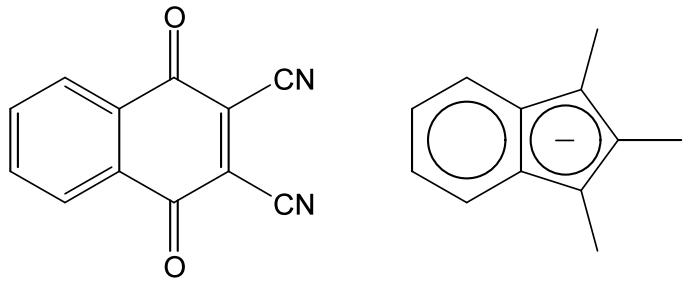

Figure 24. 2,3-Dicyanonaphtho-1,4-quinone (left) and 1,2,3-trimethylindenyl anion (right).

The chosen molecule, 2,3-dicyanonaphtho-1,4-quinone (Figure 24), is a versatile one-electron acceptor with a first reduction wave potential (+0.05 V *vs* SCE)[84] only slightly less positive than TCNE or TCNQ (-0.11 and -0.07 V, respectively).[85] DCNQ reacts readily with decamethylferrocene to form the CT salt, $FeCp^*_2[DCNQ]$,[86,87] an unusual metamagnet that exhibits slight hysteresis centered on zero applied field due to canting of the moments in the nominally antiferromagnetic state. The basic shape of the Cp* anion

is very similar to the 1,2,3-trimethylindenyl anion, so we predicted an analogous stacking pattern in the crystal structure, as is observed. $[(Ind^{3Me\text{-}1,2,3})_2Fe]^+[DCNQ]^-$ crystallizes in the same orthorhombic space group (*Pbca*) as its decamethylferrocene analogue, consisting of alternating stacks of donors and acceptors. The indenyl rings are essentially parallel, and are neither eclipsed, nor staggered, but rather twisted at 102.4°. The DCNQ ring systems are aligned to within 0.35° of the indenyl rings both above and below.

To further promote the ring alignment of the donor and acceptor in the solid state, the complex $[(Ind^{2Me\text{-}1,3/Si\text{-}2})_2Fe]^+[DCID]^-$ was synthesized. In conjunction with the π-π stacking, it was designed to fit a single methyl of each trimethylsilyl group in between the two cyano- portions of the acceptor. Given that the compound only produces a non-crystalline black powder (microcrystalline at best), the actual arrangement of the radicals in the solid state is unknown. The compound exhibits no magnetic ordering down to 1.8 K. The DCNQ analogue gives the same non-crystalline result, probably indicating the exchange of the methyl in the 2-position for a trimethylsilyl group is heavily diminishing the ability of the compounds to stack.

Conclusion

With the assumption that improved donor–acceptor alignment could enhance magnetic exchange in bis(indenyl)-based CT-salts, it seemed reasonable that an acceptor with two fused rings would provide better π-π stacking with $(Ind')_2M$ complexes than could

single ring species such as TCNQ or DDQ. The constitutional isomers DCNQ and DCID were chosen for this purpose. We have found that the CT salts of $[(Ind^{3Me\text{-}1,2,3})_2Fe]^+[TCNE]^-$ and $[(Ind^{3Me\text{-}1,2,3})_2Fe]^+[TCNQ]^-$ exhibit no evidence for magnetic order down to 1.8 K, consonant with previous data for $[(Ind^*)_2Fe]^+[TCNQ]^-$.[76] Hence the present results are consistent with the enhanced coupling in $[(Ind^{3Me\text{-}1,2,3})_2Fe]^+[DCNQ]^-$ being attributable to the geometric similarity of the DCNQ molecule and the 1,2,3-trimethylindenyl anion. Efficacious non-metallocene donors clearly exist as potential building blocks for CT salt magnets, and large, multi-ring donor-acceptor combinations appear promising for this purpose.

Attempts to vary the donor ring substituents without drastically altering the overall shape of the donor have been largely successful by the inclusion of a trimethylsilyl group in the 2-position of the ring, with or without the methyl groups in the 1- and 3-positions. Also, due to the recent mapping of the relative strength of electron donation to the metal center through substituent positions of the indenyl ligand,[10] backside (4-, 5-, 6-, and 7-position) substitution has been examined as a possible route to vary the shape of the donor without substantially affecting its oxidation potential. The ligands employed ($Ind^{2Me\text{-}4,7}$, $Ind^{Bzo\text{-}5,6}$, $Ind^{2Me\text{-}1,3/Si\text{-}2}$, and $Ind^{Si\text{-}2}$) in CT salt complexes with DCID and DCNQ have not displayed magnetic ordering. Yet through this study we have discovered that variations in the donor should also be accompanied by a rematching of the acceptor if the goal is to achieve bulk magnetism.

While no ferro- or antiferromagnetic complexes have been observed for the CT salts containing donor molecules with variations in substituent type ($SiMe_3$ or Me), number, and location on the ring, the McConnell II mechanism predicts a necessary magnetic ordering from the use of donors with two or more unpaired electrons in degenerate orbitals.[82] The simplest way to achieve this is to vary the metal center of the $(Ind')_2M$ electron donors. Bis(indenyl)chromium(II) complexes have been shown to exhibit a variety of spin states both in solution and in the solid state.[8-10] The combination of the $[(Ind^{3Me-1,2,3})_2M]^+[DCNQ]^-$ or $[DCID]^-$ CT salt framework with the unpaired spins of a d^4 chromium center did not produce a magnetically ordered species. While the slightly longer metal–C_5 ring distance may produce longer Cr···Cr distances in the 1-D chain structure, it should not affect the indenyl ring–acceptor distance, which is the critical component to coupling the positive and negative spin densities. Although this result appears to contradict both McConnell mechanisms for magnetic ordering, the unfortunate lack of crystallinity of the compound provides no structural evidence by which the differing theories of Kahn and McConnell can be tested.

CHAPTER III

MONO OR BIS(INDENYL)MANGANESE(II) COMPLEXES AND THEIR REACTIONS WITH WEAKLY COORDINATING GASES

Introduction

Homoleptic bis(indenyl) complexes of the first-row transition metals (Ind_2M; M = V, Cr, Fe, Co, and Ni) have been known for decades. Most bis(indenyl) complexes of the first row transition metals have been known since shortly after the discovery of their respective metallocenes, such as the discovery of bis(indenyl)iron(II) in 1954.[2] Notably absent from the list of metals is manganese. Given the wide range of uses for derivatives of cyclopentadienyl manganese systems (from anti-knock agents in gasoline[88] to CT salt magnets[89]), it is surprising that the typically more reactive[90] indenyl analogue has not been synthesized. There has only been one reference to it: a 1958 patent that describes bis(indenyl)manganese(II) as a brown solid.[91] Given the polymeric nature of Cp_2Mn, bis(indenyl)manganese(II) would be of interest for both its structural and magnetic properties.

Substituted bis(indenyl)manganese(II) complexes are also non-existent in the literature, suggesting possible inherent instability. This is consistent with prior investigations into the synthesis of such complexes.[80] Bulky substituents that tend to reduce metal center reactivity, such as the trimethylsilyl group, have not been thoroughly examined in an in-

denyl ligand framework for their ability to encapsulate and protect a manganese center. Once stable complexes are synthesized through the use of various substituted ligands, their reactivity with small molecules will be explored.

Mono-ring complexes of manganese(II) and their reactions with H_2 and N_2. Transition metal complexes that bind dinitrogen have been known since 1965,[92] and the first complex of manganese with N_2 was reported in 1967,[93] although characterization demonstrating any metal–nitrogen interaction was wanting. The first verifiable complex was $CpMn(CO)_2N_2$,[94] which exhibits a dinitrogen stretch at 2165 cm^{-1}.[95] Most of the manganese complexes display a linear (end-on) dinitrogen ligand (i.e., a M–N–N bond angle of 180°), as would be expected based on the isoelectronic nature of N_2 and CO. End-on complexes of dinitrogen with transition metals experience the same π-backbonding as with carbonyl complexes (Figure 25), and the stronger electron donating metal center produces a lower C–O stretching energy. More recently, there has been an effort to examine other coordination types of the N_2 ligand, specifically side-on and bridging.[96-99] In these coordination modes, the non-polarity of the N–N bond leads to the lack of a characteristic stretching frequency in the IR spectrum. ^{15}N NMR and x-ray crystallography are typical methods of characterization; however, the high lability of the N_2 ligand along with the paramagnetism of the complexes limit the applicability of these techniques.

In most transition metal complexes, the bis(indenyl) framework is much more reactive than its cyclopentadienyl counterpart.[16,18,22,90,100-102] Chirik, et al., has recently reported

the use of the indenyl ligand in zirconium complexes that bind dinitrogen.[59,103] In these compounds, variations of the substituents on the 1- and 3-positions alter the ability of the compounds to bind N_2. Certain substituted (Cp)(indenyl)zirconium(IV) dichloride complexes, which are stable to N_2 for weeks, react quickly to form dimeric systems through bridging N_2 ligands once the metal centers are reduced to zirconium(II). We found the indenyl manganese(II) system attractive for its exposed metal center and small energetic differences between coordination modes of the ligands, supporting the weak binding associated with metal–N_2 interactions.

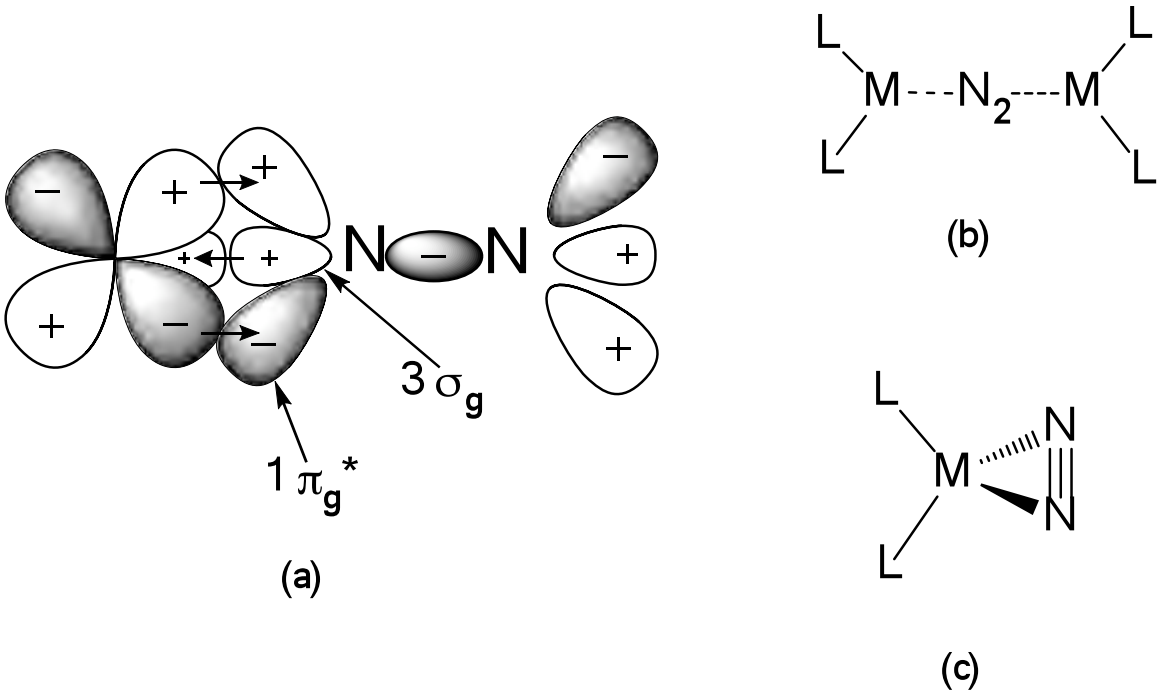

Figure 25. (a) Orbital interactions showing the bonding of an end-on dinitrogen ligand to a metal *d* orbital. Bridging (b) and side-on (c) dinitrogen ligands typically do not show IR stretching frequencies.

Transition metal complexes that bind H_2 (without oxidizing to a metal hydride) are even more rare, with the first discovery in 1984.[104] In this case, an agostic interaction to a hydrogen on a cyclohexyl or isopropyl group is interrupted by H_2, then reengaged by the removal of the H_2 atmosphere. This reversibility is characteristic of the binding of the neutral H_2 ligand. In one case of an indenyl ruthenium complex, the ring is protonated, forming a cationic ruthenium hydride with the indenyl ligand slipping to an η^6-bound six-membered ring.[105] To our knowledge there have been no reports of reversible binding of the H_2 ligand in an indenyl complex.

There have been relatively few paramagnetic species known to coordinate N_2,[106] but of the few, most tend to have only one or two unpaired electrons.[107-110] Diphosphine ligands are often used in complexes known to bind N_2,[111,112] but there has also been some work with the Cp and indenyl ligands.[59,103,113] Here we report on the first manganese(II) system to bind N_2.

Experimental

General Considerations. All manipulations were performed with the rigorous exclusion of air and moisture using Schlenk or glovebox techniques. Proton (^{1}H) NMR experiments were obtained on a Bruker DPX-300 spectrometer at 300 MHz, or a Bruker DPX-400 at 400 MHz, and were referenced to residual proton resonances of THF-d_8 (δ 3.58) and $CDCl_3$ (δ 7.26). Elemental analyses were performed by Desert Analytics (Tuc-

son, AZ). Melting points were determined on a Laboratory Devices Mel-Temp apparatus in sealed capillaries. Mass spectra were obtained using a Hewlett-Packard 5890 Series II gas chromatograph/mass spectrometer.

Materials. Anhydrous manganese(II) chloride (99.98%) was purchased from Alfa Aesar and used as received. Indene, 2-methylindene, *n*-butyl lithium, potassium bis(trimethylsilyl)amide, *p*-toluenesulfonic acid, and anhydrous, unstabilized tetrahydrofuran (THF) were purchased from Aldrich and used as received. Chlorotrimethylsilane, 2-bromo-1-indanol, and anhydrous pentane were purchased from Acros and used as received. Hexanes, toluene, and diethyl ether were distilled under nitrogen from potassium benzophenone ketyl. $CDCl_3$ (Cambridge Isotope) was dried with 4A molecular sieves prior to use. Toluene-d_8 (Aldrich) and THF-d_8 (Cambridge Isotope) were vacuum distilled from Na/K (22/78) alloy and stored over 4A molecular sieves prior to use.

Magnetic Measurements. Solution magnetic susceptibility measurements were performed on a Bruker DRX-400 spectrometer using the Evans' NMR method.[31-35] 5–10 mg of the paramagnetic material was dissolved in toluene-d_8 in a 1.0 mL volumetric flask. The solution was thoroughly mixed, and approximately 0.5 mL was placed in a NMR tube containing a toluene-d_8 capillary. The calculations required to determine the number of unpaired electrons based on the data collected have been described elsewhere.[36]

Solid state magnetic susceptibility data were obtained by Prof. Gordon T. Yee (Virginia Tech) on a Quantum Designs MPMS SQUID magnetometer in a field of 70,000 G.

Control of the sample temperature ranges from 1.8 to 300 K. To handle the extremely air- and moisture-sensitive compounds, the previously described sample holder was used;[14] the diamagnetic susceptibility of the sample holder was accepted as the average value of the measurements on several identical sample holders. The diamagnetic correction for each complex was estimated from Pascal's constants.

Synthesis of 1-Methylindene, $HInd^{Me\text{-}1}$, and 1,3-Dimethylindene, $HInd^{2Me\text{-}1,3}$. Indene (90%) was purified by vacuum distillation (150 mTorr and 25 °C) from a yellow oil to a clear, colorless liquid. In a 250 mL Schlenk flask under N_2, 15.0 g (0.129 mol) of indene was dissolved in 100 mL of diethyl ether, and the flask was chilled to 0 °C. Dropwise addition of a 2.5 M hexane solution of *n*-butyl lithium (52 mL, 0.129 mol) through an addition funnel led to the immediate formation of lithium indenide. After stirring for 2 h, the reaction was maintained at 0 °C, and 20.1 g (0.142 mol) of methyl iodide was added dropwise into the flask. The reaction was then warmed to room temperature and was allowed to continue stirring for 4 h. The reaction was quenched via the addition of a cold, dilute solution of NH_4Cl in water. The mixture was stirred to allow the complete dissolution of the precipitated lithium chloride in the aqueous layer. The aqueous layer was separated and washed with hexanes (2 × 20 mL). The hexanes layers were combined, dried with anhydrous $MgSO_4$, filtered, and the solvent was removed by rotary evaporation. The product, which was isolated in quantitative yield, was confirmed to be $HInd^{Me\text{-}1}$ with GC/MS ($m^+ = 130$) and ^1H NMR.[47]

To add a second methyl group to the indene, a portion of the 1-methylindene was degassed and returned to the glovebox. In a 250 mL Schlenk flask under N_2, 7.00 g (0.0538 mol) of 1-methylindene was dissolved in 100 mL of diethyl ether, and the flask was chilled to 0 °C. Dropwise addition of a 2.5 M hexane solution of *n*-butyl lithium (22.5 mL, 0.0538 mol) through an addition funnel led to the immediate formation of lithium 1-methylindenide. After stirring for 2 h, the reaction was maintained at 0 °C, and 7.64 g (0.0538 mol) of methyl iodide was added dropwise into the flask. The reaction was then warmed to room temperature and was allowed to continue stirring for 4 h. The reaction was quenched via the addition of a cold, dilute solution of NH_4Cl in water. The mixture was stirred to allow the complete dissolution of the precipitated lithium chloride in the aqueous layer. The aqueous layer was separated and washed with hexanes (2 × 20 mL). The hexanes layers were combined, dried with anhydrous $MgSO_4$, filtered, and the solvent was removed by rotary evaporation. The product, which was isolated in quantitative yield, was confirmed to be $HInd^{2Me\text{-}1,3}$ with GC/MS ($m^+ = 144$) and ^1H NMR.[114]

Synthesis of 1,3-bis(trimethylsilyl)indene, $HInd^{2Si\text{-}1,3}$. Indene (90%) was purified by vacuum distillation (150 mTorr and 25 °C) from a yellow oil to a clear, colorless liquid. In a 250 mL Schlenk flask under N_2, 15.0 g (0.129 mol) of indene was dissolved in 100 mL of diethyl ether, and the flask was chilled to 0 °C. Dropwise addition of a 2.5 M hexane solution of *n*-butyl lithium (52 mL, 0.129 mol) through an addition funnel led to the immediate formation of lithium indenide. Stirring was maintained as the solution

warmed to room temperature. After 14 hours, trimethylsilyl chloride (14.0 g, 0.129 mol) was slowly syringed into the flask. The reaction was quenched via the addition of a cold, dilute solution of NH_4Cl in water. The mixture was stirred to allow the complete dissolution of the precipitated lithium chloride in the aqueous layer. The aqueous layer was separated and washed with hexanes (2 × 20 mL). The hexanes layers were combined, dried with anhydrous $MgSO_4$, and transferred to another 250 mL Schlenk flask under N_2. *n*-Butyl lithium (52 mL of a 2.5 M solution, 0.129 mol) in hexane was added dropwise at 0 °C. The solution was refluxed for 2 h. On cooling to 0 °C, trimethylsilyl chloride (14.0 g, 0.129 mol) was slowly syringed into the flask. The reaction was quenched via the addition of a cold, dilute solution of NH_4Cl in water. The mixture was stirred to allow the complete dissolution of the precipitated lithium chloride in the aqueous layer. The aqueous layer was separated and washed with hexanes (2 × 20 mL). The hexanes layers were combined, dried with anhydrous $MgSO_4$, and the solvent was removed with rotary evaporation. The product (22.5g, 67% yield) was a light yellow oil that was confirmed to be 1,3-bis(trimethylsilyl)indene with GC/MS ($m^+ = 260$) and ^1H NMR prior to further use.[48]

Synthesis of 4,7-Dimethylindene, $HInd^{2Me\text{-}4,7}$. Synthesis of this compound was described in Chapter 1.

Synthesis of 2-Trimethylsilylindene, $HInd^{Si\text{-}2}$. In a 500 mL round bottom flask, 2-bromoindan-1-ol (10.0 g, 0.0469 mol) was dissolved in 250 mL of toluene, and the flask was fitted with a Dean-Stark trap and condenser. The solution was warmed to 50

°C for full dissolution of the indanol. A few crystals of *p*-toluenesulfonic acid were added to the solution, and the solution was refluxed until slightly more than 0.5 mL of water was collected in the trap. After cooling to room temperature, the solution was washed with dilute $NaHCO_3$ solution and separated into aqueous and organic layers. The aqueous layer was washed twice with 20 mL of toluene, and the organic layers were combined and dried over $MgSO_4$. After filtration, the toluene was removed by rotary evaporation to yield 2-bromoindene (7.96 g, 0.0408 mol, 87% yield) as orange crystals. GC/MS characterization of 2-bromoindene (m^+ = 194, 196) was consistent with the expected spectra of this compound.

The 2-bromoindene was brought into the glovebox, and added to 35 mL of anhydrous THF in a 125 mL addition funnel. Magnesium turnings (4.0 g, 0.163 mol) and 50 mL of anhydrous THF were added to a 500 mL 3-neck round bottom flask fitted with the addition funnel, reflux condenser, rubber septum, and magnetic stir bar. The flask was placed on a Schlenk line, and 2 mL of bromoethane was syringed into the flask to activate the magnesium turnings. After about 5 minutes the THF began to boil, so this solution was syringed out of the flask and discarded. To avoid contamination with trace amounts of ethyl magnesium bromide, the turnings were washed 3 times with 40 mL of anhydrous THF. Eighty mL of THF was added to the Mg^0 turnings before 5 mL of the solution of 2-bromoindene was quickly added to the flask to initiate the reaction. After the reaction was cooled to -15 °C, the remaining solution was added dropwise over 90 minutes. Upon

complete addition of the 2-bromoindene solution, the reaction was warmed to room temperature, and 4.5 g (5.2 mL, 0.0414 mol) of trimethylsilyl chloride was added over 5 minutes. The reaction was refluxed for 1 h with constant stirring. After being allowed to cool to room temperature, the reaction was stirred for 14 h. Cold water was added to quench the reaction, and MgBrCl precipitated from solution. The mixture was decanted to remove any unreacted magnesium, and the mixture was washed with water until no more MgBrCl was noticeable. Diethyl ether (200 mL) was also added to the mixture to get a separation of the organic and aqueous layers. The ether layer was dried over $MgSO_4$ before filtration. The removal of solvent via rotary evaporation resulted in a yellow-orange oil. This product was purified to a clear, colorless liquid by vacuum distillation over 45–48 °C and 110 mTorr pressure. The product (1.71 g) was formed in 19% overall yield. It was confirmed to be 2-trimethylsilylindene with GC/MS ($m^+ = 188$).

Synthesis of Potassium 2-Trimethylsilylindenide, K[Ind$^{Si\text{-}2}$]. 2-Trimethylsilyl)indene (1.71 g, 0.00910 mol) was degassed and dissolved in 20 mL of toluene in a 250 mL Erlenmeyer flask. Potassium bis(trimethylsilyl)amide, $K[N(SiMe_3)_2]$ (1.72 g, 0.00864 mol), was dissolved in toluene and added dropwise to the indene while stirring. The reaction was stirred for 14 h before adding 100 mL of hexanes. A white precipitate formed and was filtered over a medium-porosity glass frit. The precipitate was washed with hexanes (2 × 30 mL) and dried under vacuum to yield 2.06 g (88%). The product was confirmed to be K[Ind$^{Si\text{-}2}$] by ^{1}H NMR (400 MHz) in THF-d_8: δ 0.34 (singlet, 9H, $Si(CH_3)_3$);

5.67 (singlet, 2H, *CH* in 1,3-position); 6.31 (doublet of doublets, 2H, *CH* in 4,7-position); 7.09 (multiplet, 2H, *CH* in 5,6-position).

Synthesis of Potassium 1-Methylindenide, K[Ind^{Me-1}]. 1-Methylindene (5.00 g, 0.0384 mol) was degassed and dissolved in 20 mL of toluene in a 250 mL Erlenmeyer flask. Potassium bis(trimethylsilyl)amide, K[N(SiMe$_3$)$_2$] (6.90 g, 0.0446 mol), was dissolved in toluene and added dropwise to the indene while stirring. The reaction was stirred 14 h before adding 100 mL of hexanes. A white precipitate formed and was filtered over a medium-porosity glass frit. The precipitate was washed with hexanes (2 × 30 mL) and dried under vacuum to obtain 4.81 g (83% yield). The product was confirmed to be K[Ind^{Me-1}] by comparison with the ^{1}H NMR spectrum of the known Li[Ind^{Me-1}].[115]

Synthesis of Potassium 1,3-Dimethylindenide, K[Ind$^{2Me-1,3}$]. 1,3-Dimethylindene (1.70 g, 0.0118 mol) was degassed and dissolved in 20 mL of toluene in a 250 mL Erlenmeyer flask. Potassium bis(trimethylsilyl)amide, K[N(SiMe$_3$)$_2$] (2.25 g, 0.0113 mol), was dissolved in toluene and added dropwise to the indene while stirring. The reaction was stirred 14 h before adding 100 mL of hexanes. A bright yellow precipitate formed and was filtered over a medium-porosity glass frit. The precipitate was washed with hexanes (2 × 30 mL) and dried under vacuum to yield 1.765 g (86%). The product was confirmed to be K[Ind$^{2Me-1,3}$] by comparison with the ^{1}H NMR spectrum of the known Li[Ind$^{2Me-1,3}$].[116]

Synthesis of Potassium 4,7-Dimethylindenide, K[Ind$^{2Me-4,7}$]. Synthesis of this compound was described in Chapter 1.

Synthesis of Potassium 2-Methylindenide, K[Ind^{Me-2}]. 2-Methylindene (5.00 g, 0.0384 mol) was degassed and dissolved in 20 mL of toluene in a 250 mL Erlenmeyer flask. Potassium bis(trimethylsilyl)amide, K[N(SiMe$_3$)$_2$] (6.90 g, 0.0446 mol), was dissolved in toluene and added dropwise to the indene while stirring. The reaction was stirred 14 h before adding 100 mL of hexanes. A light yellow precipitate formed and was filtered over a medium-porosity glass frit. The precipitate was washed with hexanes (2 × 30 mL) and dried under vacuum to yield 5.37 g (92%). The product was confirmed to be K[Ind^{Me-2}] by ^{1}H NMR (400 MHz) in THF-d_8: δ 2.38 (singlet, 3H, *CH*$_3$); 5.71 (singlet, 2H, *CH* in 1,3-position); 6.29 (doublet of doublets, 2H, *CH* in 4,7-position); 7.11 (multiplet, 2H, *CH* in 5,6-position).[78]

Synthesis of Potassium 1,3-Bis(trimethylsilyl)indenide, K[Ind$^{2Si-1,3}$]. 1,3-Bis(trimethylsilyl)indene (4.00 g, 0.0154 mol) was degassed and dissolved in 20 mL of toluene in a 250 mL Erlenmeyer flask. Potassium bis(trimethylsilyl)amide K[N(SiMe$_3$)$_2$] (2.92 g, 0.0146 mol) was dissolved in toluene and added dropwise to the indene while stirring. The reaction was stirred 24 h before adding 150 mL of hexanes. A white precipitate formed and was filtered over a medium-porosity glass frit. The precipitate was washed with hexanes (2 × 30 mL) and dried under vacuum to yield 3.40 g (78%). The product was confirmed to be K[Ind$^{2Si-1,3}$] by ^{1}H NMR (400 MHz) in THF-d_8: δ 0.23 (singlet, 18H, 6 *CH*$_3$

on $SiMe_3$); 6.53 (doublet of doublets, 2H, *CH* in 4,7-position); 6.95 (singlet, 1H, *CH* in 2-position); 7.49 (doublet of doublets, 2H, *CH* in 5,6-position).[80]

Attempted Synthesis of 1-Methylindenyl Manganese(II) Chloride, $(Ind^{Me\text{-}1})MnCl$. $MnCl_2$ (0.3033 g, 2.41 mmol) was added to a 250 mL Erlenmeyer flask fitted with a stir bar. THF (40 mL) was added and the flask was stirred at –25 °C for 1 h to disperse the $MnCl_2$. Lithium 1-methylindenide (0.3281 g, 2.41 mmol) was dissolved in 100 mL of THF and added to a 125 mL addition funnel. The $Li[Ind^{Me\text{-}1}]$ was added drop-wise into the flask containing $MnCl_2$. The mixture became olive green and it was allowed to stir for 7 h. Inspection of the reaction revealed a large amount of unreacted $MnCl_2$, so the reaction was brought to reflux for 30 min. The color changed to golden, and all the $MnCl_2$ dissolved. After stirring at room temperature for 14 h, the solution had not visibly changed, so the THF was removed under vacuum over several hours, leaving a brown-black solid. Upon stirring with pentane, the insoluble solid was dispersed into a fine, light brown powder. The pentane was decanted and the solid was collected in a Soxhlet extraction apparatus. An extraction was performed with 25 mL of toluene, yielding an orange solution. No crystals grew from toluene solutions at cold temperatures, or by the diffusion of aliphatic solvents into toluene solutions. Upon allowing the toluene solution to evaporate over several days, yellow orange crystalline material formed in 7% yield (37 mg); however, it was acicular and unsuitable for x-ray crystallography. Satisfactory elemental analysis could not be obtained.

Attempted Synthesis of 2-Methylindenyl Manganese(II) Chloride, $(Ind^{Me-2})MnCl$. $MnCl_2$ (0.3800 g, 3.03 mmol) was added to a 250 mL Erlenmeyer flask fitted with a stir bar. THF (50 mL) was added and the flask was stirred for 1 h to disperse the $MnCl_2$. Potassium 2-methylindenide (0.5100 g, 3.03 mmol) was dissolved in 100 mL of THF and added to a 125 mL addition funnel. The $K[Ind^{Me-2}]$ was added dropwise over 2 h into the flask containing $MnCl_2$. The reaction was allowed to stir overnight before the removal of the solvent under vacuum left an orange oil. Pentane (30 mL) was added to the flask with stirring, causing the oil to precipitate a yellow powder. The pentane was decanted, and the yellow precipitate was collected in a Soxhlet extraction apparatus. An extraction was performed with 30 mL of hexanes and resulted in an orange solution and a light yellow solid. The solution was placed in the freezer at 10 °C and gradually cooled to –15 °C over the course of 2 days. A ring of white and orange solid had deposited around the inside of the flask, so the remaining solution was allowed to evaporate at room temperature. After 3 days, diamond-shaped orange crystals had formed above the orange and white material. The crystals were air and moisture sensitive, and the compound proved to be highly paramagnetic, as evidenced by the absence of detectable ^1H NMR resonances. After crystals had been selected for structural characterization, the amount of product remaining was too small for further analysis.

Synthesis of Bis(2-methylindenyl)manganese(II), $(Ind^{Me-2})_2Mn$. $MnCl_2$ (0.302 g, 2.41 mmol) was added to a 250 mL Erlenmeyer flask fitted with a stir bar. THF

(20 mL) was added and the flask was stirred at –25 °C for 1 h to disperse the $MnCl_2$. Potassium 2-methylindenide (0.810 g, 4.82 mmol) was dissolved in 10 mL of THF at room temperature and added dropwise into the flask containing $MnCl_2$, yielding an orange solution. After 1 d of stirring, the solvent was removed under vacuum to leave a light cream-colored solid in the flask. Pentane and hexanes (50:50 of 3 × 10 mL) was added to extract the organometallic product from KCl. A toluene extract (3 × 10 mL) was also collected; however, no crystals grew from solutions at cold temperatures or by the diffusion of aliphatic solvents into the toluene solution. Removal of the toluene solvent under vacuum produced an orange oil that proved difficult to characterize. When the reaction was conducted in BHT-stabilized THF, the aryloxide product $(Ind^{Me\text{-}2})_3Mn_2(BHT)$ was isolated.

Synthesis of Bis(1-methylindenyl)manganese(II), $(Ind^{Me\text{-}1})_2Mn$. $MnCl_2$ (0.302 g, 2.41 mmol) was added to a 250 mL Erlenmeyer flask fitted with a stir bar. THF (20 mL) was added and the flask was stirred at –25 °C for 1 h to disperse the $MnCl_2$. Potassium 1-methylindenide (0.810 g, 4.82 mmol) was dissolved in 100 mL of THF and added to a 125 mL addition funnel. The $K[Ind^{Me\text{-}1}]$ was added dropwise into the flask containing $MnCl_2$. The mixture became olive green and it was allowed to stir for 7 h. Inspection of the reaction revealed a large amount of unreacted $MnCl_2$, so the reaction was brought to reflux for 30 min. The color changed to golden, and all the $MnCl_2$ had dissolved. After stirring at room temperature for 14 h, the solution had not visibly changed, so the THF was removed under vacuum over several hours, leaving a brown-black solid. Upon stirring

with pentane, this insoluble solid was dispersed into a fine, light brown powder. A Soxhlet extraction was performed with 25 mL of toluene, yielding an orange solution. No crystals grew from solutions at cold temperatures or by the diffusion of aliphatic solvents into the toluene solution. Upon allowing the toluene solution to evaporate over several days, highly-branched, yellow-orange crystalline material formed in 37% yield. Satisfactory elemental analysis could not be obtained.

Synthesis of Bis(1,3-dimethylindenyl)manganese(II), $(Ind^{2Me-1,3})_2Mn$. $MnCl_2$, (0.2066 g, 1.64 mmol) was added to a 125 mL Erlenmeyer flask fitted with a stir bar and 30 mL of THF. The flask was stirred at –30 °C for 1 h to disperse the $MnCl_2$. Potassium 1,3-dimethylindenide (0.5988 g, 3.28 mmol) was dissolved in 10 mL of THF and chilled to –30 °C. The $K[Ind^{2Me-1,3}]$ was added dropwise to the flask containing $MnCl_2$. The reaction was allowed to stir overnight at –30 °C before the removal of the solvent under vacuum left an orange oil. The oil was insoluble in pentane and hexanes, but adding diethyl ether precipitated KCl, leaving an orange solution. Upon filtration and evaporation of this solution, 0.414 g of an orange oil remained (74% yield). This oil was dissolved in toluene, and after several attempts at crystallization, the best result was a yellow-orange powder (mp 226–229 °C (dec)). Solution magnetic susceptibility measurements with ^1H NMR showed highly paramagnetic material (μ_B = 5.47 for the assumed $(Ind^{2Me-1,3})_2Mn$ complex).

Synthesis of Bis(4,7-dimethylindenyl)manganese(II), $(Ind^{2Me-4,7})_2Mn$. $MnCl_2$ (0.1084 g, 0.864 mmol) was added to a 125 mL Erlenmeyer flask fitted with a stir bar and 30 mL of THF. The flask was stirred at –25 °C for 45 min. to disperse the $MnCl_2$. Potassium 4,7-dimethylindenide (0.314 g, 1.72 mmol) was dissolved in 10 mL of THF and chilled to –25 °C. The $K[Ind^{2Me-4,7}]$ was added dropwise to the flask containing $MnCl_2$. The reaction was allowed to stir overnight at room temperature before the removal of the solvent under vacuum left an orange residue. Three extractions with pentane (20 mL each) were performed yielding a colorless solution. This solution contained a colorless oil which was later determined to be coupled $Ind^{2Me-4,7}$. The orange precipitate was extracted into 40 mL of toluene, and 30 mL of this solution was placed in the freezer at –20 °C for 3 days. Dark orange crystalline blocks grew from the solution in 26% yield (0.0582g), mp 260-265 °C. Magnetic susceptibility was not obtained due to the lack of solubility in toluene. Anal. Calcd. for $C_{22}H_{22}Mn$: C, 77.41; H, 6.50. Found: C, 78.86; H, 6.72.

Synthesis of 2,4,7-Trimethylindenyl Manganese(II) Chloride, $(Ind^{3Me-2,4,7})MnCl$. $MnCl_2$ (0.3178 g, 2.53 mmol) was added to a 250 mL Erlenmeyer flask fitted with a stir bar. THF (50 mL) was added and the flask was stirred for 1 h to break up the $MnCl_2$. Potassium 2,4,7-trimethylindenide (0.4976 g, 2.53 mmol) was dissolved in 100 mL of THF and added to a 125 mL addition funnel. The $K[Ind^{3Me-2,4,7}]$ was added dropwise over 2 h into the flask containing $MnCl_2$. The reaction was allowed to stir overnight before the removal of the solvent under vacuum left an orange oil. Pentane (30 mL) was

added to the flask with stirring, causing the precipitation of a yellow powder that was removed by filtration. After several washes (5 × 10 mL), the bright-yellow pentane filtrates were combined in a 125 mL Erlenmeyer flask. The flask was slowly cooled from room temperature to –20 °C over 5 days. Long yellow crystalline rods grew from this solution, mp 130–133 °C. Anal. Calcd. for $C_{12}H_{13}MnCl \cdot THF$: C, 60.10; H, 6.62; Mn, 17.18. Found: C, 60.10; H, 6.84; Mn, 17.2. Solution magnetic susceptibility (μ_{eff}^{298K}): 1.7 μ_B.

Synthesis of Bis(2,4,7-trimethylindenyl)manganese(II), $(Ind^{3Me\text{-}2,4,7})_2Mn$. $MnCl_2$ (0.4630 g, 3.68 mmol) was added to a 250 mL Erlenmeyer flask fitted with a stir bar. THF (50 mL) was added and the flask was stirred for 1 h to disperse the $MnCl_2$. Potassium 2,4,7-trimethylindenide (1.45 g, 7.38 mmol) was dissolved in 100 mL of THF and added to a 125 mL addition funnel. The $K[Ind^{3Me\text{-}2,4,7}]$ was added dropwise over 2 h into the flask containing $MnCl_2$. The reaction was allowed to stir overnight before the removal of the solvent under vacuum left an orange oil. Pentane (30 mL) was added to the flask with stirring, causing the precipitation of a yellow powder that was removed by filtration. After several washes (5 × 10 mL), the orange pentane filtrates were combined into a 125 mL Erlenmeyer flask. The pentane solvent was allowed to evaporate at room temperature over 2 days, affording a dark orange crystalline solid. Anal. Calcd. for $C_{24}H_{26}Mn$: C, 78.03; H, 7.09; Mn, 14.87. Found: C, 78.64; H, 7.31; Mn, 14.9. Solution magnetic susceptibility (μ_{eff}^{298K}): 5.68 μ_B.

Synthesis of Bis(2-trimethylsilylindenyl)manganese(II), $(Ind^{Si-2})_2Mn$. $MnCl_2$ (0.154 g, 1.22 mmol) was added to a 125 mL Erlenmeyer flask fitted with a stir bar and 20 mL of THF. The starting material was pulverized into a fine powder by stirring at –30 °C for 30 min. Potassium 2-trimethylsilylindenide (0.554 g, 2.45 mmol) was dissolved in 30 mL of THF and was added dropwise over 15 min into the flask containing $MnCl_2$. The reaction immediately turned bright orange, and it was allowed to stir overnight before the removal of the solvent under vacuum. A dark orange solid remained, and pentane (30 mL) was added to the flask with stirring. The resulting orange solution was filtered to remove a yellow precipitate. After several washes (5 × 10 mL), the bright orange pentane filtrates were combined in a 125 mL Erlenmeyer flask. This flask was canted and placed under a slight vacuum, allowing the pentane solvent to evaporate at room temperature over 2 h, affording red-orange crystalline rods, mp 118–122 °C. Anal. Calcd. for $C_{24}H_{30}Si_2Mn$: C, 67.10; H, 7.04; Found: C, 68.87; H, 7.21. Solution magnetic susceptibility (μ_{eff}^{298K}): 5.72 μ_B.

Synthesis of Bis(1,3-bis(trimethylsilyl)indenyl)manganese(II), $(Ind^{2Si-1,3})_2Mn$. $MnCl_2$ (0.0424 g, 0.337 mmol) was added to a 125 mL Erlenmeyer flask fitted with a stir bar and 20 mL of THF. The starting material was pulverized into a fine powder by stirring at 0 °C for 30 min. Potassium 1,3-bis(trimethylsilyl)indenide (0.2011 g, 0.673 mmol) was dissolved in 30 mL of THF and was added dropwise over 15 min into the flask containing $MnCl_2$. The reaction immediately turned bright orange, and it was allowed to

stir overnight before the removal of the solvent under vacuum. A waxy white and orange solid remained, and pentane (20 mL) was added to the flask with stirring. A light orange solution was filtered to remove a yellow precipitate. After several washes (3 × 10 mL), the bright orange pentane filtrates were combined into a 125 mL Erlenmeyer flask. This flask was canted and the pentane solvent was allowed to evaporate at room temperature over 24 h, affording orange crystalline plates, mp 170–174 °C. Anal. Calcd. for $C_{30}H_{41}Si_4Mn$: C, 62.78; H, 8.08; Found: C, 61.79; H, 8.09. Solution magnetic susceptibility (μ_{eff}^{298K}): 5.87 μ_B.

Synthesis of Bis(indenyl)manganese(II), $(Ind)_2Mn(thf)_2$. $MnCl_2$ (0.1574 g, 1.25 mmol) was added to 30 mL of THF in a 125 mL Erlenmeyer flask fitted with a stir bar. This flask was kept at –25 °C for the duration of the reaction. Potassium indenide (0.3859 g, 2.50 mmol) was dissolved in 15 mL of THF and slowly added to the flask. The reaction turned yellow-orange and was allowed to stir overnight. The following day, the THF was removed under vacuum. Extractions with pentane, toluene, and diethyl ether yielded only lightly colored solutions, so a THF extraction was performed. Each extraction mixture was filtered over a medium-porosity glass frit. After no crystals had grown from several attempts with the individual solutions, the filtrates were combined. In three weeks, orange crystals had deposited on the sides of the flask (0.135 g, 19% yield). Anal. Calcd. for $C_{26}H_{30}O_2Mn$: C, 72.72; H, 7.04; Mn, 12.79; Found: C, 71.65; H, 6.87; Mn, 12.12. Solution magnetic susceptibility (μ_{eff}^{298K}): 5.56 μ_B.

Reaction of 2,4,7-Trimethylindenyl Manganese(II) Chloride with N_2. Solutions of approximately 0.015 M to 0.045 M ($Ind^{3Me-2,4,7}$)MnCl(thf) in toluene or pentane or a mixture of the two were prepared in a 300 mL pressure vessel. These yellow solutions were degassed, chilled to 0°C, and kept under an evacuated atmosphere before the introduction of nitrogen. Upon pressurizing the flask to approximately 1 atm, the yellow solutions turned emerald green. Further cooling of the solutions to -78 °C produced deep blue solutions. Warming the solutions to room temperature rapidly caused the blue color to revert to yellow. Reaction vessels charged with 100 psi of N_2 have yielded initially green solutions at room temperature, but the color fades to yellow over 2 minutes. After their formation at -78 °C and 1 atm of N_2, deep blue solutions persist under vacuum if the temperature is not increased; however, the solid that is deposited from the removal of solvent is yellow. Attempts to isolate this blue compound have been unsuccessful.

Reaction of 2,4,7-Trimethylindenyl Manganese(II) Chloride with H_2. A solution of approximately 0.015 M ($Ind^{3Me-2,4,7}$)MnCl in a mixture of toluene and pentane was prepared in a 10 mL pressure vessel. The solution was degassed and cooled to -78 °C. Hydrogen gas was pressurized to 20 psi above the solution, and the yellow color quickly changed to a deep purple. This reaction was reversible by warming to room temperature; however, the compound was still O_2-sensitive, as evidenced by the characteristic brown MnO_2 precipitate observed upon exposure.

General Procedures for X-ray Crystallography. A suitable crystal of each sample was located, attached to a glass fiber, and mounted on a Bruker SMART APEX II CCD Platform diffractometer for data collection at 173(2) K or 100(2) K. Data collection and structure solutions for all molecules were conducted at the X-ray Crystallography Facility at the University of Rochester by Dr. William W. Brennessel or at the University of California, San Diego by Dr. Arnold L. Rheingold. Data resolution of 0.84 Å was considered in the data reduction (SAINT 7.53A, Bruker Analytical Systems, Madison, WI). The intensity data were corrected for absorption and decay (SADABS). All calculations were performed using the current SHELXTL suite of programs.[45] Final cell constants were calculated from a set of strong reflections measured during the actual data collection. Relevant crystal and data collection parameters for each of the compounds are given in Appendix B.

The space groups were determined based on systematic absences (where appropriate) and intensity statistics. A direct-methods solution was calculated that provided most of the non-hydrogen atoms from the E-map. Several full-matrix least-squares/difference Fourier cycles were performed that located the remainder of the non-hydrogen atoms. All non-hydrogen atoms were refined with anisotropic displacement parameters. All hydrogen atoms were placed in ideal positions and refined as riding atoms with relative isotropic displacement parameters.

X-ray Crystallography of $(Ind^{Me-2})_3Mn_2(BHT)$. Bright yellow crystalline blocks of $(Ind^{Me-2})_3Mn_2(BHT)$ (BHT = butylhydroxytoluene anion) were obtained by preparing a concentrated hexanes solution at room temperature and allowing for the slow evaporation of the solvent. After some initial precipitation of amorphous solid, crystals grew along the walls of the flask. The crystals were dried under vacuum prior to data collection. An initial set of cell constants was calculated from reflections produced from four sets of 20 frames. These sets of frames were oriented such that orthogonal wedges of reciprocal space were surveyed. This produced orientation matrices determined from 38 reflections. The final cell constants were calculated from the *xyz* centroids of 3861 strong reflections as described in the general procedures.

Data was collected using MoKα radiation (graphite monochromator) with a frame time of 45 s and a detector distance of 3.98 cm. A randomly oriented region of reciprocal space was surveyed to the extent of 1 sphere, and to a resolution of 0.84 Å. Three major sections of frames were collected with 0.50° steps in ω at four different ϕ settings and a detector position of –38° in 2θ.

The space group $P2_1/c$ was determined as described in the general procedures. One of the terminal 2-methylindenyl ligands is modeled as disordered over two positions (55:45). The final full matrix least-squares refinement converged to $R1$ = 0.0465 and $wR2$ = 0.1270 (F^2, all data).

X-ray Crystallography of $(Ind^{2Me-4,7})_2Mn$. Dark orange crystals of $(Ind^{2Me-4,7})_2Mn$ were harvested by preparing a concentrated toluene solution, which was cooled to –30 °C. The crystals were separated from the mother liquor and dried under vacuum prior to data collection. An initial set of cell constants was calculated from reflections produced from three sets of 20 frames. These sets of frames were oriented such that orthogonal wedges of reciprocal space were surveyed. This produced orientation matrices determined from 40 reflections. The final cell constants were calculated from the *xyz* centroids of 3353 strong reflections as described in the general procedures.

Data was collected using MoKα radiation (graphite monochromator) with a frame time of 45 s and a detector distance of 3.98 cm. A randomly oriented region of reciprocal space was surveyed to the extent of 1 sphere, and to a resolution of 0.84 Å. Three major sections of frames were collected with 0.50° steps in ω at four different ϕ settings and a detector position of –38° in 2θ.

The space group *C*2/*c* was determined as described in the general procedures. The final full matrix least-squares refinement converged to $R1 = 0.3547$ and $wR2 = 0.2960$ (F^2, all data).

X-ray Crystallography of $[K(1,4\text{-dioxane})_{1.5}][(Ind^{2Me-4,7})_3Mn]$. Bright orange crystals of $[K(1,4\text{-dioxane})_{1.5}][(Ind^{2Me-4,7})_3Mn]$ were harvested by preparing a concentrated 1,4-dioxane solution. The crystals were separated from the mother liquor and dried under vacuum prior to data collection. An initial set of cell constants was calculated from

reflections produced from three sets of 20 frames. These sets of frames were oriented such that orthogonal wedges of reciprocal space were surveyed. This produced orientation matrices determined from 40 reflections. The final cell constants were calculated from the *xyz* centroids of 4170 strong reflections as described in the general procedures.

Data was collected using MoKα radiation (graphite monochromator) with a frame time of 45 s and a detector distance of 5.00 cm. A randomly oriented region of reciprocal space was surveyed to the extent of 1 sphere, and to a resolution of 0.84 Å. Three major sections of frames were collected with 0.50° steps in ω at four different ϕ settings and a detector position of –38° in 2θ.

The space group $P6_3$ was determined as described in the general procedures. There is one position for the Mn atom and one for the K atom that accounts for the major component. The structure shows disorder from a minor component involving 6 additional Mn atom positions and 2 additional K atom positions. The disorder is such that the edge of each major component's indenyl five-membered ring is nearly co-linear with the edge of each minor component's five-membered ring in the same plane, and the six-membered rings are shared (although the fused carbon atoms are shifted by one atom). Although the *R*1 value decreases by nearly a percent if these peaks are refined, the overall model was not improved significantly. Ultimately, this minor disorder was not modeled. One of the terminal dioxane solvent molecules is modeled as disordered over two positions (54:46). Possible non-merohedral twin laws were also examined, but without success. The final full

matrix least-squares refinement converged to $R1$ = 0.0758 and $wR2$ = 0.2191 (F^2, all data).

X-ray Crystallography of (Ind$^{3Me-2,4,7}$)MnCl. Yellow crystalline rods of (Ind$^{3Me-2,4,7}$)MnCl were harvested by preparing a concentrated pentane solution, which was slowly cooled to –30 °C. The crystals were separated from the mother liquor and dried under vacuum prior to data collection. An initial set of cell constants was calculated from reflections produced from three sets of 20 frames. These sets of frames were oriented such that orthogonal wedges of reciprocal space were surveyed. This produced orientation matrices determined from 37 reflections. The final cell constants were calculated from the *xyz* centroids of 7683 strong reflections as described in the general procedures.

Data was collected using MoKα radiation (graphite monochromator) with a frame time of 45 s and a detector distance of 3.98 cm. A randomly oriented region of reciprocal space was surveyed to the extent of 1 sphere, and to a resolution of 0.84 Å. Three major sections of frames were collected with 0.50° steps in ω at four different ϕ settings and a detector position of –38° in 2θ.

The space group $P\bar{1}$ was determined as described in the general procedures. There are two independent molecules in the asymmetric unit, both centered on crystallographic inversion centers; thus one half of each is unique. One of the THF ligands is modeled as disordered over two positions (58:42). The final full matrix least-squares refinement converged to $R1$ = 0.0470 and $wR2$ = 0.1419 (F^2, all data).

X-ray Crystallography of $(Ind^{Si\text{-}2})_2Mn$. Bright orange crystals of $(Ind^{Si\text{-}2})_2Mn$ were harvested by preparing a concentrated pentane solution and allowing it to evaporate at room temperature. The crystals were dried under vacuum prior to data collection. An initial set of cell constants was calculated from reflections produced from three sets of 20 frames. These sets of frames were oriented such that orthogonal wedges of reciprocal space were surveyed. This produced orientation matrices determined from 54 reflections. The final cell constants were calculated from the *xyz* centroids of 6014 strong reflections as described in the general procedures.

Data was collected using MoKα radiation (graphite monochromator) with a frame time of 60 s and a detector distance of 3.98 cm. A randomly oriented region of reciprocal space was surveyed to the extent of 1 sphere, and to a resolution of 0.84 Å. Three major sections of frames were collected with 0.30° steps in ω at four different ϕ settings and a detector position of –28° in 2θ.

The space group $P2_1/c$ was determined as described in the general procedures. There are two independent molecules in the unit cell, both centered on crystallographic inversion centers; thus one half of each is unique. The final full matrix least-squares refinement converged to $R1 = 0.0317$ and $wR2 = 0.0858$ (F^2, all data).

X-ray Crystallography of $(Ind^{2Si\text{-}1,3})_2Mn$. Orange crystalline plates of $(Ind^{2Si\text{-}1,3})_2Mn$ were harvested by preparing a concentrated pentane solution and allowing it to evaporate at room temperature. The crystals were dried under vacuum prior to data collec-

tion. An initial set of cell constants was calculated from reflections produced from three sets of 20 frames. These sets of frames were oriented such that orthogonal wedges of reciprocal space were surveyed. This produced orientation matrices determined from 46 reflections. The final cell constants were calculated from the *xyz* centroids of 9917 strong reflections as described in the general procedures.

Data was collected using MoKα radiation (graphite monochromator) with a frame time of 60 s and a detector distance of 3.98 cm. A randomly oriented region of reciprocal space was surveyed to the extent of 1 sphere, and to a resolution of 0.84 Å. Three major sections of frames were collected with 0.30° steps in ω at four different ϕ settings and a detector position of –28° in 2θ.

The space group $Pna2_1$ was determined as described in the general procedures. There are two independent molecules in the asymmetric unit; however, they appear to be chemically identical. The final full matrix least-squares refinement converged to $R1$ = 0.0530 and $wR2$ = 0.1385 (F^2, all data).

X-ray Crystallography of $(Ind)_2Mn(thf)_2$. Orange crystals of $(Ind)_2Mn(thf)_2$ were harvested by preparing a solution of 2:2:2:1 pentane, toluene, diethyl ether, and THF. The solution sat undisturbed for 3 weeks at room temperature while crystals grew. The crystals were dried under vacuum prior to data collection. An initial set of cell constants was calculated from reflections produced from three sets of 20 frames. These sets of frames were oriented such that orthogonal wedges of reciprocal space were surveyed. This

produced orientation matrices determined from 28 reflections. The final cell constants were calculated from the *xyz* centroids of 5278 strong reflections as described in the general procedures.

Data was collected using MoKα radiation (graphite monochromator) with a frame time of 60 s and a detector distance of 3.98 cm. A randomly oriented region of reciprocal space was surveyed to the extent of 1 sphere, and to a resolution of 0.84 Å. Three major sections of frames were collected with 0.30° steps in ω at four different ϕ settings and a detector position of –28° in 2θ.

The space group $P\bar{1}$ was determined as described in the general procedures. There are two independent but nearly identical molecules in the asymmetric unit. The final full matrix least-squares refinement converged to $R1 = 0.0308$ and $wR2 = 0.0819$ (F^2, all data).

Results

Ligand Synthesis. Various alkylated and trimethylsilylated indenes were prepared by modifications of standard procedures.[27,37,47-49] These included $HInd^{Me-2}$, $HInd^{2Me-4,7}$, $HInd^{3Me-2,4,7}$, $HInd^{Si-2}$, $HInd^{2Me-1,3}$, $HInd^{2Si-1,3}$. Once the desired hydrocarbon ring was synthesized and purified by vacuum distillation, the alkali metal indenide salt was prepared via deprotonation reaction with a strong base. Reactions with potassium bis(trimethylsilyl)amide were performed in toluene, followed by precipitation of the potassium indenide salt by the addition of hexanes. The indenides were isolated from

bis(trimethylsilyl)amine by filtration and rigorous washing with additional hexanes. The indenides were similarly isolated and washed prior to reactions with transition metal salts.

Synthesis of Substituted Bis(indenyl)manganese(II) and Indenyl Manganese(II) Chloride Complexes. Once the appropriate indenide salts were prepared, the corresponding bis(indenyl)manganese(II) complexes could be readily synthesized by salt metathesis elimination reactions in THF. Butylhydroxytoluene (BHT) is a stabilizer found in small quantities (0.025%) in THF. The butylhydroxytoluene anion is likely formed from the deprotonation of BHT with the various potassium indenide ligands. In reactions where larger volumes of THF are used, this presents a problem, as noted in isolation of a BHT/Mn aryloxide complex in the attempt to form $(Ind^{Me\text{-}2})_2Mn$. This small amount of $K^+[BHT]^-$ reacted as an aryloxide with the $MnCl_2$, becoming a bridging ligand between two manganese centers. As a result, all subsequent reactions were performed in unstabilized THF. In each case, one or two equivalents of the appropriate alkali metal indenide salt was allowed to react with anhydrous manganese(II) chloride in THF (eq 4); the resulting mixtures were generally stirred overnight to ensure complete reaction. Following the removal of THF under vacuum, a less polar solvent (pentane, hexanes, or toluene) was added to extract the manganese species, precipitating the alkali metal chloride in the process. The solubility of bis(indenyl)manganese(II) complexes in most non-polar solvents provides an efficient means by which to separate the desired materials from the rest of the reaction mixture.

$$n\,A[Ind'] + MnCl_2 \xrightarrow{THF} \xrightarrow{Hex\ or\ Pent} (Ind')_n MnCl_x + n\,ACl \qquad (4)$$

$n = 1,\ x = 1;\ or\ n = 2,\ x = 0$

$A = Li\ or\ K$

Solid State Structures

$(Ind^{2Si\text{-}1,3})_2Mn$. Crystals of $(Ind^{2Si\text{-}1,3})_2Mn$ were harvested from a pentane solution as orange plates. An ORTEP of the molecule is given in Figure 26, which indicates the numbering scheme referred to in the text; selected bond lengths and angles are shown in Table 6.

The average Mn–C ring distance observed for this species (2.42(1) Å) is lengthened from that observed in other bis(indenyl) complexes of first row transition metal species. This particular ligand set $(Ind^{2Si\text{-}1,3})_2M$ is known and has been structurally characterized for vanadium (see Chapter 4), chromium,[8] and iron[77] which all have shorter M–C bond distances (av 2.30(1) Å, 2.20(2) Å, and 2.09(1) Å, respectively). This distance must be less of a function of the steric bulk of the ligand and more due to the ionic radius of each metal appropriate for the observed spin-state.

Among the known $(Ind^{2Si\text{-}1,3})_2M$ complexes, there is a similar degree of rotation between the ligands that alleviates the steric strain. For these compounds, this twist occurs over the range of 86.3° to 94.3°, while the manganese complex lies outside this range at

96.99°. The trimethylsilyl groups are bent out of the C_5 planes by an average of 0.233 Å, with a maximum value of 0.265 Å. Each trimethylsilyl group that is situated between the two of the other ligand, Si(2) and Si(4), is pushed farther out of the plane than the less sterically hindered $SiMe_3$ groups. This is consistent with other out-of-plane bending distances for $SiMe_3$ of the known complexes, although $(Ind^{2Si\text{-}1,3})_2Cr$ has by far the largest at 0.42 Å. As with the analogous complexes, the indenyl rings are bound in an η^5 fashion to the manganese center and exhibit a range (Δ_{Mn-C} = 0.102 Å) that is also comparable. The molecule is moderately bent, with an angle of 7.99° between the two C_5 planes, and yet the chromium analogue has an even more noticeable angle between the planes (11.5°).

Table 6. Selected Bond Distances and Angles for $(Ind^{2Si\text{-}1,3})_2Mn$.

Atoms	Distance (Å)	Atoms	Distance (Å)
Mn(1)–C(1)	2.524(4)	Mn(1)–C(10)	2.474(4)
Mn(1)–C(2)	2.424(4)	Mn(1)–C(11)	2.318(4)
Mn(1)–C(3)	2.304(4)	Mn(1)–C(12)	2.307(4)
Mn(1)–C(4)	2.340(4)	Mn(1)–C(13)	2.476(4)
Mn(1)–C(5)	2.494(4)	Mn(1)–C(14)	2.545(4)

Δ_{M-C}	0.102 Å
hinge angle	3.805°
fold angle	0.923°
angle between C_5 ring planes	7.986°
twist	96.99°

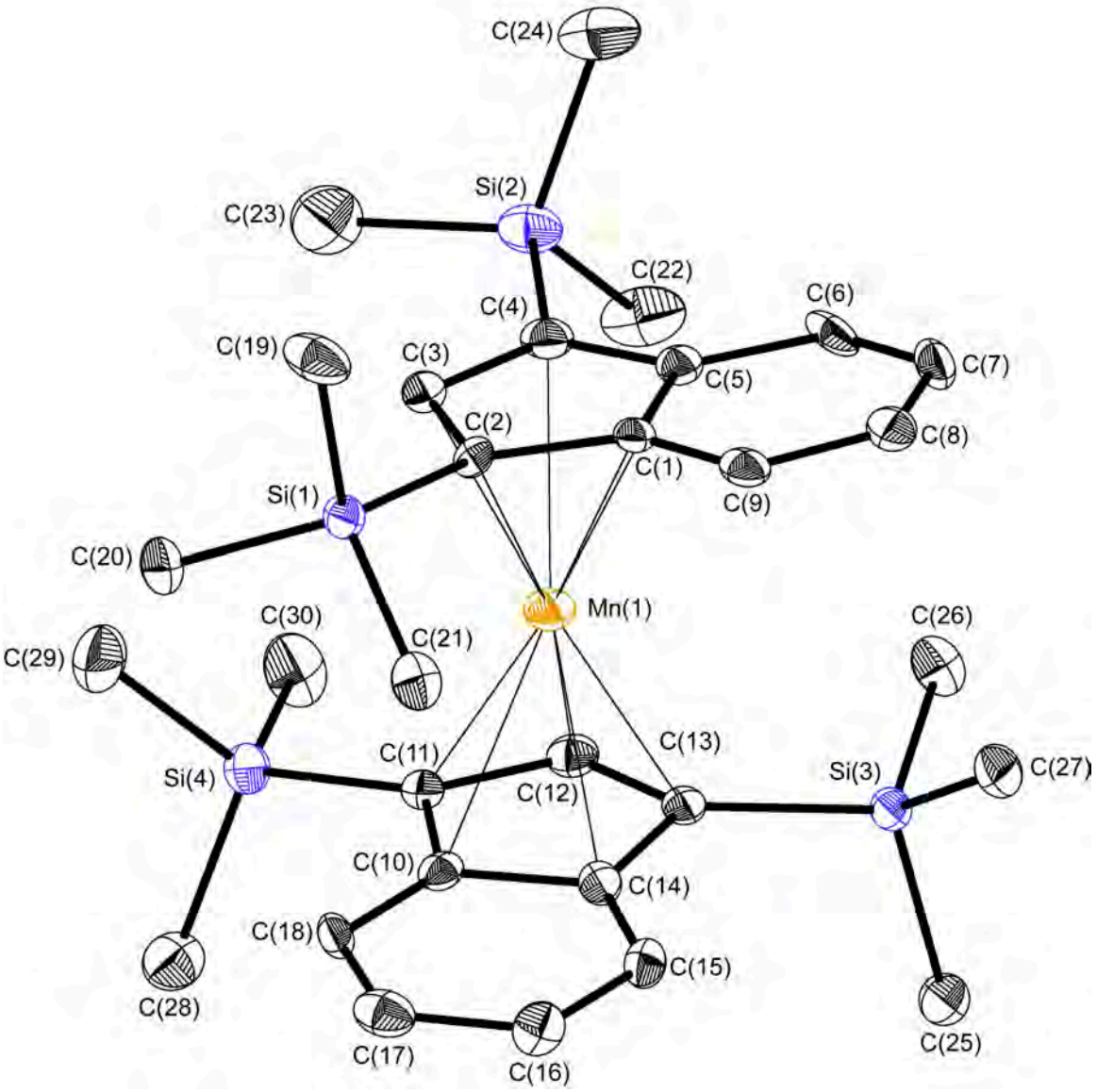

Figure 26. ORTEP of the non-hydrogen atoms of $(Ind^{2Si-1,3})_2Mn$ illustrating the numbering scheme used in the text. Thermal ellipsoids are shown at the 50% level.

$(Ind^{Si\text{-}2})_2Mn$. Crystals of $(Ind^{Si\text{-}2})_2Mn$ were harvested from a pentane solution as orange blocks. Only half of the molecule is unique, as the manganese lies on an inversion center. An ORTEP of the molecule is given in Figure 27, which indicates the numbering scheme referred to in the text; selected bond lengths and angles are shown in Table 7.

The average Mn–C ring distance observed for this species (2.41(3) Å) is virtually identical to that observed in $(Ind^{2Si\text{-}1,3})_2Mn$. The ligands are bound in an η^5 fashion to the manganese center, and are staggered 180° with respect to on another. The trimethylsilyl group is bent out of the C_5 plane by 0.277 Å, which is slightly longer than the distances found in $(Ind^{2Si\text{-}1,3})_2Mn$. Given that the molecule could rotate to a gauche conformation to alleviate some of this angle bending, this more sterically hindered molecule overcomes the $SiMe_3$ bending by crystal packing forces. The inversion center necessarily removes any non-coplanarity between the C_5 rings. This, as an adjunct to the small degree of ring slippage (Δ_{Mn-C} = 0.088 Å), suggests the core of the molecule is much like an η^5,η^5-manganocene.

Table 7. Selected Bond Distances and Angles for $(Ind^{Si\text{-}2})_2Mn$.

Atoms	Distance (Å)	Angle	Degree
Mn(1)–C(1)	2.4821(15)	hinge	2.650
Mn(1)–C(2)	2.3257(15)	fold	0.526
Mn(1)–C(3)	2.3131(14)	C_5 ring planes	0
Mn(1)–C(4)	2.3989(15)	twist	180
Mn(1)–C(5)	2.5249(15)		
	Δ_{M-C} = 0.088 Å		

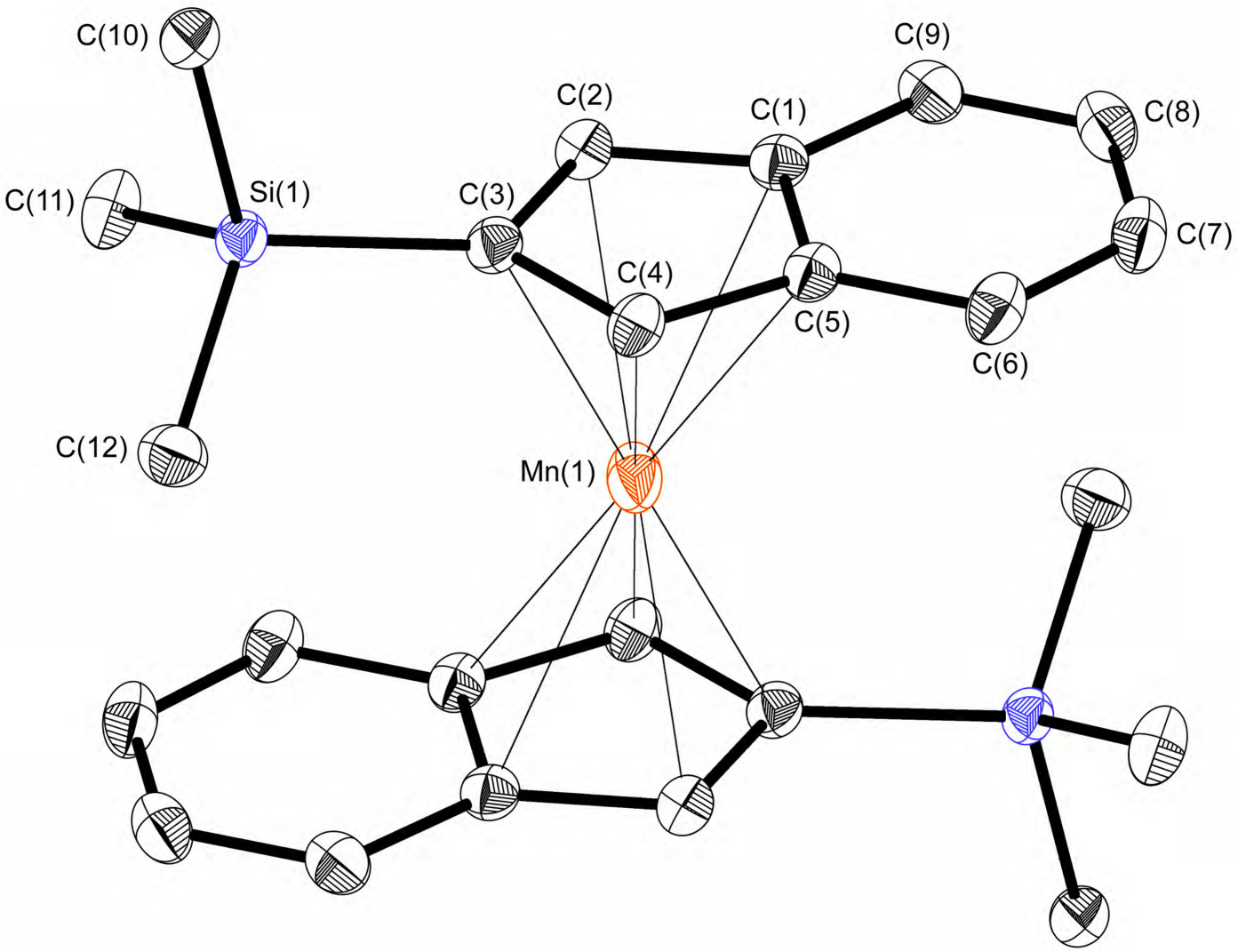

Figure 27. ORTEP of the non-hydrogen atoms of $(Ind^{Si\text{-}2})_2Mn$ illustrating the numbering scheme used in the text. Thermal ellipsoids are shown at the 50% level.

$(Ind^{Me\text{-}2})_2(\mu\text{-}Ind^{Me\text{-}2})Mn_2(\mu\text{-}BHT)$. Crystals of $(Ind^{Me\text{-}2})_3Mn_2(BHT)$ were harvested from a pentane solution as yellow plates. An ORTEP of the molecule is given in Figure 28, which indicates the numbering scheme referred to in the text; selected bond lengths and angles are shown in Table 8.

Deprotonated butylhydroxytoluene is found as a bridging ligand in the complex (see the Results section for a discussion of the provenance of this ligand). The average Mn–O distance is 2.045(3) Å.

There are two terminal and one bridging 2-methylindenyl groups. The terminal groups appear to slip to an η^3 coordination, yet the Mn(1)–C(8) and Mn(1)–C(9) distances (2.56 Å and 2.58 Å, respectively) are not significantly longer than the same positions of the $(Ind^{2Si\text{-}1,3})_2Mn$ molecule (2.55 Å). If all ten Mn–C distances are considered, the average distance is 2.48(2) Å, only slightly elongated from the accepted η^5 coordination of the rings in the previously mentioned complexes. The amount of ring slippage (Δ_{Mn-C} = 0.198 Å) suggests the ligands have shifted toward an η^3 coordination, although this number typically approaches 0.3 Å before a C_5 ring is considered η^3-bound.[117] The view of the $(Ind^{Me\text{-}2})Mn$ fragment orthogonal to the C_5 plane shows the centering of the manganese atom as somewhat skewed toward the front portion of the ring. The hinge angles (4.36° and 4.97°) are also more noticeable in this complex than in the η^5-bound ligands of the manganese complexes with trimethylsilyl substituents (Figures 26 and 27).

There is no question as to the hapticity of the bridging 2-methylindenyl ligand; it is η^1-bound to both manganese atoms. The angle Mn(1)–C(19)–C_5 ring plane is 108.3° and Mn(2)–C(21)–C_5 ring plane is 102.8°, and both Mn–C(20) distances are greater than 2.95 Å. The distances of the 1- and 3-positions to the metal centers are 2.259(1) Å and 2.282(1) Å (C(19)–Mn(1) and C(21)–Mn(2), respectively), with a hinge angle of 4.33°. The Mn(1)–Mn(2) distance in the complex is 3.56 Å, well outside the range for metal–metal bonding.[118,119]

Table 8. Selected Bond Distances and Angles for $(Ind^{Me-2})_3Mn_2(BHT)$.

Bridging		Terminal	
Atoms	Distance (Å)	Atoms	Distance (Å)
Mn(1)–O(1)	2.0373(9)	Mn(1)–C(1)	2.3892(14)
Mn(2)–O(1)	2.0528(9)	Mn(1)–C(2)	2.3543(13)
Mn(1)–C(19)	2.2589(13)	Mn(1)–C(3)	2.4151(14)
Mn(2)–C(21)	2.2822(13)	Mn(1)–C(8)	2.5584(13)
Mn(1)–Mn(2)	3.5574(7)	Mn(1)–C(9)	2.5773(13)
		Mn(2)–C(10)	2.417(6)
		Mn(2)–C(11)	2.386(5)
		Mn(2)–C(12)	2.448(9)
		Mn(2)–C(17)	2.624(4)
		Mn(2)–C(18)	2.637(4)
		Δ_{M-C} = 0.198 Å	
hinge = 4.33°		hinge = 4.36°, 4.97°	

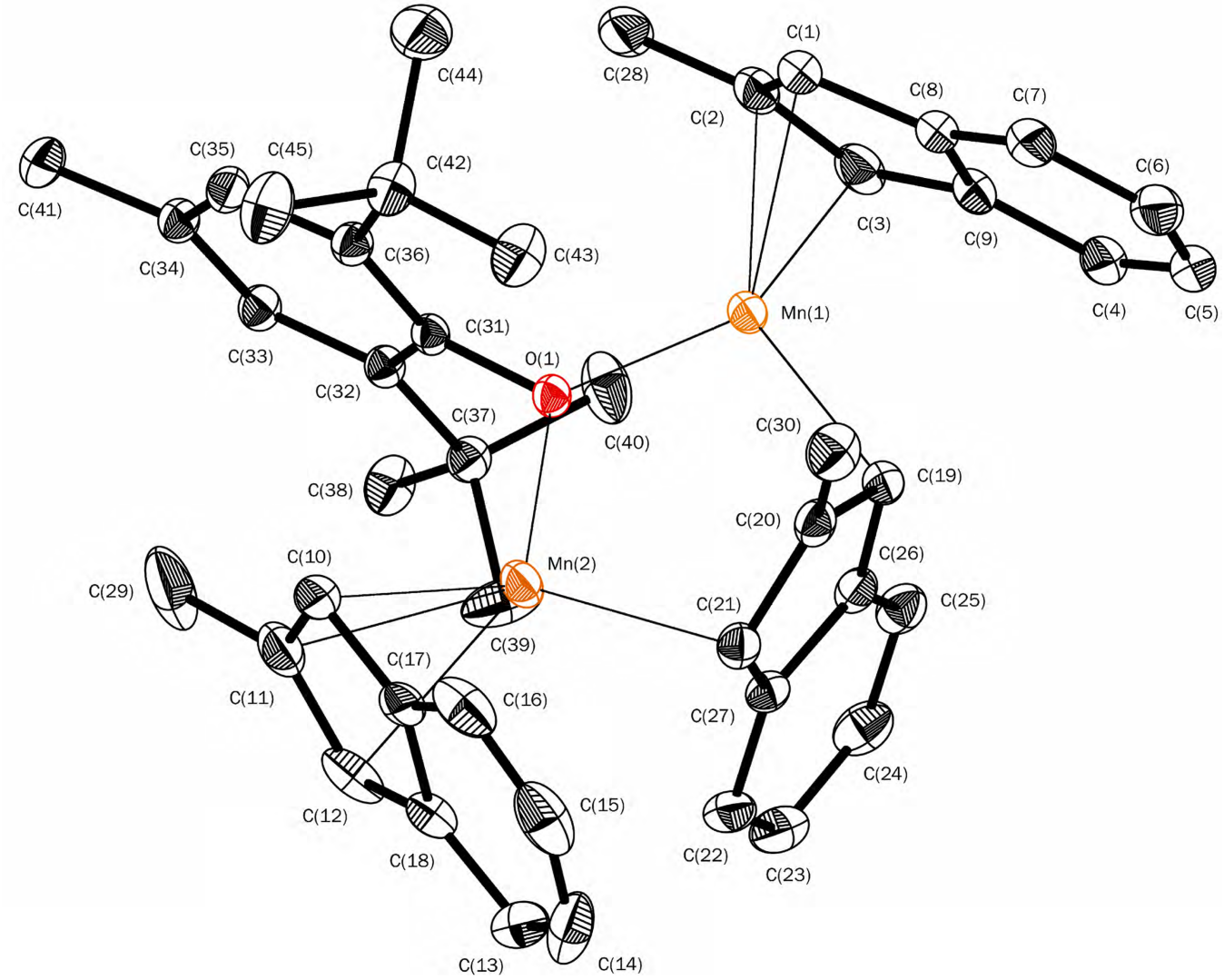

Figure 28. ORTEP of the non-hydrogen atoms of (μ-Ind^{Me-2})(Ind^{Me-2})$_2$$Mn_2$(μ-BHT) illustrating the numbering scheme used in the text. Thermal ellipsoids are shown at the 50% level.

$((Ind^{2Me-4,7})_2Mn)_8$. Crystals of the octameric $((Ind^{2Me-4,7})_2Mn)_8$ were harvested from a toluene solution as dark orange blocks. Only a poor resolution structure could be solved for the molecule, so a connectivity structure is shown in Figure 29. As a result, bond lengths and distances will not be discussed.

The structure is based on an octameric ring of manganese atoms. The structure contains a crystallographic 2-fold axis to complete the octamer, making only four Mn atoms unique. Each manganese center has three 4,7-dimethylindenyl ligands around it. Only one of these ligands is terminal, with each one of these on the "circumference" of the octagon. The terminal ligands appear to be somewhat slipped, but η^5-bound to the manganese centers. Looking along the plane of the Mn_8 ring, the terminal ligands alternate in their coordination above and below the ring.

There are also four bridging ligands in the unique half of the molecule. Of the four, only one employs an η^2-coordination to both manganese centers. The other three ligands are η^2-bound to one metal atom and η^1-bound to the other. These bridging ligands also alternate their positions above and below the Mn_8 ring.

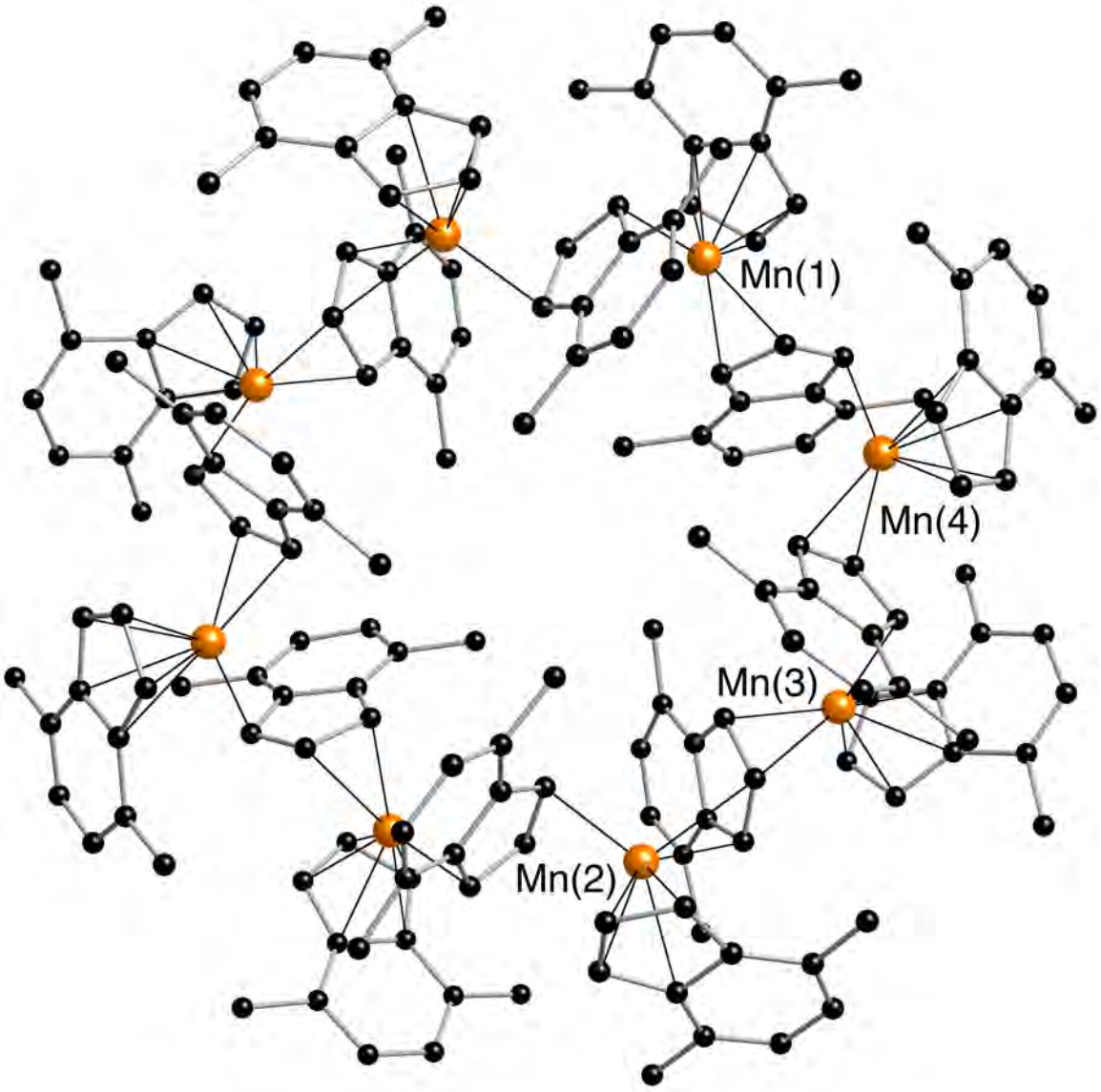

Figure 29. Ball and stick model of the non-hydrogen atoms of $((Ind^{2Me\text{-}4,7})_2Mn)_8$.

$[K_6(dioxane)_9][(Mn(Ind^{2Me\text{-}4,7})_3]_4[Mn(Ind^{2Me\text{-}4,7})_3]_2$. Crystals were harvested from a concentrated 1,4-dioxane solution as yellow hexagonal plates. An ORTEP of the molecule is given in Figure 30, which indicates the numbering scheme referred to in the text; selected bond lengths and angles are shown in Table 9.

There are six crystallographically different manganese atoms in the asymmetric unit; however, there are essentially only two distinct types. All six have very similar carbon bonding distances and arrangements of the indenyl ligands. The general coordination geometry around each manganese atom is a paddlewheel of η^2-bound 4,7-dimethylindenyl ligands. There are three ligands around each manganese center, similar to the octameric structure above. What makes half of the $[Mn(Ind^{2Me\text{-}4,7})_3]$ anions unique from the other half is the coordination to the cation, i.e., the indenyl ligands are involved in cation–π bonding to the potassium through either the 5-membered rings in one half of the molecules (K–C distances range from 3.00 Å to 3.24 Å), or the 6-membered rings in the other half (K–C distances range from 3.00 Å to 3.47 Å). Every potassium cation is co-ordinated by a 6-membered ring, a 5-membered ring, and one oxygen atom on each of two dioxane molecules. This coordination extends in two-dimensions, forming a layer of cations and anions. One of the two dioxane molecules bound to the potassium cation is bridging to a separate potassium cation of another layer, essentially creating a bilayer system held together with the bridging dioxane molecules, and no interactions between separate bilayers.

There is crystallographically imposed C_3 symmetry relating the three indenyl rings on each manganese center. The propeller-like twist of the ligands is left handed in one half of the molecules and right-handed in the other half, but these halves are not specific to the η^5- or η^6-binding character of the indenyl ligands to the potassium atoms. The indenyl ligands are not significantly bent along the hinge (0.58° to 1.96°) or fold axis (1.63° to 3.91°), as might be expected from the coordination to metals on both sides of the rings. The η^2-coordination is evident from the range of manganese bond distances to C(1) and C(2) (Mn–C(1) = 2.29 Å to 2.34 Å, Mn–C(2) = 2.37 Å to 2.42 Å) which are significantly shorter than the distances to C(3) and C(8) (Mn–C(3) = 2.86 Å to 2.91 Å, Mn–C(8) = 2.78 Å to 2.84 Å). There are a few other compounds known to exhibit η^2-coordination of a Cp to a manganese center,[120] and yet one of these is the manganocene polymer.[121] Those distances reported for η^2-coordination (2.44 Å and 2.62 Å) are much longer than the distances reported here.

This particular structure is quite similar to that of $[(\eta^2\text{-Cp})_3\text{MnK}\cdot 1.5\text{thf}]$,[120] in which three Cp ligands are arranged in a paddlewheel around each Mn center, and each Cp is cation-π bound to a potassium counter ion. With THF as the solvent molecule, this structure forms a single layer with *ca.* 9.5 Å between sheets. As a comparison, the thickness of a single sheet of the bilayer is *ca.* 8.1 Å, and the distance between bilayers is 16.0 Å, making the crystals fragile in two dimensions.

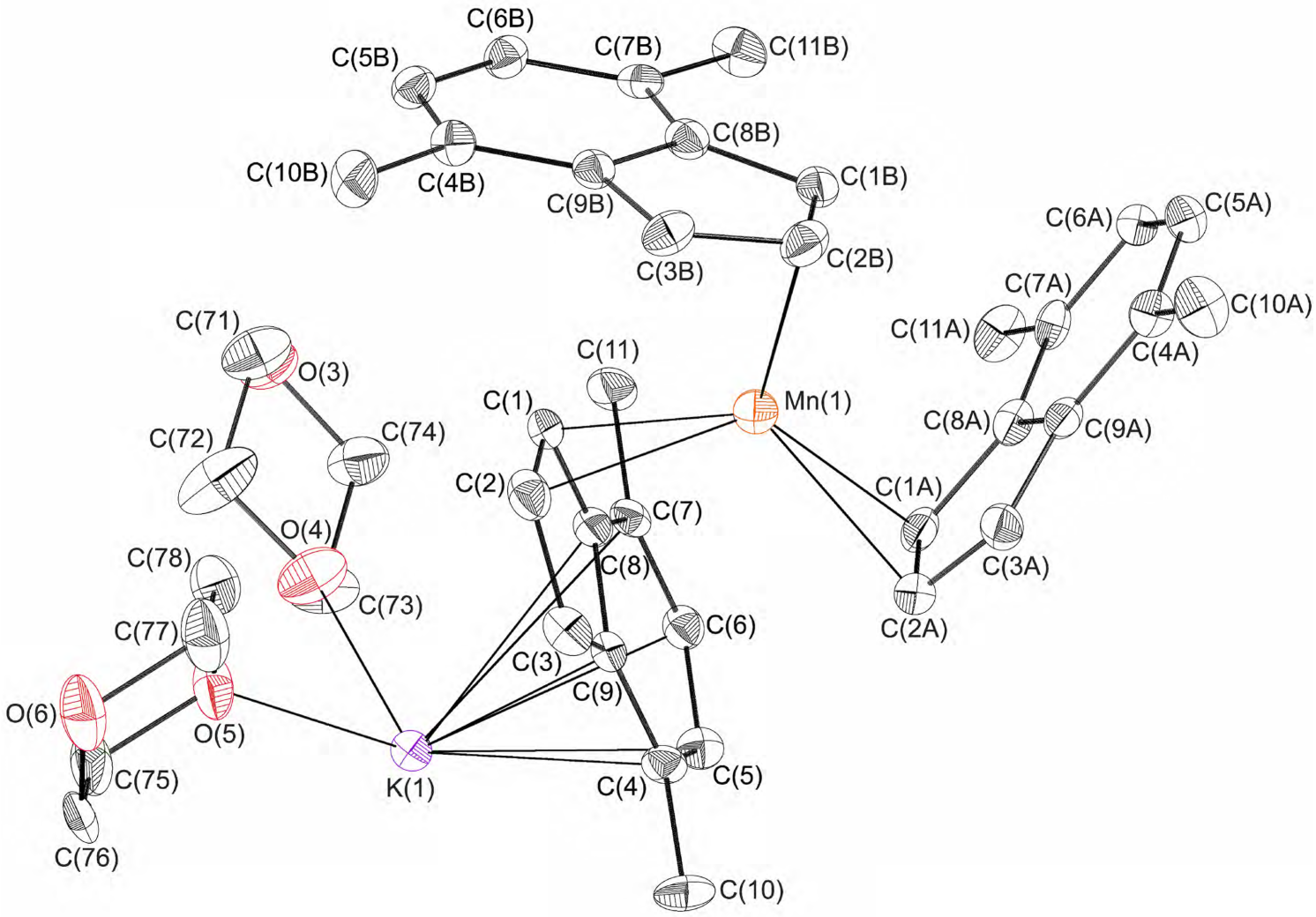

Figure 30. ORTEP of the non-hydrogen atoms of $[K_6(dioxane)_9][(Mn(Ind^{2Me\text{-}4,7})_3]_4$ $[Mn(Ind^{2Me\text{-}4,7})_3]_2$ illustrating the numbering scheme used in the text. Thermal ellipsoids are shown at the 50% level.

Table 9. Selected Bond Distances and Angles for $[K_6(dioxane)_9][(Mn(Ind^{2Me-4,7})_3]_4[Mn(Ind^{2Me-4,7})_3]_2$.

Atoms	Distance (Å)	Atoms	Distance (Å)
Mn(1)–C(1)	2.337(4)	Mn(1)–C(2)	2.404(5)
Mn(2)–C(1)	2.330(5)	Mn(2)–C(2)	2.374(5)
Mn(3)–C(1)	2.332(5)	Mn(3)–C(2)	2.419(5)
Mn(4)–C(1)	2.298(5)	Mn(4)–C(2)	2.397(5)
Mn(5)–C(1)	2.311(5)	Mn(5)–C(2)	2.418(5)
Mn(6)–C(1)	2.285(5)	Mn(6)–C(2)	2.413(5)
(η^5 to K):	hinge = 1.97°	fold = 1.63°	
(η^6 to K):	hinge = 0.58°	fold = 3.91°	

$(Ind)_2Mn(thf)_2$. Crystals of $(Ind)_2Mn(thf)_2$ were harvested from a mixture of THF, diethyl ether, toluene, and pentane as orange blocks. An ORTEP of the molecule is given in Figure 31, which indicates the numbering scheme referred to in the text; selected bond lengths and angles are shown in Table 10.

There are two unsubstituted indenyl ligands and two THF solvent molecules on each manganese atom. One of the indenyl ligands is σ-bound while the other is η^3-bound to the metal. This can be observed from looking at their bond distances. In the η^3-bound ligand, the Mn–C distances range from 2.3441(15) Å to 2.5503(16) Å for the 3 allylic carbons, and 2.827 Å to 2.854 Å for the bridgehead carbons. For the σ-bound ligand, the Mn–C(11) and Mn–C(18) distances are 2.793 Å and 2.824 Å, respectively, well beyond the Mn–C(10) bond distance of 2.2222(14) Å.

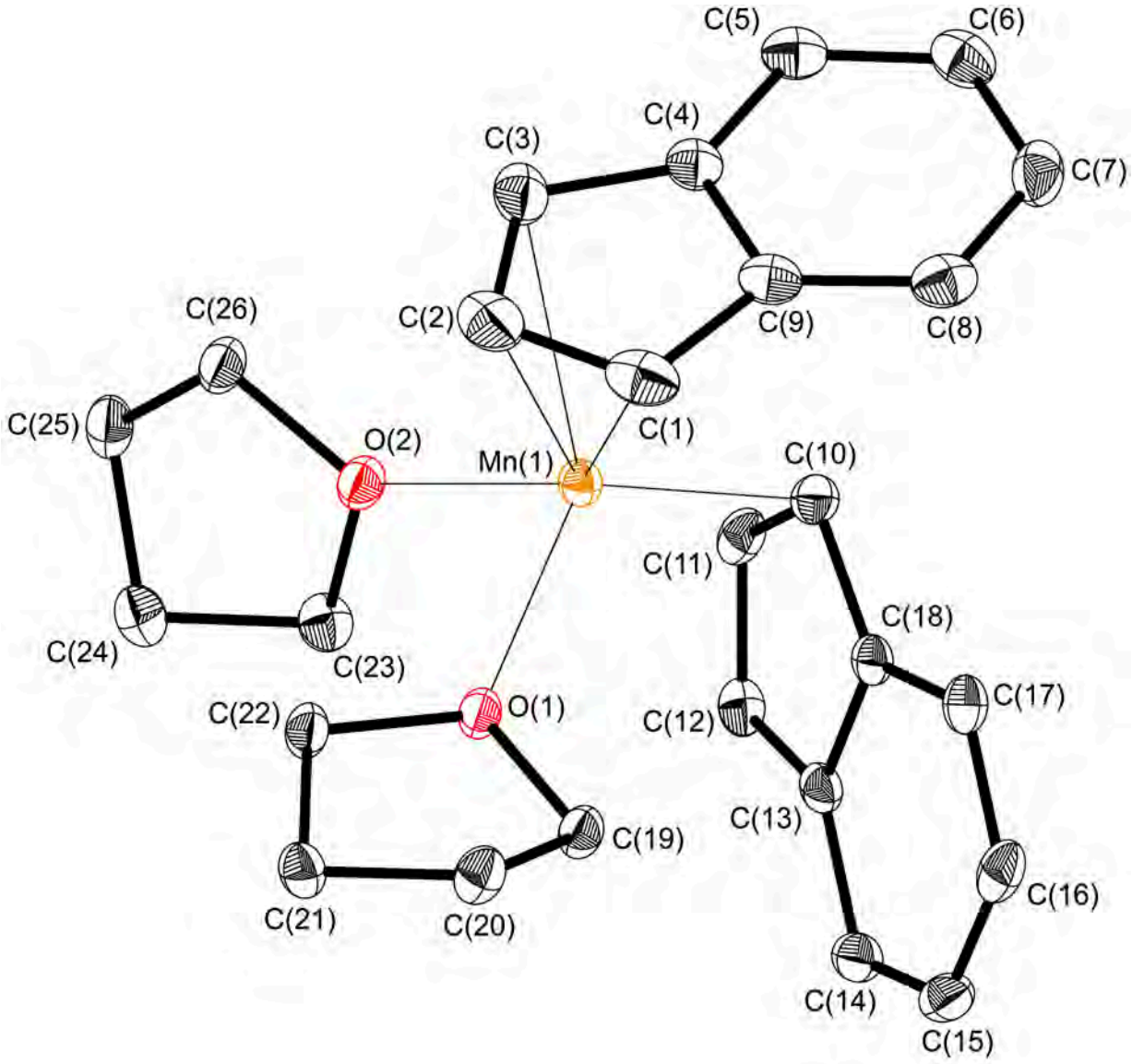

Figure 31. ORTEP of the non-hydrogen atoms of $(Ind)_2Mn(thf)_2$ illustrating the numbering scheme used in the text. Thermal ellipsoids are shown at the 50% level.

The small hinge and fold angles indicate the indenyl ligands are minimally distorted, and the amount of ring slippage (Δ_{Mn-C} = 0.375 Å) confirms the ligand is η^3–bound. The coordination geometry around the manganese center appears to be pseudo-tetrahedral, with 109(5)° as the average bond angle between ligands,[122] although the actual bond angles range from 84.69(4)° to 134.28(5)°. The Mn–O distances of 2.16 Å are slightly longer than the Mn–O distances found in the BHT adduct, but this is expected given the ionic nature of the oxygen atom in BHT.

Given the noticeably different bond distances of each indenyl ring to the manganese atom, it might be expected that the C–C bond distances would differ from each other and from those found in a typical η^5-bound indenyl ring, owing to the localization of the charge in the former. In the σ-bound case, a shortening of the C(11)–C(12) bond to a value (1.378 Å) that reflects some double-bond character is observed, and the rest of the front side bonds are slightly lengthened (Figure 32). Any affect on the aromaticity of the C_5 ring in the η^3-bound ligand is negligible. Both 6-membered rings exhibit subtle alternating single and double bond character, which is very similar to the amount displayed in η^5-bound ligands, e.g., as in $(Ind^{Si\text{-}2})_2Mn$ shown at the top of the figure.

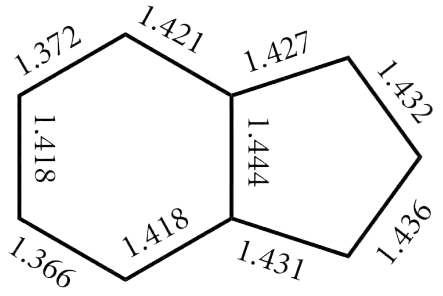

η^5-bound from $(Ind^{Si\text{-}2})_2Mn$

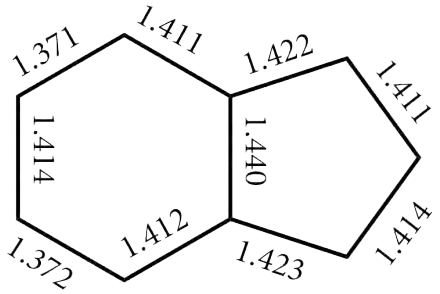

η^3-bound

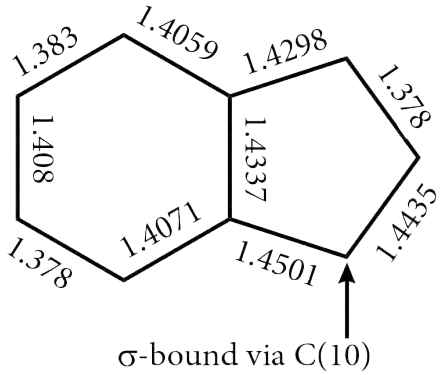

σ-bound via C(10)

Figure 32. C–C bond distances in $(Ind)_2Mn(thf)_2$ showing the aromaticity differences in the C_5 rings between the η^3-bound and σ-bound ligands, also compared with the η^5-bound ligand in $(Ind^{Si\text{-}2})_2Mn$.

Table 10. Selected Bond Distances and Angles for $(Ind)_2Mn(thf)_2$.

Atoms	Distance (Å)	Atoms	Distance (Å)
Mn(1)–C(1)	2.5503(16)	C(1)–C(2)	1.411(3)
Mn(1)–C(2)	2.3441(15)	C(2)–C(3)	1.414(2)
Mn(1)–C(3)	2.5027(15)	C(3)–C(4)	1.423(2)
Mn(1)–C(10)	2.2222(14)	C(4)–C(9)	1.440(5)
Mn(1)–O(1)	2.1613(10)	C(9)–C(1)	1.422(2)
Mn(1)–O(2)	2.1648(10)	C(10)–C(11)	1.4435(19)
		C(11)–C(12)	1.378(2)
		C(12)–C(13)	1.4298(19)
		C(13)–C(18)	1.4337(18)
Δ_{Mn-C} = 0.375 Å		C(18)–C(10)	1.4501(18)
(η^3 to Mn):	hinge = 2.82°	fold = 1.95°	
(σ to Mn):	hinge = 3.23°	fold = 2.92°	

[(Ind$^{3Me-2,4,7}$)MnCl(thf)]$_2$. Crystals of [(Ind$^{3Me-2,4,7}$)MnCl(thf)]$_2$ were harvested from pentane as yellow rods. Only one-half of the molecule is unique, as there is an inversion center between the two manganese atoms. An ORTEP of the molecule is given in Figure 33, which indicates the numbering scheme referred to in the text; selected bond lengths and angles are shown in Table 11.

This structure is the first of the type [(Ind′)MnCl]$_2$, although there are Cp analogues known, [(1,2,4-(*t*Bu)$_3$Cp)MnCl(thf)][123] and [($CH_3C_5H_4$)MnCl(PEt_3)]$_2$.[124] The indenyl compound is dimeric through bridging chlorides. Though the Mn–Cl bond distances (2.483 Å and 2.424 Å) are slightly different from each other, their dissimilarity is chemically insignificant; the previously mentioned Cp complex shows an even smaller disparity (2.482 Å and 2.480 Å). Although outside of a bonding distance,[118,119] the manganese atoms are noticeably closer (3.380 Å) than in the Cp complex (3.514 Å). The Mn–O distance of 2.095 Å is slightly shorter than those in the (Ind)$_2$Mn(thf)$_2$ complex. These findings are consistent with a low-spin manganese(II) system.

The indenyl ligand appears to have a blended η^2- and η^5-bonding character, i.e., the distances to C(1) and C(2) are much shorter (by av 0.19 Å), while the rest of the C_5 ring is still within or very close to previously observed Mn–C bonding distances. Taking a view orthogonal to the C_5 plane, the Mn atom is within the ring, but shifted toward the C(1) position rather than directly below the centroid. The 2-position methyl group is bent

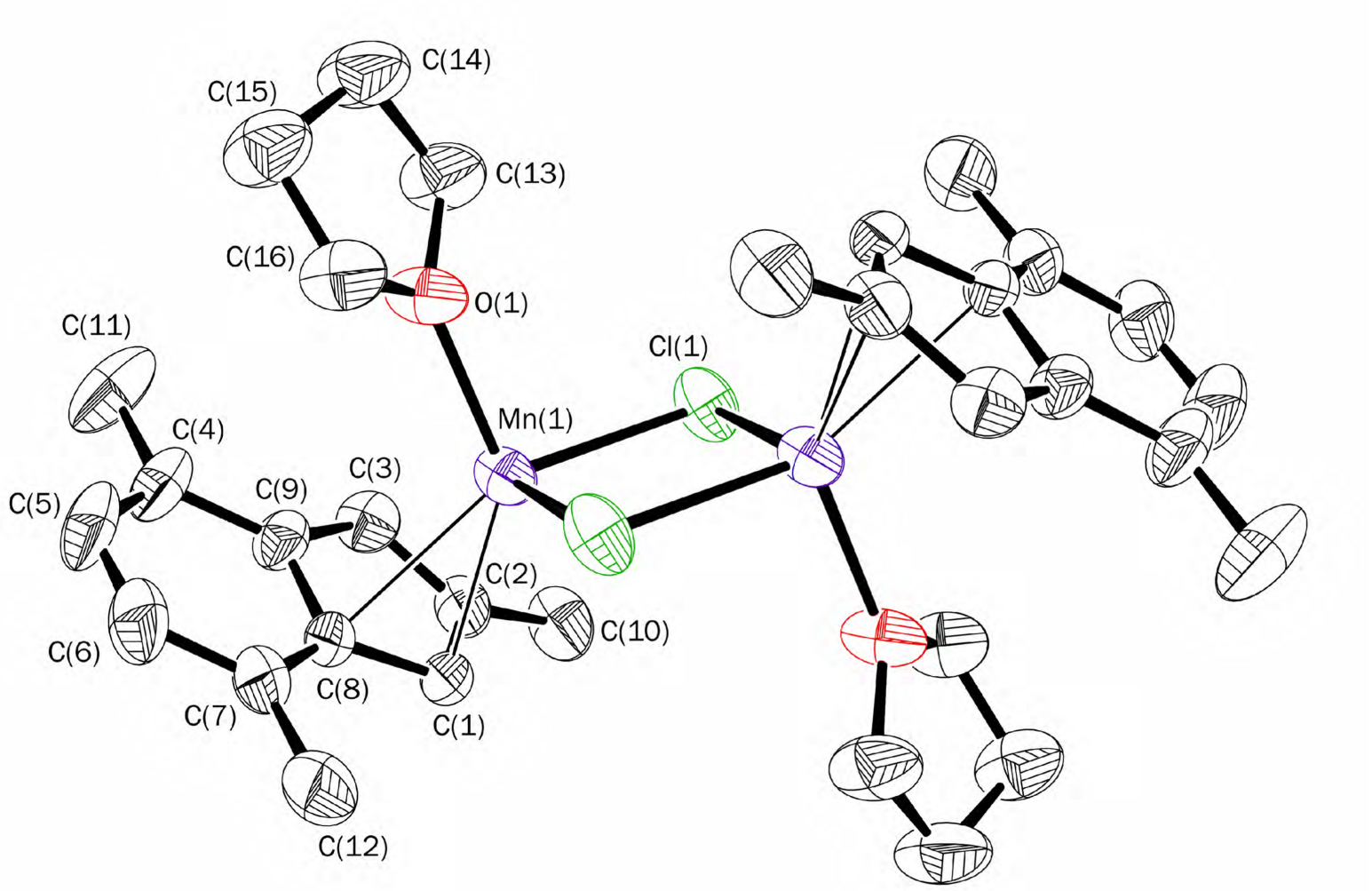

Figure 33. ORTEP of the non-hydrogen atoms of $[(Ind^{3Me\text{-}2,4,7})MnCl(thf)]_2$ illustrating the numbering scheme used in the text. Thermal ellipsoids are shown at the 50% level.

0.109 Å out of the C_5 plane. The hinge (3.108°) and fold angles (2.269°) are comparable to other complexes described in this chapter.

Table 11. Selected Bond Distances and Angles for the (Ind$^{3Me-2,4,7}$)MnCl(thf) dimer.

Atoms	Distance (Å)	Angle	Degree
Mn(1)–C(1)	2.3250(18	hinge	3.108
Mn(1)–C(2)	2.3822(18	fold	2.269
Mn(1)–C(3)	2.525(2)		
Mn(1)–C(8)	2.4917(17)		
Mn(1)–C(9)	2.6241(19)		
Mn(1)–Cl(1)	2.4237(5)		
Mn(1)–Cl(1A)	2.4831(6)		
Mn(1)–O(1)	2.0945(14)		

Computational Results

The lack of an unsolvated parent complex, as a reference to which other bis(indenyl) manganese(II) complexes could be compared, warranted an investigation into the preferred geometry and spin-state of the unsubstituted, homoleptic bis(indenyl)manganese(II). Similar to the calculations on bis(indenyl)chromium(II),[78] the influence of the complex's rotational conformation on the stability of the high-spin and low-spin states was examined via the use of density functional theory (DFT) calculations.

The geometries were optimized with the use of the PW91 functional and the TZ2P basis set (TZ2P+ for the manganese atom) in ADF.[125-127] After optimization, the frequen-

cies and energies were calculated using the same functional and basis set. From Table 12, the gauche conformational isomers are the most stable, with less than 1 kcal/mol separating the high-spin and low-spin state. In all conformations, the high-spin state is favored, although never by more than 3 kcal/mol. Despite several attempts with various imposed symmetries (C_i, C_s, C_{2h}), the staggered, high-spin molecule consistently gave 3 imaginary frequencies. Under no imposed symmetry, the molecule rotated to a gauche conformation, and was found to be a minimum.

Table 12. Calculated Relative Thermodynamics of $(Ind)_2Mn$.

rotational conformation	unpaired electrons	Imaginary frequencies (cm^{-1})	ΔH^0 at 298 K/1 atm (kcal/mol)	ΔG^0 at 298 K/1 atm (kcal/mol)
eclipsed	5	1 (-51)	2.78	4.40
gauche	5	0	0	0
staggered	5	3(-20,-35,-68)	0.60	7.96
eclipsed	1	0	3.24	7.22
gauche	1	0	0.96	0.99
staggered	1	1 (-19)	2.29	8.85

Discussion

In contrast to the low-spin or spin-crossover behavior observed in methyl substituted cyclopentadienyl manganese(II) compounds,[15,128,129] methyl substituted bis(indenyl)manganese(II) complexes have been found to be high-spin ($S = {}^5/_2$) at room temperature. As had been previously determined in the case of $(Cp^{3i})_2Mn$, increasing the

steric bulk of the Cp ligands by adding isopropyl groups to form $(Cp^{4i})_2Mn$ forced longer Mn–C distances, making a high-spin heavily alkylated manganocene complex possible.[14,15,130] This unexpected increase in number of unpaired *d* electrons from that of Cp^*_2Mn[128] was obtained in spite of the extra electron donating groups. However, the use of sterically bulky groups to influence the spin-state may not translate favorably into the development of charge-transfer salt complexes due to their interfering with intermolecular π– π interactions and hence 1-D cation/anion stacks. To combat this problem, the indenyl ligand has been employed for its extended π system and its poorer electron donation to the metal. With this ligand being a slightly weaker electron donor than Cp, we may be able to fine tune the magnetic properties of the neutral bis(indenyl)manganese(II) system by site-specific substitution, as in the case of bis(indenyl)chromium.[9,10] To get a sense of the magnetic properties of these complexes, the use of isopropyl,[80] $SiMe_3$, and methyl groups as substituents on the indenyl ligand has been studied; to date, all such complexes have displayed a high-spin state.

The average Mn–C bond distances for high-spin Cp'_2Mn complexes are typically around 2.4 Å, while low-spin complexes average around 2.1 Å, making the spin-state of similar species easily determined through a bond distance analysis of crystal structures.[128] The high-spin values are found in the homoleptic, η^5-bound species $(Ind^{2Si\text{-}1,3})_2Mn$ and $(Ind^{Si\text{-}2})_2Mn$ (2.42(1) Å and 2.41(3) Å, respectively). The spin-only value of an S = 5/2 complex should equal 5.92 μ_B. Solution magnetic susceptibility measurements support the

presence of high-spin manganese centers (5.87 μ_B for $(Ind^{2Si\text{-}1,3})_2Mn$ and 5.72 μ_B for $(Ind^{Si\text{-}2})_2Mn$).

Other substituted bis(indenyl)manganese(II) complexes display varying hapticities among bridging and terminally bound ligands. The two homoleptic species formed from the 4,7-dimethylindenyl ligand show three ligands around each manganese center with Mn–C distances of *ca.* 2.3 Å to 2.4 Å, indicative of high-spin complexes. The high-spin nature of these complexes in the solid state at 100(2) K is intriguing, considering that this same ligand supports a low-spin chromium complex at 173(2) K that undergoes a low-spin/high-spin equilibrium upon warming to room temperature. Of course, the coordination geometry around the manganese center, along with the energetic favorability of 5 unpaired electrons, is likely strongly influencing its spin-state as well. The same arrangement of Cp ligands into the paddlewheel configuration also leads to a high-spin complex,[120] even though the Cp ligand is typically considered a stronger donor ligand. However, this is not surprising considering the high-spin state of the manganese in Cp_2Mn.[131]

An increase in the donor character of the Cp ligand is afforded by the addition of alkyl donating groups, such as those in 1,1′-dimethylmanganocene[132]. This simple modification from the parent Cp_2Mn was enough to narrow the HOMO–LUMO gap to an energy that supports a spin-crossover state. As an adjunct to this work, methylation of the C_5 ring on the indenyl ligand and the subsequent incorporation into manganese(II) complexes were pursued. The tendency of these compounds to form orange to red oils that

show signs of decomposition after 1 d initially hindered characterization. However, more recently it has been discovered that the use of sources of higher purity $MnCl_2$, solvents without added stabilizers, and less than two full equivalents of the methylated indenide per manganese atom, has produced complexes not subject to decomposition upon standing.

In the case of $(Ind^{Me\text{-}2})_3Mn_2(BHT)$, each of the two terminal indenyl ligands have average Mn–C distances (2.48(2) Å if assumed to be η^5-bound, or 2.40(1) if assumed to be η^3-bound) that suggest a high-spin state. The certainty of the spin-state from the bridging indenyl ligand is more ambiguous due to its Mn–C distances (2.26(1) Å and 2.28(1) Å) that lie between the low-spin and high-spin values, although there are no known examples of an indenyl ligand bridging in this fashion. The discovery of this molecule also led us to the use of unstabilized THF to prevent any further adventitious contamination of our products.

Given the need for a stronger donating ligand, the more heavily methylated indene, 2,4,7-trimethylindene, was synthesized and deprotonated. The reaction of two equivalents of the ligand to one equivalent of $MnCl_2$ produced bright-orange, acicular crystals that were unsuitable for x-ray crystallography. Elemental analysis for C, H, and Mn confirmed the composition of $(Ind^{3Me\text{-}2,4,7})_2Mn$, and this compound was established to be high-spin by solution magnetic susceptibility methods (5.68 μ_B). This result would suggest the need for stronger donor substituents such as isopropyl or *t*-butyl groups to promote a

spin-crossover or low-spin complex; however, there is evidence that compounds containing *t*-butyl groups favor a high-spin state due to the steric bulk of the substituents,[8] and there has been a report of the high-spin complex bis(1,3-diisopropyl)manganese(II).[80] It is feasible that the use of the $Ind^{2tBu\text{-}1,3}$ ligand could force a suitable gauche arrangement around a manganese center that would accommodate a low-spin complex without the overriding intramolecular steric repulsion of the *t*-butyl groups. A second option would be to add methyl groups to the C_5 ring as in the 1,2,3-trimethylindenyl ligand, but the thermal stability of manganese complexes formed with this ligand thus far have been too short for isolation.

Bis(indenyl)manganese(II), which had previously eluded characterization and was described in the patent literature as a brown solid,[91] was isolated in this work as a THF-solvate. In the solid state, it is a monomer having one η^3-bound ligand, one σ–bound ligand, and two coordinated THF molecules, giving the manganese center an approximate tetrahedral arrangement of ligands. The combination of coordination modes of the indenyl ligands makes the molecule only the second of its kind.[133] This compound has an average Mn–C bond length to the η^3-bound indenyl of 2.466(3) Å, indicative of a high-spin complex. Solution magnetic susceptibility measurements (5.56 μ_B) confirmed this observation. This is the expected spin-state given that the unsubstituted ligand is a weaker donor than other methylated ligands that also support the high-spin state. While the structure of the homoleptic base-free complex is yet to be determined, DFT calculations

have suggested the complex would energetically favor a gauche conformation by at least 4 kcal/mol. Although efforts to synthesize this molecule are ongoing, the small calculated energy difference between conformations is unlikely to outweigh crystal packing forces, and so the solid state structure is not readily predictable.

Mono-ring complexes of manganese(II) and their reactions with N_2. The indenyl ligand has been proven to exhibit a wide range of coordination modes and bond distances to manganese(II). This fact, paired with the high-spin d^5 metal, leaves more of the metal exposed to coordination by some of the weakest electron donating ligands. Also, the structural variances among indenyl manganese complexes confirm the lack of LFSE associated with high-spin d^5 complexes. Assuming the molecular orbital/geometry combinations are not tightly coordinated, a complex may have a low-energy ligand rearrangement available. Should the ligands rearrange around the metal due to the energy of solution, a coordination site on the manganese atom may open for a small molecule to bind. For the purpose of testing this hypothesis, molecules with little evidence for steric congestion and coordinative saturation were synthesized using the 2-methylindenyl, 4,7-dimethylindenyl, or 2,4,7-trimethylindenyl ligands. Hydrocarbon solutions of one equivalent of the $K^+[Ind^{Me-2}]^-$ or $K^+[Ind^{3Me-2,4,7}]^-$ ligands with $MnCl_2$ were bright yellow at room temperature, however upon cooling to below -40 °C, the solutions became dark blue. This color change was initially investigated as a spin-state transformation, but the solution magnetic susceptibility was constant from 20 °C to -70 °C. The observed blue

color only occurred in the presence of a N_2 atmosphere, and the solution remained yellow while cooled to -78 °C under vacuum, indicating that a simple thermochromic transformation was not occurring. When the manganese complexes were dissolved in a coordinating solvent (i.e., THF), the color change did not take place even at low temperatures, suggesting that the N_2 binding was blocked by the solvent.

To attempt to characterize this Mn–N_2 interaction, variable temperature solution magnetic susceptibility measurements were recorded for the complex under vacuum and also under a nitrogen atmosphere. No differences in the two spectra were observed, suggesting the color change is not the result of a spin-crossover species, although the HOMO–LUMO gap must be affected to allow a new transition. A comparison of the blue and yellow solution IR spectra was also made, however there was no observable metal-bound dinitrogen stretch. This strongly suggests the N_2 is bound via side-on or bridging coordination modes, as either case would limit the visibility of the N–N stretch due to the lack of change in the molecule's polarity. Molecules known to coordinate N_2 in this fashion have no reported N–N stretch.[103,134,135]

Evacuated flasks containing pentane or toluene solutions of (2,4,7-trimethylindenyl)manganese(II) chloride were bright yellow at -78 °C. Once the flask was pressurized with H_2, the solution became deep purple, suggesting H_2 binding. The H_2 ligand proved to be highly labile, as the solution reverted to bright yellow upon warming to room temperature.

Conclusions

The parent bis(indenyl)manganese(II), albeit solvated with THF, has been prepared and structurally authenticated for the first time. The insolubility of potassium indenide in anything but strongly coordinating solvents makes the formation of the base-free manganese species all but impossible via salt metathesis reactions. Characterization of the molecule revealed that it is in the high-spin state in solution, along with having Mn–C bond distances associated with high-spin manganese in the solid-state, consistent with its closest analogue, manganocene. DFT calculations have shown the gas phase homoleptic molecule would adopt a gauche conformation, with the HS case favored over the LS by only 1 kcal/mol.

As anticipated from manganocene and its derivatives, bis(indenyl)manganese(II) complexes display a diverse range of Mn–C bond distances and hapticities of the indenyl ligand. The coordination environment around the metal center varies from distorted-tetrahedral to the well known bis(indenyl) framework of pseudo-octahedral. Indenyl ligands with only methyl substituents do not provide enough steric hindrance to prevent access to the manganese center. The divergence from the typical sandwich compounds observed in transition metal complexes is unexpected, although not surprising due to the larger metal radius and the fact that in high-spin d^5 complexes there is no ligand field stabilization energy. Bulky substituents, such as $SiMe_3$, tend to enforce η^5,η^5-bound ligands

due to their better encapsulation of the metal, which also blocks coordination of ancillary ligands.

Manganese centers bonded to two or more indenyl ligands favor the high-spin state regardless of the coordination environment. In the cases of methyl substitution on the indenyl ring, the ease of ring slippage combined with the lack of steric bulk allows for more than two ligands (indenyl, solvent, or otherwise) to bind to the metal center. The promotion of low-spin or spin-crossover complexes would be more likely with the use of more heavily methylated ligands, however these have not been found to generate stable manganese complexes. Alternative substituents that have been investigated include ethyl and isopropyl groups.[80]

Mono-ring complexes of manganese(II) chloride have been shown to bind reversibly dinitrogen and dihydrogen. These are the first examples of manganese(II) complexes with this capability, reversible or otherwise; however, the extreme lability of the ligands has made the interactions difficult to characterize.

CHAPTER IV

STRUCTURAL CHARACTERIZATION AND REACTIVITY OF THE FIRST SUBSTITUTED BIS(INDENYL)VANADIUM(II) COMPLEXES

Introduction

All known bis(cyclopentadienyl)vanadium(II) complexes are high-spin ($S = {}^3/_2$), even in the case of Cp^*_2V,[136] which decreases the likelihood that a low-spin or spin-crossover complex could be synthesized based on the strong electron donation properties of ligands in a vanadium sandwich framework. However, the indenyl ligand is known to exhibit strong rotational conformation preferences in transition metal complexes through the use of sterically demanding substituents. In the case of substituted bis(indenyl)chromium(II) complexes, such changes in the ligand conformations, and hence the symmetry of the complex, result in spin-state modifications derived from the interaction of the 3*d* metal orbitals with the π_3, π_4, and π_5 indenyl orbitals.[8-10] The rotational modifications in these complexes produce spin states not observed in substituted chromocenes; these ligand substitutions will be employed in the formation of substituted bis(indenyl)vanadium complexes.

The parent bis(indenyl)vanadium(II) has previously been synthesized, but lacks high quality structural characterization due to a mixture of staggered and eclipsed isomers present in the crystal lattice.[7] The structural confirmation of vanadium complexes with vari-

ous methylated or trimethylsilylated indenyl rings should provide a picture of the substitutions necessary to vary the rotational conformation of these complexes.

Another advantage of varying the rotational conformation along with the steric bulk of the ligands is the possibility of exploring of the reactivity of the metal complexes. The parent Ind_2V is a 15 e^- complex that readily binds two carbonyl ligands to form a 17 e^- complex with the aid of one indenyl ligand undergoing an η^5 to η^3 haptotropic slip.[7] However, Cp_2V and Cp^*_2V complexes only bind a single carbonyl ligand while maintaining the η^5 hapticity of both rings. Modifications that increase the steric bulk of the ligands should encumber the uptake of CO, so that the ability of substituted bis(indenyl)vanadium complexes to bind to multiple CO ligands cannot be confidently predicted.

Experimental

General Considerations. All manipulations were performed with the rigorous exclusion of air and moisture using Schlenk or glovebox techniques. Proton (^{1}H) NMR experiments were obtained on a Bruker DPX-300 spectrometer at 300 MHz, or a Bruker DPX-400 at 400 MHz, and were referenced to residual proton resonances of THF-d_8 (δ 3.58) and $CDCl_3$ (δ 7.26). Elemental analyses were performed by Desert Analytics (Tucson, AZ). Melting points were determined on a Laboratory Devices Mel-Temp apparatus in sealed capillaries. Mass spectra were obtained using a Hewlett-Packard 5890 Series II

gas chromatograph/mass spectrometer. FTIR spectra were recorded using a Thermo Mattson Satellite Spectrometer.

Materials. Anhydrous vanadium(III) chloride was purchased from Strem Chemicals and used as received. Potassium nitrite, potassium nitrate, chromium(III) oxide, and *t*-butyl isocyanide were purchased from Aldrich and used as received. Anhydrous pentane was purchased from Acros and used as received. Hexanes, toluene, and diethyl ether were distilled under nitrogen from potassium benzophenone ketyl. Carbon monoxide was purchased from A-L Compressed Gases and passed through a drying column (anhydrous $CaSO_4$) prior to use. Anhydrous tetrahydrofuran (THF) was purchased from Aldrich and dried over 4A molecular sieves prior to use. Toluene-d_8 (Aldrich) was vacuum distilled from Na/K (22/78) alloy and stored over 4A molecular sieves prior to use.

Magnetic Measurements. Solution magnetic susceptibility measurements were performed on a Bruker DRX-400 spectrometer using the Evans' NMR method.[31-35] 5–10 mg of the paramagnetic material was dissolved in toluene-d_8 in a 1.0 mL volumetric flask. The solution was thoroughly mixed, and approximately 0.5 mL was placed in a NMR tube containing a toluene-d_8 capillary. The calculations required to determine the number of unpaired electrons based on the data collected have been described elsewhere.[36]

Synthesis of 1,3-Bis(trimethylsilyl)indene ($HInd^{2Si\text{-}1,3}$), 2,4,7-Trimethylindene ($HInd^{3Me\text{-}2,4,7}$), 2-Methylindene ($HInd^{Me\text{-}2}$), Potassium 1,3-Bis(trimethylsilyl)indenide, ($K[Ind^{2Si\text{-}1,3}]$), Potassium 2,4,7-

Trimethylindenide ($K[Ind^{3Me-2,4,7}]$), and Potassium 2-Methylindenide ($K[Ind^{Me-2}]$). See Chapter 3.

Synthesis of 4,7-Dimethylindene ($HInd^{2Me-4,7}$) and Potassium 4,7-Dimethylindenide, ($K[Ind^{2Me-4,7}]$). See Chapter 1.

Synthesis of Vanadium(II) Chloride, VCl_2. Following a known procedure,[80] anhydrous vanadium(III) chloride (5.00 g, 0.0318 mol) was added to 150 mL of THF in a 250 mL Schlenk flask fitted with a stir bar and condensing column. This mixture was stirred and refluxed overnight to produce a salmon-colored powder that was isolated in quantitative yield by removal of the solvent under vacuum.

The resulting $VCl_3 \cdot 3THF$ (0.386 g, 1.03 mmol) was added to 30 mL of THF in a 125 mL Erlenmeyer flask fitted with a stir bar. A slight excess of aluminum powder (0.0300 g, 1.11 mmol) and a catalytic amount of KH (0.001 g) was added to the flask. After stirring overnight, the maroon mixture had turned blue-green. Filtration yielded a clear blue-green solution of $[VCl_2]$ in THF, assumed to be formed in quantitative yield.

Synthesis of Bis(2,4,7-trimethylindenyl)vanadium(II), $(Ind^{3Me-2,4,7})_2V$. A 40 mL solution of anhydrous VCl_2 (1.03 mmol) in THF was added to a 125 mL Erlenmeyer flask fitted with a magnetic stirring bar. Potassium 2,4,7-trimethylindenide (0.325 g, 2.06 mmol) was dissolved in 10 mL of THF and added dropwise to the flask while stirring. The mixture initially turned emerald green and continued to darken before it was allowed to stir overnight. The solvent was removed under vacuum, and 50 mL of hexanes

was added to dissolve the residue. The mixture was filtered through a medium-porosity glass frit, and the filtrate was collected in a 250 mL modified round bottom flask, which was placed in a –30 °C freezer. After 48 h, no crystals had grown, so the solution was concentrated to 20 mL and returned to the freezer. Dark green crystals of $(Ind^{3Me\text{-}2,4,7})_2V$ were observed and isolated by cannulation of the mother liquor on a Schlenk line. The crystals were dried under vacuum and brought into the glovebox (0.248 g, 66%) mp 142–146 °C. Anal. Calcd. for $C_{24}H_{26}V$: C, 78.89; H, 7.17; V, 13.94. Found: C, 77.94; H, 6.73; V, 13.88. Solution magnetic susceptibility (μ_{eff}^{298K}): 3.45.

Synthesis of Bis(2-methylindenyl)vanadium(II), $(Ind^{Me\text{-}2})_2V$. A 40 mL solution of anhydrous VCl_2 (0.747 mmol) in THF was added to a 125 mL Erlenmeyer flask fitted with a magnetic stirring bar. Potassium 2-methylindenide (0.251 g, 1.49 mmol) was dissolved in 10 mL of THF and added dropwise to the flask while stirring. The mixture initially turned emerald green and continued to darken before it was allowed to stir overnight. The solvent was removed under vacuum, and 30 mL of pentane was added to dissolve the residue. The mixture was filtered through a medium-porosity glass frit, and the filtrate was collected in a 125 mL Erlenmeyer flask, which was placed in the freezer and slowly cooled to –30 °C. After 48 h, large dark green plates had grown, so the solvent was removed under vacuum, affording more crystals of $(Ind^{Me\text{-}2})_2V$ in 66% total yield (0.153 g), mp 129–131 °C. Anal. Calcd. for $C_{20}H_{18}V$: C, 77.66; H, 5.87; V, 16.47. Found: C, 76.59; H, 5.95; V, 16.1. Solution magnetic susceptibility (μ_{eff}^{298K}): 3.64.

Synthesis of Bis(4,7-dimethylindenyl)vanadium(II), $(Ind^{2Me-4,7})_2V$. A 40 mL solution of anhydrous VCl_2 (0.985 mmol) in THF was added to a 125 mL Erlenmeyer flask fitted with a magnetic stirring bar. Potassium 4,7-dimethylindenide (0.359 g, 1.97 mmol) was dissolved in 10 mL of THF and added dropwise to the flask while stirring. The mixture initially turned emerald green and continued to darken before it was allowed to stir overnight. The solvent was removed under vacuum, and 30 mL of pentane was added to dissolve the residue. The mixture was filtered through a medium-porosity glass frit, and the filtrate was collected in a 125 mL Erlenmeyer flask. The majority of the filtrate was a dark green solution, but a small amount of a dense brown oil also came through the frit, which seemed to dissolve as more filtrate entered the flask. Together in solution, the two substances were placed in a –30 °C freezer. After 48 h, no crystals had grown, so the solvent was slowly removed under vacuum to yield dark green crystals of $(Ind^{2Me-4,7})_2V$ (0.207 g, 62%) mp 152–155 °C. Anal. Calcd. for $C_{22}H_{22}V$: C, 78.33; H, 6.57; V, 15.10. Found: C, 76.92; H, 6.91; V, 16.0. Solution magnetic susceptibility (μ_{eff}^{298K}): 3.57.

Synthesis of Bis(1,3-bis(trimethylsilyl)indenyl)vanadium(II), $(Ind^{2Si-1,3})_2V$. A 40 mL solution of anhydrous VCl_2 (1.13 mmol) in THF was added to a 125 mL Erlenmeyer flask fitted with a magnetic stirring bar. Potassium 1,3-bis(trimethylsilyl)indenide (0.673 g, 2.26 mmol) was dissolved in 10 mL of THF and added dropwise to the flask while stirring. The mixture initially turned light brown and

continued to darken before it was allowed to stir overnight. The solvent was removed under vacuum, and 50 mL of hexanes was added to dissolve the residue. The mixture was filtered through a medium-porosity glass frit, and the filtrate was collected in a 250 mL modified round bottom flask, which was placed in a –30 °C freezer. After 48 h, no crystals had grown, so the solution was allowed to slowly evaporate at RT. Large brown crystals of $(Ind^{2Si\text{-}1,3})_2V$ were obtained in 43% yield (0.274 g) mp 132–138 °C. Anal. Calcd. for $C_{30}H_{46}Si_4V$: C, 63.22; H, 8.14. Found: C, 63.54; H, 8.43. Solution magnetic susceptibility (μ_{eff}^{298K}): 3.48.

Attempted Reaction of Bis(1,3-bis(trimethylsilyl)indenyl)vanadium(II) with Carbon Monoxide. In a 50 mL Schlenk flask fitted with a stir bar, 0.061 g of $(Ind^{2Si\text{-}1,3})_2V$ was dissolved in a 60:40 mixture of hexanes:diethyl ether to give a light brown solution. Carbon monoxide was bubbled through the solution for 15 min at RT, but no reaction was observed. An IR spectrum of the solution under CO confirmed there was no coordination.

Reaction of Bis(2,4,7-trimethylindenyl)vanadium(II) with Carbon Monoxide (CO). In a 50 mL Schlenk flask fitted with a stir bar, 0.124 g of $(Ind^{3Me\text{-}2,4,7})_2V$ was dissolved in a 50:50 mixture of hexanes:diethyl ether to give an emerald green solution. Immediately upon bubbling carbon monoxide through the solution, a dark brown color was observed. The solution was saturated with CO for 5 min although no further color change was observed. An IR spectrum of the solution contained a single CO

peak at 1882 cm^{-1}. Upon isolating the solid by slow evaporation of the solvents, dark green crystals grew and were reanalyzed by FTIR, but no CO peak was observed. Further experiments showed the binding of CO was reversible in solution by purging with N_2 or Ar. Attempted crystal growth of CO adducts under a CO atmosphere at RT and -30 °C was unsuccessful.

Reaction of Bis(4,7-dimethylindenyl)vanadium(II) with Carbon Monoxide (CO). Under the same reaction conditions as the previous experiment, $(Ind^{2Me-4,7})_2V$ was treated with CO, forming a brown-green solution that quickly (1 min) reversed to dark green upon standing in a N_2 atmosphere.

Reaction of Bis(2-methylindenyl)vanadium(II) with Carbon Monoxide (CO). Under the same reaction conditions as the previous experiment, $(Ind^{Me-2})_2V$ was treated with CO, forming a dark brown solution that slowly (5 min) reversed to dark green upon standing in a N_2 atmosphere.

Reaction of Bis(2,4,7-trimethylindenyl)vanadium(II) with Nitric Oxide (NO). Excess nitric oxide was synthesized by the combination of 1.68 g of KNO_2, 0.67 g of KNO_3, and 1.00 g of Cr_2O_3. These solids were combined and ground to a uniform light green powder with a mortar and pestle. This mixture was added to one of two fused 125 mL Schlenk flasks along with a glass stir bar. To the adjoining flask was added a solution of $(Ind^{3Me-2,4,7})_2V$ (0.120 g) in 40 mL of hexanes. The glassware was taken out of the drybox and placed on the Schlenk line. The entire apparatus was degassed to favor the

formation and dissolution of NO. The flask with the solids was placed in a 400 °C oil bath and the green mixture immediately grew pale. As the valve connecting the two flasks was opened, the green solution noticeably darkened to a coffee-black suspension. Under a N_2 purge, the compound did not revert to its green color, and further attempts to isolate and characterize the compound proved unsuccessful as the compound was insoluble in aliphatic, aromatic, and ethereal solvents.

Reaction of Bis(2,4,7-trimethylindenyl)vanadium(II) with *t*-Butyl Isocyanide (*t*-BuNC). In a 125 mL Erlenmeyer flask, 0.1523 g (0.417 mmol) of $(Ind^{3Me-2,4,7})_2V$ was dissolved in 40 mL of diethyl ether. *t*-BuNC (0.0693g, 0.834 mmol) was dissolved in 10 mL of diethyl ether and added dropwise to the flask. The green solution immediately darkened to brown and material precipitated from solution. Further attempts to isolate and characterize this compound proved unsuccessful as the compound was insoluble in aliphatic, aromatic, and ethereal solvents.

Computational Details. Geometry optimizations along with frequency calculations were performed using the GAUSSIAN 03 suite of programs.[38] Density functional theory was employed with the use of the PW91PW91 functional which incorporates the 1991 gradient-corrected correlation and exchange functional of Perdew and Wang.[137] The standard Pople basis set 6-31+G(d,p) was used,[138] and, in conjunction with the PW91PW91 functional, has been shown to consistently predict carbonyl stretching frequencies with good accuracy, approximately 15–25 cm^{-1} below experimental values. All

15 e^- complex calculations were performed in the high-spin state with the relative ligand conformations geometrically optimized prior to frequency calculations.

General Procedures for X-ray Crystallography. A suitable crystal of each sample was located, attached to a glass fiber, and mounted on a Siemens SMART Platform CCD diffractometer for data collection. Data collection and structure solutions for all molecules were conducted at the X-ray Crystallography Laboratory at the University of Minnesota by Benjamin E. Kucera or at the University of California, San Diego by Dr. Arnold L. Rheingold. Data resolution of 0.84 Å was considered in the data reduction (SAINT 6.01 and SAINT 6.35, Bruker Analytical Systems, Madison, WI). The intensity data were corrected for absorption and decay (SADABS). All calculations were performed on computers using the current SHELXTL suite of programs.[45] Final cell constants were calculated from a set of strong reflections measured during the actual data collection. Relevant crystal and data collection parameters for each of the compounds are given in Appendix B.

The space groups were determined from unit cell parameters and intensity statistics. A direct-methods solution was calculated that provided most of the non-hydrogen atoms from the E-map. Several full-matrix least-squares/difference Fourier cycles were performed that located the remainder of the non-hydrogen atoms. All non-hydrogen atoms were refined with anisotropic displacement parameters. All hydrogen atoms were placed in ideal positions and refined as riding atoms with relative isotropic displacement parameters.

X-ray Crystallography of $(Ind^{3Me-2,4,7})_2V$. Dark green crystals of $(Ind^{3Me-2,4,7})_2V$ were harvested by preparing a concentrated hexanes solution, which was cooled to –30 °C. The crystals were separated from the mother liquor via cannulation and dried under vacuum prior to data collection. An initial set of cell constants was calculated from reflections produced from three sets of 20 frames. These sets of frames were oriented such that orthogonal wedges of reciprocal space were surveyed. This produced orientation matrices determined from 105 reflections. The final cell constants were calculated from the *xyz* centroids of 4056 strong reflections as described in the general procedures.

Data was collected using MoKα radiation (graphite monochromator) with a frame time of 30 s and a detector distance of 4.9 cm. A randomly oriented region of reciprocal space was surveyed to the extent of 1 sphere, and to a resolution of 0.84 Å. Four major sections of frames were collected with 0.30° steps in ω at four different ϕ settings and a detector position of –28° in 2θ.

The space group $P2_1/n$ was determined as described in the general procedures. Despite a β angle near 90°, no valid solution could be obtained using an orthorhombic setting. Therefore a pseudo-merohedral twin law of the form [1 0 0 0 – 1 0 0 0 –1] was applied. The ratio of the twin components refined to 66:34. The final full matrix least-squares refinement converged to $R1 = 0.0487$ and $wR2 = 0.1029$ (F^2, all data).

X-ray Crystallography of $(Ind^{2Si-1,3})_2V$. Dark brown crystals of $(Ind^{2Si-1,3})_2V$ were harvested by preparing a concentrated hexanes solution and allowing it to slowly

evaporate at room temperature. The crystals were separated from the mother liquor and dried under vacuum prior to data collection. An initial set of cell constants was calculated from reflections produced from three sets of 20 frames. These sets of frames were oriented such that orthogonal wedges of reciprocal space were surveyed. This produced orientation matrices determined from 105 reflections. The final cell constants were calculated from the *xyz* centroids of 9401 strong reflections as described in the general procedures.

Data was collected using a graphite monochromator with a frame time of 30 s and a detector distance of 4.9 cm. A randomly oriented region of reciprocal space was surveyed to the extent of 1 sphere, and to a resolution of 0.84 Å. Four major sections of frames were collected with 0.30° steps in ω at four different ϕ settings and a detector position of –28° in 2θ.

The space group *C*2/*c* was determined as described in the general procedures. The final full matrix least-squares refinement converged to $R1 = 0.0488$ and $wR2 = 0.0877$ (F^2, all data).

X-ray Crystallography of $(Ind^{Me\text{-}2})_2V$. Dark green crystals of $(Ind^{Me\text{-}2})_2V$ were harvested by preparing a concentrated pentane solution and allowing it to evaporate slowly at room temperature. The crystals were separated from the mother liquor and dried under vacuum prior to data collection. An initial set of cell constants was calculated from reflections produced from three sets of 20 frames. These sets of frames were ori-

ented such that orthogonal wedges of reciprocal space were surveyed. This produced orientation matrices determined from 105 reflections. The final cell constants were calculated from the *xyz* centroids of 2949 strong reflections as described in the general procedures.

Data was collected using a graphite monochromator with a frame time of 30 s and a detector distance of 4.9 cm. A randomly oriented region of reciprocal space was surveyed to the extent of 1 sphere, and to a resolution of 0.83 Å. Four major sections of frames were collected with 0.30° steps in ω at four different ϕ settings and a detector position of –28° in 2θ.

The space group *C*2/*c* was determined as described in the general procedures. The final full matrix least-squares refinement converged to $R1 = 0.0321$ and $wR2 = 0.0838$ (F^2, all data).

X-ray Crystallography of $(Ind^{2Me\text{-}4,7})_2V$. Dark brown crystals of $(Ind^{2Me\text{-}4,7})_2V$ were harvested by preparing a concentrated pentane solution and allowing it to slowly evaporate at room temperature. The crystals were separated from the mother liquor and dried under vacuum prior to data collection. An initial set of cell constants was calculated from reflections produced from three sets of 20 frames. These sets of frames were oriented such that orthogonal wedges of reciprocal space were surveyed. This produced orientation matrices determined from 105 reflections. The final cell constants were calculated from the *xyz* centroids of 5578 strong reflections as described in the general procedures.

Data was collected using a graphite monochromator with a frame time of 30 s and a detector distance of 4.9 cm. A randomly oriented region of reciprocal space was surveyed to the extent of 1 sphere, and to a resolution of 0.83 Å. Four major sections of frames were collected with 0.30° steps in ω at four different ϕ settings and a detector position of –28° in 2θ.

The space group *Cc* was determined as described in the general procedures. The final full matrix least-squares refinement converged to $R1 = 0.0348$ and $wR2 = 0.0854$ (F^2, all data).

Results

Ligand Synthesis. After the desired indene ring was synthesized and purified by vacuum distillation, the alkali metal indenide salt was prepared via deprotonation reaction with a strong base. Reactions with potassium bis(trimethylsilyl)amide were performed in toluene, followed by precipitation of the potassium indenide salt by the addition of hexanes. The indenides were isolated from bis(trimethylsilyl)amine by filtration and rigorous washing with additional hexanes. Reactions with *n*-butyl lithium were performed in a combination of pentane and hexanes, followed by precipitation of the lithium indenide salt by the addition of a small volume of diethyl ether. The indenides were similarly isolated and washed prior to reactions with transition metal salts.

Synthesis of Substituted Bis(indenyl)vanadium(II) Complexes. Once the appropriate indenide salts were prepared, the corresponding bis(indenyl)vanadium(II) complexes could be readily synthesized by salt metathesis elimination reactions. The source of vanadium(II) was prepared via the reduction of vanadium(III) chloride with one equivalent of aluminum powder, and subsequently treated with two equivalents of the appropriate alkali metal indenide salt in THF (eq 5); the resulting mixtures were generally stirred overnight to ensure complete reaction. Following the removal of THF under vacuum, a less polar solvent (pentane, hexanes, or toluene) was added to extract the vanadium species, precipitating the alkali metal chloride in the process. The solubility of these bis(indenyl)vanadium(II) complexes in most non-polar solvents provides an efficient means by which to separate the desired materials from the rest of the reaction mixture.

(5)

$$2\,K[Ind'] + [VCl_2] \xrightarrow{THF} \xrightarrow{Hex\ or\ Pent} (Ind')_2V + 2\,KCl$$

Solid State (SQUID) Magnetic Susceptibility Measurement of Bis(2-methyl-indenyl)vanadium(II). A crystalline sample of $(Ind^{Me\text{-}2})_2V$ was examined with a SQUID magnetometer, and complete data from that measurement can be found in Appendix C. Figure 34 shows the recorded magnetic moment (μ_{eff}) of $(Ind^{Me\text{-}2})_2V$ as a function of temperature.

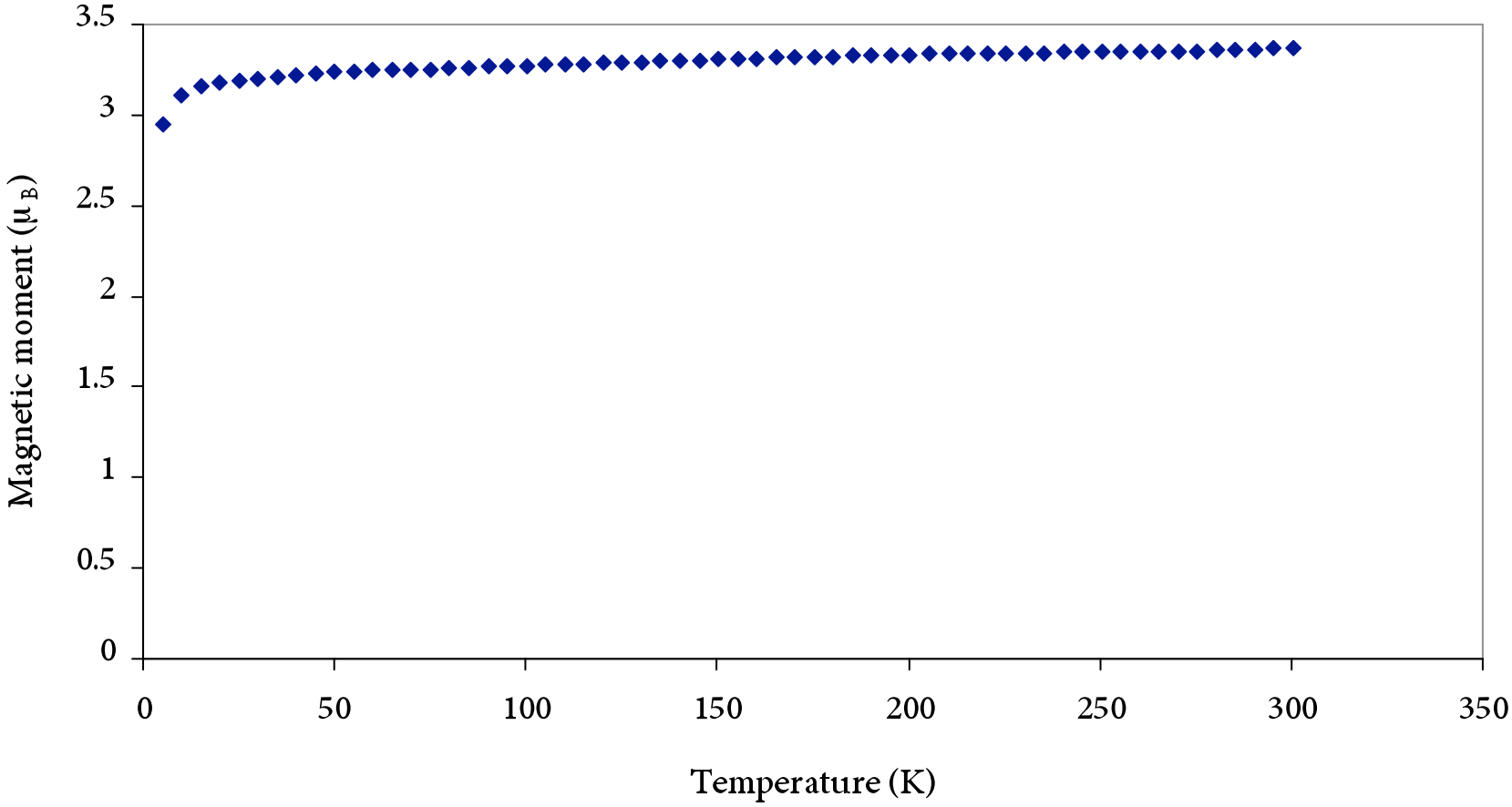

Figure 34. SQUID data for $(Ind^{Me\text{-}2})_2V$ showing the compound's high-spin nature in the solid state.

Solid State Structures

$(Ind^{2Si-1,3})_2V$. Crystals of $(Ind^{2Si-1,3})_2V$ were harvested from a hexanes solution as dark brown plates. An ORTEP of the molecule is given in Figure 35, which indicates the numbering scheme referred to in the text; selected bond lengths and angles are shown in Table 13.

The crystal structure has two independent $(Ind^{2Si-1,3})_2V$ molecules along with one *n*-hexane molecule in the asymmetric unit. The two vanadium molecules are very similar in all bond distances and angles, so only one will be discussed. The molecule is in a gauche conformation with the ligands rotated 86.56° from eclipsed. Similar to other transition metal complexes of this ligand,[8,77] the trimethylsilyl groups that lie between those of the opposing ligand are more sterically strained. Groups Si(2) and Si(3) are noticeably bent out of the C_5 ring plane by an average distance of 0.273 Å, somewhat more than groups Si(1) and Si(4), which average 0.210 Å.

The average V–C bond distance is 2.30(1) Å, which is the second longest metal–carbon distance known for this particular ligand set. Only the analogous manganese complex (see Chapter 3), with its 5 unpaired electrons, has longer distances, suggesting this molecule must also possess a high-spin state ($S = {}^3/_2$). The C_5 rings in this compound have a smaller angle between them than the rings of the manganese analogue. This fact, in conjunction with the lack of significantly increased bending along the hinge or fold angles, implies the molecule is not more strained than its manganese counterpart. As a final

point of comparison with the manganese molecule, $(Ind^{2Si-1,3})_2V$ possesses slightly shorter methyl–methyl contact distances (3.965 Å; cf. 3.992 Å for manganese) and shorter methyl–C_6 ring contact distances (3.621 Å; cf. 3.772 Å for manganese). At metal–C_5 ring distances shorter than about 2.3 Å, twisting of the ligands does not relieve all steric congestion. In the case of $(Ind^{2Si-1,3})_2Cr$, there is much more distortion of the ligands due to the shorter Cr–C bonds, significantly increasing the out-of-plane bending of the trimethylsilyl groups.[8]

Table 13. Selected Bond Distances and Angles for $(Ind^{2Si-1,3})_2V$.

Atoms	Distance (Å)	Atoms	Distance (Å)
V(1)–C(1)	2.264(3)	V(1)–C(21)	2.255(3)
V(1)–C(2)	2.310(4)	V(1)–C(22)	2.305(3)
V(1)–C(3)	2.321(3)	V(1)–C(23)	2.327(3)
V(1)–C(8)	2.316(3)	V(1)–C(28)	2.336(3)
V(1)–C(9)	2.291(4)	V(1)–C(29)	2.287(4)

Δ_{M-C}	0.040 Å
hinge angle	3.430°
fold angle	2.054°
angle between C_5 ring planes	5.800°
twist	86.56°

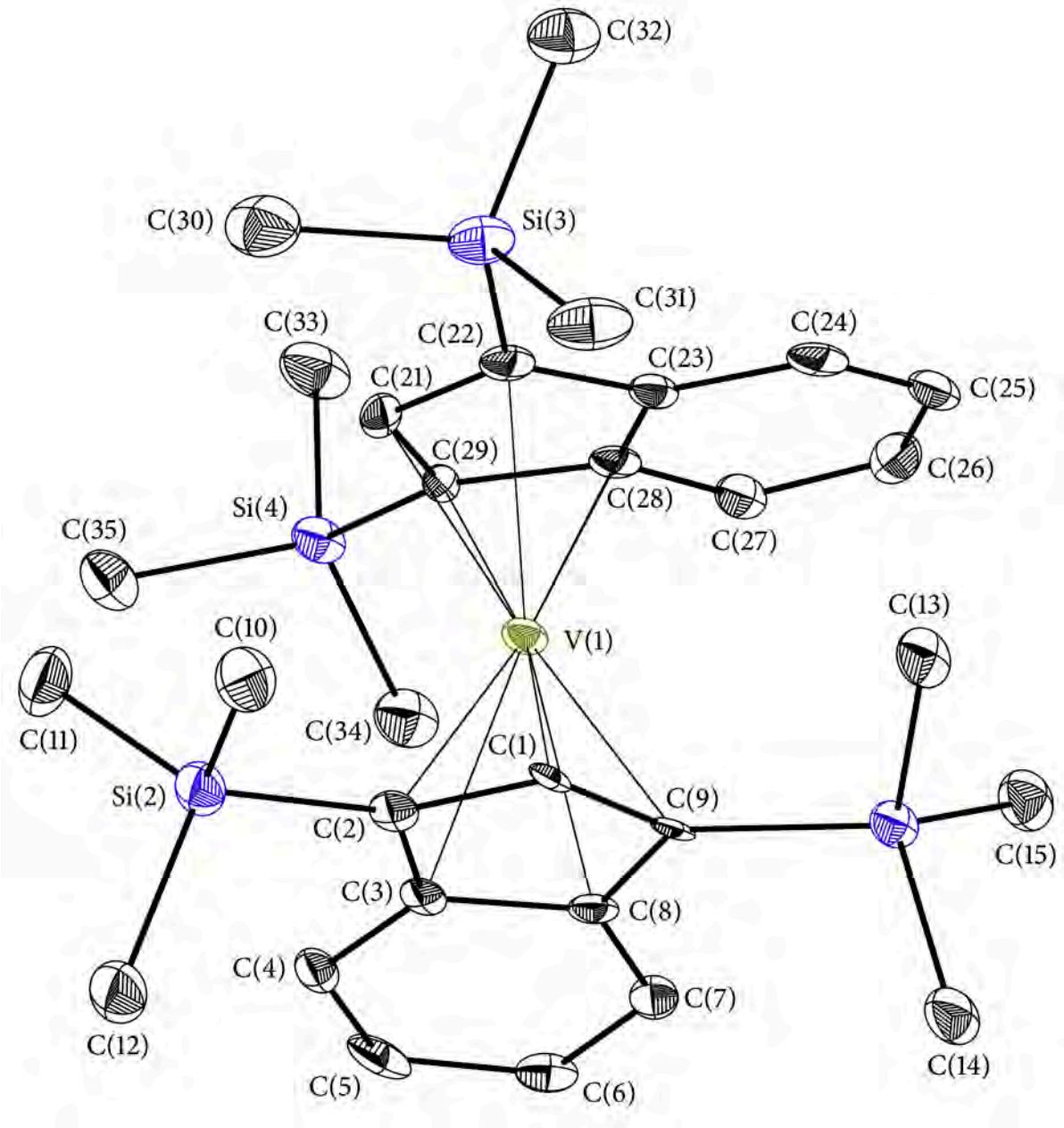

Figure 35. ORTEP of the non-hydrogen atoms of $(Ind^{2Si-1,3})_2V$ illustrating the numbering scheme used in the text. Thermal ellipsoids are shown at the 50% level.

$(Ind^{3Me\text{-}2,4,7})_2V$. Crystals of $(Ind^{3Me\text{-}2,4,7})_2V$ were harvested from a hexanes solution as dark green blocks. An ORTEP of the molecule is given in Figure 36, which indicates the numbering scheme referred to in the text; selected bond lengths and angles are shown in Table 14.

The crystal structure has four independent molecules in the asymmetric unit. The four molecules are very similar in all bond distances and angles, so only one will be discussed. The molecule possesses an eclipsed conformation with the ligands only slightly rotated from completely eclipsed (4.77°). The chromium analogue of this compound crystallizes with both eclipsed and staggered conformations in the unit cell,[10] but only the eclipsed molecule will be examined for comparisons.

The average V–C bond distance is 2.28(1) Å, similar to that found in $(Ind^{2Si\text{-}1,3})_2V$, and expectedly longer than the low-spin (S = 1) chromium analogue (2.168(5) Å). Relative to the C_5 ring plane, the methyl substituents at C(3) and C(15) are bent by 2.4° and 1.3°, respectively. While not attributable to their proximity (3.992 Å, which is just at the van der Waal's contact distance), this slight distortion observed in the vanadium complex is much more pronounced in the chromium species with the methyl groups bending out of the ring plane by 6.7°. The flexing of the methyl substituents in the vanadium complex is more noticeable on the C_6 ring owing to the closer contact distances of 3.922 Å and 3.802 Å. This oddity is caused by the unusually large fold angle (4.44°) in only one of the ligands which actually bends *toward* the other ring. This could be the result of a 15 e^-

complex desiring more electron density around the metal. Bis(indenyl)zirconium(II) complexes are known to have η^5-,η^9-bound ligands, accommodated by much larger fold angles (37°) in the η^9-bound ligand of (η^9-1,3-diisopropylindenyl)-(η^5-1,3-diisopropylindenyl)zirconium.[139] The extreme bending of the ligand in the zirconium case is attributed to the lack of C_6 ring substituents in conjunction with a rotation to the gauche conformation. This configuration affords an 18 e^- complex, rather than an extremely electron deficient η^5,η^5-bound complex. In (cyclopentadienyl)(pentalene) vanadium(III) complexes, the pentalene ligand is bent (≤ 43°) at the bridgehead atoms, also allowing for an 18 e^- complex.[140]

Table 14. Selected Bond Distances and Angles for $(Ind^{3Me\text{-}2,4,7})_2V$.

Atoms	Distance (Å)	Atoms	Distance (Å)
V(1)–C(1)	2.297(4)	V(1)–C(13)	2.286(4)
V(1)–C(2)	2.265(4)	V(1)–C(14)	2.276(4)
V(1)–C(3)	2.277(4)	V(1)–C(15)	2.298(4)
V(1)–C(4)	2.264(4)	V(1)–C(16)	2.268(4)
V(1)–C(5)	2.298(4)	V(1)–C(17)	2.269(4)
Δ_{M-C}		0.002 Å	
hinge angles		2.663°, 2.263°	
fold angles		1.421°, 4.443°	
angle between C_5 ring planes		0.848°	
twist		4.774°	

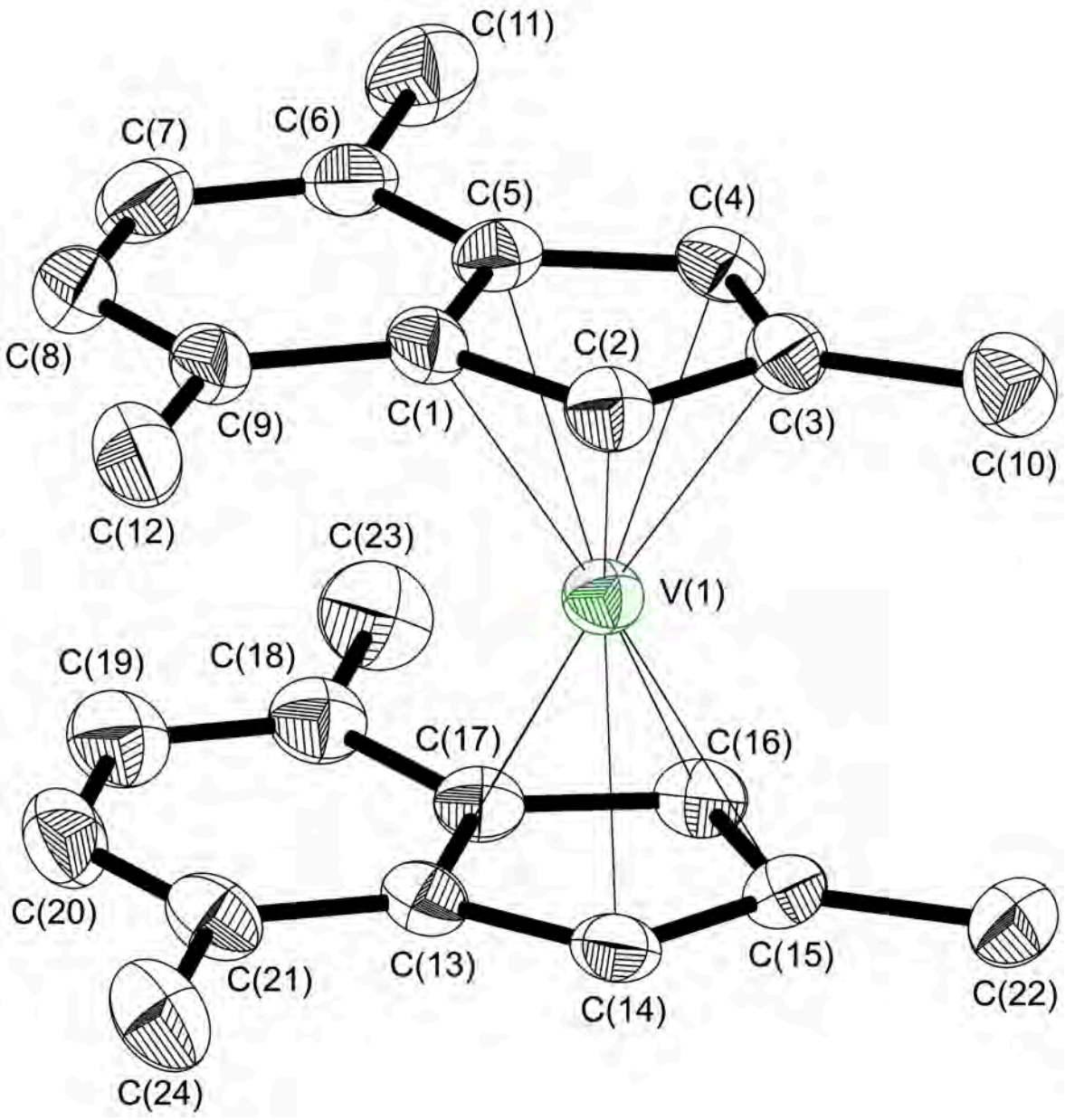

Figure 36. ORTEP of the non-hydrogen atoms of $(Ind^{3Me-2,4,7})_2V$ illustrating the numbering scheme used in the text. Thermal ellipsoids are shown at the 50% level.

$(Ind^{Me-2})_2V$. Crystals of $(Ind^{Me-2})_2V$ were harvested from a pentane solution as dark green plates. Only half of the molecule is unique, as the vanadium lies on an inversion center. An ORTEP of the molecule is given in Figure 34, which indicates the numbering scheme referred to in the text; selected bond lengths and angles are shown in Table 15.

The average V–C ring distance observed for this species (2.268(4) Å) is virtually identical to that observed in $(Ind^{3Me-2,4,7})_2V$. The ligands are bound in an η^5 fashion to the vanadium center, and are staggered 180° with respect to one another. The methyl group is bent out of the C_5 plane by 0.035 Å (1.34°), which is similar to the out-of-plane bending angles found in $(Ind^{3Me-2,4,7})_2V$. The inversion center necessarily causes the C_5 rings to be perfectly parallel. This, in conjunction with the small degree of ring slippage (Δ_{Mn-C} = 0.011 Å), suggests the core of the molecule is much like vanadocene.

Table 15. Selected Bond Distances and Angles for $(Ind^{Me-2})_2V$.

Atoms	Distance (Å)	Angle	Degree
V(1)–C(1)	2.256(2)	hinge	2.017
V(1)–C(2)	2.274(2)	fold	3.793
V(1)–C(3)	2.261(2)	C_5 ring planes	0
V(1)–C(8)	2.273(2)	twist	180
V(1)–C(9)	2.277(2)		

Δ_{M-C} = 0.011 Å

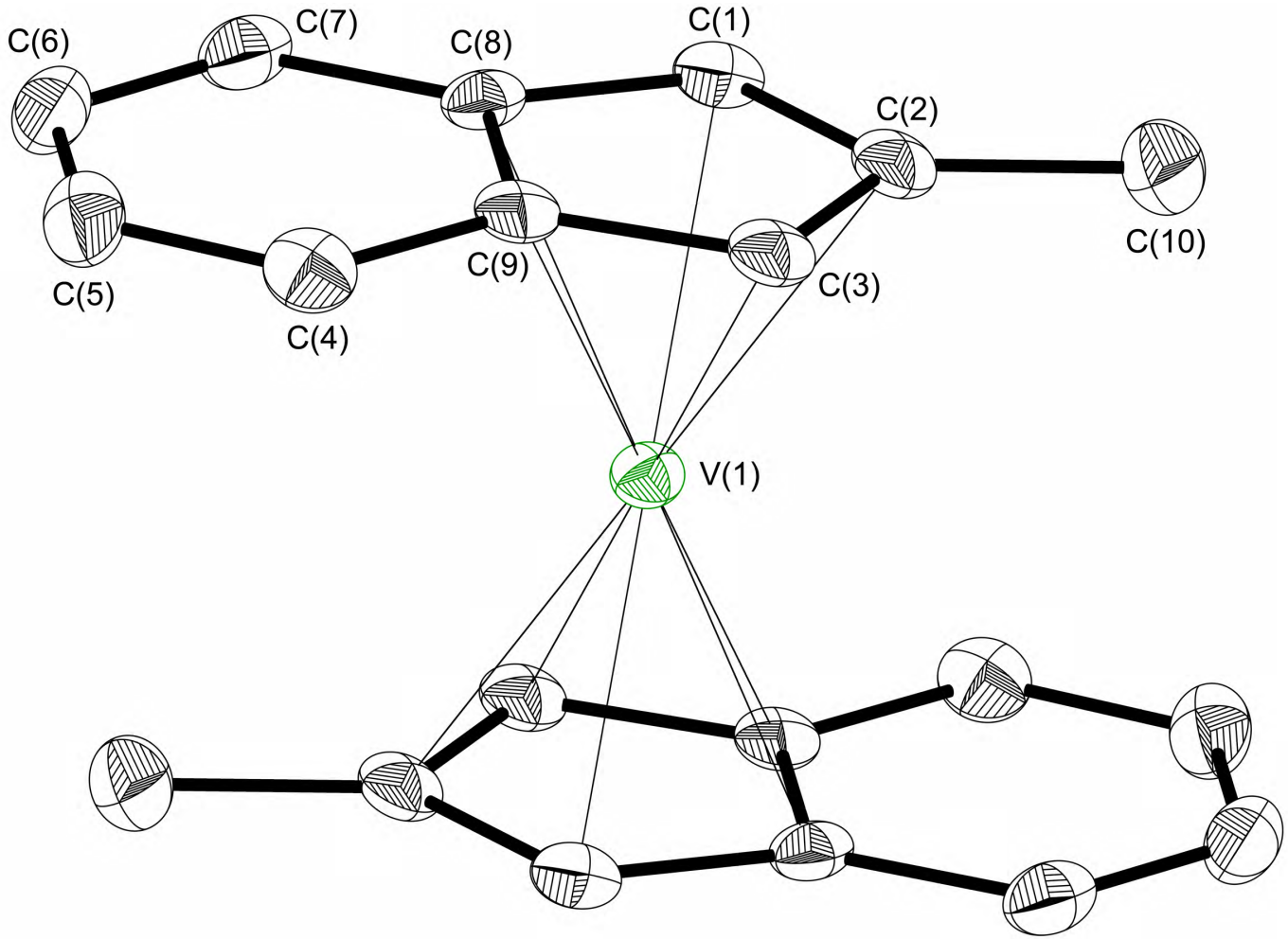

Figure 37. ORTEP of the non-hydrogen atoms of $(Ind^{Me-2})_2V$ illustrating the numbering scheme used in the text. Thermal ellipsoids are shown at the 50% level.

$(Ind^{2Me-4,7})_2V$. Crystals of $(Ind^{2Me-4,7})_2V$ were harvested from a pentane solution as dark green plates. There are two independent molecules in the unit cell, however they have nearly identical bond lengths and angles, so only one will be discussed here. An ORTEP of the molecule is given in Figure 38, which indicates the numbering scheme referred to in the text; selected bond lengths and angles are shown in Table 16.

The average V–C ring distance observed for this species (2.270(9) Å) is virtually identical to that observed in both $(Ind^{3Me-2,4,7})_2V$ and $(Ind^{Me-2})_2V$. The ligands are bound in an η^5 fashion to the vanadium center, and are rotated 21.2° from perfectly eclipsed. This is a more noticeable twist than in the chromium analogue (8.6°, Chapter 1). The Me···Me contact distances of 3.884 Å and 3.925 Å are elongated from those in the chromium case, methyl groups range from 0.19° to 2.27°, which are similar to the out-of-plane bending angles found for the C_6 ring methyl groups of $(Ind^{3Me-2,4,7})_2V$.

Table 16. Selected Bond Distances and Angles for $(Ind^{2Me-4,7})_2V$.

Atoms	Distance (Å)	Atoms	Distance (Å)
V(1)–C(1)	2.285(3)	V(1)–C(12)	2.268(3)
V(1)–C(2)	2.258(3)	V(1)–C(13)	2.259(3)
V(1)–C(3)	2.265(3)	V(1)–C(14)	2.274(3)
V(1)–C(4)	2.263(3)	V(1)–C(15)	2.268(3)
V(1)–C(5)	2.285(3)	V(1)–C(16)	2.279(3)
Δ_{M-C}		0.015 Å	
hinge angles		2.300°, 2.214°	
fold angles		2.387°, 2.844°	
angle between C_5 ring planes		1.830°	
twist		21.175°	

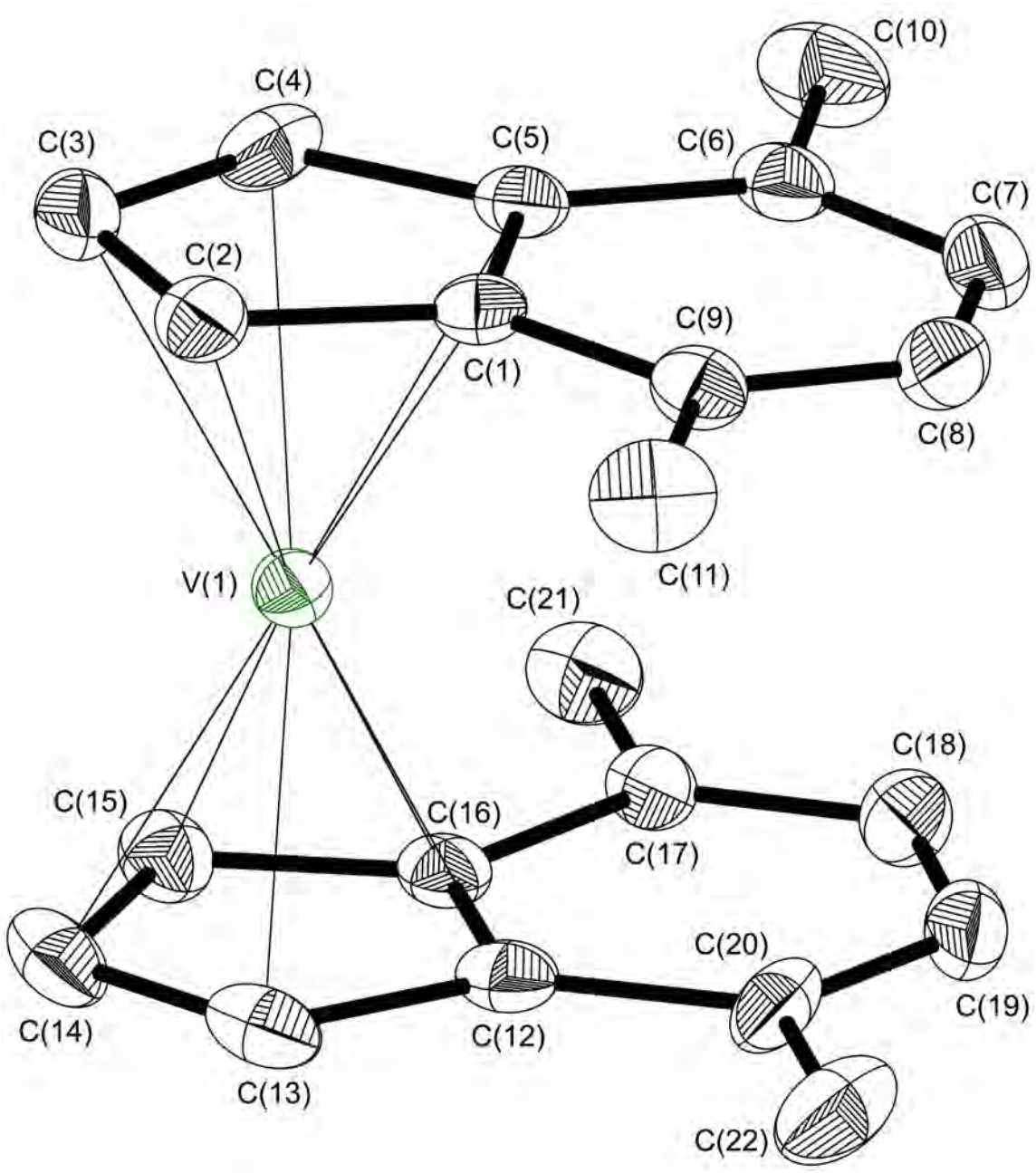

Figure 38. ORTEP of the non-hydrogen atoms of $(Ind^{2Me\text{-}4,7})_2V$ illustrating the numbering scheme used in the text. Thermal ellipsoids are shown at the 50% level.

Computational Results

The parent bis(indenyl)vanadium(II) has been known since 1986,[7] and it was isolated as dark green crystals the following year.[141] The crystal structure was not satisfactorily determined due to the presence of both staggered and eclipsed ring conformations occurring in the lattice. For a basis of comparison, DFT calculations have been performed on this parent molecule in three conformations (staggered, eclipsed, and gauche). The functional and basis set PW91PW91/6-31+G(d,p) was used throughout this study, and was used here to determine the relative energies of the three conformations. As expected, only a very slight energy difference exists among rotational conformers, which is consistent with the lack of a preferred rotamer in the solid state. The energetic similarity among these calculated minima is not indicative of a low rotational barrier, as this barrier has been shown to be much higher than in Cp complexes.[142] Results are listed in Table 17.

The uptake of a single molecule of CO by $(Ind)_2V$ was studied by this method to determine the preferred geometric conformation of the molecule, along with the energy

Table 17. Calculated Relative Thermodynamics of $(Ind)_2V$

rotational conformation	unpaired electrons	Number of Imaginary frequencies	relative ΔG^0 at 298 K and 1 atm (kcal/mol)
eclipsed	3	0	+2.3
gauche	3	0	0
staggered	3	0	+2.0

change and stretching frequency of the monocarbonyl. While the variance of 20 cm^{-1} between calculated ν_{CO} values seems large, it corresponds to an energy difference of only 0.06 kcal/mol, and is within the estimated accuracy of the functional and basis set used. Three geometric minima were found, with their ΔG^0 values varying by only 1.4 kcal/mol. The conformations are depicted in Figure 39, and their corresponding carbonyl stretching frequencies and relative energies are presented in Table 18.

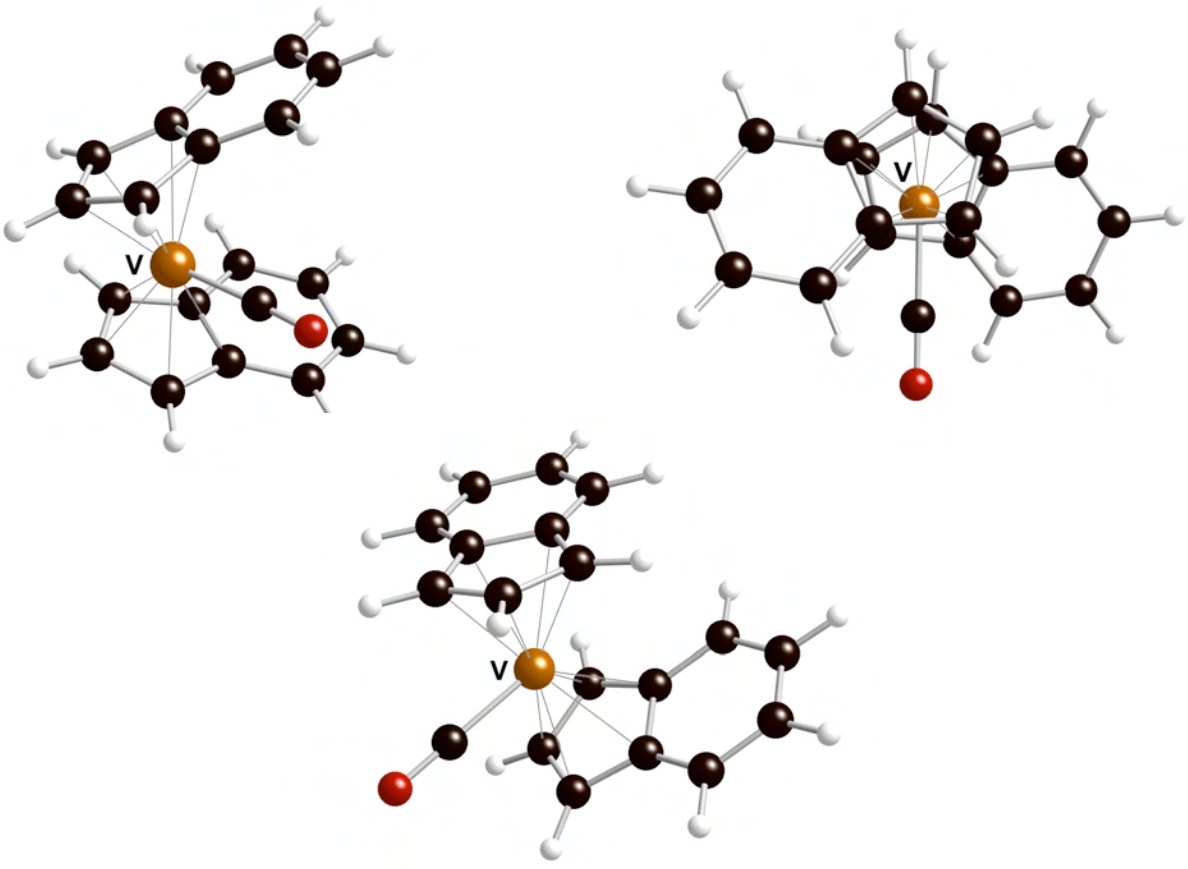

Figure 39. Calculated geometric minima of $(Ind)_2V(CO)$, forming eclipsed (upper left), "inner gauche" (upper right), and "outer gauche" (lower) conformations.

Table 18. Calculated relative thermodynamics of $(Ind)_2V(CO)$

rotational conformation	unpaired electrons	Imaginary frequencies (cm^{-1})	C–O stretching frequency (cm^{-1})	ΔG^0 at 298 K/1 atm (kcal/mol)
Eclipsed	1	0	1910	0
"inner gauche"	1	0	1905	+1.3
"outer gauche"	1	0	1890	+1.4

The carbonylation of bis(indenyl)vanadium(II) is known to form the dicarbonyl complex, which has been crystallographically characterized.[7] While not imposed in the crystal structure, C_S symmetry was enforced to perform DFT calculations on this molecule. The resulting minimum was in good agreement with the known compound for most V–C bond distances, as well as with the carbonyl stretching frequencies. Comparisons between the calculated and x-ray structures are shown in Table 19.

Table 19. Calculated *vs* Real Bond Distances and Stretching Frequencies of $(Ind)_2V(CO)_2$

	(η^5-Ind)–V distance (Å)	(η^3-Ind)–V distance (Å)	V–CO distance (Å)	carbonyl stretching frequencies (cm^{-1})
calculated structure (C_S)	2.412 2.269 2.239	2.363 2.179	1.916	1916 (asymmetric) 1954 (symmetric)
x-ray structure	2.388, 2.387 2.260, 2.272 2.237	2.360, 2.379 2.186	1.946, 1.953	1926 (asymmetric) 1978 (symmetric)

The calculated ΔG^0 values at 298 K and 1 atm for $(Ind)_2V$, $(Ind)_2V(CO)$, and $(Ind)_2V(CO)_2$ have been compared to assess the energetic favorability of the dicarbonyl formation. The binding of a single carbonyl has been determined to be spontaneous by 11.5 kcal/mol, while uptake of the second carbonyl is favored by an additional 15.9 kcal/mol, suggesting the monocarbonyl species to be a transient intermediate to the dicarbonyl complex. This was verified by the unsuccessful attempts to isolate or even detect the presence of the monocarbonyl adduct.[143]

FTIR Spectra

In a study of the steric and electronic effects of various positions of methyl and trimethylsilyl substituents in bis(indenyl)vanadium(II) complexes, a carbonylation reaction at 1 atm with each compound was carried out and the resulting infrared stretching frequencies were recorded. The reaction of CO with $(Ind^{2Si\text{-}1,3})_2V$ did not produce a color change, hence the observed spectrum (indicating the lack of a carbonyl stretch) is not shown. The methyl substituted compounds did undergo a color change from dark green to various shades of brown, and their IR spectra (Figure 40) confirm the presence of at least one V–CO bond in each case.

The single peak at 1882 cm^{-1} of $(Ind^{3Me\text{-}2,4,7})_2V$ + CO (Figure 40) indicates a monocarbonyl complex was formed. In comparison with the calculated $(Ind)_2V(CO)$ stretching frequencies (1910–1890 cm^{-1}), we observed a lowering of the $(Ind^{3Me\text{-}2,4,7})_2V(CO)$ carbonyl

peak due to the added electron donation of the methyl substituents. Upon the use of additional CO pressure (1.36 atm), the growth of dicarbonyl resonances was not observed.

The reaction of $(Ind^{Me\text{-}2})_2V$ + CO yields a classic dicarbonyl stretching pattern with the symmetric stretch registering at 1961 cm^{-1} and the asymmetric stretch at 1895 cm^{-1}. This naturally suggests that the removal of the methyl groups in the 4- and 7-positions allowed one of the indenyl rings to slip to an η^3-hapticity, accommodating the second carbonyl. To see what effect the 4- and 7-position methyl substituents have on carbonylation, the spectrum of $(Ind^{2Me\text{-}4,7})_2V$ + CO was recorded. The strong peak at 1909 cm^{-1} is suggestive of the formation of a monocarbonyl product; however, it is accompanied by a much less intense peak at 1965 cm^{-1}. This anomaly might be explained by the presence of a small amount of the dicarbonyl species, in which case the asymmetric stretch is overlapped by the monocarbonyl peak.

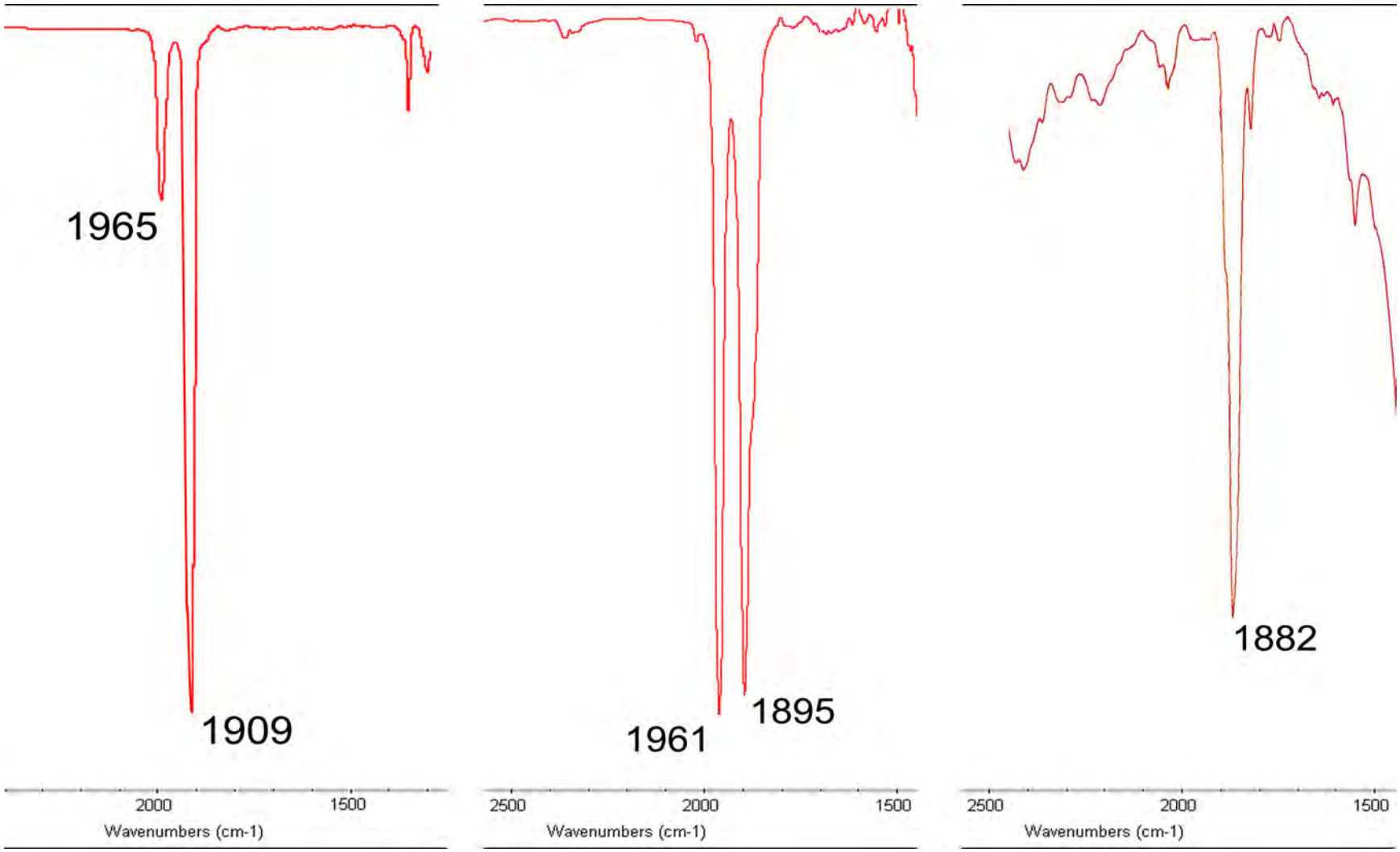

Figure 40. FTIR solution spectra of $(Ind^{3Me\text{-}2,4,7})_2V$, $(Ind^{2Me\text{-}4,7})_2V$, and $(Ind^{Me\text{-}2})_2V$ (from left to right) upon reaction with CO (1 atm).

Discussion

Vanadocene and decamethylvanadocene are both high-spin ($S = {}^3/_2$) complexes, suggesting the lowering of the spin-state to $S = ½$ in a bis(indenyl)vanadium(II) complex by the addition of electron donor substituents to the rings is unlikely. As observed in bis(indenyl)chromium(II) complexes, the symmetry of the molecules plays an important role in defining the spin states. This idea was investigated through the synthesis of the complexes $(Ind^{2Si\text{-}1,3})_2V$ and $(Ind^{3Me\text{-}2,4,7})_2V$. The trimethylsilylated compound was expected to exist in a gauche conformation, while the less bulky ligands of the latter complex could more easily rotate to an eclipsed or staggered arrangement, both of which happen to be present in the case of chromium.[10] While neither molecule is centrosymmetric in the solid state (a requirement for high-spin complexes of bis(indenyl)chromium), this breaking of the symmetry did not produce low-spin molecules. Of course, in the case of $(Ind^{2Si\text{-}1,3})_2V$, a low-spin molecule would force even greater steric repulsions due to the shortened V–C distances.

One obvious difference between the two molecules is the relative accessibility of the vanadium centers. The gauche conformation in $(Ind^{2Si\text{-}1,3})_2V$ leads to a more highly encapsulated metal compared to the more accessible metal center provided by the less bulky rings of $(Ind^{3Me\text{-}2,4,7})_2V$. This can be better understood by viewing the space filling models in Figure 41. This distinction was examined for its effect on the reactivity of each complex in the presence of carbon monoxide, as the parent $(Ind)_2V$ is known to form a stable dicarbonyl.

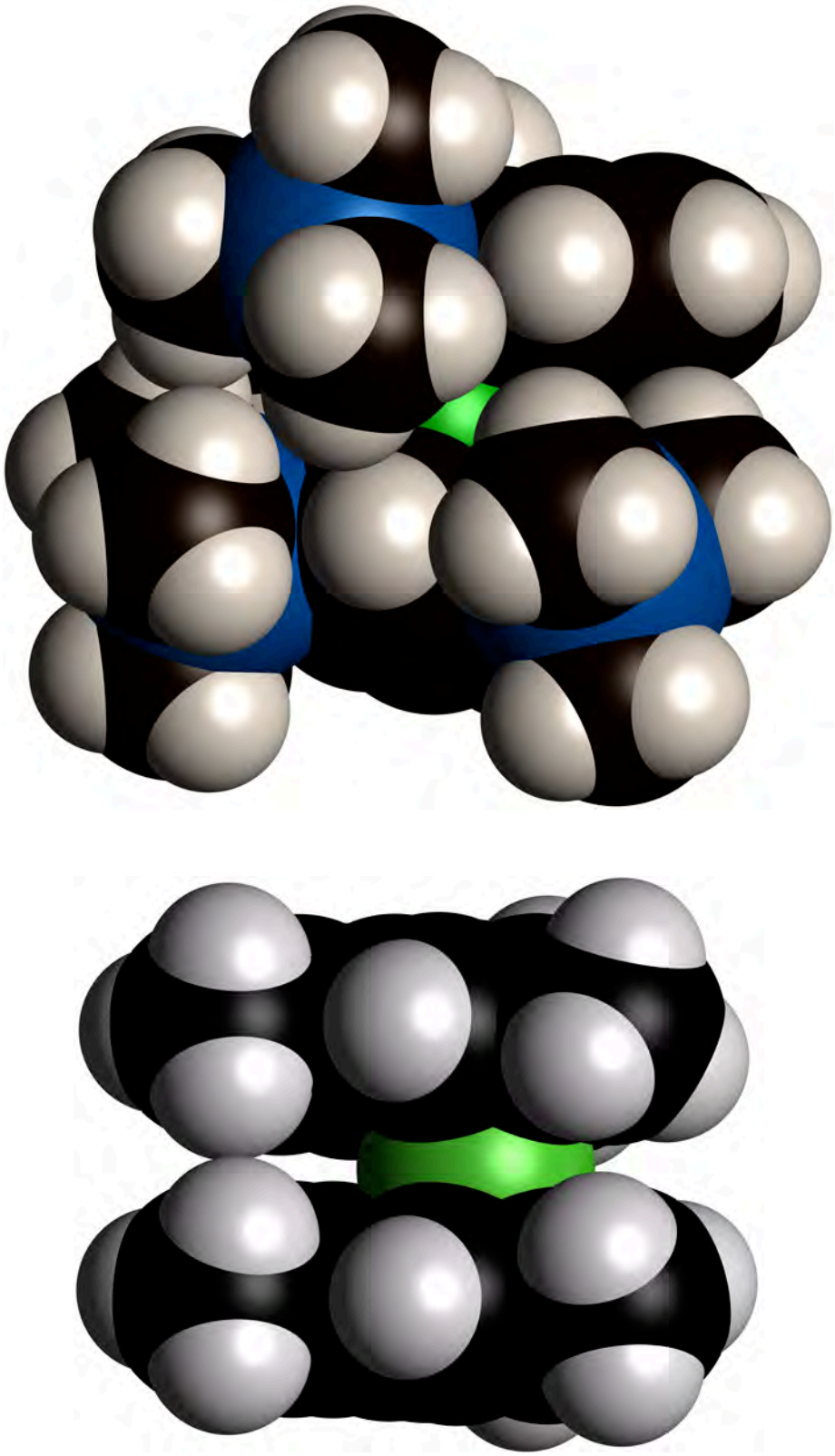

Figure 41. Space filling models of $(Ind^{2Si\text{-}1,3})_2V$ (top) and $(Ind^{3Me\text{-}2,4,7})_2V$ (bottom).

The lack of reaction of $(Ind^{2Si-1,3})_2V$ with CO, even under increased pressure, was not as surprising as the formation of the monocarbonyl complex $(Ind^{3Me-2,4,7})_2V(CO)$. The three methyl substituents on each ring, along with the ligated CO, must provide enough steric congestion to prevent the rotation of the complex to the staggered conformation, inhibiting the binding of the second carbonyl. The formation of monocarbonyl complexes from Cp_2V and Cp^*_2V is known.[136,144] These 17 e^- species are favored over the dicarbonyl complexes due to the large energy barrier of the η^5 to η^3 haptotropic slip of the Cp ligand required to bind a second carbonyl. The more heavily methylated bis(1,2,3,4,5,6,7-heptamethyl-indenyl)chromium(II) complex,[21] with even shorter metal–carbon bonds than those observed in the vanadium compound, forms a dicarbonyl,[115] suggesting steric hindrance of the three methyl groups alone is not the dominant factor preventing further carbonylation. The commonality between the structurally characterized dicarbonyl complexes of vanadium and chromium is the indenyl rings are staggered in the solid state, although it is unclear whether this conformation persists in solution. As noted in the crystal structure description, one of the indenyl rings in $(Ind^{3Me-2,4,7})_2V$ is slightly bent toward the opposing ring, possibly due to a van der Waals attraction between the methyl groups. The rotation of the rings in $(Ind^{3Me-2,4,7})_2V$ from eclipsed to a staggered conformation necessary to accommodate both carbonyl ligands may simply be too high of an energy barrier to surmount.

As a test of this theory, the molecules $(Ind^{2Me-4,7})_2V$ and $(Ind^{Me-2})_2V$ were synthesized. In the case of $(Ind^{Me-2})_2V$, the dicarbonyl was formed with CO peaks shifted to lower frequencies than those in $(Ind)_2V(CO)_2$. This is expected given that the Ind^{Me-2} ligand is a better electron donor, promoting stronger V–CO bonds due to more V–CO backbonding. The carbonylation reaction of $(Ind^{2Me-4,7})_2V$ produces an unanticipated IR spectrum, which, earlier in this chapter, was suggested to be the overlap of the combination of a dicarbonyl complex with a monocarbonyl complex. According to this interpretation, a higher ratio of eclipsed to staggered ligand conformations exists in solution. The symmetric stretch of this dicarbonyl molecule at 1965 cm^{-1} is indistinguishable from the analogous stretch of $(Ind^{Me-2})_2V(CO)_2$ at 1961 cm^{-1} since the accuracy of the spectrometer was set to ± 2 cm^{-1}. The stretch of the monocarbonyl $(Ind^{2Me-4,7})_2V(CO)$ at 1909 cm^{-1} is appropriately shifted to a higher frequency from that of $(Ind^{3Me-2,4,7})_2V(CO)$ (1882 cm^{-1}). The only apparent inconsistency in these spectra is the dicarbonyl's ($(Ind^{2Me-4,7})_2V(CO)_2$) having slightly higher energy stretches than in $(Ind^{Me-2})_2V(CO)_2$.

We previously determined the $Ind^{2Me-4,7}$ ligand to be a better donor than the Ind^{Me-2} ligand (see Chapter 1); however, the ability of the 4- and 7-positions to donate to a metal center on an η^3 slipped ring may very well be compromised. The crystal structure of $(Ind)_2V(CO)_2$ shows the C(1)–C(8) and C(3)–C(9) distances of the η^3–bound ring have elongated to 1.455(6) Å, as compared with the bond distances of the same bonds on the η^5–bound ring (1.421(7) Å), thereby disrupting the delocalization of one C_5 ring. This lowers the ability of the C_6 ring substituents to donate electron density to the metal cen-

ter, while the 1- and 3-positions would be less affected. The V–C(2) bond distance of the η^3–bound ring is the shortest of any ring carbon, likely enhancing the electron donation from the 2-position substituent. This allows for overall better donation from the indenyl ligands in $(Ind^{Me\text{-}2})_2V(CO)_2$, weakening the CO stretching energies relative to those of $(Ind^{2Me\text{-}4,7})_2V(CO)_2$.

Conclusion

Ligand-substituted molecules of bis(indenyl)vanadium(II) have been crystallographically characterized for the first time. These compounds exist in the high-spin state at all recorded temperatures regardless of substituent types, positions, or resulting rotational conformation of the ligands. Although still O_2 sensitive, the reactivity of the vanadium center toward CO in $(Ind^{2Si\text{-}1,3})_2V$ has been blocked. By replacing the sterically demanding trimethylsilyl substituents with more compact methyl groups, carbon monoxide becomes a strongly coordinated ligand, as evidenced by the low IR stretching frequencies. It remains, however, highly labile. The slight variations in methyl substitution patterns has unexpectedly led to tremendous carbonylation reactivity differences, the results of which are highly suggestive of large energetic barriers preventing conformational rearrangements even in solution. This is not inconsistent with the calculated slight energy difference between rotamers, but it does suggest the presence of a high energy transition state.

CHAPTER V

SUMMARY AND FUTURE DIRECTIONS

Although the ligand field of the cyclopentadienyl ring is stronger than that of the indenyl ligand, the ability of the indenyl ring to vary its hapticity more easily in transition metal complexes has allowed for a larger diversity in both the structure and reactivity of early to middle first row (metallocene-type) transition metal complexes. This has been accomplished through the use of methyl or trimethylsilyl substituted indenyl rings.

Trimethylsilyl groups have been employed as sterically demanding substituents, with their placements on the ring designed to impose a specific rotational conformation of the ligands without substantially altering the electron donation of the ring. Substitution of the 1- and 3-positions of the indenyl ring with $SiMe_3$ groups, followed by complexation of two indenyl rings to a metal, has consistently produced gauche conformations. The average metal–carbon bond distances of the $(Ind^{2Si\text{-}1,3})_2M$ framework, where M = V, Cr,[8] Mn, or Fe,[77] are shown in Table 20 and plotted in Figure 42. As can be seen from the rest of the data in Table 20, there are no correlations between other geometrical aspects with the spin-state of the molecules.

Table 20. Comparisons among $(Ind^{2Si-1,3})_2M$, Where M = Fe, Cr, V, and Mn.

complex	unpaired electrons	average M–C distance (Å)	angle between C_5 ring planes	rotation from eclipsed
$(Ind^{2Si-1,3})_2Fe$	0	2.09(1)	5.8°	94.3°
$(Ind^{2Si-1,3})_2Cr$	2	2.20(2)	9.99°	86.3°
$(Ind^{2Si-1,3})_2V$	3	2.30(1)	5.8°	86.6°
$(Ind^{2Si-1,3})_2Mn$	5	2.42(1)	7.99°	97.0°

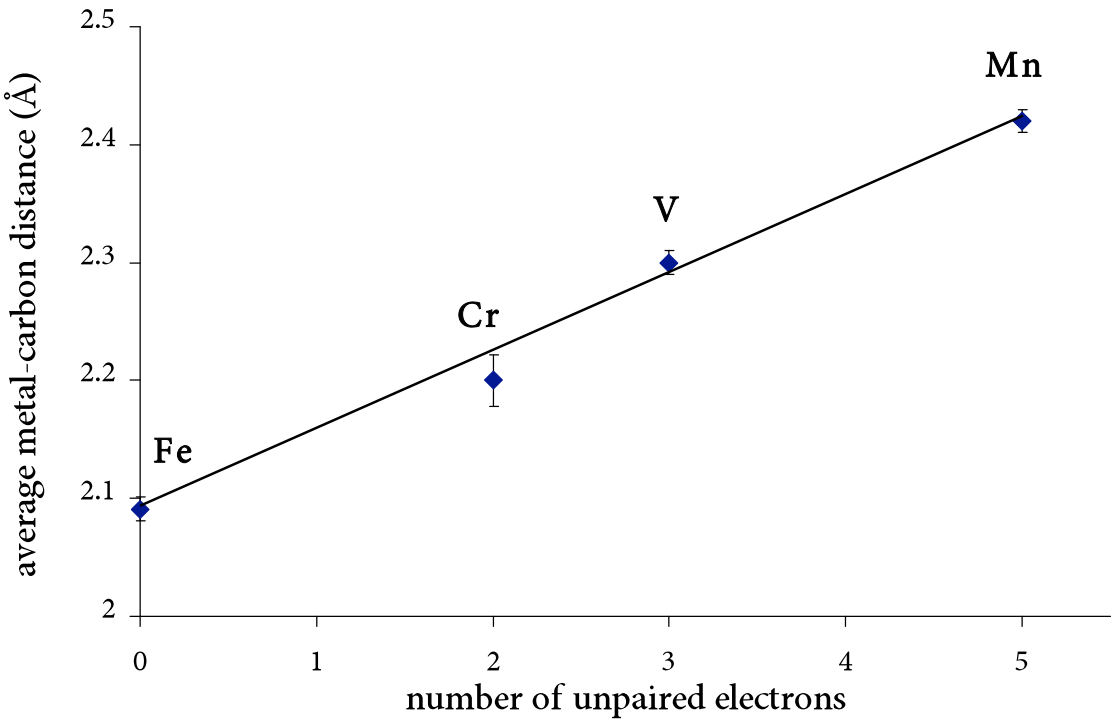

Figure 42. Plot showing the linear relationship of the average M–C distance of $(Ind^{2Si-1,3})_2M$ with the number of unpaired electrons in the molecules; M = Fe, Cr, V, and Mn.

The methylated indenyl rings Ind^{Me-2}, $Ind^{2Me-4,7}$, and $Ind^{3Me-2,4,7}$ have been studied in complexes of vanadium, chromium,[9,10] and manganese. In the cases of vanadium and chromium, the rotational conformations of the complexes with the same ligands are consistent, except with the $Ind^{3Me-2,4,7}$ ligand set. For $(Ind^{3Me-2,4,7})_2Cr$, there are both eclipsed and staggered conformations present in a 2:1 ratio in the solid state. As determined in Chapter 1, the inversion center of the staggered form leads to nonbonding combinations of orbitals 42 and 44 (Figures 12 and 13). This lack of interaction with a metal *d* orbital, allows orbital 48 to be sufficiently low in energy to be singly occupied, resulting in a high-spin molecule.

In the vanadium analog to $(Ind^{3Me-2,4,7})_2Cr$, only the eclipsed conformation is present in the solid state. Assuming the Hückel calculations can be extended to the vanadium system of one less electron, a prediction of the spin-state of the system can be made. Although the symmetry has been relaxed to allow bonding interactions with orbitals 42 and 43, one fewer *d* electron means the energy gap between orbitals 47 and 48 no longer determines the spin-state. The relatively small difference in energy between orbitals 46 and 47, regardless of symmetry, ensures a high-spin molecule (3 unpaired electrons). This is experimentally observed; both the eclipsed ($(Ind^{2Me-4,7})_2V$ and $(Ind^{3Me-2,4,7})_2V$) and staggered ($(Ind^{Me-2})_2V$) molecules possess 3 unpaired electrons in solution as well as the in solid state.

Attempts to produce monomeric sandwich complexes of manganese with the methylated indenyl ligands have been unsuccessful thus far. High-spin complexes of methyl-substituted bis(indenyl)manganese(II) have been shown to possess a large degree of structural variations in the solid state not observed in substituted bis(indenyl)vanadium(II) or chromium(II) complexes. Bonding modes of the indenyl ligands include terminal η^1-, η^2-, η^3-, and η^5-, along with bridging η^1,η^1- and η^1,η^2-ligands.

Efforts to produce monomeric, methyl-substituted bis(indenyl)manganese(II) complexes are still underway. These sandwich frameworks are desirable as π-stacking, one-electron donors for use in CT salts. Once oxidized to Mn(III) (a d^4 system like Cr(II)), spin-crossover behavior may result. If magnetic ordering is also observed in the range of temperatures that produces the spin-state change, the system would likely possess bistability—a highly desirable property for magnetic materials involving hysteresis due to a system possessing two distinct low-energy states under the same conditions.

Systems that could possess this kind of magnetism are under investigation at this time. To determine the type and degree of magnetism present in a sample over a nearly 300° range of temperatures approaching absolute zero, a superconducting quantum interference device (SQUID) is used.

Although the present methyl substituted indenyl manganese(II) complexes are not structurally suited for incorporation into CT salts, [(Ind')MnCl(thf)] has been shown to exhibit reactivity with select nonpolar gases such as N_2, H_2, and C_2H_4. Attempts to stabi-

lize such interactions via indenyl ring substitutions have been mostly ineffective, although substituents other than methyl groups (i.e., trimethylsilyl, ethyl, and isopropyl) are yet to be studied. Because metal to ligand backbonding is crucial to the stabilization of the $Mn\cdots N_2$ interaction, strong σ-donors, such as alkyl phosphines, will be examined as replacements for the coordinated THF ligands. Finally, the bridging halides will be varied to produce [(Ind')MnF(L)] and [(Ind')MnI(L)]. By optimizing the complex with most suitable indenyl ring, halide, and σ-donor, the extreme lability of the nonpolar gases may be stabilized to produce an isolable and more easily studied product. The binding of such gases as N_2 and C_2H_4 may be useful in the design of catalytic system for ammonia and polyolefin production.

Appendix A

SYNTHESIS AND STRUCTURAL CHARACTERIZATION OF INDENYL ZINC(II) COMPLEXES AND THEIR SUBSEQUENT ATTEMPTED REDUCTIONS TO ZINC(I)

The following work was undertaken in an attempt to extend the work of Carmona[145] on Zn(I)-containing cyclopentadienyl compounds to complexes with the indenyl ligand. The original goal was not achieved, owing to rapid formation of zinc metal when reduction of Zn(II) precursors was attempted. In the course of the project, the first crystallographically characterized indenyl zinc iodide species was isolated.

Experimental

Synthesis and Attempted Reduction of Bis(indenyl)zinc(II), $(Ind)_2Zn$. 1.23 g (3.85 mmol) of ZnI_2 was added to a 125 mL Erlenmeyer flask along with a stir bar and 10 mL of THF. To the mixture was added 1.170 g (7.58 mmol) of potassium indenide dissolved in 20 mL of THF. After stirring overnight, the reaction mixture was colorless and was dried under vacuum before extracting with 20 mL of a 50/50 hexanes/diethyl ether mixture. 0.0204 g (0.509 mmol) of KH was added and the mixture continued stirring at –30 °C for 2 h. The THF was removed under vacuum, and 7 mL of pentane was added to extract the organozinc complex. After filtering over a medium porosity glass frit, the filtrate was a faint yellow solution. Upon removal of the solvent at –30 °C over 12 h, a light yellow oil remained which decomposed with warming to RT.

Attempted Synthesis of Bis(1,2,3-trimethylindenyl)dizinc(I), $(Ind^{3Me-1,2,3})_2Zn_2$ (route 1). All chemicals, solvents, and glassware were chilled and kept at –30 °C at all steps during this synthesis. ZnI_2 (0.1626 g, 0.509 mmol) was added to a 10 mL

vial along with a stir bar and 3 mL of THF. To the mixture was added 0.200 g (1.02 mmol) of potassium 1,2,3-trimethylindenide in 3 mL of cold THF with stirring. The reaction mixture lightened from a dark yellow in 5 min as KI precipitated from solution. After about 30 min of stirring, 0.0204 g (0.509 mmol) of KH was added, and the reaction was allowed to stir for 2 h. The THF was removed under vacuum, and 7 mL of pentane was added to extract the organozinc product. After filtering over a medium porosity glass frit, the filtrate was a faint yellow solution. Upon removal of the solvent at –30 °C, a light yellow oil was isolated which subsequently decomposed with warming to RT.

Attempted Synthesis of Bis(1,2,3-trimethylindenyl)dizinc(I), ($Ind^{3Me-1,2,3}$)$_2Zn_2$ (route 2). All chemicals, solvents, and glassware were chilled and kept at –30 °C during all steps of this synthesis. ZnI_2 (0.1626 g, 0.509 mmol) was added to a 10 mL vial along with a stir bar and 3 mL of THF. To the mixture was added 0.200 g (1.02 mmol) of potassium 1,2,3-trimethylindenide in 3 mL of cold THF with stirring. The reaction mixture lightened from a dark yellow in 5 min as KI precipitated from solution. After about 30 min of stirring, 0.51 mL (1.0 M, 0.51 mmol) of diethyl zinc was added, and the mixture continued stirring for 2 h. The THF was removed under vacuum, and 7 mL of hexanes was added to extract the organozinc product. After filtering over a medium porosity glass frit, the filtrate was faintly yellow, which upon removal of the solvent at –30 °C over 12 h, left clear, colorless crystals. There were two distinct crystalline materials in the flask, one of which was stable enough to obtain an x-ray structure (Figure 43). The

larger crystals decompose instantly upon exposure to room temperature, depositing zinc metal.

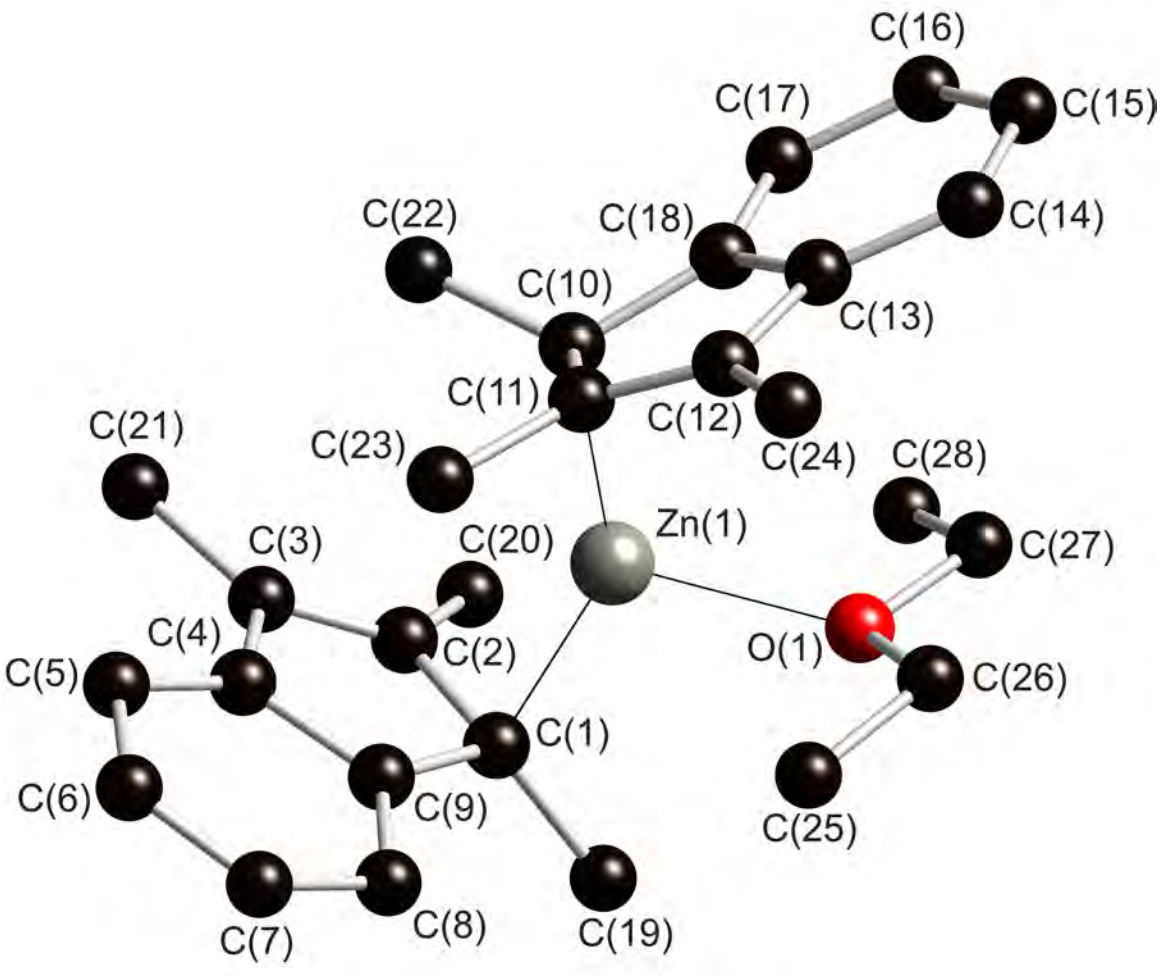

Figure 43. Ball and stick model of the non-hydrogen atoms of $(Ind^{3Me\text{-}1,2,3})_2Zn(Et_2O)$. Poor crystallographic data prevent rigorous structural interpretations.

Synthesis of 1,3-Bis(trimethylsilyl)indenyl Zinc(II) Iodide, $(Ind^{2Si\text{-}1,3})ZnI$. ZnI_2 (0.1936 g, 0.607 mmol) was added to a 250 mL Erlenmeyer flask fitted with a stir bar. THF (50 mL) was added and the flask was stirred for 1 h to disperse the ZnI_2.

Potassium 1,3-bis(trimethylsilyl)indenide (0.1811 g, 0.606 mmol) was dissolved in 100 mL of THF and added to a 125 mL addition funnel. The K[$Ind^{2Si-1,3}$] was added dropwise over 2 h into the flask containing ZnI_2. The reaction was allowed to stir overnight before the removal of the solvent under vacuum left white precipitate and a colorless oil. Pentane (30 mL) was added to the flask with stirring, causing the oil to dissolve. The precipitate was removed by filtration. After several washes (4 × 10 mL), the pentane filtrates were combined into a 125 mL Erlenmeyer flask. The flask was slowly cooled from room temperature to –20 °C over 5 days. Golden crystalline rods grew from the solution, mp 182–190 °C. The structure was confirmed to be dimeric by x-ray analysis (Figure 44).

Attempted Syntheses of Bis(1,3-bis(trimethylsilyl)indenyl)dizinc(I), [($Ind^{2Si-1,3}$)Zn]$_2$. To a solution of [($Ind^{2Si-1,3}$)ZnI(thf)]$_2$ in 40 mL of THF was slowly added one equivalent of a reducing agent (NaK alloy, sodium naphthenide, C_8K, or potassium metal). After removal of the THF solvent under vacuum, an aliphatic solvent (pentane or hexanes) was added to promote precipitation of the alkali metal iodide salt. Any indenyl zinc product was isolated by filtration, followed by the removal of the solvent by evaporation under reduced pressure. The product was often a mixture of starting material with zinc metal, and no zinc(I) species were isolated.

Attempted Syntheses of 1,3-Bis(trimethylsilyl)indenyl)zinc(I) Hydride, [($Ind^{2Si-1,3}$)ZnH]$_2$. To a stirring solution of 0.160 g (0.153 mmol) of [($Ind^{2Si-1,3}$)ZnI]$_2$ in 40 mL of THF was slowly added one equivalent of potassium hydride (6.1 mg, 0.15

mmol). After typical workup of the reaction (removal of THF, extraction into hexanes, filtration, and evaporation of the hexanes), only an oil remained. ^{1}H NMR showed the same characteristic peaks of $[(Ind^{2Si\text{-}1,3})ZnI]_2$.

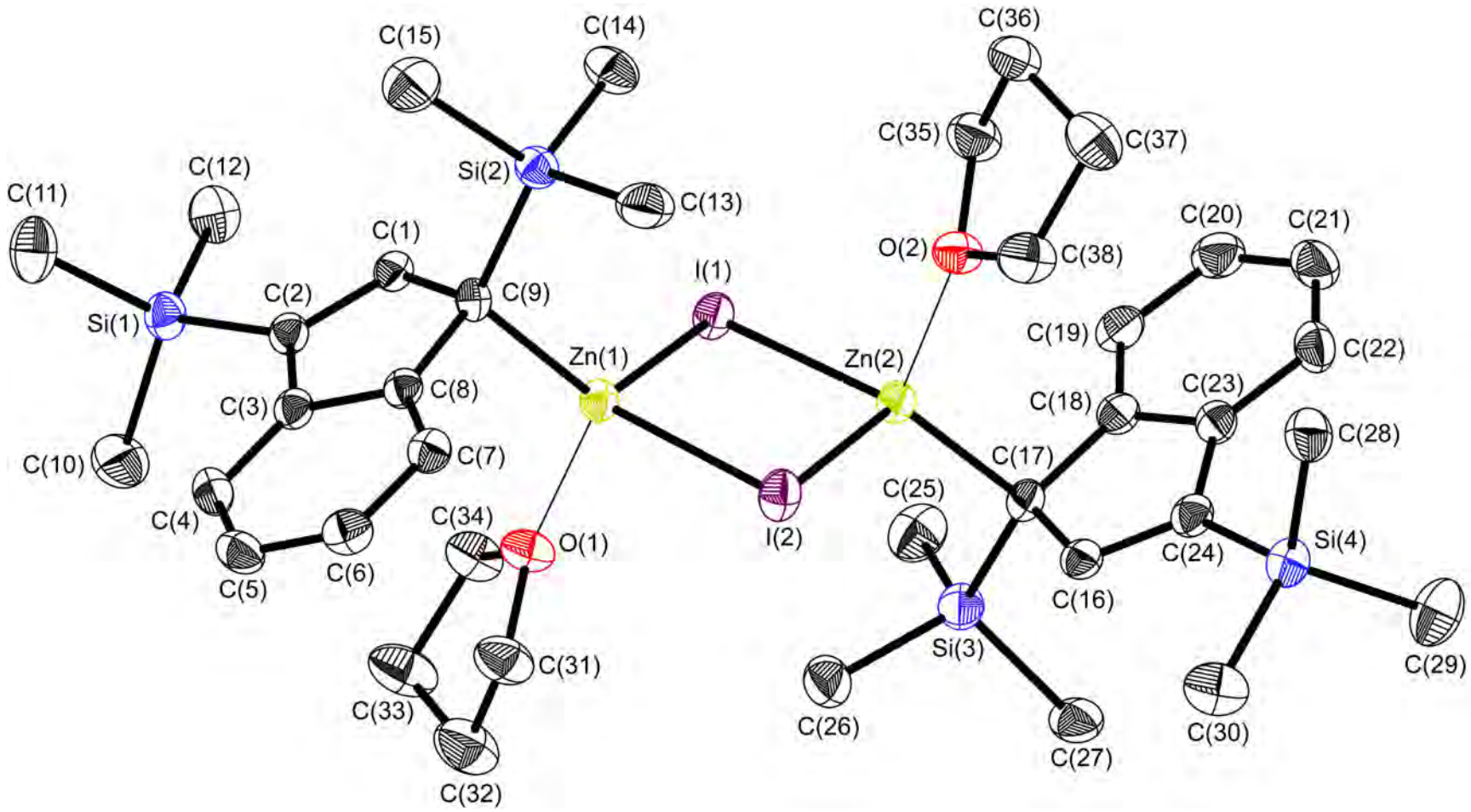

Figure 44. ORTEP of the non-hydrogen atoms of $[(Ind^{2Si\text{-}1,3})ZnI(thf)]_2$. Thermal ellipsoids are displayed at the 50% level.

Appendix B

CRYSTAL DATA AND ATOMIC FRACTIONAL COORDINATES FOR X-RAY STRUCTURAL DETERMINATIONS

Table 21. Crystal data and structure refinement for $(Ind^{2Me-4,7})_2Cr$.

Empirical formula	$C_{22}H_{22}Cr$	
Formula weight	338.40	
Temperature	173(2) K	
Wavelength	0.71073 Å	
Crystal system	Monoclinic	
Space group	*Cc*	
Unit cell dimensions	*a* = 15.3746(14) Å	aα = 90°
	b = 18.3542(16) Å	bβ = 108.440(2)°
	c = 12.656(1) Å	gγ = 90°
Volume	3388.0(5) $Å^3$	
Z	8	
Density (calculated)	1.327 g/cm^3	
Absorption coefficient	0.672 mm^{-1}	
F(000)	1424	
Crystal color, morphology	red-black, plate	
Crystal size	0.36 x 0.32 x 0.12 mm^3	
Theta range for data collection	1.78 to 25.05°	
Index ranges	-18 ≤£*h* ≤ 18, -21 ≤ *k* ≤ 21, -15 ≤ *l* ≤£11	
Reflections collected	10472	
Independent reflections	5033 [R_{int} = 0.0346]	
Observed reflections	4432	
Completeness to theta = 25.05°	99.8%	
Absorption correction	Multi-scan	
Max. and min. transmission	0.9237 and 0.7939	
Refinement method	Full-matrix least-squares on F^2	
Data / restraints / parameters	5033 / 2 / 424	
Goodness-of-fit on F^2	1.042	
Final *R* indices [$I>2\sigma(I)$]	*R*1 = 0.0364, *wR*2 = 0.0835	
R indices (all data)	*R*1 = 0.0458, *wR*2 = 0.0893	
Absolute structure parameter	0.26(2)	
Largest diff. peak and hole	0.251 and -0.194 $e^-/Å^3$	

Table 22. Atomic coordinates ($\times 10^4$) and equivalent isotropic displacement parameters ($Å^2 \times 10^3$) for $(Ind^{2Me\text{-}4,7})_2Cr$. U_{eq} is defined as 1/3 of the trace of the orthogonalized U^{ij} tensor.

atoms	x	y	z	U_{eq}
Cr(1)	1000(1)	790(1)	988(1)	34(1)
C(1)	787(3)	1956(2)	516(3)	31(1)
C(2)	1675(3)	1705(2)	529(4)	39(1)
C(3)	1536(3)	1141(2)	-284(4)	49(1)
C(4)	584(3)	1027(2)	-777(4)	43(1)
C(5)	111(3)	1541(2)	-317(3)	36(1)
C(6)	-838(3)	1649(2)	-486(4)	47(1)
C(7)	-1072(3)	2157(3)	154(5)	55(1)
C(8)	-406(4)	2558(2)	980(4)	59(1)
C(9)	514(3)	2478(2)	1180(4)	41(1)
C(10)	1238(4)	2895(2)	2050(4)	72(2)
C(11)	-1536(3)	1225(3)	-1372(4)	78(2)
C(12)	1003(3)	548(2)	2727(3)	34(1)
C(13)	1812(3)	287(2)	2547(4)	42(1)
C(14)	1545(4)	-233(2)	1664(4)	53(1)
C(15)	579(4)	-284(2)	1288(4)	49(1)
C(16)	225(3)	201(2)	1953(3)	38(1)
C(17)	-680(3)	390(2)	1931(4)	48(1)
C(18)	-770(3)	901(2)	2666(4)	53(1)
C(19)	-4(4)	1244(2)	3432(4)	53(1)
C(20)	875(3)	1085(2)	3476(3)	42(1)
C(21)	1703(4)	1436(3)	4287(4)	64(1)
C(22)	-1481(3)	16(3)	1104(4)	69(2)
Cr(2)	4619(1)	1757(1)	1741(1)	28(1)
C(23)	4792(3)	1997(2)	99(3)	33(1)
C(25)	4138(3)	2787(2)	1044(4)	48(1)
C(26)	5107(3)	2816(2)	1561(3)	46(1)
C(27)	5525(3)	2334(2)	973(4)	38(1)
C(24)	3952(3)	2270(2)	172(3)	37(1)

C(28)	6447(3)	2114(3)	1166(4)	54(1)
C(29)	6595(4)	1580(3)	505(5)	65(2)
C(30)	5881(4)	1243(3)	-358(4)	58(1)
C(31)	4988(3)	1435(2)	-577(3)	41(1)
C(32)	4211(4)	1105(2)	-1487(4)	59(1)
C(33)	7209(3)	2485(3)	2071(5)	85(2)
C(34)	4737(3)	592(2)	2200(3)	33(1)
C(35)	3841(3)	864(2)	2048(4)	35(1)
C(36)	3906(3)	1427(2)	2844(3)	39(1)
C(37)	4841(3)	1516(2)	3469(3)	38(1)
C(38)	5362(3)	994(2)	3092(3)	33(1)
C(39)	6325(3)	879(2)	3412(4)	45(1)
C(40)	6623(3)	382(3)	2833(5)	58(1)
C(41)	6038(4)	-20(2)	1950(5)	62(2)
C(42)	5082(4)	68(2)	1595(4)	47(1)
C(43)	4423(4)	-341(2)	653(4)	75(2)
C(44)	6957(3)	1307(3)	4363(4)	68(1)

Table 23. Crystal data and structure refinement for $(Ind^{Me-4})_3Cr_2Cl$.

Empirical formula	$C_{30}\ H_{27}\ Cl\ Cr_2$	
Formula weight	526.99	
Temperature	173(2) K	
Wavelength	0.71073 Å	
Crystal system	Monoclinic	
Space group	$P2_1/c$	
Unit cell dimensions	a = 24.675(4) Å	a α = 90°
	b = 6.7882(10) Å	b β = 95.473(2)°
	c = 16.172(2) Å	g γ = 90°
Volume	2696.5(7) $Å^3$	
Z	4	
Density (calculated)	1.387 g/cm^3	
Absorption coefficient	0.926 mm^{-1}	
F(000)	1168	
Crystal color, morphology	brown, needle	
Crystal size	0.30 x 0.05 x 0.05 mm^3	
Theta range for data collection	0.83 to 25.05°	
Index ranges	-29£≤ h ≤ 29, -8 ≤ k ≤£6, -19 ≤ l ≤ 19	
Reflections collected	15782	
Independent reflections	4718 [R_{int} = 0.0921]	
Observed reflections	2425	
Completeness to theta = 25.05°	99.1%	
Absorption correction	Multi-scan	
Max. and min. transmission	0.9552 and 0.7686	
Refinement method	Full-matrix least-squares on F^2	
Data / restraints / parameters	4718 / 169 / 367	
Goodness-of-fit on F^2	1.043	
Final R indices [I>2σ(I)]	R1 = 0.0849, wR2 = 0.1924	
R indices (all data)	R1 = 0.1619, wR2 = 0.2190	
Largest diff. peak and hole	0.684 and -0.425 $e^-/Å^3$	

Table 24. Atomic coordinates ($\times 10^4$) and equivalent isotropic displacement parameters ($Å^2 \times 10^3$) for $(Ind^{Me\text{-}4})_3Cr_2Cl$. U_{eq} is defined as 1/3 of the trace of the orthogonalized U^{ij} tensor.

atoms	x	y	z	U_{eq}
Cr(1)	3231(1)	3069(2)	7956(1)	42(1)
Cr(2)	2285(1)	3042(2)	7757(1)	42(1)
Cl(1)	2759(1)	6004(3)	7676(1)	49(1)
C(1)	4157(3)	2373(16)	7974(6)	70(3)
C(2)	3832(4)	621(14)	7876(6)	71(3)
C(3)	3532(3)	810(14)	7094(5)	65(3)
C(4)	3621(3)	2669(14)	6774(5)	59(2)
C(5)	4027(4)	3655(14)	7312(6)	68(3)
C(6)	4275(4)	5593(16)	7273(7)	82(3)
C(7)	4639(5)	6000(20)	7891(9)	112(4)
C(8)	4802(4)	4777(19)	8563(7)	83(4)
C(9)	4562(4)	2940(20)	8644(7)	110(4)
C(10)	4713(5)	1580(20)	9269(7)	142(6)
C(11)	2903(5)	4614(16)	9631(6)	49(2)
C(12)	3171(4)	2919(15)	9274(5)	50(2)
C(13)	2722(4)	1694(16)	8991(5)	49(2)
C(14)	2219(4)	2675(16)	9064(5)	51(2)
C(15)	2332(5)	4505(16)	9465(8)	53(2)
C(16)	1957(5)	6102(16)	9702(5)	60(3)
C(17)	2216(5)	7545(18)	10070(7)	77(3)
C(18)	2779(5)	7850(30)	10252(16)	63(3)
C(19)	3131(5)	6387(16)	9993(6)	63(3)
C(20)	3701(5)	6580(20)	10102(8)	87(4)
C(21)	1360(4)	2320(20)	7385(7)	81(4)
C(22)	1690(4)	579(16)	7429(7)	62(3)
C(23)	2040(4)	807(18)	6789(6)	53(3)
C(24)	1955(4)	2650(19)	6415(6)	55(3)
C(25)	1542(5)	3649(19)	6797(6)	67(3)
C(26)	1272(5)	5490(20)	6735(10)	99(5)

C(27)	849(5)	5910(20)	7245(10)	102(5)
C(28)	683(7)	4480(30)	7810(11)	104(6)
C(29)	937(5)	2800(30)	7927(9)	103(6)
C(30)	775(5)	1310(30)	8519(8)	112(7)

Table 25. Crystal data and structure refinement for $[(Ind^{Bzo\text{-}5,6})_2Cr]_2$.

Empirical formula	$C_{55.5}\ H_{40}\ Cr_2$	
Formula weight	810.88	
Temperature	100(2) K	
Wavelength	0.71073 Å	
Crystal system	Monoclinic	
Space group	*C*2/*c*	
Unit cell dimensions	*a* = 33.888(10) Å	α= 90°
	b = 16.944(5) Å	β= 101.661(5)°
	c = 15.386(5) Å	γ = 90°
Volume	8653(5) Å^3	
Z	8	
Density (calculated)	1.245 g/cm^3	
Absorption coefficient	0.540 mm^{-1}	
F(000)	3368	
Crystal size	0.21 × 0.04 × 0.01 mm^3	
Crystal color, habit	purple blade	
Theta range for data collection	2.20 to 25.55°	
Index ranges	$-38 \le h \le 38$, $-19 \le k \le 19$, $-17 \le l \le 17$	
Reflections collected	27973	
Independent reflections	6783 [R_{int} = 0.0230]	
Completeness to theta = 24.00°	99.5 %	
Absorption correction	Empirical	
Refinement method	Full-matrix least-squares on F^2	
Data / restraints / parameters	2169 / 2 / 528	
Goodness-of-fit on F^2	0.951	
Final *R* indices [I>2σ(I)]	*R*1 = 0.0789, *wR*2 = 0.2043	
R indices (all data)	*R*1 = 0.2177, *wR*2 = 0.1771	
Absolute structure parameter	0.014	
Extinction correction	none	
Largest diff. peak and hole	0.014 and -0.33 e$^-$/Å^3	

Table 26. Atomic coordinates and equivalent isotropic displacement parameters (Å^2) for $[(Ind^{Bzo\text{-}5,6})_2Cr]_2$. U_{eq} is defined as 1/3 of the trace of the orthogonalized U^{ij} tensor.

atoms	x	y	z	U_{eq}
Cr(1)	0.13929 (5)	0.04911 (9)	0.01408 (9)	0.0480 (5)
Cr(2)	0.20114 (5)	0.03497 (9)	0.01293 (9)	0.0458 (5)
C(1)	0.1240 (3)	−0.0386 (7)	0.1091 (6)	0.064 (3)
C(2)	0.1331 (3)	0.0322 (7)	0.1557 (6)	0.055 (3)
C(3)	0.0989 (3)	0.0833 (7)	0.1228 (6)	0.043 (3)
C(4)	0.0904 (3)	0.1576 (6)	0.1488 (5)	0.040 (3)
C(5)	0.0559 (3)	0.1950 (7)	0.1052 (6)	0.051 (3)
C(6)	0.0432 (4)	0.2722 (8)	0.1304 (6)	0.068 (3)
C(7)	0.0098 (4)	0.3097 (8)	0.0860 (8)	0.081 (4)
C(8)	−0.0173 (4)	0.2698 (9)	0.0127 (8)	0.093 (5)
C(9)	−0.0067 (3)	0.1977 (10)	−0.0112 (7)	0.079 (4)
C(10)	0.0283 (4)	0.1570 (8)	0.0313 (6)	0.055 (3)
C(11)	0.0377 (3)	0.0833 (8)	0.0054 (6)	0.060 (3)
C(12)	0.0727 (4)	0.0442 (7)	0.0512 (6)	0.052 (3)
C(13)	0.0896 (4)	−0.0304 (7)	0.0429 (6)	0.065 (3)
C(21)	0.1550 (3)	0.0320 (6)	−0.1259 (5)	0.037 (2)
C(22)	0.1875 (3)	−0.0210 (6)	−0.1180 (5)	0.040 (3)
C(23A)	0.1603 (4)	−0.2407 (6)	−0.1381 (5)	0.043 (3)
C(23)	0.1703 (3)	−0.0992 (6)	−0.1222 (5)	0.041 (3)
C(24)	0.1854 (3)	−0.1735 (6)	−0.1308 (5)	0.052 (3)
C(26)	0.1749 (4)	−0.3185 (7)	−0.1506 (6)	0.072 (4)
C(27)	0.1500 (5)	−0.3816 (7)	−0.1552 (7)	0.082 (5)
C(28)	0.1103 (5)	−0.3723 (8)	−0.1508 (7)	0.072 (4)
C(29)	0.0949 (4)	−0.2987 (8)	−0.1395 (6)	0.070 (4)
C(30)	0.1197 (4)	−0.2315 (6)	−0.1319 (5)	0.045 (3)
C(31)	0.1048 (3)	−0.1571 (7)	−0.1207 (5)	0.050 (3)
C(32)	0.1302 (4)	−0.0906 (6)	−0.1167 (5)	0.041 (3)
C(33)	0.1195 (3)	−0.0075 (6)	−0.1137 (5)	0.047 (3)
C(41)	0.1794 (3)	0.1562 (6)	0.0485 (6)	0.043 (3)
C(42)	0.2118 (3)	0.1596 (5)	−0.0009 (5)	0.044 (3)
C(43)	0.1928 (3)	0.1939 (5)	−0.0874 (6)	0.038 (2)
C(44)	0.2095 (3)	0.2076 (5)	−0.1609 (5)	0.038 (2)
C(45)	0.1831 (3)	0.2315 (5)	−0.2411 (6)	0.035 (2)
C(46)	0.1984 (3)	0.2417 (5)	−0.3199 (6)	0.042 (3)
C(47)	0.1719 (4)	0.2616 (5)	−0.3984 (6)	0.051 (3)
C(48)	0.1301 (3)	0.2773 (6)	−0.4007 (6)	0.052 (3)
C(49)	0.1153 (3)	0.2688 (5)	−0.3254 (6)	0.050 (3)
C(50)	0.1421 (3)	0.2448 (5)	−0.2428 (6)	0.043 (3)

C(51)	0.1251 (3)	0.2302 (5)	−0.1659 (6)	0.040 (3)
C(52)	0.1508 (3)	0.2048 (5)	−0.0901 (6)	0.036 (2)
C(53)	0.1412 (3)	0.1760 (5)	−0.0059 (5)	0.046 (3)
C(61)	0.2252 (3)	−0.0339 (7)	0.1350 (6)	0.059 (3)
C(62)	0.2312 (3)	−0.0793 (5)	0.0634 (6)	0.042 (3)
C(63)	0.2640 (3)	−0.0402 (6)	0.0314 (6)	0.049 (3)
C(64)	0.2845 (3)	−0.0577 (6)	−0.0360 (6)	0.052 (3)
C(65)	0.3144 (3)	−0.0106 (6)	−0.0538 (7)	0.052 (3)
C(66)	0.3343 (4)	−0.0283 (7)	−0.1239 (7)	0.071 (4)
C(67)	0.3624 (4)	0.0203 (8)	−0.1418 (9)	0.088 (4)
C(68)	0.3741 (4)	0.0870 (10)	−0.0931 (12)	0.110 (5)
C(69)	0.3550 (4)	0.1083 (7)	−0.0248 (10)	0.093 (4)
C(70)	0.3242 (4)	0.0601 (7)	−0.0014 (8)	0.065 (3)
C(71)	0.3037 (3)	0.0798 (6)	0.0657 (7)	0.058 (3)
C(72)	0.2741 (3)	0.0308 (6)	0.0839 (6)	0.044 (3)
C(73)	0.2480 (3)	0.0354 (6)	0.1423 (6)	0.053 (3)

Table 27. Crystal data and structure refinement for $(Ind^{2Me\text{-}1,3/Si\text{-}2})_2Fe$.

Empirical formula	$C_{28}H_{38}Si_2Fe$	
Formula weight	486.61	
Crystal color, morphology	deep purple, needle	
Temperature	100(2) K	
Wavelength	0.71073 Å	
Crystal system	Orthorhombic	
Space group	$P2_12_12_1$	
Unit cell dimensions	a = 10.9707(10) Å	α = 90°
	b = 14.9054(14) Å	β = 90°
	c = 15.9760(15) Å	γ = 90°
Volume	2612.4(4) $Å^3$	
Z	4	
Density (calculated)	1.237 g/cm^3	
Absorption coefficient	0.682 mm^{-1}	
F(000)	1040	
Crystal size	0.34 x 0.11 x 0.10 mm^3	
Theta range for data collection	1.87 to 28.25°	
Index ranges	$-14 \leq h \leq 14$, $-19 \leq k \leq 18$, $-20 \leq l \leq 20$	
Reflections collected	22684	
Independent reflections	6023 (R_{int} = 0.0285)	
Completeness to theta = 25.00°	100.0 %	
Absorption correction	None	
Max. and min. transmission	0.9349 and 0.8012	
Refinement method	Full-matrix least-squares on F^2	
Data / restraints / parameters	6023 / 0 / 290	
Goodness-of-fit on F^2	1.026	
Final R indices [I>2σ(I)]	R1 = 0.0372, wR2 = 0.0915	
R indices (all data)	R1 = 0.0403, wR2 = 0.0936	
Absolute structure parameter	0.014(13)	
Largest diff. peak and hole	0.597 and -0.297 $e^-/Å^3$	

Table 28. Atomic coordinates and equivalent isotropic displacement parameters ($Å^2$) for $(Ind^{2Me-1,3/Si-2})_2Fe$. U(eq) is defined as 1/3 of the trace of the orthogonalized U^{ij} tensor.

atoms	x	y	z	U(eq)
Fe(1)	0.0850(1)	0.1342(1)	0.2087(1)	0.021(1)
Si(1)	0.3929(1)	0.2019(1)	0.3876(1)	0.041(1)
Si(2)	0.8880(1)	0.295(1)	0.2239(1)	0.046(1)
C(1)	0.5609(3)	0.2904(2)	0.0735(1)	0.034(1)
C(2)	0.6704(3)	0.3206(2)	0.0453(2)	0.045(1)
C(3)	0.7747(3)	0.3223(2)	0.0976(2)	0.045(1)
C(4)	0.7704(2)	0.2940(2)	0.1789(2)	0.036(1)
C(5)	0.6562(2)	0.2637(2)	0.2121(2)	0.026(1)
C(6)	0.6202(2)	0.2342(2)	0.2939(1)	0.028(1)
C(7)	0.4914(2)	0.2156(2)	0.2921(2)	0.028(1)
C(8)	0.4508(2)	0.2305(1)	0.2071(2)	0.025(1)
C(9)	0.5511(2)	0.2620(2)	0.1591(1)	0.024(1)
C(10)	0.7028(3)	0.2347(2)	0.3689(2)	0.051(1)
C(11)	0.3237(2)	0.2201(2)	0.1745(2)	0.038(1)
C(12)	0.4617(5)	0.1357(4)	0.4735(3)	0.108(2)
C(13)	0.3615(4)	0.3183(2)	0.4242(2)	0.061(1)
C(14)	0.2436(4)	0.1486(3)	0.3651(3)	0.102(2)
C(21)	0.4462(3)	0.0309(2)	0.0615(2)	0.041(1)
C(22)	0.3341(3)	0.0019(2)	0.0837(2)	0.049(1)
C(23)	0.3074(3)	-0.0260(2)	0.1670(2)	0.050(1)
C(24)	0.3931(2)	-0.0251(2)	0.2283(2)	0.035(1)
C(25)	0.5135(2)	0.0035(1)	0.2069(2)	0.027(1)
C(26)	0.6242(2)	0.0093(2)	0.2549(1)	0.026(1)
C(27)	0.7212(2)	0.0381(2)	0.2003(1)	0.028(1)
C(28)	0.6673(2)	0.0557(2)	0.1195(1)	0.029(1)
C(29)	0.5413(2)	0.0321(2)	0.1237(1)	0.029(1)
C(30)	0.7313(3)	0.0861(2)	0.0413(2)	0.043(1)
C(31)	0.6358(3)	-0.0220(2)	0.3440(1)	0.034(1)
C(32)	0.9280(3)	-0.0910(3)	0.2076(4)	0.100(2)
C(33)	0.9859(3)	0.0969(2)	0.1532(2)	0.058(1)
C(34)	0.9290(3)	0.0606(6)	0.3330(3)	0.144(3)

Table 29. Crystal data and structure refinement for $[(Ind^{3Me\text{-}1,2,3})_2Fe]^+[DCNQ]^-$.

Empirical formula	$C_{36}\,H_{30}\,Fe\,N_2\,O_2$
Formula weight	578.47
Temperature	173(2) K
Wavelength	0.71073 Å
Crystal system	Orthorhombic
Space group	*Pbca*
Unit cell dimensions	a = 17.020(1) Å a α = 90°
	b = 15.989(1) Å b β = 90°
	c = 20.364(2) Å g γ = 90°
Volume	5541.8(7) $Å^3$
Z	8
Density (calculated)	1.387 Mg/m^3
Absorption coefficient	0.581 mm^{-1}
F(000)	2416
Crystal color, morphology	maroon, needle
Crystal size	0.40 x 0.12 x 0.04 mm^3
Theta range for data collection	2.00 to 25.05°
Index ranges	-18 ≤ *h*£≤ 20, -19£≤ *k*£≤ 19,-24 ≤ *l* ≤ 24
Reflections collected	34191
Independent reflections	4896 [R_{int} = 0.1217]
Observed reflections	2606
Completeness to theta = 25.05°	99.8%
Absorption correction	Multi-scan
Max. and min. transmission	0.9771 and 0.8008
Refinement method	Full-matrix least-squares on F^2
Data / restraints / parameters	4896 / 0 / 376
Goodness-of-fit on F^2	1.055
Final R indices [I>2σ(I)]	R1 = 0.0580, wR2 = 0.1174
R indices (all data)	R1 = 0.1472, wR2 = 0.1664
Largest diff. peak and hole	0.465 and -0.544 $e^-/Å^3$

Table 30. Atomic coordinates ($\times 10^4$) and equivalent isotropic displacement parameters ($Å^2 \times 10^3$) for $[(Ind^{3Me\text{-}1,2,3})_2Fe]^+[DCNQ]^-$. U(eq) is defined as one third of the trace of the orthogonalized U^{ij} tensor.

atoms	x	y	z	U_{eq}
Fe(1)	4239(1)	2361(1)	1209(1)	22(1)
C(1)	4138(4)	1499(3)	2018(3)	27(1)
C(2)	4857(4)	1974(4)	2044(3)	25(1)
C(3)	4654(4)	2835(3)	2106(3)	27(1)
C(4)	3820(4)	2911(4)	2063(3)	28(1)
C(5)	3497(4)	2078(4)	2029(3)	27(1)
C(6)	2722(4)	1770(5)	1957(3)	43(2)
C(7)	2601(5)	931(5)	1901(3)	51(2)
C(8)	3230(5)	368(5)	1902(3)	51(2)
C(9)	3991(4)	635(4)	1939(3)	41(2)
C(10)	5663(4)	1598(4)	2089(3)	40(2)
C(11)	5224(4)	3542(4)	2177(3)	42(2)
C(12)	3338(4)	3691(4)	2106(3)	44(2)
C(13)	3619(4)	2685(4)	335(3)	26(1)
C(14)	3904(4)	1834(3)	326(3)	27(1)
C(15)	4737(4)	1861(3)	351(3)	24(1)
C(16)	4986(3)	2712(4)	429(3)	24(1)
C(17)	4284(4)	3226(3)	399(2)	22(1)
C(18)	4174(4)	4108(3)	465(3)	30(1)
C(19)	3425(4)	4404(4)	464(3)	39(2)
C(20)	2768(4)	3872(4)	406(3)	43(2)
C(21)	2853(4)	3034(4)	355(3)	35(2)
C(22)	3389(4)	1074(4)	236(3)	43(2)
C(23)	5282(4)	1124(4)	308(3)	37(2)
C(24)	5804(4)	3032(3)	451(3)	32(1)
O(1)	2802(2)	2974(2)	3699(2)	37(1)
O(2)	5329(2)	902(3)	3776(2)	46(1)
N(1)	4397(3)	4388(3)	3668(3)	39(1)
N(2)	6205(3)	2922(4)	3751(3)	46(1)
C(25)	3379(3)	2498(3)	3711(3)	26(1)

C(26)	4165(3)	2808(3)	3723(2)	22(1)
C(27)	4821(3)	2263(3)	3745(3)	25(1)
C(28)	4748(3)	1377(3)	3754(3)	28(1)
C(29)	3807(4)	183(3)	3744(3)	36(2)
C(30)	3071(4)	-148(4)	3728(3)	41(2)
C(31)	2421(4)	384(4)	3715(3)	40(2)
C(32)	2532(3)	1235(4)	3716(3)	32(1)
C(33)	3279(3)	1579(3)	3721(3)	23(1)
C(34)	3934(3)	1039(3)	3742(3)	25(1)
C(35)	4283(4)	3685(3)	3691(3)	28(1)
C(36)	5597(3)	2614(4)	3751(3)	31(1)

Table 31. Crystal data and structure refinement for $(Ind^{2Si-1,3})_2Mn$.

Empirical formula	$C_{30}\ H_{46}\ Si_4\ Mn$
Formula weight	573.98
Crystal color, morphology	orange, plate
Temperature	100(2) K
Wavelength	0.71073 Å
Crystal system	Orthorhombic
Space group	$Pna2_1$
Unit cell dimensions	a = 11.315(2) Å α = 90°
	b = 16.399(3) Å β = 90°
	c = 38.383(7) Å γ = 90°
Volume	7122(2) $Å^3$
Z	8
Density (calculated)	1.071 g/cm^3
Absorption coefficient	0.520 mm^{-1}
F(000)	2456
Crystal size	0.30 x 0.20 x 0.10 mm^3
Theta range for data collection	2.19 to 27.18°
Index ranges	$-13 \le h \le 13$, $-20 \le k \le 20$, $-47 \le l \le 46$
Reflections collected	53617
Independent reflections	13864 (R_{int} = 0.0648)
Completeness to theta = 25.00°	100.0 %
Absorption correction	None
Refinement method	Full-matrix least-squares on F^2
Data / restraints / parameters	13864 / 1 / 632
Goodness-of-fit on F^2	1.158
Final R indices [I>2σ(I)]	R1 = 0.0530, wR2 = 0.1385
R indices (all data)	R1 = 0.0612, wR2 = 0.1434
Absolute structure parameter	0.014(2)
Largest diff. peak and hole	1.388 and -0.332 $e^-/Å^3$

Table 32. Atomic coordinates and equivalent isotropic displacement parameters ($Å^2 \times 10^3$) for $(Ind^{2Si-1,3})_2Mn$. U_{eq} is defined as 1/3 of the trace of the orthogonalized U^{ij} tensor.

atoms	x	y	z	U(eq)
Mn(1)	0.80907(5)	0.51016(4)	0.548702(17)	19.53(15)
Si(2)	0.88804(9)	0.70102(6)	0.59872(3)	16.2(2)
Si(4)	0.74354(10)	0.28818(7)	0.55990(3)	19.9(2)
Si(3)	1.05532(11)	0.50179(7)	0.47614(3)	21.1(3)
Si(1)	0.58178(10)	0.59303(7)	0.48280(3)	19.3(2)
C(1)	0.6032(3)	0.5638(2)	0.55945(11)	18.2(8)
C(2)	0.6514(3)	0.5966(2)	0.52717(10)	15.4(8)
C(3)	0.7528(3)	0.6426(2)	0.53747(11)	17.1(8)
C(4)	0.7757(3)	0.6373(2)	0.57454(10)	15.1(8)
C(5)	0.6783(3)	0.5899(2)	0.58839(10)	15.0(8)
C(6)	0.6468(3)	0.5682(2)	0.62304(11)	17.2(8)
C(7)	0.5445(4)	0.5233(2)	0.62896(11)	20.4(9)
C(8)	0.4737(4)	0.4954(2)	0.60065(12)	20.2(9)
C(9)	0.5003(4)	0.5144(2)	0.56651(11)	19.0(9)
C(10)	0.9447(3)	0.4049(2)	0.57183(11)	18.3(8)
C(11)	0.8524(3)	0.3720(2)	0.54956(11)	16.9(8)
C(12)	0.8787(3)	0.4039(2)	0.51509(10)	15.9(8)
C(13)	0.9789(4)	0.4570(3)	0.51494(10)	18.4(8)
C(14)	1.0206(3)	0.4577(2)	0.55105(11)	19.3(8)
C(15)	1.1181(4)	0.4980(2)	0.56687(12)	21.8(9)
C(16)	1.1401(4)	0.4851(2)	0.60206(12)	22.7(9)
C(17)	1.0680(4)	0.4333(3)	0.62226(11)	24.7(10)
C(18)	0.9709(4)	0.3931(3)	0.60801(11)	23.4(9)
C(19)	0.4332(4)	0.6457(3)	0.48409(12)	27.2(10)
C(20)	0.6810(4)	0.6474(3)	0.45109(12)	28.8(10)
C(21)	0.5575(4)	0.4840(3)	0.46834(12)	27.3(10)
C(22)	0.9419(4)	0.6497(3)	0.63937(11)	26.4(10)
C(23)	1.0156(4)	0.7210(3)	0.56867(12)	23.4(10)
C(24)	0.8188(4)	0.8015(3)	0.61149(14)	32.8(12)
C(25)	1.2089(4)	0.4578(3)	0.47374(14)	36.9(12)
C(26)	0.9699(5)	0.4756(3)	0.43586(13)	37.4(12)
C(27)	1.0671(5)	0.6167(3)	0.47779(13)	36.0(12)
C(28)	0.8259(4)	0.1895(3)	0.56313(16)	37.2(13)
C(29)	0.6686(4)	0.3076(3)	0.60258(13)	31.6(11)
C(30)	0.6318(4)	0.2823(3)	0.52365(13)	35.9(12)

Table 33. Crystal data and structure refinement for $(Ind^{Si\text{-}2})_2Mn$.

Empirical formula	$C_{24}H_{30}MnSi_2$
Formula weight	429.60
Temperature	100(2) K
Wavelength	0.71073 Å
Crystal system	Monoclinic
Space group	$P2_1/c$
Unit cell dimensions	a = 11.826(4) Å α = 90°
	b = 8.128(3) Å β = 113.469(5)°
	c = 12.663(4) Å γ = 90°
Volume	1116.4(7) Å^3
Z	2
Density (calculated)	1.278 g/cm^3
Absorption coefficient	0.705 mm^{-1}
F(000)	454
Crystal size	0.30 x 0.20 x 0.20 mm^3
Theta range for data collection	1.88 to 28.22°
Index ranges	$-15 \le h \le 15$, $-10 \le k \le 10$, $-16 \le l \le 16$
Reflections collected	9217
Independent reflections	2582 [R_{int} = 0.0246]
Completeness to theta = 25.00°	99.9 %
Absorption correction	None
Max. and min. transmission	0.8719 and 0.8164
Refinement method	Full-matrix least-squares on F^2
Data / restraints / parameters	2582 / 0 / 124
Goodness-of-fit on F^2	1.024
Final R indices [$I>2\sigma(I)$]	$R1$ = 0.0317, $wR2$ = 0.0838
R indices (all data)	$R1$ = 0.0354, $wR2$ = 0.0858
Largest diff. peak and hole	0.444 and -0.189 e$^-$/Å^3

Table 34. Atomic coordinates ($\times 10^4$) and equivalent isotropic displacement parameters ($Å^2 \times 10^3$) for $(Ind^{Si\text{-}2})_2Mn$. U(eq) is defined as 1/3 of the trace of the orthogonalized U^{ij} tensor.

atoms	x	y	z	U(eq)
Mn(1)	5000	5000	5000	28(1)
Si(1)	8124(1)	6792(1)	5962(1)	17(1)
C(1)	4440(1)	7638(2)	3929(1)	18(1)
C(2)	5497(1)	7768(2)	4994(1)	19(1)
C(3)	6475(1)	6801(2)	4913(1)	18(1)
C(4)	5998(1)	6012(2)	3811(1)	19(1)
C(5)	4758(1)	6543(2)	3192(1)	18(1)
C(6)	3866(1)	6181(2)	2072(1)	22(1)
C(7)	2729(1)	6913(2)	1708(1)	25(1)
C(8)	2420(1)	7987(2)	2435(1)	25(1)
C(9)	3244(1)	8338(2)	3526(1)	23(1)
C(10)	8966(1)	8556(2)	5652(1)	22(1)
C(11)	8203(1)	7043(2)	7449(1)	25(1)
C(12)	8852(1)	4821(2)	5808(2)	26(1)

Table 35. Crystal data and structure refinement for (μ-Ind^{Me-2})(Ind^{Me-2})$_2Mn_2$(μ -BHT).

Empirical formula	C45 H50 Mn2 O	
Formula weight	716.73	
Temperature	100.0(1) K	
Wavelength	0.71073 Å	
Crystal system	Monoclinic	
Space group	$P2_1/c$	
Unit cell dimensions	a = 19.8480(19) Å	a α = 90°
	b = 10.3790(10) Å	b β = 110.487(2)°
	c = 18.8577(17) Å	g γ = 90°
Volume	3639.0(6) $Å^3$	
Z	4	
Density (calculated)	1.308 g/cm^3	
Absorption coefficient	0.728 mm^{-1}	
F(000)	1512	
Crystal color, morphology	yellow, block	
Crystal size	0.32 x 0.24 x 0.20 mm^3	
Theta range for data collection	1.10 to 37.78°	
Index ranges	$-33 \leq h \leq 34$, $-17 \leq k \leq$£17, $-32 \leq l \leq 32$	
Reflections collected	87504	
Independent reflections	19356 [R_{int} = 0.0595]	
Observed reflections	12301	
Completeness to theta = 37.78°	99.1%	
Absorption correction	Multi-scan	
Max. and min. transmission	0.8681 and 0.8005	
Refinement method	Full-matrix least-squares on F^2	
Data / restraints / parameters	19356 / 38 / 484	
Goodness-of-fit on F^2	1.008	
Final R indices [$I>2\sigma(I)$]	$R1$ = 0.0465, $wR2$ = 0.1063	
R indices (all data)	$R1$ = 0.0896, $wR2$ = 0.1270	
Largest diff. peak and hole	0.720 and -0.599 $e^-/Å^3$	

Table 36. Atomic coordinates ($\times 10^4$) and equivalent isotropic displacement parameters ($Å^2 \times 10^3$) for (μ-Ind^{Me-2})(Ind^{Me-2})$_2$$Mn_2$($\mu$ -BHT). U_{eq} is defined as 1/3 of the trace of the orthogonalized U^{ij} tensor.

atoms	x	y	z	U_{eq}
Mn(1)	8517(1)	862(1)	2495(1)	18(1)
Mn(2)	6816(1)	-521(1)	2276(1)	25(1)
O(1)	7506(1)	335(1)	1823(1)	16(1)
C(1)	9077(1)	2845(1)	2372(1)	24(1)
C(2)	9195(1)	1926(2)	1869(1)	25(1)
C(3)	9656(1)	956(2)	2303(1)	25(1)
C(4)	10333(1)	715(2)	3748(1)	27(1)
C(5)	10428(1)	1282(2)	4435(1)	31(1)
C(6)	10075(1)	2436(2)	4483(1)	31(1)
C(7)	9621(1)	3036(2)	3844(1)	26(1)
C(8)	9515(1)	2487(1)	3129(1)	22(1)
C(9)	9877(1)	1311(1)	3082(1)	22(1)
C(10)	5583(3)	203(5)	1754(3)	31(1)
C(11)	5651(3)	-921(5)	1365(2)	32(1)
C(12)	5775(5)	-1964(5)	1872(3)	30(1)
C(13)	5829(7)	-2165(10)	3290(4)	30(1)
C(14)	5714(10)	-1432(9)	3852(6)	40(2)
C(15)	5582(7)	-117(9)	3755(5)	38(2)
C(16)	5530(7)	508(9)	3106(5)	33(1)
C(17)	5591(9)	-216(7)	2496(6)	23(1)
C(18)	5747(1)	-1578(1)	2593(1)	23(1)
C(19)	8572(1)	100(1)	3636(1)	20(1)
C(20)	7920(1)	496(1)	3715(1)	20(1)
C(21)	7431(1)	-536(1)	3550(1)	20(1)
C(22)	7607(1)	-2963(1)	3291(1)	24(1)
C(23)	8100(1)	-3841(2)	3215(1)	29(1)
C(24)	8784(1)	-3443(2)	3244(1)	29(1)
C(25)	8991(1)	-2169(2)	3363(1)	25(1)
C(26)	8507(1)	-1263(1)	3466(1)	19(1)

C(27)	7805(1)	-1662(1)	3418(1)	20(1)
C(28)	8907(1)	1994(2)	1017(1)	34(1)
C(29)	5526(3)	-1005(7)	527(2)	61(2)
C(30)	7796(1)	1787(2)	4000(1)	28(1)
C(31)	7222(1)	514(1)	1047(1)	16(1)
C(32)	7298(1)	-490(1)	567(1)	16(1)
C(33)	6986(1)	-313(1)	-211(1)	19(1)
C(34)	6606(1)	791(1)	-532(1)	19(1)
C(35)	6555(1)	1755(1)	-49(1)	20(1)
C(36)	6851(1)	1661(1)	741(1)	18(1)
C(37)	7726(1)	-1739(1)	866(1)	19(1)
C(38)	7669(1)	-2691(1)	229(1)	26(1)
C(39)	7468(1)	-2455(2)	1429(1)	38(1)
C(40)	8526(1)	-1429(2)	1248(1)	35(1)
C(41)	6263(1)	923(1)	-1377(1)	25(1)
C(42)	6766(1)	2887(1)	1171(1)	23(1)
C(43)	7011(1)	2798(2)	2038(1)	29(1)
C(44)	7200(1)	3977(2)	984(1)	34(1)
C(45)	5972(1)	3309(2)	904(1)	33(1)

Table 37. Crystal data and structure refinement for $[K_6(dioxane)_9][(Mn(Ind^{2Me\text{-}4,7})_3]_4[Mn(Ind^{2Me\text{-}4,7})_3]_2$.

Empirical formula	$C_{234}H_{270}K_6Mn_6O_{18}$	
Formula weight	3934.74	
Temperature	100.0(1) K	
Wavelength	0.71073 Å	
Crystal system	Hexagonal	
Space group	$P6_3$	
Unit cell dimensions	a = 19.125(5) Å	a α = 90°
	b = 19.125(5) Å	b β = 90°
	c = 32.076(8) Å	g γ = 120°
Volume	10160(4) $Å^3$	
Z	2	
Density (calculated)	1.286 g/cm^3	
Absorption coefficient	0.549 mm^{-1}	
F(000)	4164	
Crystal color, morphology	yellow, hexagonal plate	
Crystal size	0.28 x 0.16 x 0.06 mm^3	
Theta range for data collection	1.77 to 31.51°	
Index ranges	$-28 \le h \le 28$, $-28 \le k \le 28$, $-47 \le l \le 47$	
Reflections collected	132350	
Independent reflections	22576 [R_{int} = 0.1435]	
Observed reflections	13455	
Completeness to theta = 31.51°	100.0%	
Absorption correction	Multi-scan	
Max. and min. transmission	0.9678 and 0.8616	
Refinement method	Full-matrix least-squares on F^2	
Data / restraints / parameters	22576 / 14 / 822	
Goodness-of-fit on F^2	1.012	
Final R indices [$I>2\sigma(I)$]	$R1$ = 0.0758, $wR2$ = 0.1770	
R indices (all data)	$R1$ = 0.1425, $wR2$ = 0.2191	
Absolute structure parameter	0.21(2)	
Largest diff. peak and hole	4.709 and -0.541 $e^-/Å^3$	

Table 38. Atomic coordinates ($\times 10^4$) and equivalent isotropic displacement parameters ($Å^2 \times 10^3$) for $[K_6(dioxane)_9][(Mn(Ind^{2Me\text{-}4,7})_3]_4[Mn(Ind^{2Me\text{-}4,7})_3]_2$. U_{eq} is defined as 1/3 of the trace of the orthogonalized U^{ij} tensor.

atoms	x	y	z	U_{eq}
Mn(1)	6667	3333	6577(1)	20(1)
C(1)	5713(3)	3686(3)	6367(2)	21(1)
C(2)	5682(3)	3676(3)	6813(2)	25(1)
C(3)	5142(3)	2890(3)	6954(2)	22(1)
C(4)	4292(3)	1544(3)	6558(1)	18(1)
C(5)	4128(3)	1228(3)	6161(1)	21(1)
C(6)	4462(3)	1718(3)	5801(1)	20(1)
C(7)	4971(3)	2538(3)	5830(1)	18(1)
C(8)	5163(3)	2885(3)	6231(1)	19(1)
C(9)	4816(2)	2387(3)	6596(1)	18(1)
C(10)	3957(3)	1029(3)	6940(2)	28(1)
C(11)	5342(3)	3078(3)	5458(2)	26(1)
Mn(2)	0	0	6016(1)	21(1)
C(12)	1251(3)	1044(3)	6234(2)	23(1)
C(13)	1251(3)	1097(3)	5788(2)	22(1)
C(14)	1518(3)	595(3)	5621(2)	23(1)
C(15)	1974(3)	-337(3)	5960(2)	22(1)
C(16)	2099(3)	-573(3)	6339(2)	26(1)
C(17)	1973(3)	-269(3)	6719(2)	25(1)
C(18)	1695(3)	268(3)	6727(2)	21(1)
C(19)	1541(3)	522(3)	6335(2)	18(1)
C(20)	1704(3)	228(3)	5954(1)	19(1)
C(21)	2121(3)	-651(3)	5562(2)	34(1)
C(22)	1554(3)	594(3)	7124(2)	32(1)
Mn(3)	3333	6667	3474(1)	21(1)
C(23)	2969(3)	5357(3)	3676(2)	24(1)
C(24)	2999(3)	5340(3)	3227(2)	26(1)
C(25)	3786(3)	5595(3)	3100(2)	22(1)
C(26)	5121(3)	6086(3)	3509(2)	20(1)

C(27)	5424(3)	6243(3)	3908(2)	22(1)
C(28)	4916(3)	6080(3)	4263(2)	21(1)
C(29)	4091(3)	5752(3)	4226(1)	20(1)
C(30)	3766(3)	5604(3)	3818(1)	18(1)
C(31)	4269(3)	5756(2)	3459(1)	18(1)
C(32)	5637(3)	6262(3)	3132(2)	26(1)
C(33)	3549(3)	5589(3)	4596(2)	27(1)
Mn(4)	6667	3333	4079(1)	18(1)
C(34)	5655(3)	3568(3)	3867(1)	20(1)
C(35)	5579(3)	3523(3)	4306(2)	23(1)
C(36)	6064(3)	4295(3)	4479(1)	18(1)
C(37)	6984(3)	5690(3)	4141(2)	22(1)
C(38)	7244(3)	6056(3)	3752(2)	27(1)
C(39)	6979(3)	5617(3)	3381(2)	26(1)
C(40)	6449(3)	4797(3)	3371(2)	22(1)
C(41)	6185(3)	4413(3)	3763(2)	18(1)
C(42)	6440(3)	4844(3)	4143(2)	19(1)
C(43)	7243(3)	6160(3)	4544(2)	31(1)
C(44)	6141(4)	4318(4)	2974(2)	32(1)
Mn(5)	3333	6667	5998(1)	19(1)
C(45)	3065(3)	5394(3)	6195(2)	22(1)
C(46)	3063(3)	5361(3)	5749(2)	23(1)
C(47)	2279(3)	5123(3)	5607(2)	24(1)
C(48)	958(3)	4777(3)	5990(2)	24(1)
C(49)	642(3)	4696(3)	6380(2)	29(1)
C(50)	1113(3)	4822(3)	6747(2)	24(1)
C(51)	1915(3)	5058(3)	6728(2)	20(1)
C(52)	2266(3)	5141(2)	6327(2)	15(1)
C(53)	1781(3)	4981(3)	5955(2)	20(1)
C(54)	459(3)	4638(3)	5605(2)	36(1)
C(55)	2433(3)	5228(3)	7110(2)	26(1)
Mn(6)	0	0	4033(1)	25(1)
C(56)	1306(3)	938(3)	3879(2)	33(1)
C(57)	1324(3)	874(4)	4320(2)	41(1)
C(58)	1507(3)	275(4)	4431(2)	38(1)
C(59)	1815(3)	-655(3)	3983(2)	27(1)

C(60)	1911(3)	-819(3)	3580(2)	26(1)
C(61)	1814(3)	-408(3)	3242(2)	27(1)
C(62)	1622(3)	191(3)	3300(2)	24(1)
C(63)	1527(3)	379(3)	3712(2)	25(1)
C(64)	1634(3)	-46(3)	4054(2)	27(1)
C(65)	1884(3)	-1145(4)	4336(2)	40(1)
C(66)	1472(3)	614(3)	2946(2)	31(1)
K(1)	3079(1)	1980(1)	6056(1)	20(1)
K(2)	4673(1)	4443(1)	3978(1)	20(1)
O(1)	3554(2)	3303(2)	3536(1)	32(1)
C(67)	3489(4)	2606(3)	3339(2)	44(2)
C(68)	3378(4)	2647(4)	2877(2)	46(2)
O(2)	2691(2)	2702(2)	2783(1)	36(1)
C(69)	2753(4)	3393(3)	2988(2)	32(1)
C(70)	2856(3)	3362(3)	3447(2)	27(1)
O(3)	3583(2)	3647(2)	4596(1)	32(1)
C(71)	3964(4)	4010(3)	4976(2)	39(1)
C(72)	3396(5)	3620(3)	5334(2)	49(2)
O(4)	3148(2)	2794(2)	5355(1)	39(1)
C(73)	2744(3)	2416(3)	4976(2)	38(1)
C(74)	3292(3)	2800(3)	4601(2)	36(1)
O(5)	3200(2)	3221(2)	6448(1)	33(1)
C(75)	2548(14)	3280(30)	6645(8)	50(5)
C(76)	2636(13)	3329(17)	7105(8)	61(6)
O(6)	3396(13)	4008(18)	7238(7)	45(3)
C(77)	4051(12)	3960(20)	7038(8)	37(3)
C(78)	3942(10)	3900(20)	6579(8)	29(3)

Table 39. Crystal data and structure refinement for $(Ind)_2Mn(thf)_2$.

Empirical formula	$C_{26}H_{30}MnO_2$	
Formula weight	429.44	
Temperature	100(2) K	
Wavelength	0.71073 Å	
Crystal system	Triclinic	
Space group	$P\bar{1}$	
Unit cell dimensions	a = 9.094(2) Å	α = 80.539(4)°
	b = 9.775(3) Å	β = 72.620(4)°
	c = 13.066(3) Å	γ = 71.148(4)°
Volume	1046.0(5) $Å^3$	
Z	2	
Density (calculated)	1.363 g/cm^3	
Absorption coefficient	0.651 mm^{-1}	
F(000)	454	
Crystal size	0.30 x 0.30 x 0.20 mm^3	
Theta range for data collection	1.64 to 28.31°	
Index ranges	$-12 \le h \le 11$, $-13 \le k \le 12$, $-16 \le l \le 17$	
Reflections collected	12856	
Independent reflections	4735 [R_{int} = 0.0187]	
Completeness to theta = 25.00°	99.5 %	
Absorption correction	None	
Max. and min. transmission	0.8809 and 0.8287	
Refinement method	Full-matrix least-squares on F^2	
Data / restraints / parameters	4735 / 0 / 262	
Goodness-of-fit on F^2	1.040	
Final R indices [I>2σ(I)]	$R1$ = 0.0308, $wR2$ = 0.0810	
R indices (all data)	$R1$ = 0.0320, $wR2$ = 0.0819	
Largest diff. peak and hole	0.481 and -0.485 $e^-/Å^3$	

Table 40. Atomic coordinates ($\times 10^4$) and equivalent isotropic displacement parameters ($Å^2 \times 10^3$) for $(Ind)_2Mn(thf)_2$. U(eq) is defined as 1/3 of the trace of the orthogonalized U^{ij} tensor.

atoms	x	y	z	U(eq)
Mn(1)	3915(1)	5818(1)	2402(1)	14(1)
O(1)	3462(1)	7721(1)	3221(1)	17(1)
O(2)	5996(1)	6433(1)	1380(1)	18(1)
C(1)	3383(2)	4343(2)	4202(1)	26(1)
C(2)	5022(2)	4227(2)	3710(1)	29(1)
C(3)	5595(2)	3327(2)	2846(1)	24(1)
C(4)	4308(2)	2810(1)	2831(1)	19(1)
C(5)	4178(2)	1885(2)	2159(1)	22(1)
C(6)	2727(2)	1630(2)	2310(1)	24(1)
C(7)	1365(2)	2272(2)	3129(1)	25(1)
C(8)	1457(2)	3152(2)	3809(1)	23(1)
C(9)	2927(2)	3445(1)	3675(1)	20(1)
C(10)	2155(2)	5830(1)	1529(1)	17(1)
C(11)	2868(2)	6527(2)	527(1)	19(1)
C(12)	2101(2)	7996(2)	482(1)	19(1)
C(13)	816(2)	8304(1)	1439(1)	16(1)
C(14)	-354(2)	9597(2)	1799(1)	20(1)
C(15)	-1534(2)	9545(2)	2749(1)	21(1)
C(16)	-1573(2)	8221(2)	3357(1)	21(1)
C(17)	-430(2)	6943(2)	3028(1)	18(1)
C(18)	801(2)	6963(1)	2074(1)	15(1)
C(19)	1895(2)	8387(2)	3928(1)	18(1)
C(20)	2254(2)	8644(2)	4924(1)	20(1)
C(21)	3859(2)	8998(2)	4478(1)	18(1)
C(22)	4716(2)	8053(2)	3537(1)	19(1)
C(23)	5824(2)	7843(2)	771(1)	20(1)
C(24)	7428(2)	8126(2)	571(1)	21(1)
C(25)	8591(2)	6609(2)	399(1)	21(1)
C(26)	7709(2)	5680(2)	1250(1)	21(1)

Table 41. Crystal data and structure refinement for $[(Ind^{3Me\text{-}2,4,7})MnCl(thf)]_2$.

Empirical formula	$C_{32}H_{42}Cl_2Mn_2O_2$	
Formula weight	639.44	
Temperature	173.0(5) K	
Wavelength	0.71073 Å	
Crystal system	Triclinic	
Space group	$P\bar{1}$	
Unit cell dimensions	a = 9.5845(5) Å	a α = 85.269(1)°
	b = 9.6973(5) Å	b β = 88.141(1)°
	c = 17.1564(10) Å	g γ = 83.660(1)°
Volume	1578.99(15) Å^3	
Z	2	
Density (calculated)	1.345 g/cm^3	
Absorption coefficient	0.995 mm^{-1}	
F(000)	668	
Crystal color, morphology	yellow, block	
Crystal size	0.28 x 0.20 x 0.18 mm^3	
Theta range for data collection	1.19 to 35.63°	
Index ranges	$-15 \le h \le 15$, $-15 \le k \le 15$, $-28 \le l \le 28$	
Reflections collected	35286	
Independent reflections	14299 [R_{int} = 0.0303]	
Observed reflections	9523	
Completeness to theta = 35.63°	98.2%	
Absorption correction	Multi-scan	
Max. and min. transmission	0.8412 and 0.7681	
Refinement method	Full-matrix least-squares on F^2	
Data / restraints / parameters	14299 / 10 / 356	
Goodness-of-fit on F^2	1.031	
Final R indices [$I>2\sigma(I)$]	$R1$ = 0.0470, $wR2$ = 0.1246	
R indices (all data)	$R1$ = 0.0762, $wR2$ = 0.1419	
Largest diff. peak and hole	1.015 and -0.428 e$^-$/Å^3	

Table 42. Atomic coordinates ($\times 10^4$) and equivalent isotropic displacement parameters ($Å^2 \times 10^3$) for $[(Ind^{3Me\text{-}2,4,7})MnCl(thf)]_2$. U_{eq} is defined as 1/3 of the trace of the orthogonalized U^{ij} tensor.

atoms	x	y	z	U_{eq}
Mn(1)	4312(1)	8590(1)	433(1)	41(1)
Cl(1)	6286(1)	8858(1)	-466(1)	51(1)
C(1)	4865(2)	8096(2)	1743(1)	44(1)
C(2)	5567(2)	6986(2)	1355(1)	46(1)
C(3)	4577(2)	6165(2)	1109(1)	46(1)
C(4)	1880(2)	6249(2)	1355(2)	56(1)
C(5)	784(2)	7034(3)	1692(2)	67(1)
C(6)	939(2)	8267(3)	2031(2)	60(1)
C(7)	2221(2)	8748(2)	2074(1)	50(1)
C(8)	3396(2)	7936(2)	1773(1)	39(1)
C(9)	3234(2)	6707(2)	1386(1)	42(1)
C(10)	7135(2)	6713(3)	1245(1)	64(1)
C(11)	1712(3)	4939(3)	978(2)	87(1)
C(12)	2391(3)	10079(3)	2437(2)	69(1)
O(1)	2788(1)	8334(2)	-375(1)	52(1)
C(13)	2945(3)	7639(3)	-1078(2)	68(1)
C(14)	1510(3)	7790(4)	-1423(2)	80(1)
C(15)	518(3)	8173(3)	-779(2)	71(1)
C(16)	1348(2)	8953(3)	-289(1)	58(1)
Mn(2)	6246(1)	786(1)	4464(1)	33(1)
Cl(2)	6324(1)	-1315(1)	5345(1)	41(1)
C(17)	8505(2)	524(2)	3600(1)	35(1)
C(18)	7461(2)	-280(1)	3379(1)	35(1)
C(19)	6279(2)	623(2)	3129(1)	33(1)
C(20)	5806(2)	3320(2)	2969(1)	35(1)
C(21)	6464(2)	4498(2)	3041(1)	44(1)
C(22)	7847(2)	4426(2)	3298(1)	47(1)
C(23)	8639(2)	3194(2)	3505(1)	41(1)
C(24)	8002(2)	1953(1)	3447(1)	32(1)

C(25)	6600(2)	2025(1)	3164(1)	30(1)
C(26)	7599(2)	-1838(2)	3395(1)	47(1)
C(27)	4343(2)	3375(2)	2680(1)	45(1)
C(28)	10143(2)	3120(2)	3742(2)	63(1)
O(2)	6816(1)	2172(1)	5247(1)	44(1)
C(29)	6138(11)	3608(8)	5181(5)	48(2)
C(30)	7125(6)	4453(4)	5559(3)	68(1)
C(31)	7861(6)	3389(4)	6153(3)	68(1)
C(32)	8110(20)	2087(16)	5670(20)	71(1)

Table 43. Crystal data and structure refinement for $(Ind^{2Si-1,3})_2V$.

Empirical formula	$C_{31.5}H_{49.5}Si_4V$	
Formula weight	591.51	
Temperature	100(2) K	
Wavelength	0.71073 Å	
Crystal system	Monoclinic	
Space group	$P2_1/c$	
Unit cell dimensions	a = 10.9860(11) Å	α a= 90°
	b = 16.3123(16) Å	βb= 93.467(2)°
	c = 38.234(4) Å	γ = 90°
Volume	6839.3(12) $Å^3$	
Z	8	
Density (calculated)	1.149 g/cm^3	
Absorption coefficient	0.448 mm^{-1}	
F(000)	2540	
Crystal size	0.30 x 0.30 x 0.07 mm^3	
Theta range for data collection	1.64 to 26.00°	
Index ranges	$-13 \le h \le 13$, $-20 \le k \le 20$, $-46 \le l \le 47$	
Reflections collected	52657	
Independent reflections	13450 [R_{int} = 0.1154]	
Completeness to theta = 26.00°	99.9 %	
Absorption correction	None	
Refinement method	Full-matrix least-squares on F^2	
Data / restraints / parameters	13450 / 0 / 658	
Goodness-of-fit on F^2	0.798	
Final R indices [I>2σ(I)]	$R1$ = 0.0488, $wR2$ = 0.0786	
R indices (all data)	$R1$ = 0.1187, $wR2$ = 0.0877	
Largest diff. peak and hole	0.563 and -0.446 $e^-/Å^3$	

Table 44. Atomic coordinates ($\times 10^4$) and equivalent isotropic displacement parameters ($Å^2 \times 10^3$) for $(Ind^{2Si-1,3})_2V$. U(eq) is defined as 1/3 of the trace of the orthogonalized U^{ij} tensor.

atoms	x	y	z	U(eq)
V(1)	753(1)	7055(1)	1405(1)	14(1)
Si(1)	1641(1)	9264(1)	1515(1)	17(1)
Si(2)	-1815(1)	7171(1)	700(1)	20(1)
Si(3)	2620(1)	6229(1)	690(1)	21(1)
Si(4)	91(1)	5147(1)	1904(1)	16(1)
C(1)	112(3)	8146(2)	1078(1)	16(1)
C(2)	464(3)	8457(2)	1415(1)	14(1)
C(3)	-373(3)	8094(2)	1646(1)	13(1)
C(4)	-541(3)	8208(2)	2010(1)	18(1)
C(5)	-1495(3)	7827(2)	2155(1)	21(1)
C(6)	-2282(3)	7306(2)	1954(1)	21(1)
C(7)	-2156(3)	7170(2)	1612(1)	16(1)
C(8)	-1197(3)	7574(2)	1442(1)	14(1)
C(9)	-885(3)	7587(2)	1082(1)	16(1)
C(10)	-2062(4)	6039(2)	721(1)	27(1)
C(11)	-1031(3)	7420(2)	291(1)	28(1)
C(12)	-3337(3)	7694(2)	692(1)	31(1)
C(13)	2477(3)	9090(2)	1946(1)	27(1)
C(14)	861(3)	10277(2)	1530(1)	26(1)
C(15)	2708(3)	9291(2)	1154(1)	28(1)
C(21)	1143(3)	5738(2)	1272(1)	15(1)
C(22)	2124(3)	6220(2)	1143(1)	16(1)
C(23)	2741(3)	6558(2)	1455(1)	17(1)
C(24)	3819(3)	7049(2)	1500(1)	20(1)
C(25)	4269(3)	7221(2)	1833(1)	21(1)
C(26)	3693(3)	6940(2)	2130(1)	20(1)
C(27)	2636(3)	6495(2)	2097(1)	16(1)
C(28)	2140(3)	6285(2)	1757(1)	13(1)
C(29)	1102(3)	5783(2)	1642(1)	14(1)
C(30)	1516(4)	5609(2)	410(1)	29(1)

C(31)	2757(4)	7292(2)	518(1)	26(1)
C(32)	4157(3)	5739(2)	687(1)	32(1)
C(33)	874(3)	4170(2)	2038(1)	29(1)
C(34)	-327(3)	5669(2)	2311(1)	23(1)
C(35)	-1274(3)	4906(2)	1616(1)	22(1)
C(102)	8239(5)	-20(3)	89(1)	70(2)
C(103)	9434(4)	210(3)	-84(1)	70(2)
C(101)	7059(5)	356(3)	-89(1)	80(2)

Table 45. Crystal data and structure refinement for $(Ind^{3Me-2,4,7})_2V$.

Empirical formula	$C_{24}H_{26}V$	
Formula weight	365.39	
Temperature	173(2) K	
Wavelength	0.71073 Å	
Crystal system	Monoclinic	
Space group	$P2_1/n$	
Unit cell dimensions	a = 20.069(3) Å	aα = 90°
	b = 15.620(2) Å	bβ = 90.075(2)°
	c = 24.618(4) Å	gγ = 90°
Volume	7717(2) Å^3	
Z	16	
Density (calculated)	1.258 g/cm^3	
Absorption coefficient	0.517 mm^{-1}	
F(000)	3088	
Crystal color, morphology	green, block	
Crystal size	0.30 x 0.25 x 0.20 mm^3	
Theta range for data collection	0.83 to 25.07°	
Index ranges	-23 ≤£h ≤£23, -18 ≤ k ≤ 18, -29 ≤ l ≤ 29	
Reflections collected	70501	
Independent reflections	13658 [R_{int} = 0.0694]	
Observed reflections	11215	
Completeness to theta = 25.07°	99.7%	
Absorption correction	Multi-scan	
Max. and min. transmission	0.9037 and 0.8604	
Refinement method	Full-matrix least-squares on F^2	
Data / restraints / parameters	13658 / 0 / 926	
Goodness-of-fit on F^2	1.060	
Final R indices [I>2sigma(I)]	R1 = 0.0487, wR2 = 0.0965	
R indices (all data)	R1 = 0.0659, wR2 = 0.1029	
Largest diff. peak and hole	0.384 and -0.412 e$^-$/Å^3	

Table 46. Atomic coordinates ($\times 10^4$) and equivalent isotropic displacement parameters ($Å^2 \times 10^3$) for $(Ind^{3Me\text{-}2,4,7})_2V$. U_{eq} is defined as 1/3 of the trace of the orthogonalized U_{ij} tensor.

atoms	x	y	z	U_{eq}
V1	9499(1)	8340(1)	2885(1)	26(1)
C1	8795(2)	7852(2)	2218(2)	30(1)
C2	8414(2)	8267(2)	2636(2)	31(1)
C3	8597(2)	9139(2)	2645(2)	30(1)
C4	9110(2)	9274(2)	2257(2)	31(1)
C5	9230(2)	8485(2)	1982(2)	30(1)
C6	9681(2)	8251(3)	1558(2)	35(1)
C7	9680(2)	7420(3)	1399(2)	41(1)
C8	9256(2)	6796(3)	1628(2)	40(1)
C9	8813(2)	6987(2)	2037(2)	34(1)
C10	8297(2)	9811(3)	3009(2)	43(1)
C11	10112(2)	8918(3)	1289(2)	49(1)
C12	8357(2)	6333(2)	2275(2)	42(1)
C13	10105(2)	7321(2)	3334(2)	29(1)
C14	9735(2)	7805(2)	3724(2)	31(1)
C15	9965(2)	8665(2)	3713(2)	31(1)
C16	10461(2)	8733(2)	3300(2)	30(1)
C17	10555(2)	7908(2)	3069(2)	28(1)
C18	10950(2)	7615(3)	2620(2)	35(1)
C19	10889(2)	6783(3)	2473(2)	43(1)
C20	10456(2)	6200(3)	2747(2)	40(1)
C21	10064(2)	6455(2)	3170(2)	35(1)
C22	9715(2)	9380(3)	4072(2)	41(1)
C23	11405(2)	8236(3)	2332(2)	49(1)
C24	9594(2)	5854(3)	3450(2)	46(1)
V2	7031(1)	8173(1)	4920(1)	27(1)
C25	7817(2)	7732(2)	4305(2)	30(1)
C26	7300(2)	8187(3)	4024(2)	32(1)
C27	7301(2)	9042(2)	4208(2)	32(1)

C28	7793(2)	9131(2)	4621(2)	29(1)
C29	8125(2)	8327(2)	4683(2)	29(1)
C30	8633(2)	8040(3)	5046(2)	35(1)
C31	8813(2)	7202(3)	5010(2)	41(1)
C32	8519(2)	6619(3)	4638(2)	42(1)
C33	8025(2)	6862(3)	4288(2)	37(1)
C34	6852(2)	9743(3)	4004(2)	41(1)
C35	8942(2)	8654(3)	5443(2)	45(1)
C36	7707(2)	6258(3)	3892(2)	47(1)
C37	6536(2)	7147(2)	5449(2)	31(1)
C38	6040(2)	7558(2)	5119(2)	31(1)
C39	5998(2)	8429(2)	5273(2)	28(1)
C40	6487(2)	8584(2)	5683(1)	29(1)
C41	6816(2)	7786(2)	5797(2)	29(1)
C42	7352(2)	7578(3)	6159(2)	37(1)
C43	7569(2)	6745(3)	6148(2)	48(1)
C44	7279(2)	6113(3)	5811(2)	46(1)
C45	6769(2)	6288(3)	5459(2)	38(1)
C46	5530(2)	9072(2)	5033(2)	37(1)
C47	7636(2)	8247(3)	6531(2)	49(1)
C48	6457(2)	5620(3)	5100(2)	50(1)
V3	4760(1)	8293(1)	2734(1)	26(1)
C49	5868(2)	8487(2)	2914(2)	32(1)
C50	5516(2)	9273(2)	3004(2)	32(1)
C51	5069(2)	9137(2)	3443(2)	32(1)
C52	5107(2)	8264(3)	3603(2)	35(1)
C53	5613(2)	7862(2)	3288(2)	33(1)
C54	5852(2)	7001(3)	3269(2)	43(1)
C55	6329(2)	6814(3)	2888(2)	52(1)
C56	6578(2)	7429(3)	2525(2)	51(1)
C57	6367(2)	8256(3)	2526(2)	41(1)
C58	4612(2)	9798(3)	3682(2)	42(1)
C59	5584(3)	6350(3)	3660(2)	59(1)
C60	6651(2)	8922(3)	2149(2)	55(1)
C61	4485(2)	7867(2)	1881(1)	29(1)
C62	4171(2)	8674(2)	1990(2)	30(1)

C63	3708(2)	8547(2)	2424(2)	31(1)
C64	3748(2)	7689(2)	2595(2)	29(1)
C65	4215(2)	7250(2)	2261(2)	30(1)
C66	4461(2)	6395(2)	2270(2)	34(1)
C67	4965(2)	6204(3)	1918(2)	39(1)
C68	5241(2)	6809(3)	1554(2)	41(1)
C69	5021(2)	7631(3)	1525(2)	33(1)
C70	3261(2)	9220(2)	2661(2)	40(1)
C71	4159(2)	5751(3)	2644(2)	48(1)
C72	5302(2)	8294(3)	1143(2)	48(1)
V4	7800(1)	3228(1)	5559(1)	28(1)
C73	8024(2)	3399(2)	4656(2)	30(1)
C74	8126(2)	4199(2)	4925(2)	31(1)
C75	8659(2)	4096(3)	5301(2)	34(1)
C76	8876(2)	3239(3)	5283(2)	34(1)
C77	8495(2)	2797(2)	4879(2)	32(1)
C78	8511(2)	1933(3)	4695(2)	38(1)
C79	8062(2)	1711(3)	4301(2)	45(1)
C80	7585(2)	2298(3)	4090(2)	45(1)
C81	7554(2)	3130(3)	4253(2)	36(1)
C82	8958(2)	4796(3)	5650(2)	49(1)
C83	9033(2)	1336(3)	4909(2)	55(1)
C84	7060(2)	3760(3)	4027(2)	50(1)
C85	6767(2)	2715(3)	5785(2)	32(1)
C86	6864(2)	3530(3)	6038(2)	34(1)
C87	7398(2)	3453(3)	6418(2)	34(1)
C88	7655(2)	2614(3)	6379(2)	34(1)
C89	7264(2)	2141(3)	5995(2)	35(1)
C90	7310(2)	1289(3)	5802(2)	39(1)
C91	6873(2)	1052(3)	5405(2)	45(1)
C92	6390(2)	1617(3)	5193(2)	48(1)
C93	6325(2)	2440(3)	5360(2)	41(1)
C94	7647(2)	4148(3)	6789(2)	44(1)
C95	7834(3)	694(3)	6026(2)	54(1)
C96	5821(2)	3055(3)	5135(2)	53(1)

Table 47. Crystal data and structure refinement for $(Ind^{Me-2})_2V$.

Empirical formula	$C_{20}H_{18}V$	
Formula weight	309.28	
Temperature	107(2) K	
Wavelength	1.54178 Å	
Crystal system	Monoclinic	
Space group	*C*2/*c*	
Unit cell dimensions	*a* = 19.1705(19) Å	αa= 90°
	b = 10.7408(11) Å	βb= 107.740(7)°
	c = 7.8099(8) Å	γ = 90°
Volume	1531.6(3) $Å^3$	
Z	4	
Density (calculated)	1.341 g/cm^3	
Absorption coefficient	5.304 mm^{-1}	
F(000)	644	
Crystal size	0.33 × 0.22 × 0.11 mm^3	
Theta range for data collection	4.78 to 58.97°	
Index ranges	$-15 \le h \le 21$, $-11 \le k \le 11$, $-8 \le l \le 6$	
Reflections collected	3487	
Independent reflections	1042 [R_{int} = 0.0263]	
Completeness to theta = 58.97°	94.5 %	
Absorption correction	Multi-scan	
Refinement method	Full-matrix least-squares on F^2	
Data / restraints / parameters	1042 / 0 / 98	
Goodness-of-fit on F^2	1.091	
Final R indices [I>2σ(I)]	*R*1 = 0.0321, *wR*2 = 0.0838	
R indices (all data)	*R*1 = 0.0345, *wR*2 = 0.0852	
Extinction coefficient	0.00030(14)	
Largest diff. peak and hole	0.475 and -0.287 $e^-/Å^3$	

Table 48. Atomic coordinates ($\times 10^4$) and equivalent isotropic displacement parameters ($Å^2 \times 10^3$) for $(Ind^{Me\text{-}2})_2V$. U(eq) is defined as 1/3 of the trace of the orthogonalized U^{ij} tensor.

atoms	x	y	z	U(eq)
V(1)	7500	7500	0	16(1)
C(1)	7738(1)	7862(2)	2969(3)	20(1)
C(2)	8129(1)	8760(2)	2291(3)	20(1)
C(3)	7618(1)	9491(2)	983(3)	20(1)
C(4)	6188(1)	9428(2)	-239(3)	24(1)
C(5)	5591(1)	8798(2)	-89(3)	27(1)
C(6)	5665(1)	7799(2)	1134(3)	26(1)
C(7)	6335(1)	7424(2)	2220(3)	23(1)
C(8)	6973(1)	8058(2)	2128(3)	18(1)
C(9)	6895(1)	9083(2)	874(3)	18(1)
C(10)	8945(1)	8895(2)	2854(3)	29(1)

Table 49. Crystal data and structure refinement for $(Ind^{2Me-4,7})_2V$.

Empirical formula	$C_{22}H_{22}V$	
Formula weight	337.34	
Temperature	293(2) K	
Wavelength	0.71073 Å	
Crystal system	Monoclinic	
Space group	*Cc*	
Unit cell dimensions	*a* = 15.642(5) Å	α= 90°
	b = 18.533(6) Å	β= 110.758(4)°
	c = 12.547(4) Å	γ = 90°
Volume	3401.2(19) Å^3	
Z	8	
Density (calculated)	1.318 g/cm^3	
Absorption coefficient	0.580 mm^{-1}	
F(000)	1416	
Crystal size	0.33 × 0.22 × 0.10 mm^3	
Crystal color, habit	Green blade	
Theta range for data collection	1.77 to 27.71°	
Index ranges	$-20 \le h \le 16$, $-24 \le k \le 23$, $-16 \le l \le 16$	
Reflections collected	13424	
Independent reflections	6148 [R_{int} = 0.0408]	
Completeness to theta = 25.00°	96.0 %	
Absorption correction	Multi-scan	
Refinement method	Full-matrix least-squares on F^2	
Data / restraints / parameters	6148 / 2 / 461	
Goodness-of-fit on F^2	1.067	
Final *R* indices [I>2σ(I)]	*R*1 = 0.0348, *wR*2 = 0.0854	
R indices (all data)	*R*1 = 0.0432, *wR*2 = 0.0939	
Absolute structure parameter	0.471(18)	
Extinction coefficient	0.00058(16)	
Largest diff. peak and hole	0.386 and -0.519 e$^-$/Å^3	

Table 50. Atomic coordinates ($\times 10^4$) and equivalent isotropic displacement parameters ($Å^2 \times 10^3$) for $(Ind^{2Me\text{-}4,7})_2V$. U(eq) is defined as $^1/_3$ of the trace of the orthogonalized U^{ij} tensor.

atoms	x	y	z	U(eq)
V(1)	3174(1)	1756(1)	9659(1)	19(1)
C(1)	2431(2)	998(1)	8186(2)	19(1)
C(2)	3005(2)	1476(2)	7844(2)	24(1)
C(3)	3916(2)	1330(2)	8532(3)	27(1)
C(4)	3936(2)	792(2)	9336(3)	26(1)
C(5)	3021(2)	570(1)	9128(2)	21(1)
C(6)	2626(2)	67(2)	9689(2)	24(1)
C(7)	1690(2)	6(2)	9276(3)	31(1)
C(8)	1126(2)	419(2)	8353(3)	28(1)
C(9)	1463(2)	905(2)	7793(2)	23(1)
C(10)	3242(3)	-363(2)	10673(3)	37(1)
C(11)	858(3)	1348(2)	6802(3)	35(1)
C(12)	2281(2)	2245(2)	10553(2)	23(1)
C(13)	2530(2)	2799(1)	9926(2)	27(1)
C(14)	3487(2)	2886(2)	10405(2)	28(1)
C(15)	3855(2)	2379(2)	11299(2)	24(1)
C(16)	3115(2)	1986(1)	11416(2)	21(1)
C(17)	3083(2)	1396(1)	12138(2)	22(1)
C(18)	2238(2)	1108(2)	11987(2)	28(1)
C(19)	1421(2)	1382(2)	11168(3)	29(1)
C(20)	1418(2)	1928(2)	10440(2)	26(1)
C(21)	3950(2)	1121(2)	13010(3)	31(1)
C(22)	562(2)	2198(2)	9516(3)	37(1)
V(1')	1826(1)	4199(1)	5367(1)	20(1)
C(1')	2084(2)	3009(1)	5834(2)	20(1)
C(2')	1194(2)	3199(2)	5805(3)	27(1)
C(3')	1303(2)	3714(2)	6681(3)	28(1)
C(4')	2235(2)	3870(2)	7218(2)	26(1)
C(5')	2739(2)	3427(2)	6719(2)	23(1)

C(6')	3691(2)	3367(2)	6923(3)	28(1)
C(7')	3952(2)	2902(2)	6252(3)	33(1)
C(8')	3311(3)	2499(2)	5373(3)	35(1)
C(9')	2389(2)	2540(1)	5136(3)	28(1)
C(10')	4363(3)	3808(2)	7851(3)	44(1)
C(11')	1696(3)	2120(2)	4196(3)	44(1)
C(12')	1705(2)	4486(1)	3541(2)	21(1)
C(13')	979(2)	4828(2)	3795(3)	26(1)
C(14')	1381(2)	5323(2)	4682(3)	29(1)
C(15')	2340(2)	5285(1)	5026(3)	27(1)
C(16')	2555(2)	4772(1)	4301(2)	22(1)
C(17')	3408(2)	4535(2)	4243(3)	27(1)
C(18')	3366(2)	4035(2)	3433(3)	32(1)
C(19')	2529(2)	3738(2)	2685(3)	30(1)
C(20')	1700(2)	3946(2)	2722(2)	26(1)
C(21')	4284(2)	4841(2)	5054(3)	38(1)
C(22')	806(3)	3642(2)	1936(3)	38(1)

Table 51. Crystal data and structure refinement $[(Ind^{2Si-1,3})ZnI(thf)]_2$.

Empirical formula	$C_{38}H_{62}I_2O_2Si_4Zn_2$	
Formula weight	1047.78	
Temperature	100(2) K	
Wavelength	0.71073 Å	
Crystal system	Monoclinic	
Space group	$P2_1/c$	
Unit cell dimensions	a = 16.4885(10) Å	aα = 90°
	b = 16.0594(10) Å	bβ = 111.9010(10)°
	c = 19.5253(12) Å	gγ = 90°
Volume	4797.1(5) Å^3	
Z	4	
Density (calculated)	1.451 g/cm^3	
Absorption coefficient	2.415 mm^{-1}	
F(000)	2112	
Crystal size	0.30 x 0.30 x 0.20 mm^3	
Theta range for data collection	1.69 to 28.19°	
Index ranges	$-21 \le h \le 21$, $-20 \le k \le 21$, $-25 \le l \le 25$	
Reflections collected	39671	
Independent reflections	11069 [R_{int} = 0.0302]	
Completeness to theta = 28.19°	96.9 %	
Absorption correction	None	
Max. and min. transmission	0.6438 and 0.5311	
Refinement method	Full-matrix least-squares on F^2	
Data / restraints / parameters	11069 / 0 / 434	
Goodness-of-fit on F^2	1.035	
Final R indices [I>2σ(I)]	$R1$ = 0.0297, $wR2$ = 0.0672	
R indices (all data)	$R1$ = 0.0471, $wR2$ = 0.0746	
Largest diff. peak and hole	1.032 and -0.454 e$^-$/Å^3	

Table 52. Atomic coordinates ($\times 10^4$) and equivalent isotropic displacement parameters ($Å^2 \times 10^3$) for $[(Ind^{2Si-1,3})ZnI(thf)]_2$. U(eq) is defined as 1/3 of the trace of the orthogonalized U^{ij} tensor.

atoms	x	y	z	U(eq)
I(1)	6307(1)	687(1)	4666(1)	25(1)
I(2)	8644(1)	-532(1)	5687(1)	28(1)
Zn(1)	7317(1)	-477(1)	4393(1)	22(1)
Zn(2)	7601(1)	587(1)	5982(1)	23(1)
Si(1)	5589(1)	-906(1)	1607(1)	27(1)
Si(2)	6336(1)	-2229(1)	4382(1)	24(1)
Si(3)	8298(1)	2444(1)	5945(1)	28(1)
Si(4)	9904(1)	837(1)	8621(1)	27(1)
O(1)	7869(1)	217(1)	3814(1)	29(1)
O(2)	7072(1)	-189(1)	6523(1)	28(1)
C(1)	6092(2)	-1176(2)	3165(1)	21(1)
C(2)	6300(2)	-1236(2)	2551(1)	22(1)
C(3)	7150(2)	-1646(2)	2793(1)	22(1)
C(4)	7684(2)	-1860(2)	2409(2)	27(1)
C(5)	8476(2)	-2252(2)	2779(2)	29(1)
C(6)	8745(2)	-2425(2)	3528(2)	29(1)
C(7)	8230(2)	-2212(2)	3922(2)	25(1)
C(8)	7428(2)	-1825(2)	3558(1)	21(1)
C(9)	6761(2)	-1516(2)	3836(1)	21(1)
C(10)	6168(2)	-190(2)	1189(2)	48(1)
C(11)	5223(2)	-1842(2)	1004(2)	40(1)
C(12)	4617(2)	-363(2)	1652(2)	36(1)
C(13)	7187(2)	-2602(2)	5260(2)	41(1)
C(14)	5467(2)	-1671(2)	4595(2)	33(1)
C(15)	5863(2)	-3167(2)	3808(2)	41(1)
C(16)	8980(2)	1290(2)	7099(1)	23(1)
C(17)	8152(2)	1615(2)	6564(1)	24(1)
C(18)	7649(2)	1786(2)	7038(1)	25(1)
C(19)	6804(2)	2097(2)	6866(2)	31(1)
C(20)	6478(2)	2176(2)	7420(2)	35(1)

C(21)	6978(2)	1950(2)	8146(2)	36(1)
C(22)	7811(2)	1638(2)	8325(2)	30(1)
C(23)	8153(2)	1555(2)	7771(1)	24(1)
C(24)	8999(2)	1244(2)	7805(1)	25(1)
C(25)	7260(2)	2995(2)	5402(2)	42(1)
C(26)	8762(2)	1973(2)	5295(2)	38(1)
C(27)	9072(2)	3237(2)	6531(2)	35(1)
C(28)	9528(2)	-114(2)	8973(2)	34(1)
C(29)	10266(2)	1643(2)	9366(2)	44(1)
C(30)	10842(2)	564(2)	8354(2)	41(1)
C(31)	8734(2)	90(2)	3798(2)	38(1)
C(32)	8857(2)	832(2)	3370(2)	50(1)
C(33)	7968(2)	996(2)	2828(2)	46(1)
C(34)	7391(2)	823(2)	3256(2)	34(1)
C(35)	6188(2)	-147(2)	6514(2)	37(1)
C(36)	6132(2)	-886(2)	6968(2)	37(1)
C(37)	7032(2)	-901(2)	7569(2)	39(1)
C(38)	7618(2)	-685(2)	7155(2)	39(1)

Appendix C

SQUID Magnetometer Description and Solid State Magnetic Data

To use this instrument, approximately 30 mg of sample is placed inside a superconducting sample holder that rests above the SQUID device. A biasing current is then applied to a superconducting loop possessing two Josephson junctions (each represented by × in the inset of Figure 45). The resulting magnetic field is then influenced by the magnetic character of the sample, inducing a measurable change in the magnetic flux. This is recorded in the form of impedance and later interpreted to yield the magnetic susceptibility (χ) of the sample. Plotted over a range of temperatures, χT *vs* T produces characteristic data curves that correspond to distinct magnetic ordering, such as ferro- or antiferromagnetism.

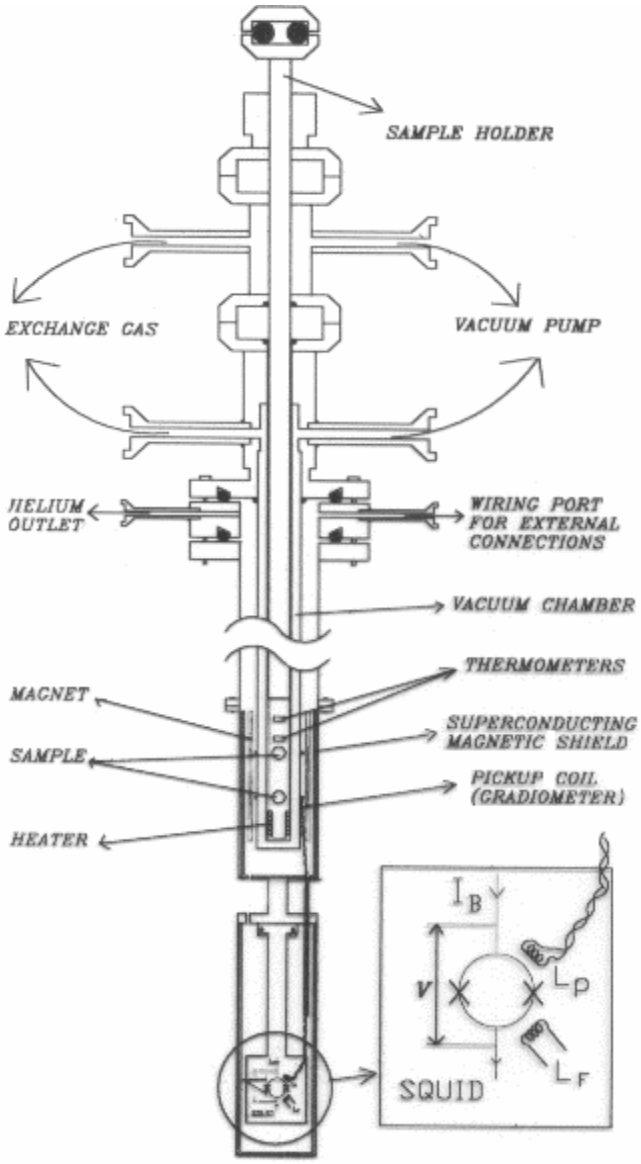

Figure 45. Schematic for a SQUID magnetometer.

Table 53. SQUID data for $[(Ind^{2Me-4,7})_2Cr$

temp (K)	χ_m	μ_{eff}	$1/\chi_m$	$\chi_m T$
2.00	0.37155	2.44	2.69	0.74
2.50	0.33037	2.57	3.03	0.83
3.00	0.28618	2.62	3.49	0.86
3.50	0.25383	2.66	3.94	0.89
4.00	0.22714	2.70	4.40	0.91
4.50	0.20631	2.73	4.85	0.93
5.00	0.18917	2.75	5.29	0.95
5.50	0.17377	2.77	5.75	0.96
6.00	0.16048	2.78	6.23	0.96
6.50	0.14919	2.79	6.70	0.97
7.00	0.13889	2.79	7.20	0.97
7.50	0.13007	2.79	7.69	0.98
8.00	0.12224	2.80	8.18	0.98
8.50	0.11532	2.80	8.67	0.98
9.00	0.10920	2.80	9.16	0.98
9.50	0.10359	2.81	9.65	0.98
10.00	0.09876	2.81	10.13	0.99
12.00	0.08348	2.83	11.98	1.00
14.01	0.07223	2.84	13.85	1.01
15.99	0.06368	2.85	15.70	1.02
18.00	0.05683	2.86	17.60	1.02
19.99	0.05130	2.86	19.49	1.03
21.99	0.04676	2.87	21.38	1.03
23.99	0.04292	2.87	23.30	1.03
26.00	0.03934	2.86	25.42	1.02
28.00	0.03667	2.87	27.27	1.03
30.00	0.03411	2.86	29.31	1.02
35.00	0.02915	2.86	34.30	1.02
40.01	0.02551	2.86	39.20	1.02
45.01	0.02271	2.86	44.04	1.02
50.01	0.02044	2.86	48.92	1.02
55.05	0.01864	2.87	53.64	1.03
60.06	0.01711	2.87	58.44	1.03
65.08	0.01582	2.87	63.23	1.03
70.09	0.01471	2.87	67.96	1.03
75.09	0.01377	2.88	72.61	1.03
80.13	0.01296	2.88	77.15	1.04

Table 53., continued

temp (K)	χ_m	μ_{eff}	$1/\chi_m$	$\chi_m T$
85.13	0.03501	7.30	28.57	6.67
90.14	0.03445	7.34	29.03	6.73
95.17	0.03390	7.37	29.50	6.79
100.10	0.03339	7.41	29.95	6.86
105.20	0.03285	7.44	30.44	6.91
110.19	0.03235	7.47	30.91	6.97
115.22	0.03186	7.50	31.39	7.02
120.23	0.03138	7.52	31.87	7.07
125.25	0.03091	7.55	32.36	7.12
130.26	0.03045	7.57	32.84	7.17
135.27	0.03001	7.60	33.33	7.22
140.29	0.02957	7.62	33.82	7.26
145.29	0.02915	7.64	34.30	7.30
150.31	0.02874	7.66	34.79	7.34
155.32	0.02834	7.68	35.29	7.38
160.33	0.02794	7.70	35.79	7.42
165.34	0.02756	7.72	36.29	7.45
170.35	0.02718	7.74	36.79	7.49
175.36	0.02682	7.76	37.29	7.52
180.38	0.02646	7.77	37.79	7.55
185.40	0.02612	7.79	38.29	7.59
190.40	0.37155	2.44	2.69	0.74
195.41	0.33037	2.57	3.03	0.83
200.41	0.28618	2.62	3.49	0.86
205.44	0.25383	2.66	3.94	0.89
210.45	0.22714	2.70	4.40	0.91
215.43	0.20631	2.73	4.85	0.93
220.45	0.18917	2.75	5.29	0.95
225.44	0.17377	2.77	5.75	0.96
230.44	0.16048	2.78	6.23	0.96
235.45	0.14919	2.79	6.70	0.97
240.46	0.13889	2.79	7.20	0.97
245.44	0.13007	2.79	7.69	0.98
250.45	0.12224	2.80	8.18	0.98
255.45	0.11532	2.80	8.67	0.98
260.45	0.10920	2.80	9.16	0.98
265.45	0.10359	2.81	9.65	0.98

Table 53., continued

temp (K)	χ_m	μ_{eff}	$1/\chi_m$	$\chi_m T$
270.45	0.09876	2.81	10.13	0.99
275.45	0.08348	2.83	11.98	1.00

Table 54. SQUID data for $[(Ind^{3Me\text{-}1,2,3})_2Fe]^+[DCNQ]^-$

temp (K)	χ_m	μ_{eff}	$1/\chi_m$	$\chi_m T$
1.79	1.1476	4.06	0.87	2.06
2.00	1.1388	4.27	0.88	2.28
2.20	1.1306	4.46	0.88	2.49
2.40	1.1218	4.64	0.89	2.69
2.60	1.1123	4.81	0.90	2.89
2.80	1.1016	4.97	0.91	3.08
3.00	1.0904	5.11	0.92	3.27
3.20	1.0767	5.25	0.93	3.44
3.40	1.0612	5.37	0.94	3.61
3.60	1.0431	5.48	0.96	3.75
3.81	1.0218	5.58	0.98	3.89
4.00	0.9996	5.66	1.00	4.00
4.20	0.9747	5.73	1.03	4.10
4.40	0.9483	5.78	1.05	4.17
4.60	0.9202	5.82	1.09	4.23
4.80	0.8956	5.86	1.12	4.30
5.00	0.8678	5.89	1.15	4.34
5.20	0.8379	5.90	1.19	4.36
5.40	0.8074	5.91	1.24	4.36
5.60	0.7765	5.90	1.29	4.35
5.80	0.7440	5.88	1.34	4.32
6.00	0.7132	5.85	1.40	4.28
6.19	0.6845	5.82	1.46	4.24
6.40	0.6551	5.79	1.53	4.19
6.60	0.6278	5.76	1.59	4.14
6.80	0.6020	5.72	1.66	4.09
7.00	0.5777	5.69	1.73	4.04
7.20	0.5541	5.65	1.80	3.99
7.40	0.5320	5.61	1.88	3.93
7.60	0.5112	5.57	1.96	3.88
7.80	0.4914	5.54	2.03	3.83
8.00	0.4728	5.50	2.12	3.78
8.20	0.4552	5.46	2.20	3.73
8.40	0.4386	5.43	2.28	3.68
8.60	0.4229	5.39	2.36	3.64
8.79	0.4083	5.36	2.45	3.59
9.00	0.3943	5.33	2.54	3.55

Table 54., continued

temp (K)	χ_m	μ_{eff}	$1/\chi_m$	$\chi_m T$
9.20	0.3807	5.29	2.63	3.50
9.40	0.3686	5.26	2.71	3.46
9.60	0.3569	5.23	2.80	3.43
9.79	0.3457	5.20	2.89	3.39
10.00	0.3351	5.18	2.98	3.35
14.99	0.1816	4.67	5.51	2.72
19.98	0.1191	4.36	8.40	2.38
24.98	0.0870	4.17	11.49	2.17
30.00	0.0678	4.03	14.75	2.03
35.00	0.0552	3.93	18.11	1.93
40.00	0.0464	3.85	21.54	1.86
45.01	0.0400	3.79	25.01	1.80
50.03	0.0350	3.74	28.55	1.75
55.05	0.0311	3.70	32.12	1.71
60.07	0.0280	3.67	35.69	1.68
65.08	0.0255	3.64	39.29	1.66
70.08	0.0233	3.62	42.84	1.64
75.13	0.0215	3.60	46.46	1.62
80.13	0.0200	3.58	50.07	1.60
85.16	0.0186	3.56	53.67	1.59
90.15	0.0175	3.55	57.25	1.57
95.16	0.0164	3.54	60.83	1.56
100.22	0.0155	3.53	64.40	1.56
105.18	0.0147	3.52	67.97	1.55
110.23	0.0140	3.51	71.53	1.54
115.25	0.0133	3.50	75.08	1.53
120.23	0.0127	3.50	78.65	1.53
125.22	0.0122	3.49	82.16	1.52
130.28	0.0117	3.49	85.64	1.52
135.29	0.0112	3.48	89.19	1.52
140.31	0.0108	3.48	92.71	1.51
145.33	0.0104	3.48	96.22	1.51
150.35	0.0100	3.47	99.72	1.51
155.34	0.0097	3.47	103.18	1.51
160.36	0.0094	3.47	106.69	1.50
165.37	0.0091	3.47	110.13	1.50
170.40	0.0088	3.46	113.61	1.50

Table 54., continued

temp (K)	χ_m	μ_{eff}	$1/\chi_m$	$\chi_m T$
175.39	0.0085	3.46	117.06	1.50
180.40	0.0083	3.46	120.49	1.50
185.42	0.0081	3.46	123.91	1.50
190.42	0.0079	3.46	127.33	1.50
195.44	0.0076	3.46	130.74	1.49
200.45	0.0075	3.46	134.11	1.49
205.45	0.0073	3.46	137.51	1.49
210.47	0.0071	3.46	140.88	1.49
215.47	0.0069	3.46	144.21	1.49
220.47	0.0068	3.46	147.57	1.49
225.47	0.0066	3.46	150.89	1.49
230.39	0.0065	3.46	154.23	1.49
235.45	0.0063	3.46	157.51	1.49
240.48	0.0062	3.46	160.81	1.50
245.45	0.0061	3.46	164.09	1.50
250.48	0.0060	3.46	167.36	1.50
255.47	0.0059	3.46	170.65	1.50
260.48	0.0057	3.46	173.95	1.50
265.48	0.0056	3.46	177.32	1.50
270.50	0.0055	3.46	180.58	1.50
275.51	0.0054	3.46	183.85	1.50
280.50	0.0053	3.46	187.06	1.50
285.50	0.0053	3.46	190.34	1.50
290.51	0.0052	3.47	193.53	1.50
295.48	0.0051	3.47	196.72	1.50
300.48	0.0050	3.47	199.88	1.50

Table 55. SQUID data for $[(Ind^{2Me\text{-}1,3/Si\text{-}2})_2Fe]^+[DCID]^-$

temp (K)	χ_m	μ_{eff}	$1/\chi_m$	$\chi_m T$
1.80	0.2804	2.01	3.57	0.51
2.00	0.2689	2.07	3.72	0.54
2.20	0.2574	2.13	3.88	0.57
2.40	0.2471	2.18	4.05	0.59
2.60	0.2380	2.22	4.20	0.62
2.80	0.2297	2.27	4.35	0.64
3.00	0.2222	2.31	4.50	0.67
3.20	0.2153	2.35	4.65	0.69
3.40	0.2090	2.38	4.78	0.71
3.60	0.2033	2.42	4.92	0.73
3.81	0.1981	2.46	5.05	0.75
4.01	0.1932	2.49	5.18	0.77
4.20	0.1887	2.52	5.30	0.79
4.40	0.1845	2.55	5.42	0.81
4.60	0.1803	2.58	5.55	0.83
4.80	0.1777	2.61	5.63	0.85
5.00	0.1746	2.64	5.73	0.87
5.20	0.1714	2.67	5.83	0.89
5.40	0.1683	2.70	5.94	0.91
5.60	0.1653	2.72	6.05	0.93
5.80	0.1625	2.75	6.15	0.94
6.00	0.1597	2.77	6.26	0.96
6.20	0.1572	2.79	6.36	0.97
6.40	0.1547	2.81	6.46	0.99
6.60	0.1522	2.83	6.57	1.00
6.80	0.1501	2.86	6.66	1.02
7.00	0.1480	2.88	6.76	1.04
7.20	0.1458	2.90	6.86	1.05
7.40	0.1439	2.92	6.95	1.06
7.60	0.1420	2.94	7.04	1.08
7.80	0.1402	2.96	7.13	1.09
7.99	0.1384	2.98	7.22	1.11
8.19	0.1367	2.99	7.31	1.12
8.40	0.1350	3.01	7.41	1.13
8.60	0.1334	3.03	7.49	1.15
8.79	0.1319	3.05	7.58	1.16
9.00	0.1304	3.06	7.67	1.17

Table 55., continued

temp (K)	χ_m	μ_{eff}	$1/\chi_m$	$\chi_m T$
9.20	0.1289	3.08	7.76	1.19
9.40	0.1275	3.10	7.84	1.20
9.60	0.1261	3.11	7.93	1.21
9.80	0.1248	3.13	8.01	1.22
10.00	0.1235	3.14	8.10	1.23
14.99	0.1019	3.50	9.81	1.53
19.98	0.0859	3.71	11.64	1.72
24.97	0.0737	3.84	13.57	1.84
30.00	0.0643	3.93	15.56	1.93
35.00	0.0559	3.96	17.88	1.96
40.00	0.0485	3.94	20.60	1.94
44.99	0.0441	3.98	22.70	1.98
50.04	0.0404	4.02	24.78	2.02
55.05	0.0373	4.05	26.84	2.05
60.06	0.0346	4.08	28.89	2.08
65.08	0.0323	4.10	30.95	2.10
70.10	0.0303	4.12	32.99	2.12
75.10	0.0285	4.14	35.03	2.14
80.12	0.0270	4.16	37.06	2.16
85.13	0.0256	4.18	39.06	2.18
90.15	0.0240	4.16	41.59	2.17
95.14	0.0232	4.21	43.04	2.21
100.18	0.0222	4.22	44.97	2.23
105.17	0.0213	4.23	46.92	2.24
110.30	0.0205	4.25	48.86	2.26
115.32	0.0197	4.26	50.80	2.27
120.30	0.0190	4.27	52.71	2.28
125.26	0.0183	4.28	54.64	2.29
130.27	0.0177	4.29	56.54	2.30
135.29	0.0171	4.30	58.44	2.32
140.30	0.0166	4.31	60.32	2.33
145.31	0.0161	4.32	62.15	2.34
150.33	0.0156	4.33	64.01	2.35
155.36	0.0152	4.34	65.85	2.36
160.36	0.0148	4.35	67.68	2.37
165.37	0.0144	4.36	69.53	2.38
170.38	0.0141	4.39	70.81	2.41

Table 55., continued

temp (K)	χ_m	μ_{eff}	$1/\chi_m$	$\chi_m T$
175.36	0.0137	4.38	73.17	2.40
180.40	0.0133	4.39	74.97	2.41
185.42	0.0130	4.40	76.75	2.42
190.44	0.0127	4.40	78.54	2.42
195.36	0.0124	4.41	80.34	2.43
200.45	0.0122	4.42	82.07	2.44
205.46	0.0119	4.43	83.80	2.45
210.46	0.0117	4.44	85.56	2.46
215.46	0.0115	4.44	87.30	2.47
220.45	0.0112	4.45	88.98	2.48
225.47	0.0110	4.46	90.72	2.49
230.46	0.0108	4.47	92.46	2.49
235.47	0.0106	4.47	94.17	2.50
240.48	0.0104	4.48	95.92	2.51
245.49	0.0102	4.48	97.64	2.51
250.48	0.0101	4.49	99.35	2.52
255.49	0.0099	4.50	101.05	2.53
260.48	0.0097	4.50	102.73	2.54
265.51	0.0096	4.51	104.40	2.54
270.49	0.0094	4.52	106.05	2.55
275.45	0.0093	4.52	107.73	2.56
280.48	0.0091	4.53	109.50	2.56
285.48	0.0090	4.53	111.13	2.57
290.51	0.0089	4.54	112.79	2.58
295.45	0.0087	4.55	114.40	2.58
300.51	0.0086	4.55	116.03	2.59

Table 56. SQUID data for $[(Ind^{3Me\text{-}2,4,7})MnCl(thf)]_2$

temp (K)	χ_m	μ_{eff}	$1/\chi_m$	$\chi_m T$
5.00	0.02599	1.02	38.48	0.13
10.00	0.03975	1.78	25.15	0.40
14.99	0.04473	2.32	22.36	0.67
19.99	0.04698	2.74	21.29	0.94
24.98	0.04833	3.11	20.69	1.21
30.00	0.04934	3.44	20.27	1.48
35.00	0.05010	3.75	19.96	1.75
40.00	0.05074	4.03	19.71	2.03
45.00	0.05123	4.29	19.52	2.31
50.02	0.05181	4.55	19.30	2.59
55.06	0.05207	4.79	19.20	2.87
60.08	0.05138	4.97	19.46	3.09
65.08	0.05119	5.16	19.54	3.33
70.10	0.05086	5.34	19.66	3.57
75.12	0.05044	5.51	19.82	3.79
80.13	0.04994	5.66	20.03	4.00
85.14	0.04936	5.80	20.26	4.20
90.15	0.04873	5.93	20.52	4.39
95.18	0.04805	6.05	20.81	4.57
100.21	0.04734	6.16	21.12	4.74
105.21	0.04661	6.26	21.46	4.90
110.20	0.04586	6.36	21.81	5.05
115.24	0.04510	6.45	22.17	5.20
120.24	0.04435	6.53	22.55	5.33
125.24	0.04359	6.61	22.94	5.46
130.27	0.04284	6.68	23.34	5.58
135.28	0.04209	6.75	23.76	5.69
140.30	0.04136	6.81	24.18	5.80
145.31	0.04065	6.87	24.60	5.91
150.33	0.03995	6.93	25.03	6.00
155.33	0.03926	6.99	25.47	6.10
160.35	0.03860	7.04	25.91	6.19
165.36	0.03796	7.09	26.34	6.28
170.37	0.03734	7.13	26.78	6.36
175.39	0.03674	7.18	27.22	6.44
180.40	0.03615	7.22	27.66	6.52
185.41	0.03558	7.26	28.11	6.60

Table 56., continued

temp (K)	χ_m	μ_{eff}	$1/\chi_m$	$\chi_m T$
190.41	0.03501	7.30	28.57	6.67
195.43	0.03445	7.34	29.03	6.73
200.43	0.03390	7.37	29.50	6.79
205.45	0.03339	7.41	29.95	6.86
210.46	0.03285	7.44	30.44	6.91
215.44	0.03235	7.47	30.91	6.97
220.44	0.03186	7.50	31.39	7.02
225.45	0.03138	7.52	31.87	7.07
230.44	0.03091	7.55	32.36	7.12
235.45	0.03045	7.57	32.84	7.17
240.47	0.03001	7.60	33.33	7.22
245.46	0.02957	7.62	33.82	7.26
250.47	0.02915	7.64	34.30	7.30
255.46	0.02874	7.66	34.79	7.34
260.46	0.02834	7.68	35.29	7.38
265.47	0.02794	7.70	35.79	7.42
270.45	0.02756	7.72	36.29	7.45
275.46	0.02718	7.74	36.79	7.49
280.46	0.02682	7.76	37.29	7.52
285.47	0.02646	7.77	37.79	7.55
290.47	0.02612	7.79	38.29	7.59
295.47	0.02578	7.81	38.79	7.62
300.47	0.02545	7.82	39.30	7.65

Table 57. SQUID data for $(Ind^{Me-2})_2V$

temp (K)	χ_m	μ_{eff}	$1/\chi_m$	$\chi_m T$
5.00	0.21714	2.95	4.61	1.09
9.99	0.12064	3.10	8.29	1.21
14.99	0.08309	3.16	12.03	1.25
19.99	0.06314	3.18	15.84	1.26
24.99	0.05100	3.19	19.61	1.27
30.00	0.04277	3.20	23.38	1.28
35.00	0.03686	3.21	27.13	1.29
40.01	0.03241	3.22	30.86	1.30
45.01	0.02889	3.23	34.62	1.30
50.02	0.02624	3.24	38.11	1.31
55.04	0.02387	3.24	41.89	1.31
60.06	0.02191	3.24	45.64	1.32
65.08	0.02024	3.25	49.40	1.32
70.09	0.01883	3.25	53.10	1.32
75.10	0.01762	3.25	56.77	1.32
80.12	0.01656	3.26	60.40	1.33
85.14	0.01561	3.26	64.07	1.33
90.15	0.01478	3.26	67.68	1.33
95.20	0.01403	3.27	71.28	1.34
100.21	0.01336	3.27	74.87	1.34
105.21	0.01275	3.28	78.44	1.34
110.23	0.01219	3.28	82.03	1.34
115.16	0.01170	3.28	85.47	1.35
120.21	0.01123	3.29	89.06	1.35
125.22	0.01080	3.29	92.56	1.35
130.26	0.01041	3.29	96.06	1.36
135.28	0.01005	3.30	99.54	1.36
140.30	0.00971	3.30	102.99	1.36
145.31	0.00939	3.30	106.47	1.36
150.33	0.00909	3.31	109.96	1.37
155.34	0.00882	3.31	113.40	1.37
160.34	0.00855	3.31	116.90	1.37
165.36	0.00831	3.32	120.37	1.37
170.36	0.00808	3.32	123.81	1.38
175.39	0.00786	3.32	127.26	1.38
180.40	0.00765	3.32	130.71	1.38
185.41	0.00746	3.33	134.12	1.38

Table 57., continued

temp (K)	X_m	μ_{eff}	$1/\chi_m$	$\chi_m T$
190.41	0.00727	3.33	137.57	1.38
195.41	0.00709	3.33	140.97	1.39
200.44	0.00693	3.33	144.36	1.39
205.44	0.00677	3.34	147.74	1.39
210.43	0.00661	3.34	151.19	1.39
215.44	0.00647	3.34	154.60	1.39
220.46	0.00633	3.34	157.99	1.40
225.43	0.00619	3.34	161.42	1.40
230.44	0.00606	3.34	164.89	1.40
235.29	0.00594	3.34	168.34	1.40
240.42	0.00582	3.35	171.80	1.40
245.45	0.00571	3.35	175.25	1.40
250.46	0.00559	3.35	178.74	1.40
255.46	0.00549	3.35	182.23	1.40
260.45	0.00538	3.35	185.75	1.40
265.49	0.00528	3.35	189.31	1.40
270.46	0.00519	3.35	192.77	1.40
275.45	0.00510	3.35	195.95	1.41
280.47	0.00502	3.36	199.16	1.41
285.46	0.00494	3.36	202.36	1.41
290.46	0.00487	3.36	205.55	1.41
295.47	0.00479	3.37	208.72	1.42
300.48	0.00472	3.37	211.90	1.42

References

(1) Fisher, E. O.; Seus, D. *Z. Naturforsch.* **1953**, *8b*, 694.

(2) Pauson, P. L.; Wilkinson, G. *J. Am. Chem. Soc.* **1954**, *76*, 2024-2026.

(3) Brintzinger, H. H.; Risher, D.; Mülhay, R.; Rieger, B.; Waymouth, R. M. *Angew. Chem., Int. Ed.* **1995**, *34*, 1143.

(4) Hitchcock, P. B.; Kerton, F. M.; Lawless, G. A. *J. Am. Chem. Soc.* **1998**, *120*, 10264-10265.

(5) Urnezius, E.; Brennessell, W. W.; Cramer, C. J.; Ellis, J. E.; von Rague Schleyer, P. *Science* **2002**, *295*, 832.

(6) Antipin, M. Y.; Lobkovsky, E.; Semenenko, K. N.; Soloveichik, G. L.; Struchkov, Y. T. *Zh. Strukt. Khim.* **1979**, *20*, 942.

(7) Kowaleski, R. M.; Rheingold, A. L.; Trogler, W. C.; Basolo, F. *J. Am. Chem. Soc.* **1986**, *108*, 2460-2461.

(8) Brady, E. D.; Overby, J. S.; Meredith, M. B.; Mussman, A. B.; Cohn, M. A.; Hanusa, T. P.; Yee, G. T.; Pink, M. *J. Am. Chem. Soc.* **2002**, *124*, 9556-9566.

(9) Meredith, M. B.; Crisp, J. A.; Brady, E. D.; Hanusa, T. P.; Yee, G. T.; Brooks, N. R.; Kucera, B. E.; Young Jr., V. G. *Organometallics* **2006**, *25*, 4945-4952.

(10) Meredith, M. B.; Crisp, J. A.; Brady, E. D.; Hanusa, T. P.; Yee, G. T.; Pink, M.; Brennessell, W. W.; Young Jr., V. G. *Organometallics* **2008**, *27*, 5464-5473.

(11) Switzer, M. E.; Wang, R.; Rettig, M. F.; Maki, A. H. *J. Am. Chem. Soc.* **1974**, *96*, 7669-7674.

(12) Smart, J. C.; Robbins, J. L. *J. Am. Chem. Soc.* **1978**, *100*, 3936-3937.

(13) Robbins, J. L.; Edelstein, N. M.; Cooper, S. R.; Smart, J. C. *J. Am. Chem. Soc.* **1979**, *101*, 3853-3857.

(14) Hays, M. L.; Burkey, D. J.; Overby, J. S.; Hanusa, T. P.; Yee, G. T.; Sellers, S. P.; Young Jr., V. G. *Organometallics* **1998**, *17*, 5521-5527.

(15) Sitzmann, H.; Schär, M. *Z. Anorg. Allg. Chem.* **1997**, *623*, 1850-1852.

(16) Hart-Davis, A. J.; Mawby, R. *J. Chem. Soc. A* **1969**, 2403.

(17) Cramer, R.; Seiwell, L. P. *J. Organomet. Chem.* **1975**, *92*, 245.

(18) Rerek, M. E.; Basolo, F. *J. Am. Chem. Soc.* **1984**, *106*, 5908.

(19) Rerek, M. E.; Ji, L. N.; Basolo, F. *J. Chem. Soc., Chem. Commun.* **1983**, 1208.

(20) Caddy, P.; Green, M.; O'Brien, E.; Smart, L. E.; Woodward, P. *Angew. Chem., Int. Ed.* **1977**, *16*, 648.

(21) O'Hare, D.; Murphy, V. J.; Kaltsoyannis, N. *J. Chem. Soc., Dalton Trans.* **1993**, 383-92.

(22) Westcott, S. A.; Kakkar, A. K.; Stringer, G.; Taylor, N. J.; Marder, T. B. *J. Orgnomet. Chem.* **1990**, *394*, 777-794.

(23) Fisher, E. O.; Hafner, W. *Z. Naturforsch.* **1953**, *8B*, 444.

(24) Weiss, E.; Fisher, E. O. *Z. Anorg. Allg. Chem.* **1956**, *284*, 69.

(25) Karol, F. J. U.S.P. 4,015,059, 1977.

(26) Heinemann, O.; Jolly, P. W.; Krüger, C.; Verhovnik, G. P. J. *Organometallics* **1996**, *15*, 5462-5463.

(27) O'Hare, D.; Green, J. C.; Marder, T. B.; Collins, S.; Stringer, G.; Kakkar, A.; Kaltsoyannis, N.; Kuhn, A.; Lewis, R.; Mehnert, C.; Scott, P.; Kurmoo, M.; Pugh, S. *Organometallics* **1992**, *11*, 48.

(28) Aoki, T.; Furusaki, A.; Tomiie, Y.; Ono, K.; Tanaka, K. *Bull. Chem. Soc. Jpn.* **1969**, *42*, 545-547.

(29) Smith, J. D.; Hanusa, T. P.; Young Jr., V. G. *J. Am. Chem. Soc.* **2001**, *123*, 6455-6456.

(30) Carlson, C. N.; Smith, J. D.; Hanusa, T. P.; Brennessell, W. W.; Young Jr., V. G. *J. Organomet. Chem.* **2003**, *683*, 191-199.

(31) Evans, D. F. *J. Chem. Soc.* **1959**, 2003-2005.

(32) Loeliger, J.; Scheffold, R. *J. Chem. Ed.* **1972**, *49*, 646-647.

(33) Grant, D. H. *J. Chem. Ed.* **1995**, *72*, 39-40.

(34) Sur, S. K. *J. Magn. Reson.* **1989**, *82*, 169-173.

(35) Lindoy, L. F.; Katovic, V.; Busch, D. H. *J. Chem. Ed.* **1972**, *49*, 117-120.

(36) Hays, M. L., Ph.D. Dissertation, Vanderbilt University, 1996.

(37) Becker, C. L.; McLaughlin, M. L. *Synlett* **1991**, *9*, 642.

(38) Gaussian 03, Revision C.02, Frisch, M. J.; Trucks, G. W.; Schlegel, H. B.; Scuseria, G. E.; Robb, M. A.; Cheeseman, J. R.; Montgomery, Jr., J. A.; Vreven, T.; Kudin, K. N.; Burant, J. C.; Millam, J. M.; Iyengar, S. S.; Tomasi, J.; Barone, V.; Mennucci, B.; Cossi, M.; Scalmani, G.; Rega, N.; Petersson, G. A.; Nakatsuji, H.; Hada, M.; Ehara, M.; Toyota, K.; Fukuda, R.; Hasegawa, J.; Ishida, M.; Nakajima, T.; Honda, Y.; Kitao, O.; Nakai, H.; Klene, M.; Li, X.; Knox, J. E.; Hratchian, H. P.; Cross, J. B.; Bakken, V.; Adamo, C.; Jaramillo, J.; Gomperts, R.; Stratmann, R. E.; Yazyev, O.; Austin, A. J.; Cammi, R.; Pomelli, C.; Ochterski, J. W.; Ayala, P. Y.; Morokuma, K.; Voth, G. A.; Salvador, P.; Dannenberg, J. J.; Zakrzewski, V. G.; Dapprich, S.; Daniels, A. D.; Strain, M. C.; Farkas, O.; Malick, D. K.; Rabuck, A. D.; Raghavachari,

K.; Foresman, J. B.; Ortiz, J. V.; Cui, Q.; Baboul, A. G.; Clifford, S.; Cioslowski, J.; Stefanov, B. B.; Liu, G.; Liashenko, A.; Piskorz, P.; Komaromi, I.; Martin, R. L.; Fox, D. J.; Keith, T.; Al-Laham, M. A.; Peng, C. Y.; Nanayakkara, A.; Challacombe, M.; Gill, P. M. W.; Johnson, B.; Chen, W.; Wong, M. W.; Gonzalez, C.; and Pople, J. A.; Gaussian, Inc., Wallingford CT, 2004.

(39) Staroverov, V. N.; Scuseria, G. E.; Tao, J.; Perdew, J. P. *J. Chem. Phys.* **2003**, *119*, 12129-12137.

(40) Furche, F.; Perdew, J. P. *J. Chem. Phys.* **2006**, *124*, 044103/1-044103/27.

(41) Rassolov, V. A.; Pople, J. A.; Ratner, M. A.; Windus, T. L. *J. Chem. Phys.* **1998**, *109*, 1223-1229.

(42) Becke, A. D. *Phys. Rev. A*, *38*, 3098-3100.

(43) Lee, C.; Yang, W.; Parr, R. G. *Phys. Rev. B* **1988**, *37*, 785-789.

(44) Meihlich, B.; Savin, A.; Stoll, H.; Preuss, H. *Chem. Phys. Lett.* **1989**, *157*, 200-206.

(45) SHELXTL V6.14, Bruker Analytical X-Ray Systems, Madison, WI (2003).

(46) Spek, A. L. *Acta. Cryst.* **1990**, *A46*, C34.

(47) Cedheim, L.; Eberson, L. *Synthesis* **1973**, 159.

(48) Ready, T. E.; Chien, J. C. W.; Rausch, M. D. *J. Organomet. Chem.* **1999**, *583*, 11-27.

(49) Davison, A.; Rakita, P. E. *J. Organomet. Chem.* **1970**, *21*, 55-58.

(50) Crossley, N. S.; Green, J. C.; Nagy, A.; Stringer, G. *J. Chem. Soc., Dalton Trans.* **1989**, 2139-2147.

(51) Gütlich, P.; Hauser, A.; Spiering, H. *Angew. Chem.* **1994**, *106*, 2109-2141.

(52) Gütlich, P.; Garcia, Y.; Woike, T. *Coord. Chem. Rev.* **2001**, *219*, 839-879.

(53) Real, J. A.; Gaspar, A. B.; Munoz, M. C. *Dalton Trans.* **2005**, 2062-2079.

(54) Switzer, M. E.; Wang, R.; Rettig, M. F.; Maki, A. H. *J. Am. Chem. Soc.* **1974**, *96*, 7669-7674.

(55) Robbins, J. L.; Edelstein, N.; Spencer, B.; Smart, J. C. *J. Am. Chem. Soc.* **1982**, *104*, 1882-1893.

(56) Curnow, O. J.; Fern, G. M. *J. Organomet. Chem.* **2005**, *690*, 3018-3026.

(57) Kamigaito, M.; Watanabe, Y.; Ando, T.; Sawamoto, M. *J. Am. Chem. Soc.* **2002**, *124*, 9994-9995.

(58) Deng, X.; Wang, B.; Xu, S.; Zhou, X.; Yang, L.; Li, Y.; Hu, Y.; Li, Y.; Zou, F. *J. Mol. Catal. A: Chem.* **2002**, *184*, 57-64.

(59) Pun, D.; Bradley, C. A.; Lobkovsky, E.; Keresztes, I.; Chirik, P. J. *J. Am. Chem. Soc.* **2008**, *130*, 14046-14047.

(60) Bazinet, P.; Tilley, T. D. *Organometallics* **2008**, *27*, 1267-1274.

(61) Crisp, J. A.; Meredith, M. B.; Hanusa, T. P.; Wang, G.; Brennessell, W. W.; Yee, G. T. *Inorg. Chem.* **2004**, *44*, 172-174.

(62) Edelstein, A. S.; Mandel, M. *J. Chem. Phys.* **1961**, *35*, 1130.

(63) Morozova, N. D.; Dyatkina, M. E. *Zh. Strukt. Khim.* **1965**, *6*, 278-282.

(64) McConnell, H. M. *J. Chem. Phys.* **1958**, *28*, 1188-1192.

(65) McConnell, H. M. *J. Chem. Phys.* **1963**, *39*, 1910.

(66) McConnell, H. M. *Proc. R. A. Welch Found. Chem. Res.* **1967**, *11*, 144.

(67) Candela, G. A.; Swartzendruber, L.; Miller, J. S.; Rice, M. J. *J. Am. Chem. Soc.* **1979**, *101*, 2755.

(68) Miller, J. S.; Epstein, A. J.; Reiff, W. M. *Chem. Rev.* **1988**, *88*, 201.

(69) Miller, J. S.; Calabrese, J. C.; Rommelmann, H.; Chittipeddi, S. R.; Zhang, J. H.; Reiff, W. M.; Epstein, A. J. *J. Am. Chem. Soc.* **1987**, *109*, 769.

(70) Broderick, W. E.; Eichhorn, D. M.; Liu, X.; Toscano, P. M.; Owens, S. M.; Hoffman, B. M. *J. Am. Chem. Soc.* **1995**, *117*, 3641-3642.

(71) Yee, G. T.; Miller, J. S. *Magnetism: Molecules to Materials*, Miller, J. S., Drillon, M. Eds., Wiley-VCH: Mannheim, Germany, 2004.

(72) Kollmar, C.; Couty, M.; Kahn, O. *J. Am. Chem. Soc.* **1991**, *113*, 7994-8005.

(73) Chi, K.-M.; Calabrese, J. C.; Reiff, W. M.; Miller, J. S. *Organometallics* **1991**, *10*, 688-693.

(74) Miller, J. S.; Glatzhofer, D. T.; O'Hare, D. M.; Reiff, W. M.; Chakraborty, A.; Epstein, A. J. *Inorg. Chem.* **1989**.

(75) Desiraju, G. R. *Crystal Engineering: The Design of Organic Solids*; Elsevier: Amsterdam, 1989.

(76) Murphy, V. J.; O'Hare, D. *Inorg. Chem.* **1994**, *33*, 1833-1841.

(77) Fern, G. M.; Klaib, S.; Curnow, O. J.; Lang, H. *J. Organomet. Chem.* **2004**, *689*, 1139-1144.

(78) Meredith, M. B. Ph.D. Dissertation, Vanderbilt University, 2004.

(79) Neelgund, G. M.; Budni, M. L. *Monatsh. Chem.* **2004**, *135*, 1395-1407.

(80) Overby, J. S. Ph.D. Dissertation, Vanderbilt University, 1997.

(81) Miller, J. S.; Reiss, A. H.; Gebert, E.; Ritski, J. J.; Salaneck, W. R.; Kovnat, L.; Cape, T. W.; Duyne, R. P. V. *J. Am. Chem. Soc.* **1979**, *101*, 7111-7113.

(82) Kollmar, C.; Kahn, O. *J. Am. Chem. Soc.* **1991**, *113*, 7987-7994.

(83) Schweizer, J.; Bencini, A.; Carbonera, C.; Epstein, A. J.; Golhen, S.; Lelievre- Berna, E.; Miller, J. S.; Ouahab, L.; Pontillon, Y.; Ressouche, E.; Zheludev, A. *Polyhedron* **2001**, *20*, 1771-1778.

(84) Chatterjee, S. *J. Chem. Soc. (B),* **1971**, *11*, 2194-2197.

(85) Khoo, S. B.; Foley, J. K.; Pons, S. *J. Electroanal. Chem.* **1986**, *215*, 273-285.

(86) Yee, G. T.; Whitton, M. J.; Sommer, R. D.; Frommen, C. M.; Reiff, W. M. *Inorg. Chem.* **2000**, *39*, 1874-1877.

(87) Hamlin, J. J.; Beckett, B. R.; Tomita, T.; Schilling, J. S.; Tyree, W. S.; Yee, G. T. *Polyhedron* **2003**, *22*, 2249-2252.

(88) Hughmark, G. A.; Sobel, B. A. *SAE Technical Paper Series* **1980**, *800393*, 10.

(89) Miller, J. S.; Dixon, D. A.; McLean, R. S.; Groski, D. M.; Flippen, R. B.; Manriquez, J. M.; Yee, G. T.; Narayan, K. S.; Epstein, A. J. *Adv. Mater.* **1990**, *3*, 309-311.

(90) Kakkar, A.; Taylor, N. J.; Marder, T. B.; Shen, J. K.; Hallinan, N.; Basolo, F. *Inorg. Chim. Acta* **1992**, *198*, 219-231.

(91) Shapiro, H.; De Witt, E. G.; Brown, J. E.; U.S.P. 2,839,552: 1958.

(92) Allen, A. D.; Harris, R. O.; Loescher, B. R.; Stevens, J. R.; Whiteley, R. N. *Chem. Rev.* **1973**, *73*, 11-20.

(93) Johnson, G. L.; Beveridge, W. D. *Inorg. Nucl. Chem. Lett.* **1967**, *3*, 323-325.

(94) Sellmann, D.; Weiss, W. *Angew. Chem.* **1977**, *89*, 918-919.

(95) Sellmann, D.; Weiss, W. *J. Organomet. Chem.* **1978**, *160*, 183-196.

(96) Chirik, P. J. *Dalton Trans.* **2007**, *1*, 16-25.

(97) Fryzuk, M. D.; Love, J. B.; Rettig, S. J.; Young Jr., V. G. *Science* **1997**, *275*, 1445.

(98) Jeffery, J.; Lappert, M. F.; Riley, P. I. *J. Organomet. Chem.* **1978**, *181*, 25.

(99) Pez, G. P.; Apgar, P.; Crissey, R. K. *J. Am. Chem. Soc.* **1982**, *104*, 482.

(100) White, C.; Mawby, R. J. *Inorg. Chim. Acta* **1970**, *4*, 261.

(101) Caddy, P.; Green, M.; O'Brien, E.; Smart, L. E.; Woodward, P. *J. Chem. Soc., Dalton Trans.* **1980**, 962.

(102) Marder, T. B.; Williams, I. D. *J. Chem. Soc., Chem. Commun.* **1987**, 1478.

(103) Pun, D.; Lobkovsky, E.; Chirik, P. J. *J. Am. Chem. Soc.* **2008**, *130*, 6047-6054.

(104) Kubas, G. J.; Ryan, R. R.; Swanson, B. I.; Vergamini, P. J.; Wasserman, H. J. *J. Am. Chem. Soc.* **1984**, *106*, 451.

(105) Hung, M. Y.; Ng, S. M.; Zhou, Z.; Lau, C. P. *Organometallics* **2000**, *19*, 3692-3699.

(106) Allen, A. D.; Bottomley, F.; Harris, R. O.; Reinsalu, V. P.; Senoff, C. V. *J. Am. Chem. Soc.* **1967**, *89*, 5595.

(107) Atkinson, L. K.; Mawby, A. H.; Smith, D. C. *Chem. Commun.* **1971**, 157.

(108) Chatt, J.; Dilworth, J.; Leigh, G. J. *Chem. Commun.* **1969**, 687.

(109) Speier, G.; Marko, L. *Inorg. Chim. Acta* **1969**, *3*, 126.

(110) Pool, J. A.; Lobkovsky, E.; Chirik, P. J. *J. Am. Chem. Soc.* **2003**, *125*, 2241.

(111) Girolami, G. S.; Salt, J. E.; Wilkinson, G.; Thornton-Pett, M.; Hursthouse, M. B. *J. Am. Chem. Soc.* **1983**, *105*, 5954-5956.

(112) Salt, J. E.; Girolami, G. S.; Wilkinson, G.; Motevalli, M.; Thornton-Pett, M.; Hursthouse, M. B. *J. Am. Chem. Soc.* **1985**, *4*.

(113) Childs, G. I.; Grills, D. C.; Gallagher, S.; Bitterwolf, T. E.; George, M. W. *J. Chem. Soc., Dalton Trans.* **2001**, 1711-1717.

(114) Bosch, A.; Brown, R. K. *Can. J. of Chem.* **1964**, *42*, 1718-1735.

(115) Brady, E. D., Ph. D. Dissertation, Vanderbilt University, 2001.

(116) Burger, U.; Thorel, P. J.; Mentha, Y. *Chimia* **1987**, *41*, 26-28.

(117) Faller, J. W.; Crabtree, R. H.; Habib, A. *Organometallics* **1985**, *4*, 929-935.

(118) Dahl, L. F.; Ishishi, E.; Rundle, R. E. *Acta. Cryst.* **1963**, *16*, 419-426.

(119) Calderon, J. L.; Fontana, S.; Frauendorfer, E.; Day, V. W.; Stults, B. R. *Inorg. Chim. Acta* **1976**, *17*, L31-L32.

(120) Bond, A. D.; Layfield, R. A.; MacAllister, J. A.; McPartlin, M.; Rawson, J. M.; Wright, D. S. *Chem. Commun.* **2001**, *19*, 1956-1957.

(121) Bunder, W.; Weiss, E. *Z. Naturforsch., Teil B,* **1978**, *33*, 1235.

(122) Calculated from the average of all C-Mn-O, O-Mn-O, and C-Mn-C angles, excluding only the intra-ring C-Mn-C angles of the η3–bound ligand.

(123) Krinsky, J. L.; Stavis, M. N.; Walter, M. D. *Acta. Crystallogr., Sect. E: Struct. Rep. Online* **2003**, *59*, m497.

(124) Kohler, F. H.; Hebendanz, N. *Angew. Chem.* **1984**, *96*, 697-699.

(125) te Velde, G.; Bickelhaupt, F. M.; van Gisbergen, S. J. A.; Fonseca Guerra, C.; Baerends, E. J.; Snijders, J. G.; Ziegler, T. *J. Comput. Chem.* **2001**, *22*, 931-967.

(126) Fonseca Guerra, C.; Snijders, J. G.; te Velde, G.; Baerends, E. J. *Theor. Chem. Acc.* **1998**, *99*, 391.

(127) Baerends, E. J.; Autschbach, J.; Bérces, A.; Bickelhaupt, F. M.; Bo, C.; Boerrigter, P. M.; Cavallo, L.; Chong, D. P.; Deng, L.; Dickson, R. M.; Ellis, D. E.; Faassen, M. v.; Fan, L.; Fischer, T. H.; Fonseca Guerra, C.; Gisbergen, S. J. A. v.; Götz, A. W.; Groeneveld, J. A.; Gritsenko, O. V.; Grüning, M.; Harris, F. E.; Hoek, P. v. d.; Jacob, C. R.; Jacobsen, H.; Jensen, L.; Kessel, G. v.; Kootstra, F.; Krykunov, M. V.; Lenthe, E. v.; McCormack, D. A.; Michalak, A.; Neugebauer, J.; Nicu, V. P.; Osinga, V. P.; Patchkovskii, S.; Philipsen, P. H. T.; Post, D.; Pye, C. C.; Ravenek, W.; Rodríguez, J. I.; Ros, P.; Schipper, P. R. T.; Schreckenbach, G.; Snijders, J. G.; Solà, M.; Swart, M.; Swerhone, D.; Velde, G. t.; Vernooijs, P.; Versluis, L.; Visscher, L.; Visser, O.; Wang, F.; Wesolowski, T. A.; Wezenbeek, E. M. v.; Wiesenekker, G.; Wolff, S. K.; Woo, T. K.; Yakovlev, A. L.; Ziegler, T., ADF2008.01, SCM, Theoretical Chemistry, Vrije Universiteit, Amsterdam, The Netherlands, http://www.scm.com.

(128) Freyberg, D. P.; Robbins, J. L.; Raymond, K. N.; Smart, J. C. *J. Am. Chem. Soc.* **1979**, *101*, 892-897.

(129) Almenningen, A.; Haaland, A.; Samdal, S. *J. Organomet. Chem.* **1978**, *149*, 219-229.

(130) Overby, J. S.; Hanusa, T. P.; Young Jr., V. G., Unpublished results.

(131) Buender, W.; Weiss, E. *Z. Naturforsch., Teil B,* **1978**, *33*, 1235.

(132) Ammeter, J. H.; Bucher, R.; Oswald, N. *J. Am. Chem. Soc.* **1974**, *96*, 7833-7835.

(133) Radius, U.; Sundermeyer, J.; Peters, K.; von Schnering, H. G. *Z. Anorg. Allg. Chem.* **2002**, *628*, 1226-1235.

(134) Bernskoetter, W. H.; Lobkovsky, E.; Chirik, P. J. *Angew. Chem., Int. Ed.* **2008**, *46*, 2858-2861.

(135) Pun, D.; Lobkovsky, E.; Chirik, P. J. *J. Am. Chem. Soc.* **2008**, *130*, 6047-6054.

(136) Gambarotta, S.; Floriani, C.; Chiesi-Villa, A.; Guastini, C. *Inorg. Chem.* **1984**, *23*, 1739.

(137) Perdew, J. P.; Wang, Y. *Phys. Rev.* **1992**, *45*, 13244-13249.

(138) Krishnan, R.; Binkley, J. S.; Seeger, R.; Pople, J. A. *J. Chem. Phys.* **1980**, *72*, 650-654.

(139) Bradley, C. A.; Keresztes, I.; Lobkovsky, E.; Young Jr., V. G.; Chirik, P. J. *J. Am. Chem. Soc.* **2004**, *126*, 16937.

(140) Jonas, K.; Gabor, B.; Mynott, R.; Aundermund, K.; Heinemann, O.; Krüger, C. *Angew. Chem. Int. Ed.* **1997**, *36*, 1712-1714.

(141) Bocarsly, J. R.; Floriani, C.; Chiesi-Villa, A.; Guastini, C. *Inorg. Chem.* **1987**, *26*, 1871-1875.

(142) Barr, R. D.; Green, M.; Marder, T. B.; Stone, F. G. A. *J. Chem. Soc., Dalton Trans.* **1984**, 1261-1262.

(143) Kowaleski, R. M., Ph.D. Dissertation, Northwestern University, 1987.

(144) Calderazzo, F.; Fachinetti, G.; Floriani, C. *J. Am. Chem. Soc.* **1974**, *96*, 3695-3696.

(145) Resa, I.; Carmona, E.; Gutierrez-Puebla, E.; Monge, A. *Science* **2004**, *305*, 1136-1138.